8107392

SHUBERT, KEITH ALAN

IMMITTANCE PROPERTIES OF LARGE FINITE DIELECTRIC COVERED PHASED ARRAYS

The Ohio State University PH.D. 1980

University Microfilms International 300 N. Zeeb Road, Ann Arbor, MI 48106

PLEASE NOTE:

In all cases this material has been filmed in the best possible way from the available copy. Problems encountered with this document have been identified here with a check mark ✓.

1. Glossy photographs ______
2. Colored illustrations ______
3. Photographs with dark background ______
4. Illustrations are poor copy ______
5. Print shows through as there is text on both sides of page ______
6. Indistinct, broken or small print on several pages ✓
7. Tightly bound copy with print lost in spine ______
8. Computer printout pages with indistinct print ✓
9. Page(s) ______ lacking when material received, and not available from school or author
10. Page(s) ______ seem to be missing in numbering only as text follows
11. Poor carbon copy ______
12. Not original copy, several pages with blurred type ______
13. Appendix pages are poor copy ______
14. Original copy with light type ______
15. Curling and wrinkled pages ______
16. Other ______

IMMITTANCE PROPERTIES OF LARGE FINITE
DIELECTRIC COVERED PHASED ARRAYS

Dissertation
Presented in Partial Fulfillment of the Requirements for
the Degree Doctor of Philosophy in the Graduate
School of The Ohio State University

By

Keith Alan Shubert, B.S.E.E., M.Sc.

******

The Ohio State University
1980

Reading Committee:

Professor Benedikt A. Munk
Professor Jack H. Richmond
Professor David L. Moffatt

Approved by

Adviser
Department of Electrical
Engineering

ACKNOWLEDGMENT

The author wishes to thank his many friends and associates at The ElectroScience Laboratory for their help throughout his career while enrolled in the Graduate School at The Ohio State University. Professor David L. Moffatt deserves special recognition for his guidance as a past advisor as well as for his review of this dissertation. A debt of gratitude is also owed to Professor Jack H. Richmond for his technical help through the years and his critical review of this manuscript. And a special debt is owed to the author's friend and advisor, Professor Benedickt A. Munk, without whose guidance, knowledge, and enthusiasm this work would have never been completed.

VITA

November 22, 1951..........Born - Kansas City, Missouri

1974.......................B.S.E.E., the Ohio State University

1975.......................M.Sc., The Ohio State University

1974-1980..................Graduate Research Associate, ElectroScience Laboratory, Department of Electrical Engineering, The Ohio State University

PUBLICATIONS

"Synthetic Radar Imagery," (co-authors, D.L. Moffatt and J.D. Young), IEEE Transactions of Antennas and Propagation, Vol. AP-25, No. 4, July 1977.

"Natural Resonances via Rational Approximants," (co-author, D.L. Moffatt), IEEE Transactions on Antennas and Propagation, Vol. AP-25, No. 5, September 1977.

FIELDS OF STUDY

Electromagnetics, Professor David L. Moffatt and Professor Robert G. Kouyoumjian

Communication Theory, Professor C.E. Warren

Mathematics, Professor J.T. Scheick

Digital Theory, Professor H. Hemami

CONTENTS

LIST OF FIGURES

CHAPTER I
INTRODUCTION

The advantages of using phased arrays of antennas in radar systems, such as the ability to track many targets through microsecond inertialess scanning and beamshaping [1,2], along with developments in phase shifting devices which perform to the standards required by theory [3], have led to their popularity and implementation in many devices and systems. In fact, the use of periodically spaced radiators has expanded into many other areas such as metallic radomes [4-13] whose use has been shown to be beneficial in controlling frequency and spatial selection of energy transmission, reflection, and reradiation. The theoretical development of these frequency sensitive surfaces (F.S.S.) has incorporated an extremely useful method for treating dielectric layers adjacent to the phased array or F.S.S. device [14,15,16]. It is this recently developed procedure which is exploited here in treating an old problem in the understanding of phased arrays.

Antenna array theory considers a phased array to be a collection of periodically spaced radiators which are fed with progressive phase in such a way as to direct energy in one direction. In what has been called "classical" phased array theory [17], the effects of each element in the array radiating energy towards all other elements in the array is ignored. This interaction among elements, characterized as mutual-coupling or mutual immittance, cannot be ignored, particularly when the elements are spaced a half-wavelength or less apart. To date, however, the non-trivial problems of studying the effects of this mutual coupling upon desirable spatial and frequency selective properties has been addressed mainly through models of arrays using an infinite number of radiators [18-23]. Although several studies have effectively investigated finite arrays with a modest number of elements [24,25,26], a gap remains between methods which describe properties of infinitely large arrays and finite arrays with fewer than 100 elements. It is the intent of this effort to not only help to fill this gap by considering large finite arrays (on the order of 1000 elements or more), but to also use the theory mentioned above to allow the use of a dielectric layer over the array which has been shown to be effective in decreasing the change in the immittance level as the array is scanned in space [27].

This theory, in the approach used by Munk and other investigators [28], begins by considering an infinite plane of equally excited Hertzian dipoles whose total vector potential is written as an infinite sum of spherical waves. An involved transform procedure converts this sum of spherical waves to a sum, or spectrum, of plane waves. The use of Maxwell's equations yields expressions for the electric and magnetic fields, each of which are a spectrum of plane waves. The formulation in terms of plane waves allows layers of dielectrics to be treated using plane wave reflection coefficients. The method presented here starts with the array of Hertzian dipoles and goes through the transform procedure but differs with the above method in that the currents on all the Hertzian dipoles are not equal. Figure 1 gives a representation of the magnitudes of the currents along the x-axis for the infinite array when all magnitudes are the same. Figure 2 shows the currents as they are considered in the new method where all amplitudes are not equal but rather, the magnitudes are considered to be periodically spaced finite "apertures" surrounded by areas of non-excited elements. The periodic spacing allows an expression for the currents to be written as a Fourier sum. The transform procedure is carried out as before and an expression for the electric field is found in terms of a spectrum of plane waves. This field is now considered to be, however, the field from an infinite number of periodically spaced finite arrays.

It is the immittance properties of finite arrays which are the topic studied here. The specific immittance properties under consideration are those between the individual array element and the feeding network. These "matching" properties have been very important in phased arrays over the years because as arrays are scanned in different directions, this match, in general, changes. Under some conditions the match can be so poor as to inhibit energy radiation in certain directions. The matching problem is at least as important as the radiation pattern shape problem. The method presented here used the field from the array, written as a spectrum of plane waves, and a test element placed in close proximity to an array element to find the self-immittance of that element. This process can be repeated for each element in the finite "aperture" and, if the finite "apertures" are spaced far enough apart, these self-immittances can be considered the immittances of elements in a finite array.

The above procedure is also applied to two-dimensional geometries where the periodic spacing in two directions gives expressions for the self-immittances of finite two-dimensional arrays. This dissertation goes through the described mathematics and presents some computer generated results for free space and dielectric coated dipole arrays and dielectric coated slot arrays. The various features of the method are discussed as they are encountered. The method is shown to be successful and some suggestions for future study are given.

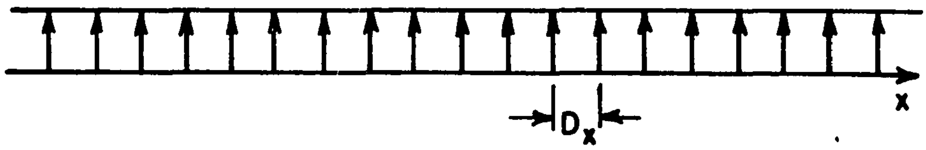

Figure 1. Representation of the magnitudes of the currents on an infinite array of dipoles, without modulation.

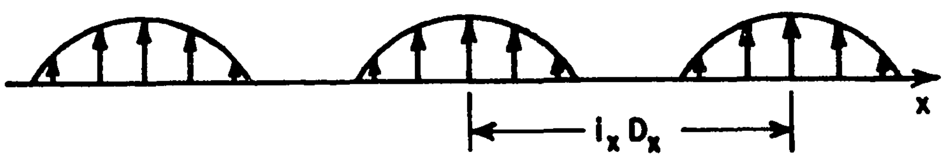

Figure 2. Representation of the magnitudes of the currents on a modulated array of dipoles creating an infinite number of finite arrays.

CHAPTER II
THE FIELD OF A CURRENT MODULATED ARRAY OF LINEAR DIPOLES

A. Introduction

In this chapter the current on the elements of an infinite phased array of dipoles is given as an expression with identical currents on each element and progressive phase as required to implement scan in a particular direction. The concept of constant magnitude is then removed to allow each element to have a unique excitation. Describing these magnitudes with a Fourier Sum allows periodic groupings of some amplitude shape in the infinite phased array. Forcing this shape to be an area of zero excitation surrounding areas of non-zero excitation makes the infinite array appear as if it were an infinite number of periodically spaced finite arrays. This idea of "modulating" the element by element currents is exploited first for the one-dimensional case and then for the two-dimensional case. The rest of the chapter is devoted to applying the methods of Reference [26] for finding the electric field radiated by these periodically spaced finite phased arrays.

B. The Current

Figure 3 represents the two-dimensional infinite phased array of identical linear dipoles where the current on each element is expressed in terms of some reference element as ($e^{j\omega t}$ time convention)

$$I = I(\ell)\, e^{-j\beta q D_x s_x}\, e^{-j\beta m D_z s_z} \tag{1}$$

$I(\ell)$ represents the current as a function of position (ℓ) which is the same on each element. The phase of each element is given by Floquet's theorem as a function of scan angle where s_x and s_z specify the scan angle and are related to angles α and η (see Figure 4) by

$$s_x = \cos(\alpha)\sin(\eta) \tag{2}$$

$$s_z = \sin(\alpha)\sin(\eta) \tag{3}$$

The direction of scan is

$$\hat{s} = \hat{x}s_x + \hat{y}s_y + \hat{z}s_z \tag{4}$$

and β is equal to 2π divided by the wavelength.

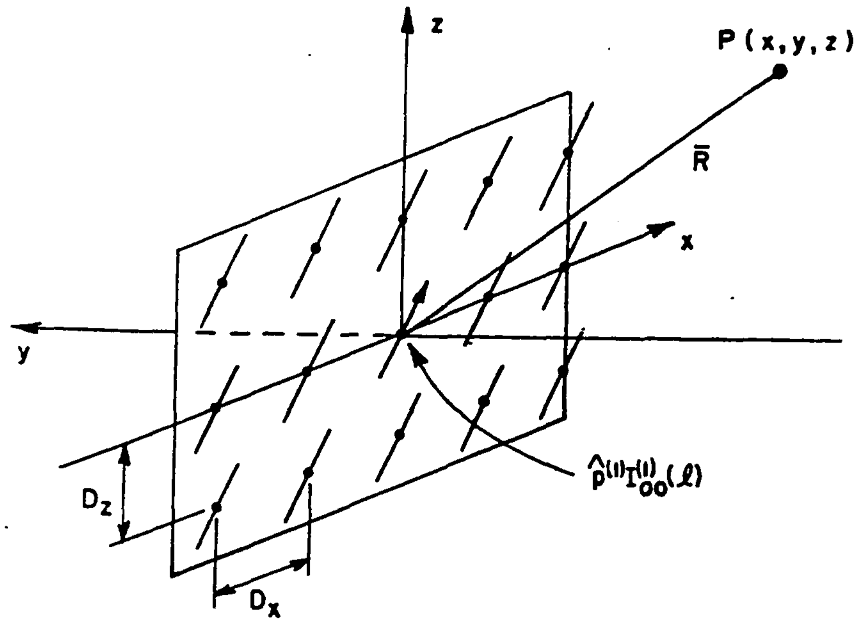

Figure 3. Part of an infinite array of arbitrarily oriented dipoles in the x-z plane.

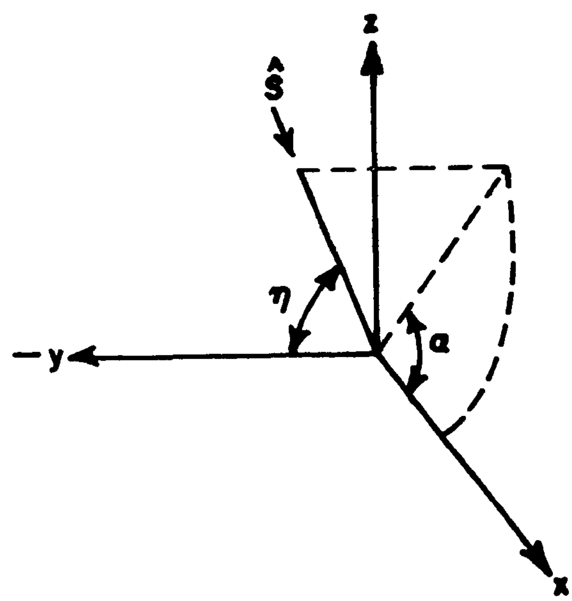

Figure 4. Relationship between vector direction of scan, $\hat{s}$, and the angles α and ν.

1. One-dimensional case

To examine the effect of "modulating" the current for the purpose of creating an infinite number of finite arrays, consider the row of dipoles along the x-axis. Their currents without modulation are given by

$$I_{q,o} = I\, e^{-j\beta q D_x s_x} \tag{5}$$

where the explicit dependence on ℓ has been dropped since all elements are identical and only the phase changes from element to element. Figure 1 is a representation of the magnitudes of these currents. Of more interest is Figure 2 where all magnitudes are not equal. The zero-magnitude elements appear to be separating an infinite number of finite apertures. If these finite apertures are periodically spaced, with distance between their centers equal to $i_x D_x$, then the current magnitude of the element located at x can be expressed as a Fourier Series with

$$I_x = I_x^{(0)} + I_x^{(1)} \cos\left(\frac{2\pi}{i_x D_x} x\right) + I_x^{(2)} \cos\left(\frac{4\pi}{i_x D_x} x\right) + \cdots \tag{6}$$

or

$$I_x = \sum_{k=0}^{\infty} \frac{I_x^{(k)}}{2} \left(e^{jk \frac{2\pi}{i_x D_x} x} + e^{-jk \frac{2\pi}{i_x D_x} x} \right) \tag{7}$$

The total expression for the magnitude and phase as a function of element position is given by substituting Equation (7) into (5) giving

$$I\Big|_{x=qD_x} = \sum_{k=0}^{\infty} \frac{I_x^{(k)}}{2} \left(e^{-j\beta q D_x \left(s_x - \frac{k\lambda}{i_x D_x}\right)} + e^{-j\beta q D_x \left(s_x + \frac{k\lambda}{i_x D_x}\right)} \right) \tag{8}$$

or

$$I\Big|_{x=qD_x} = \sum_{k=-\infty}^{\infty} \frac{1}{\varepsilon_k} I_x^{(k)}\, e^{-j\beta q D_x s_x^k} \tag{9}$$

where

$$\varepsilon_k = \begin{cases} 1 & k=0 \\ 2 & k \neq 0 \end{cases} \tag{10}$$

and

$$s_x^k = s_x + k \frac{\lambda}{i_x D_x} \tag{11}$$

with λ being the wavelength and $I_x^{(k)}$ being equal to $I_x^{(-k)}$.

Equation (9) is the current on the element located at $x=qD_x$. The expression includes the effect of "modulation" and scan at an angle as indicated by s_x and Figure 4. This expression gives the current for what might be considered one-dimensional modulation (along x) and scan in the x-y plane ($\alpha=0$, $-\pi<\eta<\pi$). Equation (9) merits careful examination, since the one-dimensional case will be simpler to analyze, but also because the two-dimensional case follows naturally from an understanding of the one-dimensional case.

Equation (9) is a Fourier Series with the $I_x^{(k)}$ being the Fourier Coefficients. They can be calculated in such a way as to give a shape similar to that of Figure 2, that is finite apertures with cosine or some other shaped distributions between the areas of zero current. An example of calculating the coefficients is given below and in Figure 5. More examples are given in Appendix D.

Arbitrary location of the z-axis at the center of one of the finite apertures allows exploitation of even Fourier Series expansion. The appropriate form of the series is,

$$f_s(x) = \sum_{n=0}^{\infty} a_n \cos\left(\frac{n\pi x}{\frac{T}{2}}\right) \tag{12}$$

where

$$a_0 = \frac{2}{T} \int_0^{\frac{T}{2}} f(x)dx \tag{13}$$

$$a_n = \frac{4}{T} \int_0^{\frac{T}{2}} f(x) \cos\left(\frac{n\pi x}{\frac{T}{2}}\right) dx, \quad n\neq 0 \tag{14}$$

For the example of Figure 5

$$\frac{T}{2} = \frac{i_x}{2} \tag{15}$$

$$a_0 = \frac{2K_x}{i_x\pi} \tag{16}$$

$$a_n = \frac{2K_x}{i_x\pi}\left[\frac{\sin\frac{\pi}{2}\left(\frac{i_x-2nK_x}{i_x}\right)}{\left(\frac{i_x-2nK_x}{i_x}\right)} + \frac{\sin\frac{\pi}{2}\left(\frac{i_x+2nK_x}{i_x}\right)}{\left(\frac{i_x+2nK_x}{i_x}\right)}\right] \tag{17}$$

Equation (9) gives the desired current magnitude at a given element. As would be expected, the k=0 term,

$$I_o = I_x^{(0)} e^{-j\beta q D_x s_x} \tag{18}$$

is exactly the same as the value in Equation (5). For broadside scan, Figure 4 and Equation (2) reveal s_x to be zero, so the zeroth term of Equation (9) is

$$I_o = I_x^{(0)} \tag{19}$$

the k = 1 term is

$$I_1 = \frac{1}{2} I_x^{(1)} e^{-j\beta q D_x \frac{\lambda}{i_x D_x}} \tag{20}$$

and the pth term is

$$I_p = \frac{1}{2} I_x^{(p)} e^{-j\beta q D_x p \frac{\lambda}{i_x D_x}} \tag{21}$$

This examination reveals that each Fourier Series term represents the current for a distinct scan angle, with the magnitude of the particular current weighted by the appropriate Fourier Coefficient. Figure 6 represents this idea for broadside scan ($s_x = 0$) and Figure 7 gives this representation for a 10 degree scan. The lengths of each of these arrows correspond to their particular Fourier Coefficient, and their angular separation is specified by λ and i_x in Equation (11). In summation, Equation (9) is interpreted as the linear superposition of currents for an infinite number of scan angles in real and imaginary space with weights determined by the Fourier Coefficients of the desired shape and size of periodically spaced finite apertures.

2. Two-dimensional case

It is now appropriate to consider the two-dimensional case. Modulating the current in the z-direction yields periodically spaced two-dimensional finite apertures surrounded by areas of zero current, as shown in Figure 8. The shape of the distribution in the apertures is arbitrary, with the condition it be expressable as a function of x times a function of z. This constraint allows the expression for the current to be separable in x and z. An added benefit is independent calculations of the x and z Fourier coefficients.

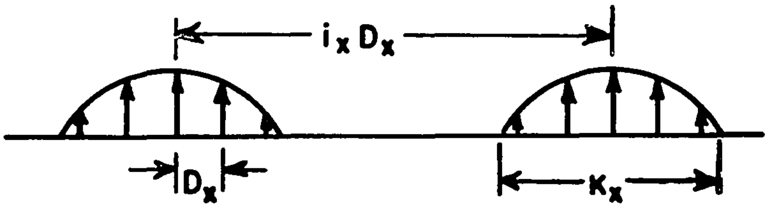

Figure 5. Parameters used in calculating the Fourier coefficients on a modulated arrow of dipoles.

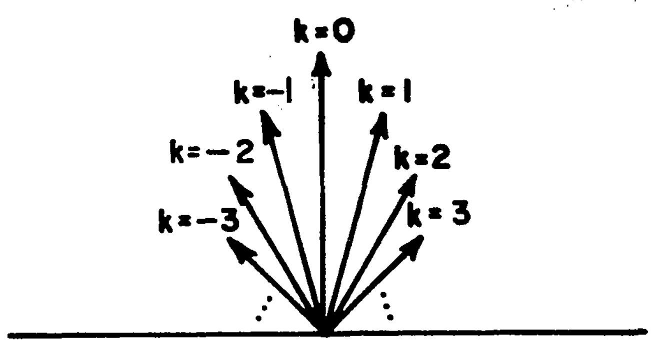

Figure 6. Representation of each term in the Fourier sum as a scan in a particular direction with the length of the arrow being the value of the Fourier coefficient, broadside scan.

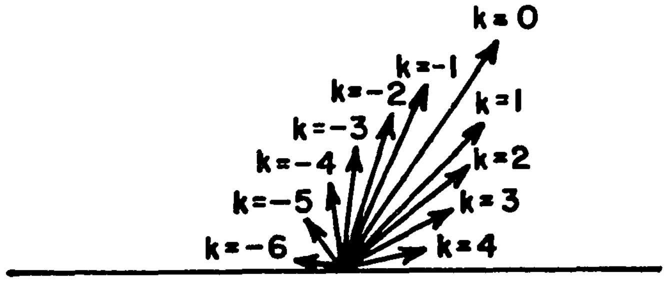

Figure 7. Representation of each term in the Fourier sum as a scan in a particular direction with the length of the array being the value of the Fourier coefficient, broadside scan.

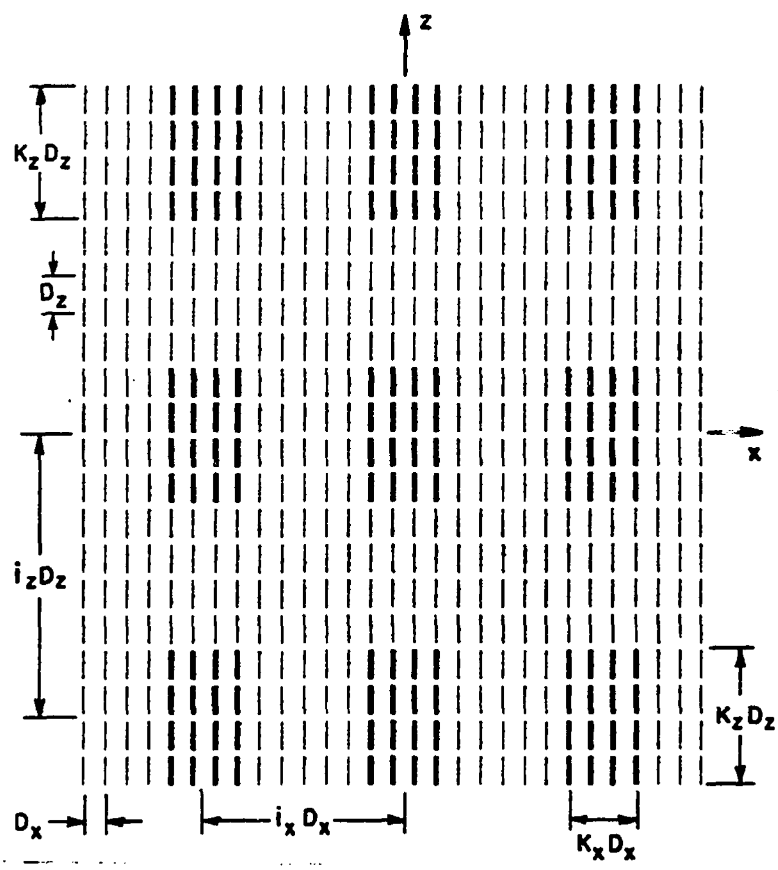

Figure 8. Top view of an infinite number of periodically spaced finite apertures in the x-z plane.

As Equation (9) evolved from Equation (5) for the one-dimensional case, an expression for the two-dimensional current can be derived from Equation (1)

$$I_{q,m} = I\, e^{-j\beta qD_x s_x}\, e^{-j\beta mD_z s_z} \tag{1}$$

Direct analogy to the x-modulated current yields for a z-modulated current along the z-axis.

$$I\big|_{z=mD_z} = \sum_{n=-\infty}^{\infty} \frac{1}{\varepsilon_n} I_z^{(n)}\, e^{-j\beta mD_z s_z^n} \tag{22}$$

$$s_z^n = s_z + n\frac{\lambda}{i_z D_z} \tag{23}$$

where i_z is the spacing between finite array centers as shown in Figure 8. Since we will require expressions for the current to be separable in x and z we can rewrite Equation (1) as

$$I_{q,m} = (I_x\, e^{-j\beta qD_x s_x})\,(I_z e^{-j\beta mD_z s_z}) \tag{24}$$

Substituting Equations (22) and (9) into (24) yields

$$I_{q,m} = \left(\sum_{k=-\infty}^{\infty} \frac{1}{\varepsilon_k}\; I_k^{(k)}\; e^{-j\beta qD_x s_x^k}\right)\left(\sum_{n=-\infty}^{\infty} \frac{1}{\varepsilon_n} I_z^{(n)}\; e^{-j\beta mD_z s_z^n}\right) \tag{25}$$

or, after rearranging and reindexing,

$$I_{q,m} = \sum_{\nu=-\infty}^{\infty} \sum_{\mu=-\infty}^{\infty} \frac{I_x^{(\nu)} I_z^{(\nu)}}{\varepsilon_\nu \varepsilon_\mu}\; e^{-j\beta qD_x s_x^\nu}\; e^{-j\beta mD_z s_z^\mu} \tag{26}$$

The physical interpretation of the two-dimensional modulated current of Equation (26) is analogous to the discussion of the one-dimensional case. Each term of (26) for a given ν and μ corresponds to a scan in a certain direction in real or imaginary space, weighted by the Fourier Coefficients $I_x^{(\nu)}$ and $I_z^{(\mu)}$ which depend on desired aperture shape and are calculated using the techniques in Appendix D. The $\nu=\mu=0$ term is in the direction which we are actually scanning. No simple drawing of the rays can be made as in Figure 7 because the rays are no longer confined to a single plane. Instead, rays fanning out in all directions must be imagined, with their angular separations specified by λ, i_x, and i_z as seen in Equations (11) and (23). Again, the total current specified by Equation (26) is merely the linear superposition of an infinite number of currents, each of which corresponds to scan in a certain direction of real or imaginary space.

As the last step in the development of the current, Equation (26) will be adapted to Hertzian dipoles of length $d\ell$ and orientation $\hat{p}^{(1)}$. The current on the Hertzian dipole located at $x=qD_x$, $z=mD_z$ is

$$\bar{I}^{(1)}_{q,m} = \hat{p}^{(1)} \sum_{\nu=-\infty}^{\infty} \sum_{\mu=-\infty}^{\infty} d\ell \, \frac{I_x^{(\nu)} I_x^{(\mu)}}{\varepsilon_\nu \varepsilon_\mu} \, e^{-j\beta q D_x s_x^\nu} \, e^{-j\beta m D_z s_z^\mu} \tag{27}$$

The superscript (1) in Equation (27) anticipates the presence of a test dipole which will be employed below in calculating individual element impedances.

C. The Electric Field

The goal of this section is to obtain a workable expression for the electric field. As a first step, an expression for the vector potential, $\bar{A}$, of the infinite array of Hertzian dipoles will be given. With future applications in mind, however, the vector potential will be shaped into a more useful form. The electric or magnetic field can then be calculated using the vector potential and classical identities. Only an explanation will be given here. The step by step derivation which parallels Reference [27] is given in Appendix A.

From the total vector potential summed over all the elements is (with μ_c being the permeability, as opposed to the index of summation μ)

$$d\bar{A}^{(1)} = \frac{\hat{p}^{(1)}\mu_c}{4\pi} \sum_{\nu=-\infty}^{\infty} \sum_{\mu=-\infty}^{\infty} \frac{I_x^{(\nu)} I_z^{(\mu)} \, d\ell}{\varepsilon_\nu \varepsilon_\mu} \sum_{q=-\infty}^{\infty} \sum_{m=-\infty}^{\infty} e^{-j\beta q D_x s_x^\nu} \, e^{-j\beta m D_z s_z^\mu} \times \frac{e^{-j\beta R_{qm}}}{R_{qm}} \tag{28}$$

where

$$R_{qm}^2 = a^2 + (mD_z - z)^2 \tag{29}$$

$$a^2 = y^2 + (qD_x - x)^2 \tag{30}$$

as shown in Figure 9. Equation (28) gives the vector potential as a summation of spherical waves. Transformation of (28) to a spectrum of plane waves is desirable for two reasons; 1) the double summation (currently over q and m) will converge faster, and 2) analysis of the presence of planar boundary conditions near the array using plane wave reflection coefficients will be expedited. This process which exploits the Poisson Sum Formula and two Fourier Transforms is shown in detail in Appendix A. The final form of the vector potential is

$$d\bar{A}^{(1)} = \hat{p}^{(1)} \sum_{\mu=-\infty}^{\infty} \sum_{\nu=-\infty}^{\infty} \frac{\mu_c I_x^{(\nu)} I_z^{(\mu)} d\ell}{2j\beta D_x D_z \varepsilon_\nu \varepsilon_\mu} \sum_{k=-\infty}^{\infty} \sum_{n=-\infty}^{\infty} \frac{e^{-j\beta \bar{R}\cdot\hat{r}_\pm}}{r_y} \tag{31}$$

where
$$\bar{R} = \hat{x}x + \hat{y}y + \hat{z}z \tag{32}$$

$$\hat{r}_\pm = \hat{x}r_x \pm \hat{y}r_y + \hat{z}r_z \qquad y \gtrless 0 \tag{33}$$

$$r_x = \left(s_x^\nu + k\frac{\lambda}{D_x}\right) = \left(s_x + k\frac{\lambda}{D_x} + \nu\frac{\lambda}{i_x D_x}\right) \tag{34}$$

$$r_z = \left(s_z^\mu + n\frac{\lambda}{D_z}\right) = \left(s_z + n\frac{\lambda}{D_z} + \mu\frac{\lambda}{i_z D_z}\right) \tag{35}$$

$$r_y = \sqrt{1 - r_x^2 - r_z^2} \tag{36}$$

Equation (31) is the desired form. It is a spectrum of plane waves, or in fact, a double infinite sum of spectra of plane waves.

The electric field is obtained using [28]

$$\bar{H} = \frac{1}{\mu_c}\nabla\mathrm{x}\,\bar{A} \tag{37}$$

and

$$\bar{E} = \frac{1}{j\omega\varepsilon_c}\nabla\mathrm{x}\,\bar{H} \tag{38}$$

giving

$$d\bar{E}^{(1)}(\bar{R}) = \sum_{\nu=-\infty}^{\infty} \sum_{\mu=-\infty}^{\infty} \frac{I_x^{(\nu)} I_z^{(\mu)} d\ell Z_c}{2D_x D_z \varepsilon_\nu \varepsilon_\mu} \sum_{k=-\infty}^{\infty} \sum_{n=-\infty}^{\infty} \frac{e^{j\beta\bar{R}\cdot\hat{r}_\pm}}{r_y} (\hat{p}^{(1)} \times \hat{r}_\pm) \times \hat{r}_\pm \tag{39}$$

where

$$Z_c = \sqrt{\frac{\mu_c}{\varepsilon_c}} \tag{40}$$

Examination of (39) reveals a spectrum of plane waves propagating in the direction $\hat{r}_\pm$ for each value of ν and μ. If r_y is real, the corresponding plane wave will propagate away from the plane of the array with no attenuation. In general, propagation occurs only for the k=n=0 term. Equations (34) through (36) reveal many more cases of r_y being pure imaginary (it must be pure real or pure imaginary). This phenomenon reveals most of the waves in the plane wave spectra to be evanescent, attenuating as their distance to the $y=0$ plane increases. The effect of modulating the current in the expression for the electric field is similar to the effect in the current. For any particular ν and μ there is a non-attenuating mode ($k=n=0$) and an infinite number of evanescent modes. To picture this physically, it is helpful to go back to the one-dimensional example of Figure 7 redrawn as Figure 10. Each arrow now represents the $k=n=0$ non-attenuating mode for different values of ν (with $\mu=0$). Each arrow in the drawing can be thought to have an infinite number of invisible arrows associated with it corresponding to the evanescent modes associated with each non-attenuating mode. Figure 10 depicts only the $\mu=0$ terms. There could be a similar drawing for each value of μ. Only the $\nu=\mu=k=n=0$ term will propagate in the direction in which the beam is being scanned. All modes will have effect in the near field of the array. They will affect array performance either through mutual impedance or through interaction with boundary conditions such as dielectric interfaces, ground planes, or other arrays which may or may not be present in the near field. So the physical interpretation made with the current still holds. The electric field as given by Equation (39) is a linear superposition of the fields which would exist as a result of scanning in the directions indicated by s_x^ν and s_z^μ in Equations (23) and (11).

Equations (34) through (36) reveal the possibility of r_y being real even if it is not the case that $k=n=0$. For these rare occurances the resulting non-attenuating mode can be considered to be contributing to grating lobes. Because the existence of grating lobes is dependant upon the interelement spacings D_x and D_z, keeping these distances small made grating lobes unlikely. In the cases found during the course of this study where this phenomenon occured, ν or μ was large. For these cases the corresponding Fourier Coefficent was sufficiently small as to make this term's effect negligible.

As Figure 9 indicates, Equation (39) is valid for the reference element being located at the origin. It is now desirable to allow the position of the reference element to be arbitrary. For the purpose of illustration, rewrite Equation (39) with the following shorthand notation; the current on the element being $I^{(0)}d\ell$, and the dependence upon field point position being $f[\overline{R}\cdot\hat{r}]$. Equation (39) now looks like

$$d\overline{E}^{(1)}(\overline{R}) = I^{(0)}d\ell\ f[\overline{R}\cdot\hat{r}] \tag{41}$$

This situation with reference element at the origin is depicted in Figure 11. This figure also shows the vector $\overline{R}'$ to which we want to move the reference element and calculate $d\overline{E}(\overline{R})$. Figure 12 shows a situation identical to this new one, where the element remains at the origin and the field point is moved to $(\overline{R}-\overline{R}')$. This yields

$$d\overline{E}^{(1)}(\overline{R}-\overline{R}') = I^{(0)}\ d\ell\ f[(\overline{R}-\overline{R}')\cdot\hat{r}] \tag{42}$$

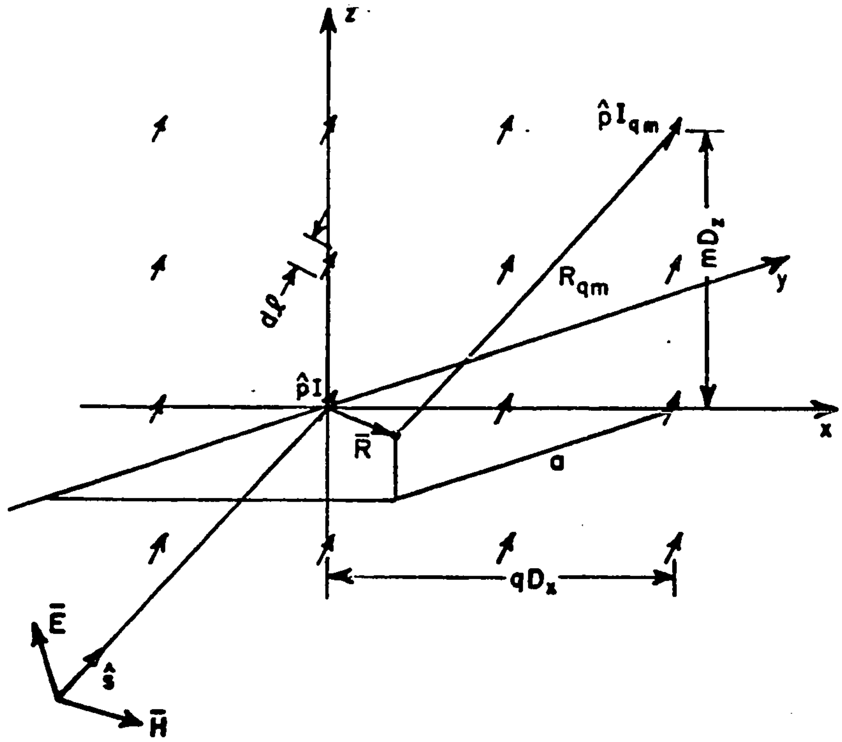

Figure 9. The field point $\bar{R}$ and an array of periodically spaced Hertzian dipoles in the x-z plane.

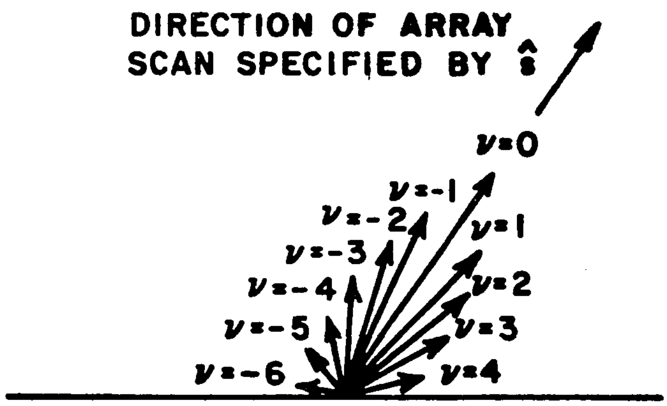

Figure 10. Representation of the propagating modes for different values of ν. Each arrow has an infinite spectrum of attenuating modes associated with it.

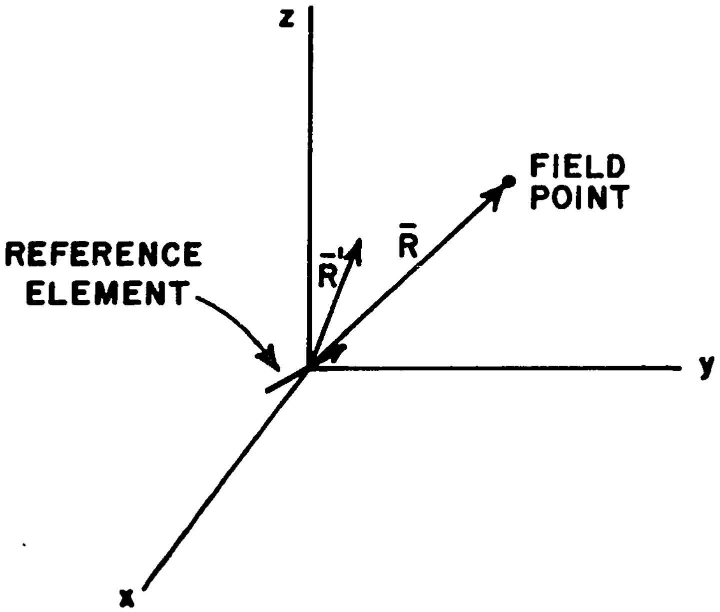

Figure 11. The field point $\overline{R}$, the reference element, and the position to which it is desired to move the reference element, $\overline{R}'$.

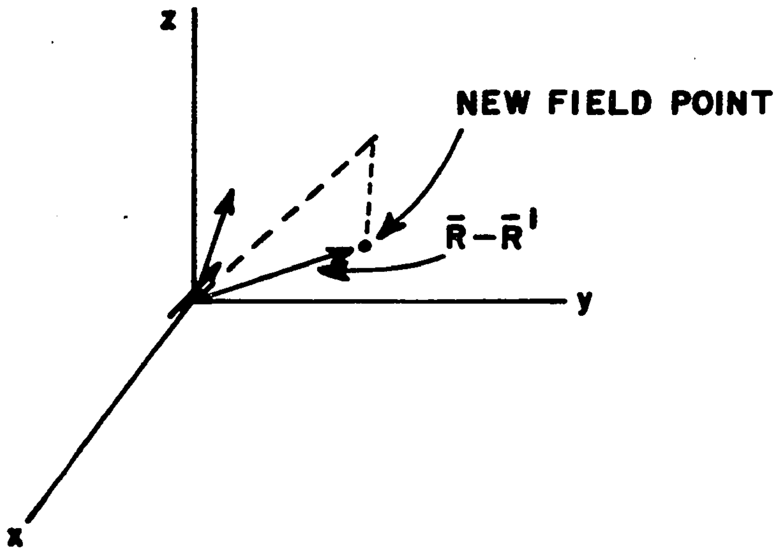

Figure 12. Displacement of the field point to $\overline{R}$-$\overline{R}'$, with the element at the origin.

As the $d\ell$ in Equation (42) indicates, the current is integrated over some finite element geometry. This integration is independent of the element's position. If the currrent situated at $\overline{R}'$ is called $I'd\ell$, the situation of Figure 13 is exactly equivalent to Figure 12 and the field of Figure 13 becomes

$$d\overline{E}^{(1)}(\overline{R}) = I'\ d\ell\ f\ [(\overline{R}-\overline{R}') \cdot \hat{r}] \tag{43}$$

Extrapolating back to Equation (39) and separating the new dependence upon $\overline{R}'$,

$$d\overline{E}^{(1)}(\overline{R}) = \sum_{\nu=-\infty}^{\infty} \sum_{\mu=-\infty}^{\infty} \frac{I_x'^{(\nu)} I_z'^{(\mu)} d\ell\ Z_c}{2D_x D_z \varepsilon_\nu \varepsilon_\mu} \sum_{k=-\infty}^{\infty} \sum_{n=-\infty}^{\infty} \frac{e^{-j\beta\overline{R}\cdot\hat{r}}}{r_y}\ \overline{e}^{(1)}\ e^{j\beta\overline{R}'\cdot\hat{r}} \tag{44}$$

$\overline{e}^{(1)}$ is the field's vector direction given by

$$\overline{e}^{(1)} = (\hat{p}^{(1)} \times \hat{r}) \times \hat{r} \tag{45}$$

and the $\pm$ on $\hat{r}$ has been dropped for convenience.

To this point, all elements have been Hertzian dipoles and the expression for their current, $(I_x'^{(\nu)}\ I_z'^{(\mu)})$, has been just the magnitude at some point. To allow for a current distribution over the geometry of an element, the current will now be considered to be

$$L_x^{(\nu)} L_z^{(\mu)} I^{(1)}(\overline{R}') = I_x'^{(\nu)}\ I_z'^{(\mu)} \tag{46}$$

where $\overline{R}'$ is allowed to move over the geometry of the element with L_x and L_z being dimensionless Fourier Coefficients. Integrating over the extent of the element, the expression for the total electric field is obtained,

$$\overline{E}^{(1)}(\overline{R}) = \frac{Z_c}{2D_x D_z} \sum_{\nu=-\infty}^{\infty} \sum_{\mu=-\infty}^{\infty} \frac{L_x^{(\nu)} L_z^{(\mu)}}{\varepsilon_\nu \varepsilon_\mu} \sum_{k=-\infty}^{\infty} \sum_{n=-\infty}^{\infty} \frac{e^{j\beta\overline{R}\cdot\hat{r}}}{r_y}\ \overline{e}^{(1)}$$

$$\times \int_a^b I^{(1)}(\overline{R}') e^{j\beta\overline{R}'\cdot\hat{r}}\ d\ell \tag{47}$$

where $\overline{R}^{(1)}$ is considered a reference point on the element, $\hat{p}^{(1)}$ the vector direction of the element at a given point, and the extent of the element to be between a and b, then

$$\overline{R}' = \overline{R}^{(1)} + \hat{p}^{(1)}\ell,\ a<\ell<b \tag{48}$$

The final result of this chapter, the electric field, is written as

$$E^{(1)}(\overline{R}) = \frac{I^{(1)}(\overline{R}^{(1)})Z_c}{2D_xD_z} \sum_{\nu=-\infty}^{\infty} \sum_{\mu=-\infty}^{\infty} \frac{L_x^{(\nu)}L_z^{(\mu)}}{\varepsilon_\nu \varepsilon_\mu} \sum_{k=-\infty}^{\infty} \sum_{n=-\infty}^{\infty} \frac{e^{-j\beta(\overline{R}-\overline{R}^{(1)})\cdot\hat{r}}}{r_y}$$

$$x\ \overline{e}^{(1)}P^{(1)} \tag{49}$$

where

$$P^{(1)} = \frac{1}{I^{(1)}(\overline{R}^{(1)})} \int_a^b I^{(1)}(\ell)e^{j\beta\ell\hat{p}^{(1)}\cdot\hat{r}}\, d\ell \tag{50}$$

Equation (50) is recognized [29] as the normalized far field pattern of a single element without the $\sin\theta$ dependence which is included in $\overline{e}^{(1)}$ (θ is the angle between $\hat{p}^{(1)}$ and $\hat{r}$). Equation (49) is separated into what might be considered the field of the array times the element pattern factor. This interpretation is useful because subsequent changing of the element size or shape affects only the pattern factor $P^{(1)}$.

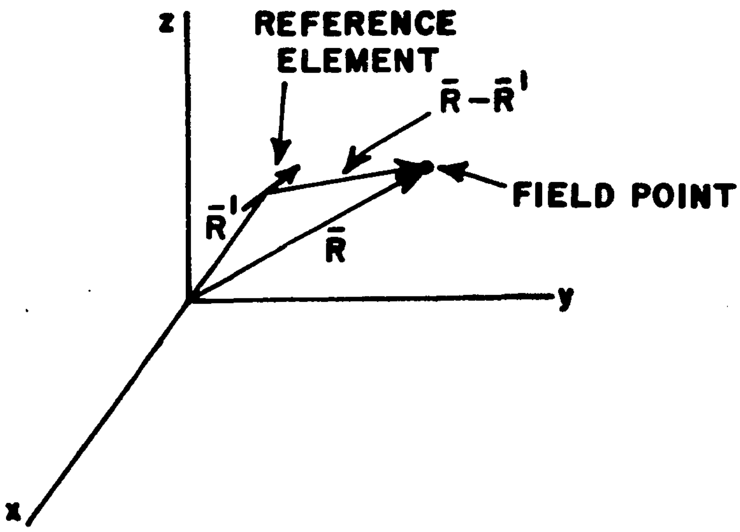

Figure 13. The element displaced to $\overline{R}'$, with the field point at $\overline{R}$. The difference between their positions is $\overline{R}$-$\overline{R}'$.

CHAPTER III

SELF-IMPEDANCE OF AN ARBITRARY ELEMENT

In order to calculate the self-impedance of any element in the array it is necessary to introduce a test dipole and find the voltage at its terminals due to the currents on the array. The self-impedance of an array element is then the ratio of the voltage on the test dipole to the current on the array element when the test dipole is one radius away. This process for the modulated dipole array in free space as well as the adaptation for the case of a slot array in a dielectric coated ground plane is given in this chapter.

A. Dipole Array in Free Space

Consider a linear dipole in free space with orientation $\hat{p}^{(2)}$ and current under transmitting conditions to be $I^{(2)}(\ell)$. According to Schellkunoff[30], when this dipole is exposed to the electric field $\overline{E}$, the voltage $v^{(2)}$ will be observed as the terminal located at $\overline{R}^{(2)}$ where

$$v^{(2)} = \frac{1}{I^{(2)}(\overline{R}^{(2)})} \int_{\text{element 2}} \overline{E} \cdot \hat{p}^{(2)} I^{(2)t}(\ell)\, d\ell \tag{51}$$

If $\overline{E}$ is a plane wave given by

$$\overline{E}(\overline{R}) = \overline{E}^{i}\, e^{-j\beta\overline{R}\cdot\hat{s}} \tag{52}$$

and $\overline{R}^{(2')}$ is the position vector for any point on the linear dipole where

$$\overline{R}^{(2')} = \overline{R}^{(2)} + \hat{p}^{(2)}\ell\ , \qquad a<\ell<b \tag{53}$$

then

$$v^{(2)}(\overline{R}^{(2)}) = \hat{p}^{(2)}\cdot\overline{E}(\overline{R}^{(2)})\ \frac{1}{I^{(2)t}(\overline{R}^{(2)})} \int_a^b I^{(2)t}(\ell) e^{-j\ell\hat{p}^{(2)}\cdot\hat{s}} d\ell \tag{54}$$

Rewriting Equation (54) as

$$v^{(2)}(\overline{R}^{(2)}) = \hat{p}^{(2)}\ \cdot\overline{E}(\overline{R}^{(2)})\ p^{(2)t} \tag{55}$$

where

$$p^{(2)t} = \frac{1}{I^{(2)}(\overline{R}^{(2)})} \int_a^b I^{(2)t}(\ell) e^{-j\beta\ell\hat{p}^{(2)}\cdot\hat{s}}\ d\ell \tag{56}$$

shows the voltage at the terminal of the test antenna to be equal to the incident field times the pattern of the test dipole under transmitting conditions, without the sin θ factor mentioned at the end of Chapter II. It is now appropriate to apply the field of the modulated array of Equation (49) as the incident field. Substituting (49) into (55) yields the voltage at the test dipole due to the current on the array as

$$V^{2,1} = \frac{I^{(1)}(\overline{R}^{(1)})Z_c}{2D_xD_z} \sum_{\nu=-\infty}^{\infty} \sum_{\mu=-\infty}^{\infty} \frac{L^x_\nu L^x_\mu}{\varepsilon_\nu \varepsilon_\mu} \sum_{k=-\infty}^{\infty} \sum_{n=-\infty}^{\infty} \frac{e^{-j\beta(\overline{R}^{(2)}-\overline{R}^{(1)})\cdot\hat{r}}}{r_y}$$

$$\times\, P^{(1)}P^{(2)}t_{\hat{p}}^{(2)} \cdot \overline{e}^{(1)} \tag{57}$$

Two steps are now required in the process of finding the self-impedance of the element in the array located at $x=qD_x$, $z=mD_z$. First, the magnitude of the current at that element must be divided into $V^{2,1}$. Second, the test dipole must be positioned one wire radius from the element in question. To take the first step, the expression of Equation (26) is used, with the definition of Equation (46) for the Fourier Coefficients. Additionally, it will be advantageous to separate those parts of the exponents which do not depend upon ν and μ.

$$I^{(1)}_{q,m}(\overline{R}^{(1)}) = I^{(1)}(\overline{R}^{(1)})\, e^{-j\beta qD_x s_x}\, e^{-j\beta mD_z s_z}$$

$$\times \sum_{\nu=-\infty}^{\infty} \sum_{\mu=-\infty}^{\infty} \frac{L^x L^z}{\varepsilon_\nu \varepsilon_\mu}\, e^{-j\beta qD_x \frac{\lambda}{i_x D_x}}\, e^{-j\beta mD_z \frac{\lambda}{i_z D_z}} \tag{58}$$

or

$$I^{(1)}_{q,m}(\overline{R}^{(1)}) = I^{(1)}(\overline{R}^{(1)})e^{-j\beta qD_x s_x}\, e^{-j\beta mD_z s_z}$$

$$\times \sum_{\nu=0}^{\infty} \sum_{\mu=0}^{\infty} L^x_\nu L^z_\mu \cos\left(2\pi\frac{q\nu}{i_x}\right)\cos\left(2\pi\frac{m\mu}{i_z}\right) \tag{59}$$

Examining the phase of equation (57) reveals some simplification. $\overline{R}^{(1)}$ is always the position of the reference element of the array. It is considered, without loss of generality, to be located at (x, y, z) = (0, b, 0). If "a" is the radius of dipoles in the array, then it is desired to have

$$\overline{R}^{(2)} = (qD_x, a+b, mD_z) \tag{60}$$

to find the self-impedance of the element located at $x=qD_x$, $z=mD_z$. The phase of Equation (57) becomes

$$e^{-j(\overline{R}^{(2)}-\overline{R}^{(1)})\cdot\hat{r}} = e^{-j\beta q D_x s_x} e^{-j\beta m D_z s_z} e^{-j\beta a r_y} \times e^{-j\,2\pi\frac{q\nu}{i_x}} e^{-j\frac{m\mu}{i_z}} \tag{61}$$

Dividing the current of Equation (58) into the voltage of (57) and taking into account (61) and the definition of mutual impedance yields the expression for the self-impedance of the element at $x=qD_x$, $z=mD_z$,

$$Z_{q,m} = -\frac{V^{2,1}}{I^{(1)}} = \frac{-Z_c}{2D_xD_z\left[\sum_{\nu=0}^{\infty} L_\nu^x\cos\left(2\pi\frac{q\nu}{i_x}\right)\right]\left[\sum_{\mu=0}^{\infty} L_\mu^z\cos\left(2\pi\frac{m\mu}{i_z}\right)\right]} \times$$

$$\times \sum_{\nu=-\infty}^{\infty}\sum_{\mu=-\infty}^{\infty} e^{-j2\pi\frac{q\nu}{i_x}} e^{-j2\pi\frac{m\mu}{i_z}} \frac{L_\nu^x L_\mu^z}{\varepsilon_\nu\varepsilon_\mu} \sum_{k=-\infty}^{\infty}\sum_{n=-\infty}^{\infty}\frac{e^{-j\beta a r_y}}{r_y}$$

$$\times\, P^{(1)}P^{(2)}\,\hat{p}^{(2)}\cdot\overline{e}^{(1)} \tag{62}$$

B. Dipole Array in a Dielectric Slab

Because the goal of this chapter is to apply Equation (62) to the geometry of either a dipole array in a dielectric slab or a slot array in a dielectric coated ground plane, it is now appropriate to introduce the geometry of Figure 14. The dipole array with reference element located at $\overline{R}^{(1)}$ is in medium 2 ($0<y<d_2$) which is between medium 1 ($y<0$) and medium 3 ($y>d_2$). The test element is also in medium 2 and for this study, the y component of $\overline{R}^{(2)}$ will be greater than the y component of $\overline{R}^{(1)}$. $\Gamma_{2,1}$ and $\Gamma_{2,3}$, as referred to on Figure 14 are plane wave reflection coefficients which will be defined.

In order to find the self-impedance of an array element in this geometry, it is necessary to first consider the form of the electric field. Returning to Equation (49), which is the field before the test dipole was introduced, and adapting it to medium 2 (as if medium 2 existed throughout all space) it becomes

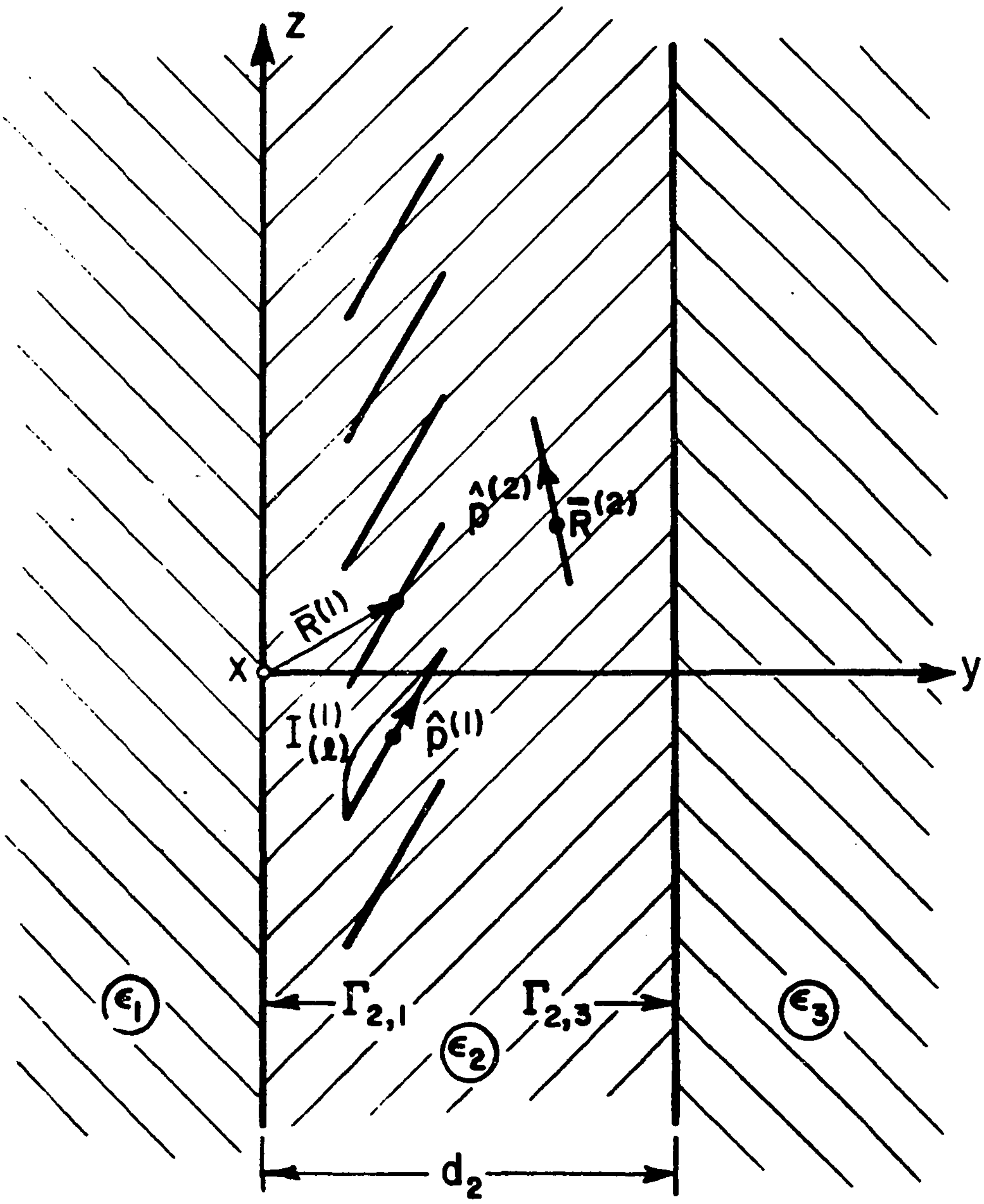

Figure 14. An infinite array of arbitrary elements located in a dielectric slab ε_2 sandwiched between two semi-infinite dielectric media ε_1 and ε_3.

$$\overline{E}^{(1)}(\overline{R}) = \frac{I^{(1)}(\overline{R}^{(1)})Z_2}{2D_xD_z} \sum_{\nu=-\infty}^{\infty} \sum_{\mu=-\infty}^{\infty} \frac{L_\nu^x L_\mu^z}{\varepsilon_\nu \varepsilon_\mu} \times$$

$$\times \sum_{k=-\infty}^{\infty} \sum_{n=-\infty}^{\infty} \frac{e^{-j\beta_2(\overline{R}-\overline{R}^{(1)})}}{r_{2y}} \overline{e}_2^{(1)} P_2^{(1)} \tag{63}$$

where

$$Z_2 = \sqrt{\frac{\mu_2}{\varepsilon_2}} \quad , \beta_2 = \frac{2\pi}{\lambda_2} \tag{64}$$

$$\hat{r}_2 = \hat{x}r_{2x} + \hat{y}r_{2y} + \hat{z}r_{2z} \tag{65}$$

$$r_{2x} = s_x + k\frac{\lambda_2}{D_x} + \nu\frac{\lambda_2}{i_xD_x} \tag{66}$$

$$r_{2z} = s_z + n\frac{\lambda_2}{D_z} + \mu\frac{\lambda_2}{i_zD_z} \tag{67}$$

$$r_{2y} = \sqrt{1 - r_{2x}^2 - r_{2z}^2} \tag{68}$$

$$\overline{e}_2^{(1)} = [\hat{p}^{(1)} \times \hat{r}_2] \times \hat{r}_2 \tag{69}$$

$$P_2^{(1)} = \frac{1}{I^{(1)}(\overline{R}^{(1)})} \int_{\text{element } 1} I^{(1)}(\ell) e^{-j\beta_2 \ell \hat{p}^{(2)} \cdot \hat{r}_2} d\ell \tag{70}$$

Introducing the interfaces at $y=0$ and $y=d_2$ requires significant alteration of the form of the electric field. Because the derivation of the new form is lengthy and available elsewhere [31], only the major steps will be outlined here.

As Figure 14 indicates, plane wave reflection coefficients will be exploited in treating the dielectric interfaces. The electric field of Equation (63) is a linear superposition of plane waves, each of which has a unique direction of propagation and polarization described by $\hat{r}_2$ and $\overline{e}_2^{(1)}$, respectively. To find the appropriate reflection coefficient for a given plane wave, it is necessary to define parallel and orthogonal reflection coefficients for the electric and magnetic fields. This is done in Appendix B in terms of the immittances of media 1 and 2. Since the terms parallel and orthogonal refer to the plane of incidence which is defined by the vector direction of propagation and the normal to the interface, the parallel and normal component of the electric and magnetic fields must be defined in terms of $\hat{r}_2$ of Equation (65), the wave polarization, and the normal to the interface in question. This is done in Appendix B of [32] which is not repeated here since it is an intermediate result. Equations which are given here relate $\hat{r}$ in two different media, such as medium a and medium b. They represent the generalized Snell's Law

$$\gamma_b r_{bx} = \gamma_a r_{ax} \tag{71}$$

$$\gamma_b r_{bz} = \gamma_a r_{az} \tag{72}$$

and for any medium c

$$r_{cy} = \sqrt{1 - r_{cx}^2 - r_{cz}^2} \tag{73}$$

Figure 15 depicts an important step in the process of calculating the field in region 2 when the dielectric interfaces at y=0 and $y=d_2$ are introduced. The waves emanating from the array element located at $y^{(1)}$ can reach the field point at y in four different "bounce" modes. After encountering the point at y, each ray "bounces" off of the dielectric interfaces an infinite number of times. The resulting mathematical expression for each of these modes is given on the right side of Figure 15. The term to the left represents the reflections and the phase delay before the wave reaches the field point at y for each mode. The term on the right represents the subsequent infinite number of bounces. This term was written as a geometric series and rewritten in fractional form. The derivation in [33] results in two transformation functions, one parallel and one orthogonal,

$$_{(\perp\,\parallel)}T_2(y^{(1)}, d_2 - y^{(2)}) =$$

$$\frac{[1 + {}_{(\perp\parallel)}{}^{E}\Gamma_{2,1}e^{-j2\beta_2 y^{(1)} r_{2y}}]\,[1 + {}_{(\perp\,\parallel)}{}^{E}\Gamma_{2,3}e^{-j2\beta_2(d_2 - y^{(2)})r_{2y}}]}{1 - {}_{(\perp\,\parallel)}{}^{E}\Gamma_{2,1}\,{}_{(\perp\,\parallel)}{}^{E}\Gamma_{2,3}e^{-j4\beta_2 d_2 r_{2y}}}$$

(74)

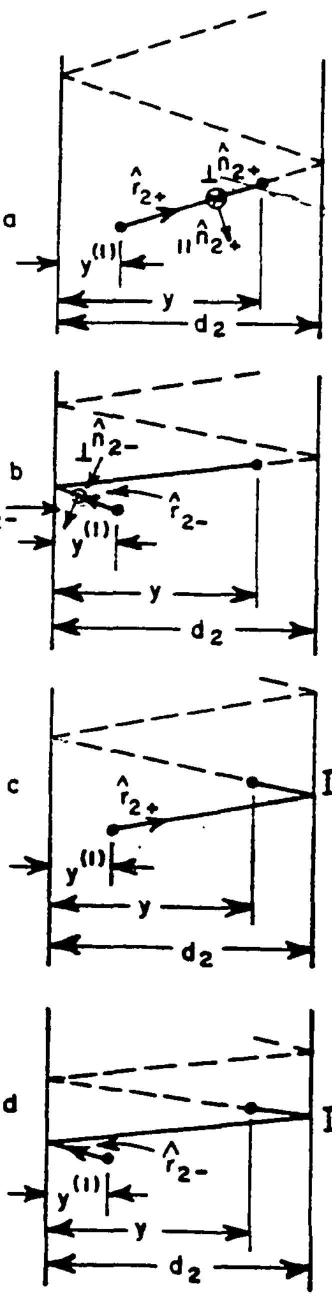

MODE a $\quad e^{-j\beta_2 (y-y^{(1)}) r_{2y}} \quad \dfrac{1}{1-\Gamma_{2,1}\Gamma_{2,3}{}^{-j2\beta_2 d_2 r_{2y}}}$

MODE b $\quad \Gamma_{2,1}\, e^{-j\beta_2 (y+y^{(1)}) r_{2y}} \quad \dfrac{1}{1-\Gamma_{2,1}\Gamma_{2,3}e^{-j2\beta_2 d_2 r_{2y}}}$

MODE c $\quad \Gamma_{2,3}\, e^{-j\beta_2 (2d_2 - y - y^{(1)}) r_{2y}} \quad \dfrac{1}{1-\Gamma_{2,1}\Gamma_{2,3}e^{-j2\beta_2 d_2 r_{2y}}}$

MODE d $\quad \Gamma_{2,1}\Gamma_{2,3}\, e^{-j\beta_2 (2d_2 - y + y^{(1)}) r_{2y}} \quad \dfrac{1}{1-\Gamma_{2,1}\Gamma_{2,3}e^{-j2\beta_2 d_2 r_{2y}}}$

Figure 15. The four different wave modes emanating from the array and being reflected from the two dielectric interfaces 2,1 and 2,3.

each of which treat the dielectric interfaces. These transformation functions along with the parallel and orthogonal components of the array and test dipole patterns, $_{(\perp\shortparallel)}P_2^{(2)t}$ and $_{(\perp\shortparallel)}P_2^{(1)}$, give the following expression for the voltage induced on the test element when the array and the test dipole are located inside medium 2 and all elements lie in a plane parallel to the x-z plane;

$$V^{2,1} = \frac{I^{(1)}(\overline{R}^{(1)})Z_2}{2D_xD_z} \sum_{\nu=-\infty}^{\infty} \sum_{\mu=-\infty}^{\infty} \frac{L_\nu^x L_\mu^z}{\varepsilon_\nu \varepsilon_\mu}$$

$$x \sum_{k=-\infty}^{\infty} \sum_{n=-\infty}^{\infty} \frac{e^{-j\beta_2(\overline{R}^{(2)}-\overline{R}^{(1)}) \cdot \hat{r}_2}}{r_{2y}}$$

$$x \left[{}_\perp P_2^{(2)t} \; {}_\perp P_2^{(1)} \; {}_\perp T_2(y^{(1)}, d_2 - y^{(2)}) \right.$$

$$\left. + {}_{\shortparallel} P_2^{(2)t} \; {}_{\shortparallel} P_2^{(1)} \; {}_{\shortparallel} T_2(y^{(1)}, d_2 - y^{(2)}) \right] \qquad (75)$$

The introduction of forcing all elements to be in a plane parallel to the x-z plane simplifies the expressions but it is also necessary in applying the relations to slots in a plane. Forcing the test element to be in a parallel plane does not imply that the element itself is parallel to an array element.

A new symbol, $\Omega_{k,n,\nu,\mu}$, is now introduced to represent the bracketed quantity in Equation (75). It is defined as

$$\Omega_{k,n,\nu,\mu} = \left[{}_\perp P_2^{(2)t} \; {}_\perp P_2^{(1)} \; {}_\perp T_2(y^{(1)}, d_2 - y^{(2)}) \right.$$

$$\left. + {}_{\shortparallel} P_2^{(2)t} \; {}_{\shortparallel} P_2^{(1)} \; {}_{\shortparallel} T_2(y^{(1)}, d_2 - y^{(2)}) \right] \qquad (76)$$

This new quantity, Ω, is extremely interesting. For each plane wave (i.e., for each value of ν, μ, k, n), there is a weight which depends upon the parallel and orthogonal components of the far field pattern factor of the test dipole under transmitting conditions, the far field pattern factor of an array element, and a transformation factor which depends upon geometry. Subsequent change in the geometry, such as changing the thickness of the dielectric layer, affects only the transformation factor. Similarly, changing the size or shape of the array element forces a change only in the pattern factor.

Finally, the self-impedance of an element in the array, situated in the geometry of Figure 14, can be written using Equations (62), (75), and (76) as

$$Z_{q,m} = \frac{Z_2}{2D_xD_z\left[\sum_{\nu=0}^{\infty} L_\nu^x \cos\left(2\pi \frac{q\nu}{l_x}\right)\right]\left[\sum_{\mu=0}^{\infty} L_\mu^z \cos\left(2\pi \frac{m\mu}{l_z}\right)\right]}$$

$$\times \sum_{\nu=-\infty}^{\infty} \sum_{\mu=-\infty}^{\infty} \frac{L_\nu^x L_\mu^z}{\varepsilon_\nu \varepsilon_\mu} e^{-j2\pi\frac{q\nu}{l_x}} e^{-j2\pi \frac{m\mu}{l_z}} \sum_{k=-\infty}^{\infty} \sum_{n=-\infty}^{\infty} \frac{e^{-j\beta_2 a r_{2y}}}{r_{2y}}$$

$$\times \Omega_{k,n,\nu,\mu} \tag{77}$$

Equation (77) is the self-impedance of the array element located at $x=qD_x$, $z=mD_z$ in a periodically modulated array of linear dipoles, located in region 2 of Figure 14.

C. Slot Array in a Dielectric Coated Ground Plane

Adapting Equation (77) to the geometry of a slot array in a dielectric coated ground plane is straightforward using well known techniques. Figure 16 shows the geometry. The slots are modeled as magnetic dipoles over a ground plane, so their admittance as slots is the quantity of interest. According to [34] the relationship between the impedance of the dipoles and the admittance of the slots is

$$Y_{q,m} = \frac{4}{Z_c^2} Z_{q,m} \tag{78}$$

where Z_c is the characteristic impedance of the medium. For Equation (77) $Z_c = Z_2$. Additionally, the magnetic dipole's being infinitesimally close to the ground plane corresponds to $y^{(1)}$ being zero in Figure 15 and in Equation (74) for the transformation factor. Using H field reflection coefficients in Equation (74) and unity for the coefficient at the interface between media 1 and 2 (as medium 1 is now a perfectly conducting ground plane), Equation (74) becomes

$$(\perp \, ^{\shortparallel}) T_2 = 2 \times \frac{1 + {}_{(\perp \, ^{\shortparallel})}{}^{H}\Gamma_{2,3}\, e^{-j2\beta_2 d_2 r_{2y}}}{1 - {}_{(\perp \, ^{\shortparallel})}{}^{H}\Gamma_{2,3}\, e^{-j2\beta_2 d_2 r_{2y}}} \tag{79}$$

The factor of two in Equation (79) occurs because of the perfectly conducting surface to the left and actually takes into consideration the doubling of the H field at this boundary. Of the factor of four in Equation (78), one factor of two is caused by the H field being doubled at the surface of a perfectly conducting ground plane. To

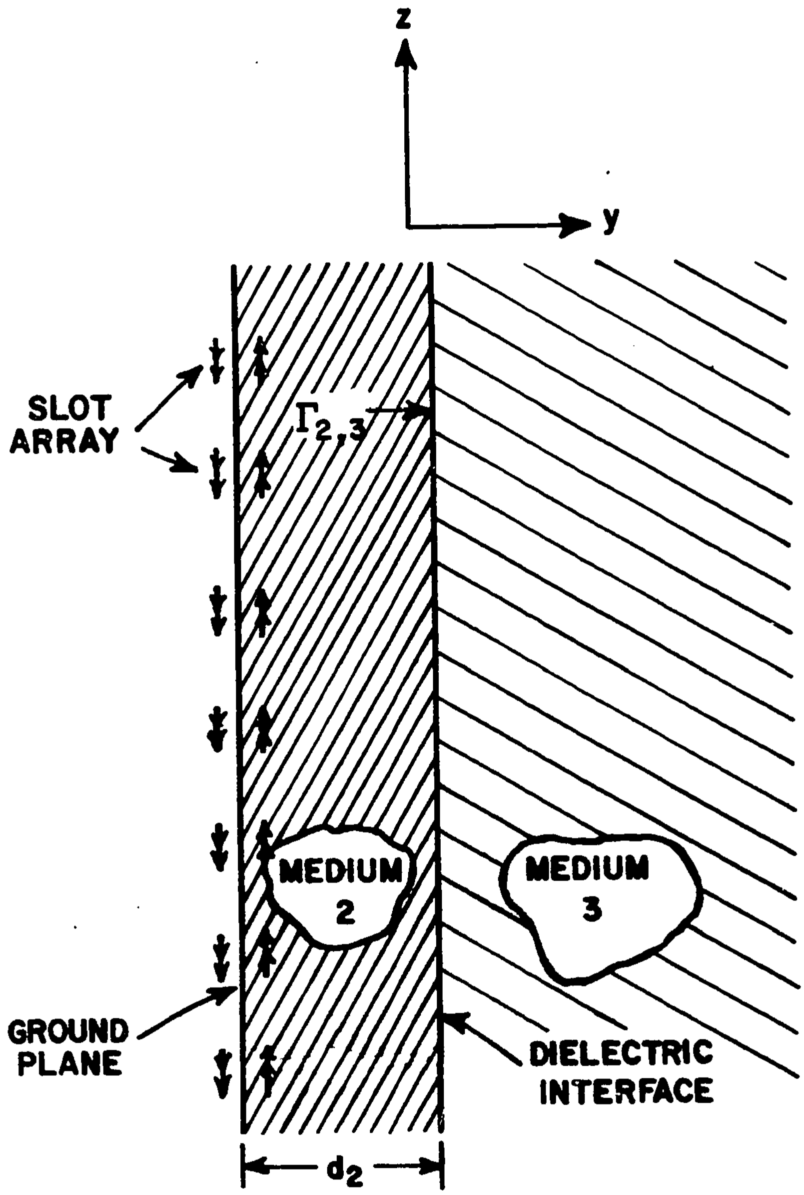

Figure 16. An infinite array of slots in a dielectric coated ground plane modeled as the complement of an infinite array of magnetic sources over a groundplane.

not duplicate this factor of two, it is best to consider the four in Equation (78) to be a two in this application. The expression for the admittance of the slot at $x=qD_x$, $z=mD_z$ looking to the right is

$$Y_{q,m} = \frac{Y_2}{2D_xD_z\left[\sum_{\nu=0}^{\infty} L_\nu^x \cos\left(2\pi \frac{q\nu}{l_x}\right)\right]\left[\sum_{\mu=0}^{\infty} L_\mu^z \cos\left(2\pi\frac{m\mu}{l_z}\right)\right]}$$

$$\sum_{\nu=-\infty}^{\infty} \sum_{\mu=-\infty}^{\infty} \frac{L_\nu^x L_\mu^z}{\varepsilon_\nu \varepsilon_\mu} e^{-j2\pi\frac{q\nu}{l_x}} e^{-j2\pi\frac{m\mu}{l_z}} \sum_k \sum_n \frac{e^{-j\beta_2 a r_{2y}}}{r_{2y}} \Omega_{k,n,\nu,\mu} \quad (80)$$

where $\Omega_{k,n,\nu,\mu}$ uses the transformation factor of Equation (79) and

$$Y_2 = \frac{1}{Z_2} = \sqrt{\frac{\varepsilon_2}{\mu_2}} \quad (81)$$

The total admittance is the sum of the admittances looking right and looking left.

CHAPTER IV
RESULTS

The results of this study take the form of admittance values of the elements of large finite arrays in various geometrical configurations and at several scan angles. The immittances were calculated using either Equation (77) or (80) with the aid of a digital computer. Because the programming of these equations is involved, Appendix G on programming considerations has been included as an intermediate between the theory and the computer code documentation. The results presented in this chapter take the form of computer generated plots of the input voltage and the resulting current and admittances at each element in an array of straight z-directed slots, or the input current with the resulting voltage and impedance at each z-directed dipole.

This chapter is divided into four sections. First, an explanation will be given of the form of the plots and the various parameters displayed. Results for the one-dimensional arrays are then given followed by the two-dimensional results. In the last section, various other topics are discussed.

A. Form of the Computer Generated Plots

The goal of this effort is to calculate and better understand the behavior of the immittances of large finite phased arrays. For the one-dimensional array, representing these immittances in plot form is a straightforward task. The input forcing function (current for dipoles or voltage for slots) and the resulting immittance (impedance or admittance) can be graphed on a plane. For a two-dimensional array, a three-dimensional representation of some sort is analogous. Because these three-dimensional plots seem to rely on interpretation, two-dimensional array data is plotted here using series of two-dimensional plots which are clearer in their depiction of the behavior of the immittances of the arrays. The text and figure titles will aid in clarifying the geometry being represented.

Figure 17 shows one format of displaying the results for a one-dimensional array (i.e., infinite in the z-direction and finite in the x-direction). There are 1049 elements in one modulation period which corresponds to i_x = 1049 (in the text) or IX = 1049 as shown on the plot. IZ as shown on the plot has no meaning here since there is no modulation in the x-direction in this example. There are 31

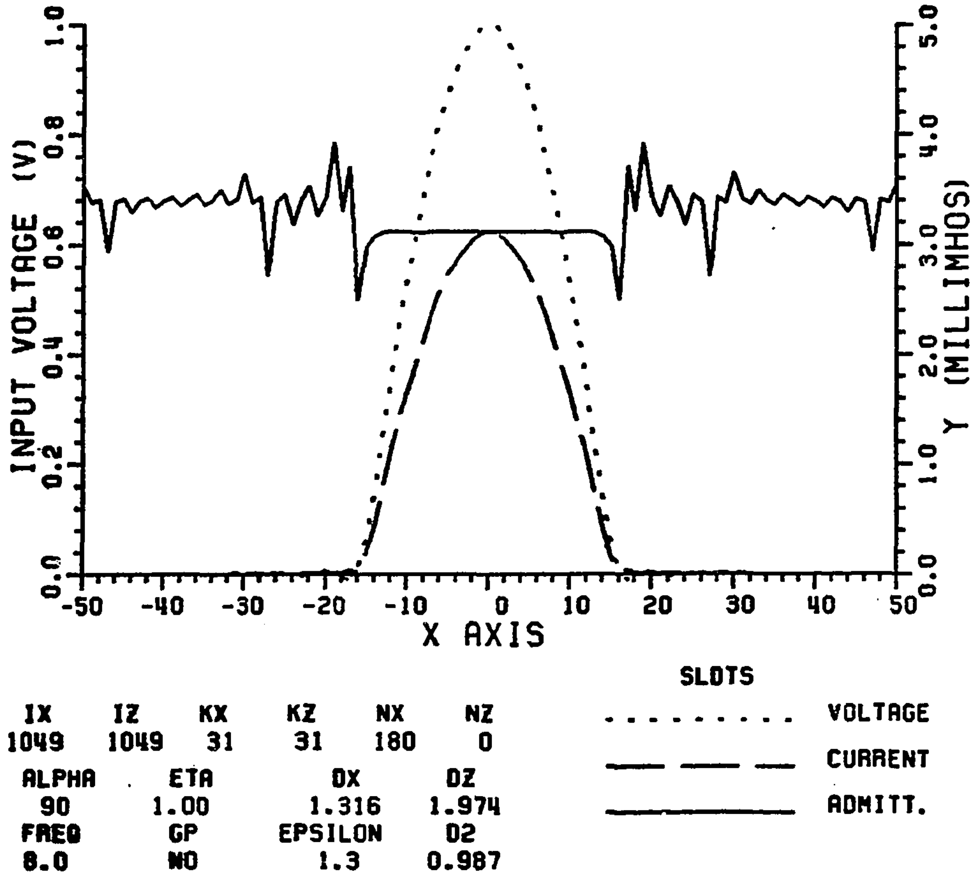

Figure 17. Example plot showing the input voltage along with the resulting current and admittance for a one-dimensional array of slots.

excited elements in the x-direction (k_x = KX = 31). Again, KZ is meaningless since there is no modulation in the z-direction. 180 Fourier terms were used along x (Nx=NX=180). NZ is given as zero since only the zero order (constant) term is used along z. Also listed on Figure 17 are the frequency in GHz, the scan angle in degrees (as defined in Figure 4), the interelement spacings Dx and Dz, and the possible presence of a ground plane to the left of the array is indicated with a "YES" or "NO" under "GP". The composition of the array, either dipoles or slots, is also given along with the relative dielectric constant of the medium surrounding the array and its thickness, d_2. The abscissa is element position along the x-axis. The model of the finite array with 31 elements extends from -15 to 15 along x. The dotted line is the voltage input at each slot with the values normalized to one volt as indicated by the ordinate on the left axis. The dashed line indicates the current at each element. The solid line is the resulting admittance at each slot with the values indicated by the ordinate at the right axis in mhos. To reduce clutter on the plot, the ordinate values of the current are not given. They can be simply calculated with knowledge of the voltage and admittance. The dipole results are given similarly.

Because the areas of zero excitation between the finite arrays are of little interest, plots of the form of Figure 18 are used in this study. The information content is the same as for Figure 17 except the area of excitation is enlarged for clarity. Additionally, the phase of the admittance or impedance has been added.

The plots of the two-dimensional arrays are given in the same format. Those plots represent only one row across the array where, in the one-dimensional case, any given plot applies to all rows. Plots along the z-direction can also be made for the two-dimensional case. They use z as the abscissa, rather than x.

Plots take one additional form in this chapter. Four plots appear on one page as in Figure 19. Each are of the form of the upper plot of Figure 18. Their parameters are identical except for their scan angles which are given. The plots are given in this form in order to ease comparison of the behavior of the immittances for several data sets.

Table I
Geometrical Parameters of the Arrays

Array	D1	D2	D3	S1	D4	S2
elements	dipoles	dipoles	dipoles	slots	dipoles	slots
#of dimensions	1	1	1	1	2	2
geometry	all free space	Fig. 39	Fig. 66	Fig. 16	Fig. 39	Fig. 16
d_2 (cm)	-	0.987	0.987	0.987	0.987	0.987
relative dielectric constant	1	1.3	1.3	1.3	1.3	1.3
element length (cm)	1.875	1.644	1.644	1.644	1.644	1.644
element width (cm)	0.1	0.0877	0.0877	0.0877	0.0877	0.0877
element thickness (cm)	0.01	0.00877	0.00877	0.00877*	0.00877	0.00877*
Dx (cm)	1.5	1.316	1.316	0.316	1.316	1.316
Dz (cm)	2.25	1.974	1.974	1.974	1.974	1.974

*Indicates thickness of ground plane containing slots.

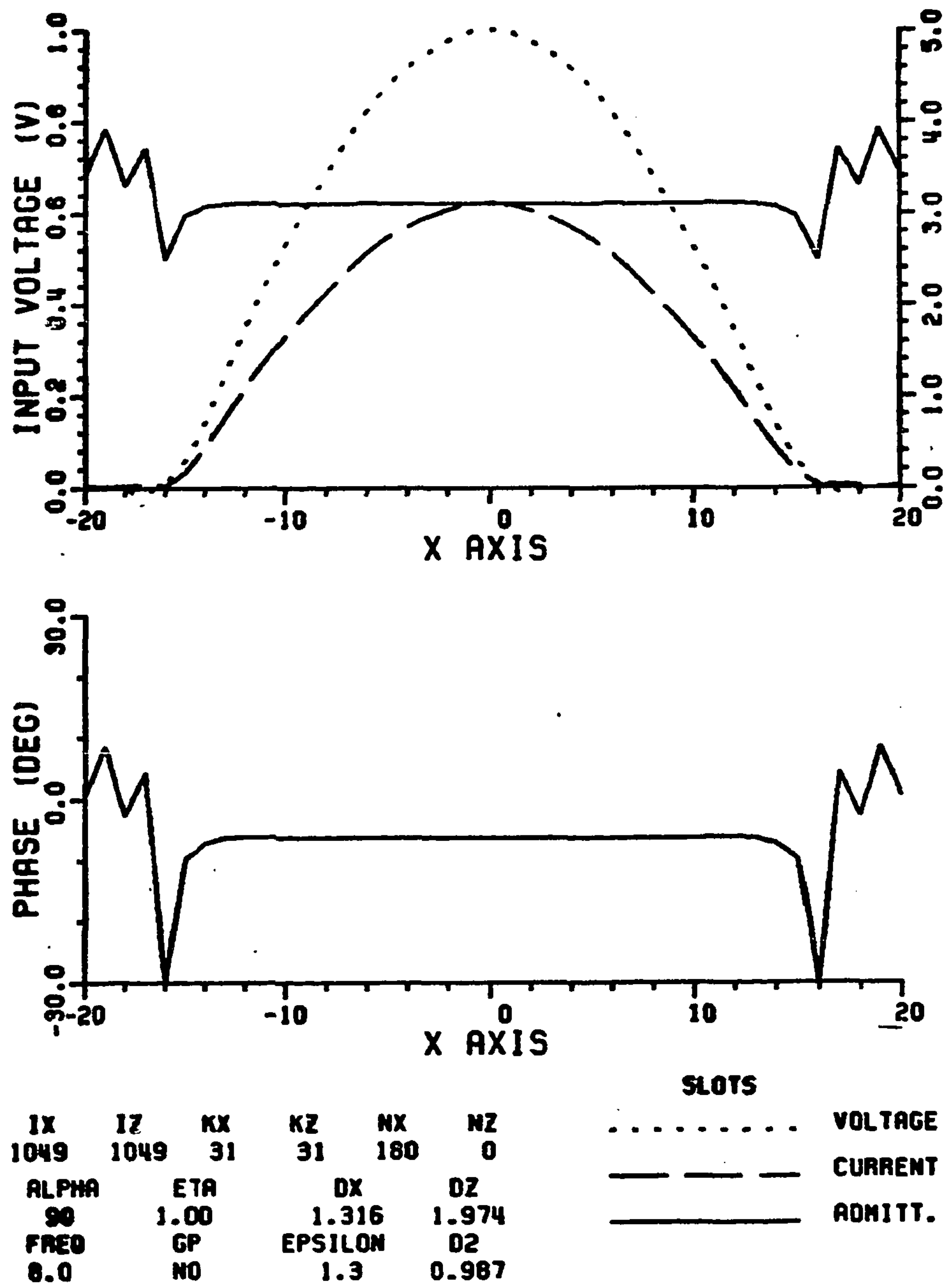

Figure 18. Example plot showing the expanded view of the voltage, current, and admittance with the addition of the phase of the admittance.

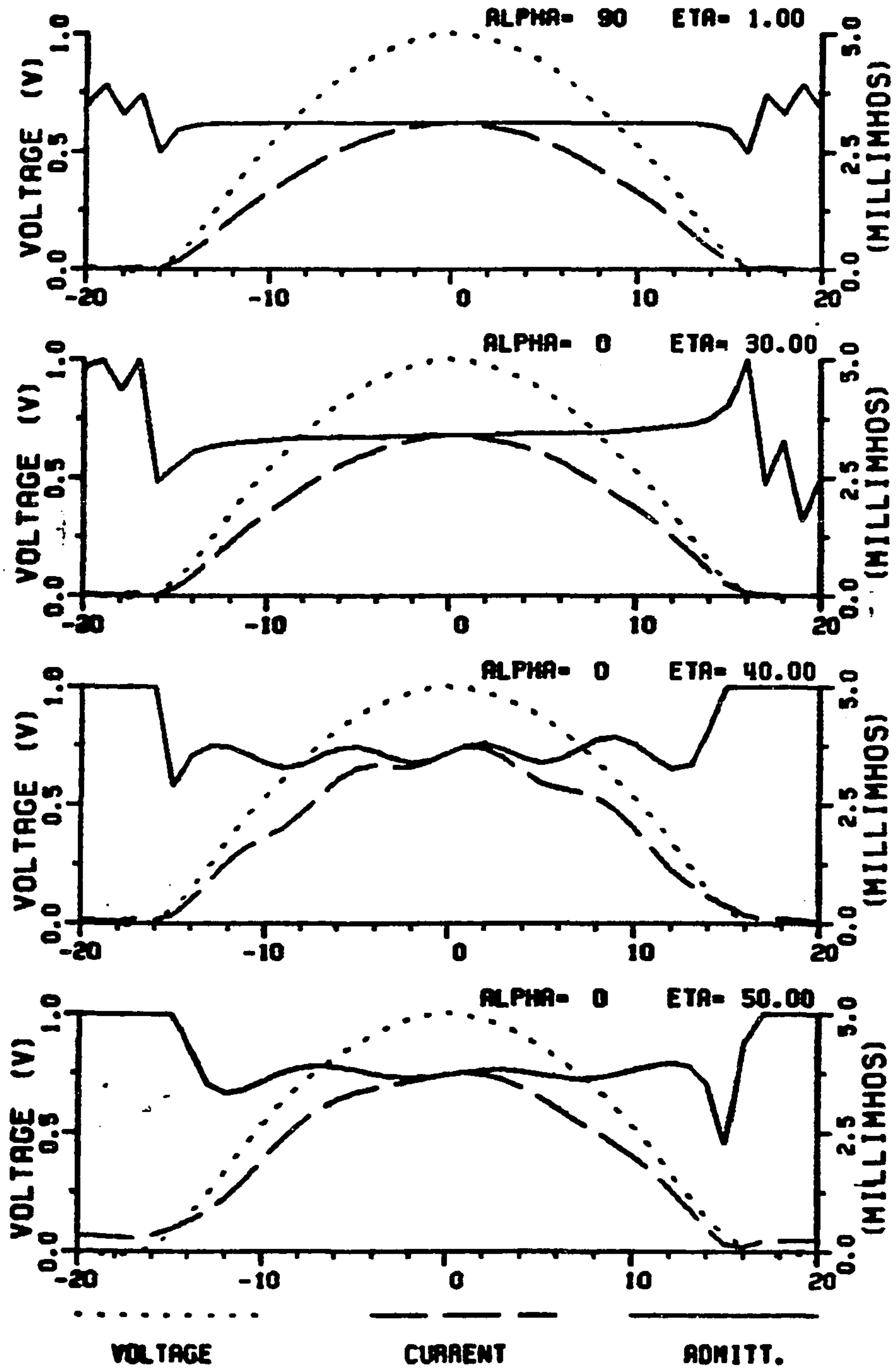

Figure 19. Example plot showing the voltage, current, and admittance for the slot array at four scan angles in the x-y plane. The scan angle is to the right in these plots.

B. One-dimensional Results

Figure 20 gives a representation of a typical one-dimensional array where the darker lines represent elements which have non-zero excitation and the lighter lines represent the areas of zero excitation between the models of the finite arrays. Dx and Dz are the interelement spacings and i_x is the period of modulation which is the distance between centers of the finite array models. Figure 20 shows only four elements excited in the x-direction with five non-excited elements between the finite array models. Arrays modeled in this study are larger, with 31 elements excited and with 318-1818 non-excited elements between the finite arrays (corresponding to i_x between 349 and 1849).

1. Dipole array in free space

The first array to be modeled, example D1, is composed of straight z-directed half-wave dipoles in free space with modulation in the x-direction (the direction of strongest coupling). Equation (77) is used to find the impedances with simplification for the one-dimentional case. To implement without modulation in the z-direction, only the constant $\mu = 0$ term is used along z. This leaves the expression for the impedance of the element located at x=qDx (there is no longer dependence upon m, position along z) as

$$Z_q = \frac{Z_2}{2D_xD_z \sum_{\nu=0}^{\infty} L_\nu^x \cos(2\pi \frac{q\nu}{i_x})} \times$$

$$\times \sum_{\nu=-\infty}^{\infty} \frac{L_\nu^x}{\varepsilon_\nu} e^{-j2\pi\frac{q\nu}{i_x}} \sum_{k=-\infty}^{\infty} \sum_{n=-\infty}^{\infty} \frac{e^{-j\beta_2 ar_{2y}}}{r_{2y}} \Omega_{k,n,\nu,0} \qquad (82)$$

Because the medium is free space, Ω of Equation (76) also simplifies. $(_{\perp \parallel})T$ becomes unity as there are no longer any dielectric interfaces to cause the bounce modes of Figure 15. For this example, medium 2 is free space and infinite in extent. As Appendix C on the pattern factor indicates, for the straight z-directed elements employed in this study, the transmitting pattern factor equals the non-transmitting pattern factor. This leaves

$$\Omega_{k,n,\nu,0} = \left[({}_\perp P_2^{(2)t})^2 + ({}_\parallel P_2^{(2)t})^2\right] \qquad (83)$$

The modeling of array D1 is done at 8 GHz (λ=3.75 cm) with dipoles of length 1.875 cm (0.5λ) and Dx and Dz 1.5 cm (0.4λ) and 2.25 cm (0.6λ), respectively. The modulation period (i_x) is 349 and 31 elements are excited in the x-direction. The flat dipoles modeled here have width 0.1 cm (.026667λ). Table I gives the geometrical parameters for all arrays discussed in this chapter. Figure 21 gives

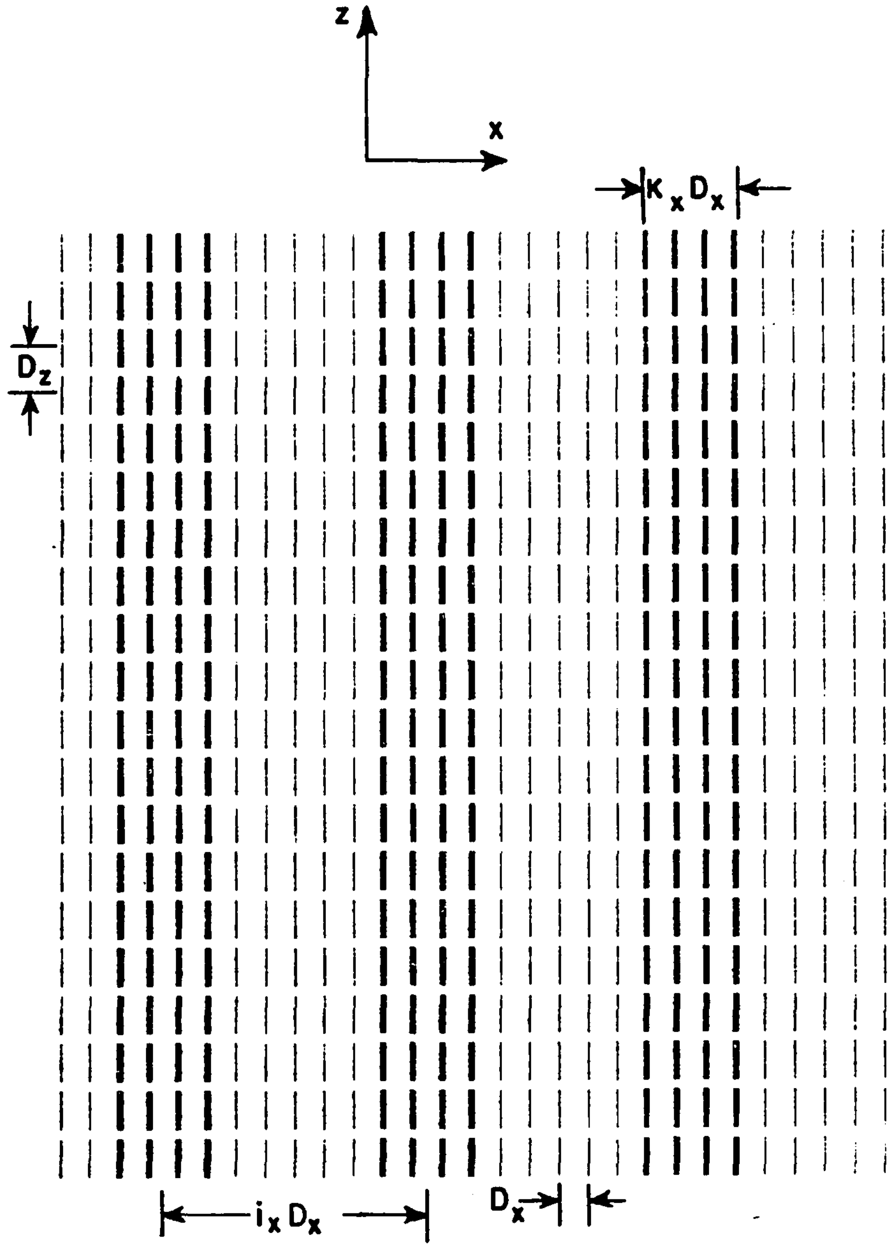

Figure 20. A view of the one-dimensional dipole array in the x-z plane. The darker lines represent the excited elements and the lighter lines represent the non-excited elements between the finite array models.

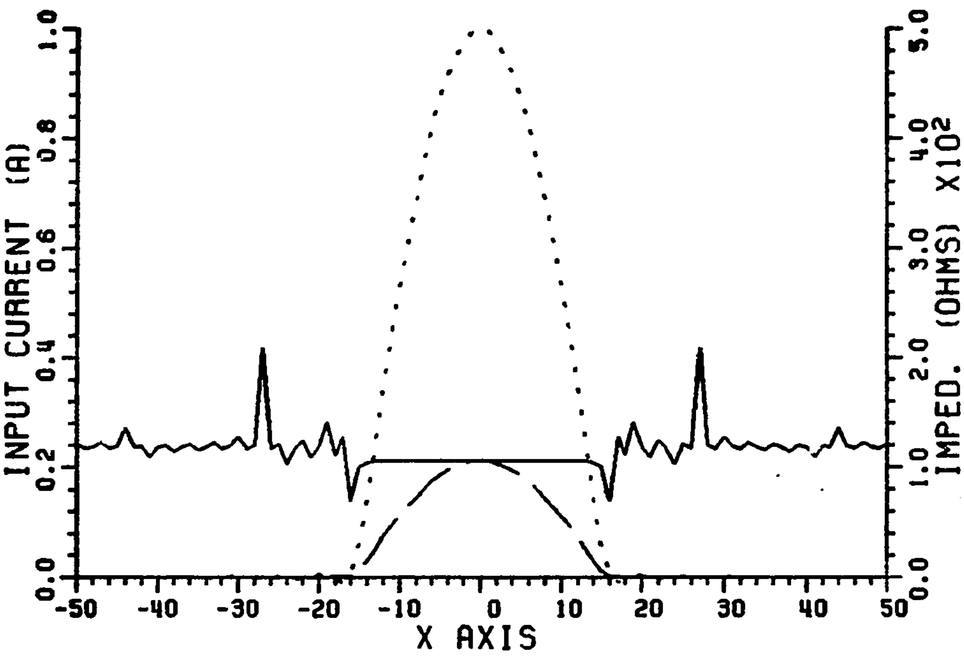

IX	IZ	KX	KZ	NX	NZ
349	349	31	31	60	0

ALPHA	ETA	DX	DZ
90	1.00	1.500	2.250
FREQ	GP	EPSILON	D2
8.0	NO	1.0	1.125

DIPOLES

. . . . CURRENT

— — — — VOLTAGE

———————— IMPED.

Figure 21. The impedance for array D1 at a broadside scan angle with a cosine distribution of the input current.

from q=-174 to q=+174. This plot displays only the points from -50 to +50. Those points omitted in the area of zero excitation have values similar to those shown in this area of Figure 21. The area of non-zero excitation is from -15 to +15 (i.e., Kx=31). The dotted line for the input current on the dipoles indicates the aperture has a cosine shaped distribution. The Fourier coefficients, L_ν^x of Equation (82), for this shape are given as Equations (D5) and (D6) of Appendix D. The dashed line gives the voltage induced at each element and the solid line indicates the resulting impedance. These results are for broadside scan. The figure indicates $\alpha=90^o$ and $\eta=1^o$ as defined in Figure 4, which is actually a 1^o scan in the y-z plane. This angle was used in order to avoid possible computer problems at true broadside but its results are nearly identical to those at broadside.

Figure 22 shows a plot of the relative magnitudes of the Fourier coefficients and the scan angles they correspond to for the geometrical parameters of array D1 with 60 Fourier terms when the finite array is scanned at broadside. While this study made no attempt to place a quantitative error on the effects of Fourier sum truncation, it is readily seen from the figures that the tapered distributions used here contain sufficient terms to give an accurate representation of immittance effects. One non-tapered distribution, a trapezoidal distribution, will be encountered below and a similar plot will be given then.

Figure 23 gives an enlarged view of array D1 at broadside scan as in Figure 21, with the addition of the phase of the impedance. It is easier to see the nearly constant value of the impedance (106 ohms) across the aperture of the finite array. For this broadside scan angle, only the two edge elements depart from this value, going down to around 95 ohms. The phase of the impedance is also nearly constant (9^o). The slight inductive nature of the half-wave dipoles is due to the addition of an incremental length to the dipoles in the computer model, to account for effects near the ends of flat dipoles with finite width and thickness. This procedure is well documented [38]. The incremental change in length affects the shape of the current which in turn affects the pattern factor $_{(1'')}P^{(2)t}$ of Equation (83)). A further discussion of this correction is included in Appendix C.

Figure 24 gives results for array D1 scanned in the x-y plane. The initial broadside angle of Figure 23 is repeated, followed by 30^o, 40^o, and 50^o scans. The symmetry about the center of the array is gone and the impedance values are no longer constant across the aperture. Figure 25 shows the enlarged plot for the 60^o scan with a new scale on the phase plot. A new phenomenon occurs here which is not present at the smaller scan angles. For previous scans, the

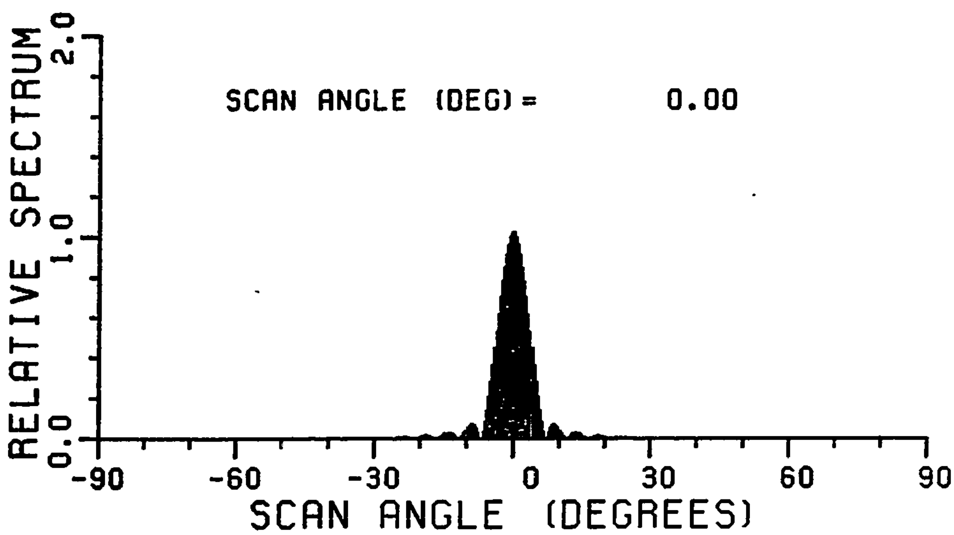

Figure 22. The spectrum of the finite array as a function of scan angle for the cosine aperture scanned at broadside with 60 Fourier terms.

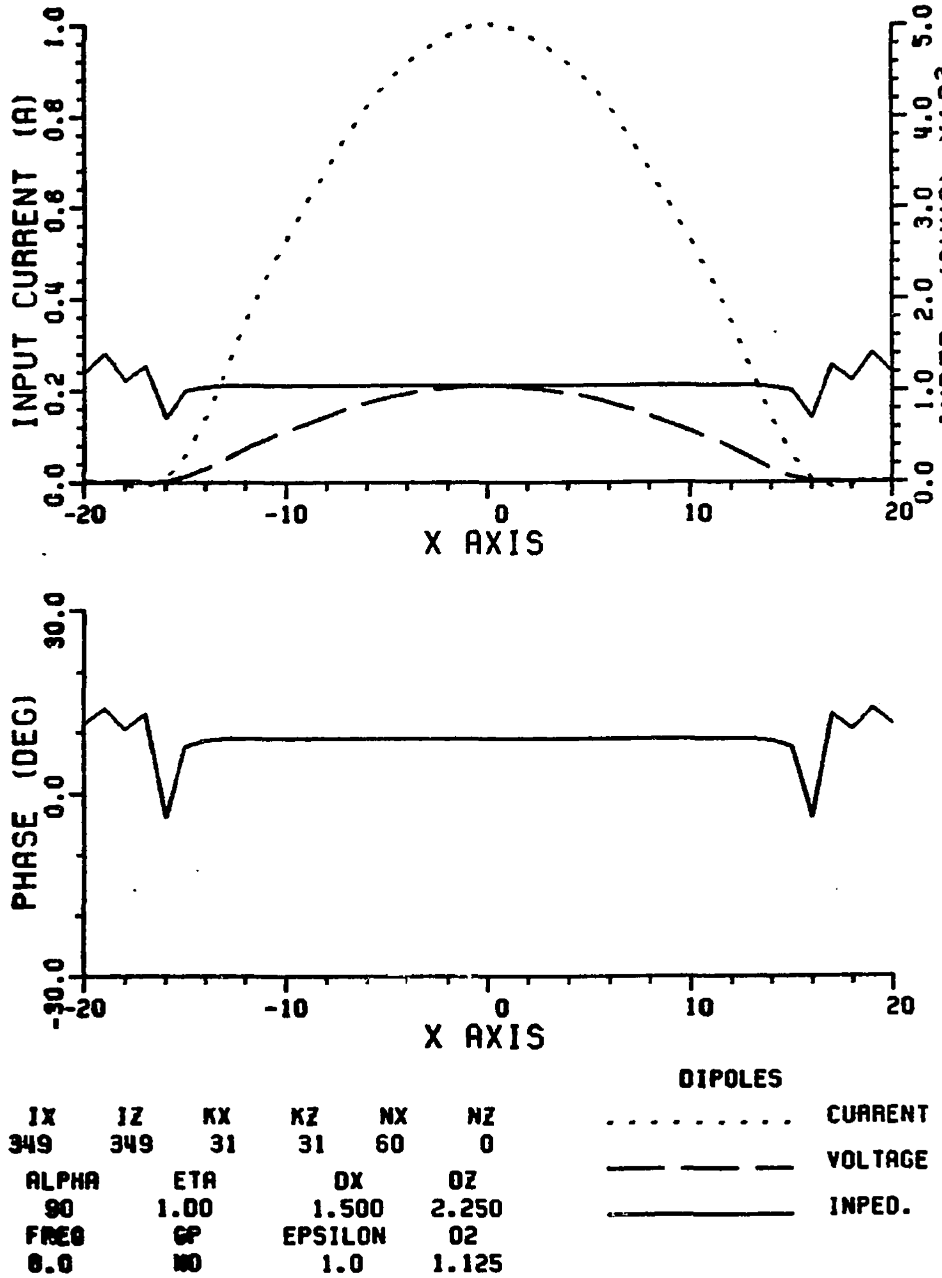

Figure 23. Expanded view of the impedance for array D1 at a broadside scan angle with a cosine distribution of the input current.

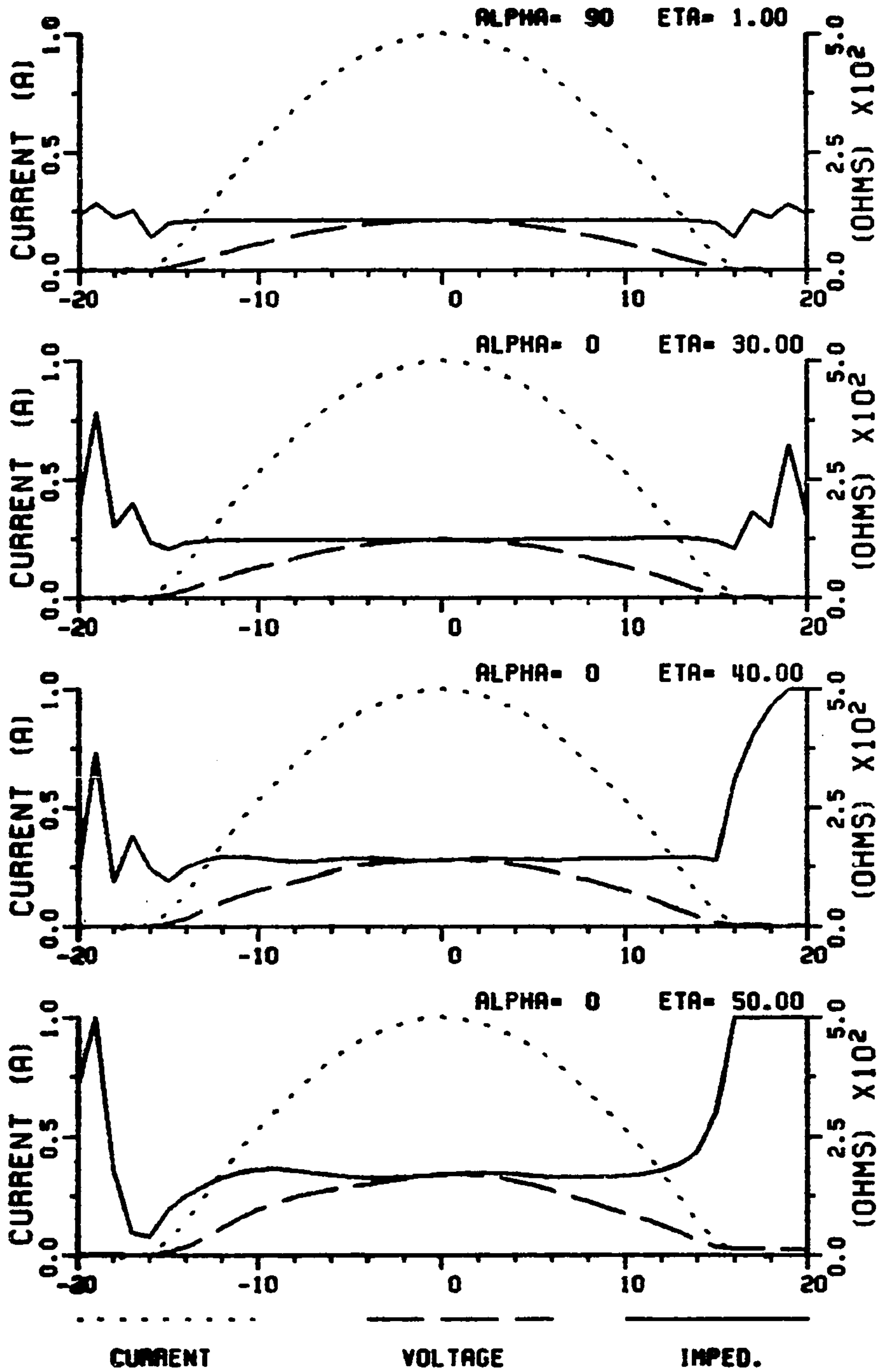

Figure 24. The impedance of array D1 at four scan angles in the x-y plane with a cosine input current. The scan angle is to the right in these plots.

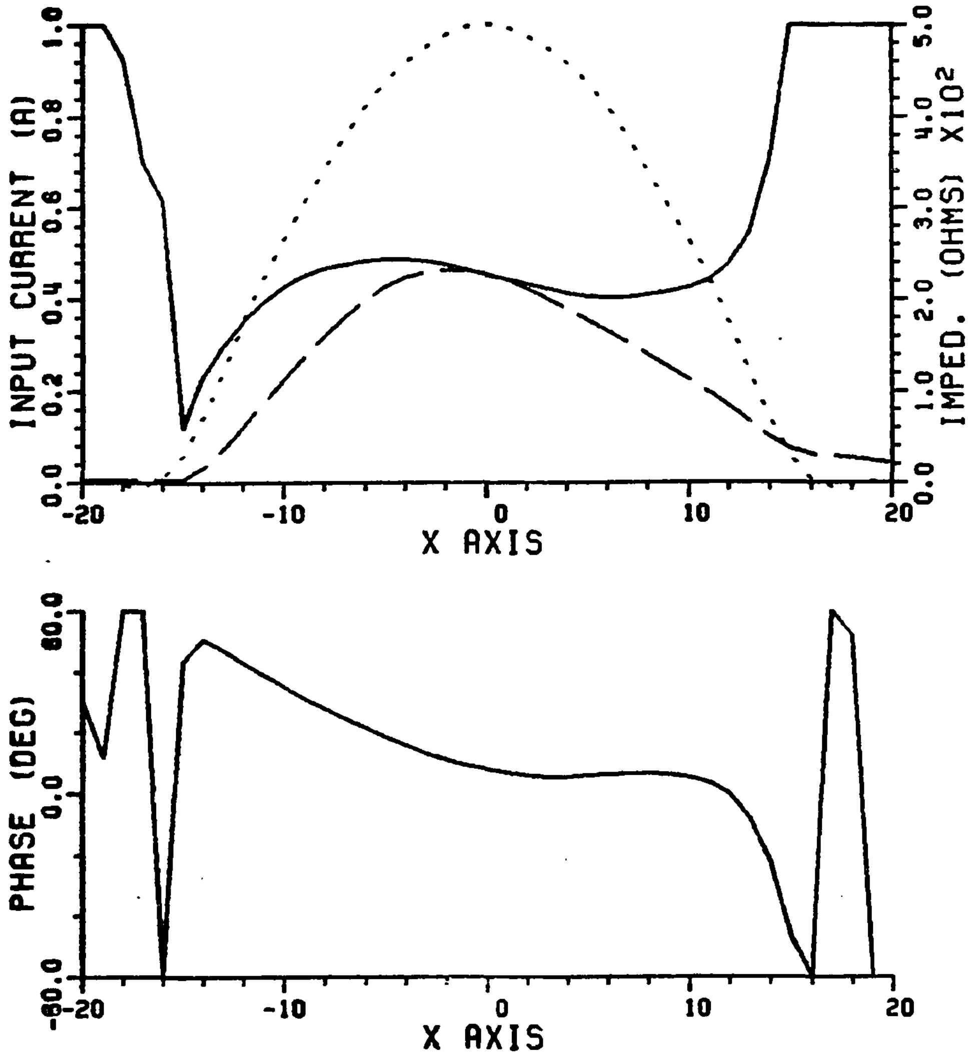

IX	IZ	KX	KZ	NX	NZ
349	349	31	31	60	0

ALPHA	ETA	DX	DZ
0	60.00	1.500	2.250
FREQ	GP	EPSILON	D2
8.0	NO	1.0	1.125

Figure 25. Expanded view of the impedance for array D1 at a 60^0 scan angle to the right with a cosine distribution of the input current.

voltage (the dashed line in the figures) goes to zero outside the finite array area. As Figure 25 indicates, the voltage does not go to zero past element 15 for the 50° or 60° scans. This phenomenon occurs at larger scan angles also.

This new, perhaps unexpected, behavior has to be considered carefully. One possible explanation is the existence of some limitation in the method, which prevents scanning past some, as yet unspecified, angle. Because this limitation would greatly reduce the utility of the method considered in this study, it is necessary to prove, at this point, the accuracy of the method in predicting the element by element impedances of large finite phased arrays at both small and large scan angles.

In order to explain why non-zero voltages on elements outside the model of the finite phased array do not affect impedance values in the area of non-zero current excitation (the array model), it is useful to consider the phased array in Figure 26. This figure shows a linear array of 9 excited dipoles with two parasitic elements at each end. This array is scanned by adjusting the relative phases of the currents on the excited elements. After a certain scan angle, a non-zero voltage will appear at the terminals of the two non-excited elements to the far right in a situation similar to the one in Figure 25. It is postulated that these elements could be removed, even though they have a non-zero voltage on them, and the impedances of the elements in the interior of the finite array would not change. This postulation is made because these non-excited elements have no current flowing on them. They can be considered to have infinite impedance at their center terminal which will not allow any even current modes to flow. Admittedly, odd current modes could exist but their magnitudes would be sufficiently small to have little effect when the element length is on the order of a half wavelength. This possible removal is the situation which the method of this study attempts to emulate. The basic hypothesis is that the behavior of the impedances in the array model is independent of the presence of the non-excited elements, whether they have a voltage induced on them or not. The removal of the non-excited elements in the present method cannot be accomplished. Another numerical method is available, howerver, which can accomplish that removal. If the present method gives impedance values which compare favorably to this other method, the credability of the new method is certainly increased.

The Moment Method computer programs of J. H. Richmond [39] were chosen to confirm the new method. For brevity. Richmond's results will henceforth be referred to as the Direct Method and the method of this study will be referred to as the Transform method. A description of the Direct method and the comparison with the Transform method is given in Appendix E, but some of the comparison results are given in this chapter.

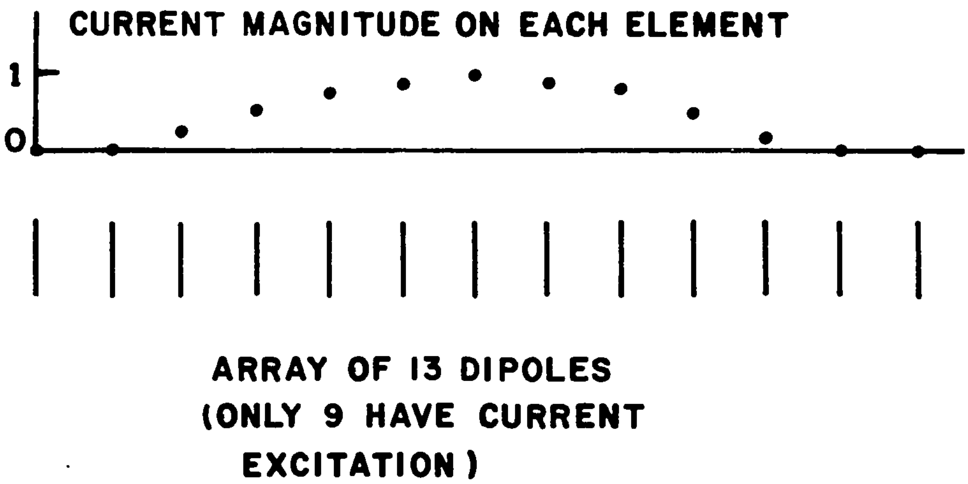

Figure 26. The array of 13 dipoles, only 9 of which have non-zero excitation, similar to those used by the mutual-impedance method is comparing results with the transform method.

The Direct method was applied to several cases where there were n excited elements per row in an array with (n+4) total elements per row, as in the example of Figure 26. Removing the non-excited elements did not affect the self-impedances of the excited elements (to at least 3 decimal digits). Comparison of the Direct method (with no parasitic elements) must be made with results of the Transform method (which, by nature must have these parasitic, but non-radiating, elements). Results for the first example, a 30° scan, are given in Figures 27 and 28. Both arrays have a cosine distribution of current magnitudes over the extent of their apertures. The agreement is excellent in the interior of the array and close near the edges. Figures 29 and 30 gives similar results for a 60° scan. Again, agreement is remarkable considering the difference in the two methods. It is interesting to note the change in shape of this impedance curve when the scan angle is increased to this large value from broadside. The impedance is no longer constant as a function of position, which indicates a relative ineffectiveness in the infinite phased array theory for predicting the behavior of a finite array of this size at a large scan angle. Increasing the width of the finite array from 31 elements to 61 elements causes a distinct change in the shape of the impedance curve as indicated by Figures 31 and 32. The impedance is now more nearly constant in the interior of the array. This phenomenon is not surprising. One would expect the infinite array to be a better approximation to the elements near the center of a finite array as the finite array increases in size, even though the infinite array cannot predict effects near the edge. It is also important to note that increasing the size of the array in the Direct method increases computation time while the Transform method's time is not affected. Of even greater importance, the Transform method can be applied to arrays immersed in a dielectric layer, whereas the Direct method cannot be so applied. Examples of arrays embedded in dielectric layers are given later in this chapter.

Array D1 was also used with other aperture shapes. The trapezoidal aperture, whose Fourier coefficients are given in Appendix D by Equations (D9) and (D10), was tried initially with 60 Fourier terms. Its spectrum, which is given as Figure 33, can be compared to the cosine spectrum of Figure 22. Because its angular spectrum does not decrease in size as rapidly as the tapered spectrum does, 90 terms were employed when considering trapezoidal distributions. The 90 term spectrum is given in Figure 34 and the broadside scan for this distribution is given in Figure 35. Gx, which indicates the size of the triangles at the edges of the array (see Figure D3), is equal to 4 in all examples here and Kx is 27 so the aperture width would remain 31 as in the other examples. The trapezoidal shape was modeled rather than the rectangular pulse shape in order to lessen

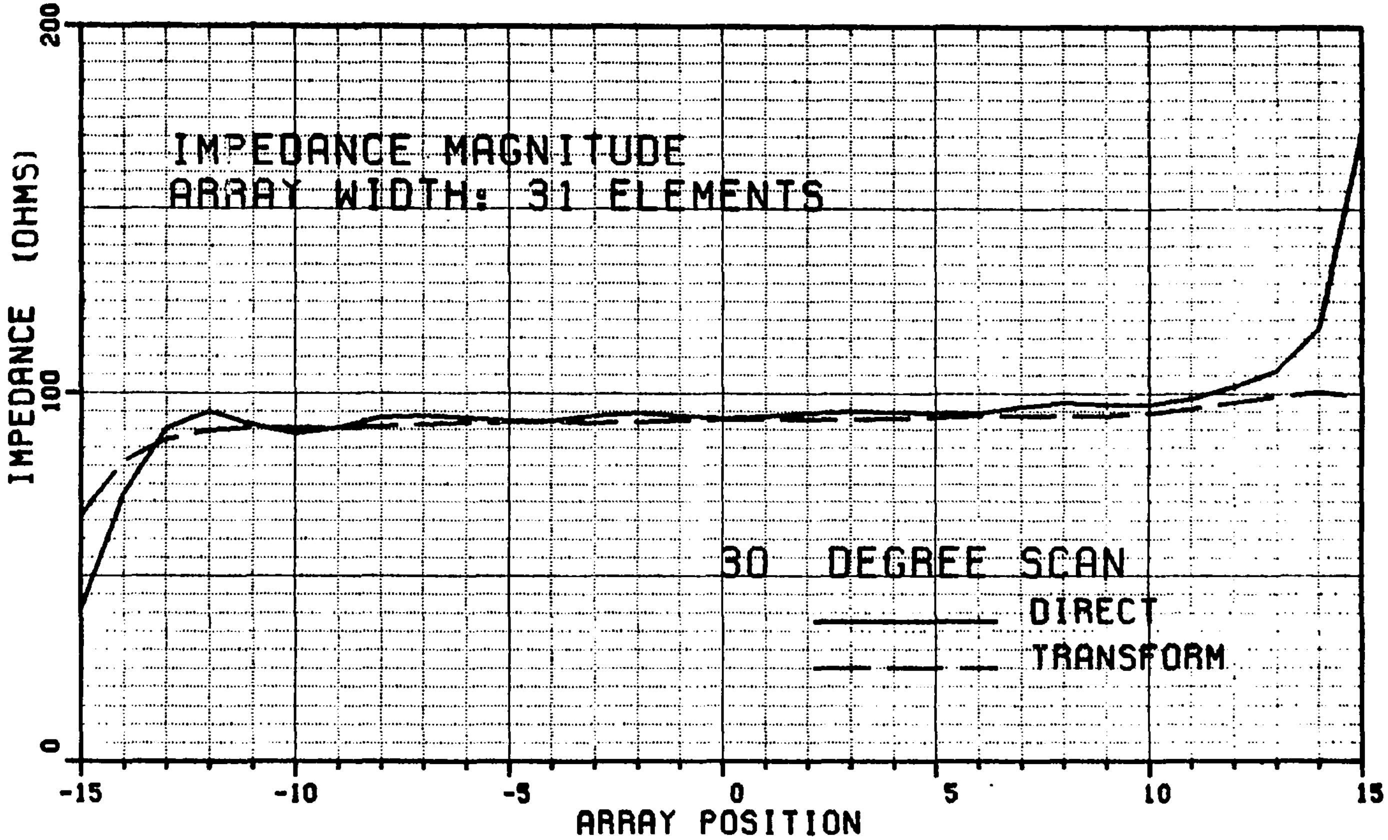

Figure 27. Comparison of impedance magnitude values between the direct and transform methods for an array 31 elements wide at a 30^{0} scan angle to the right.

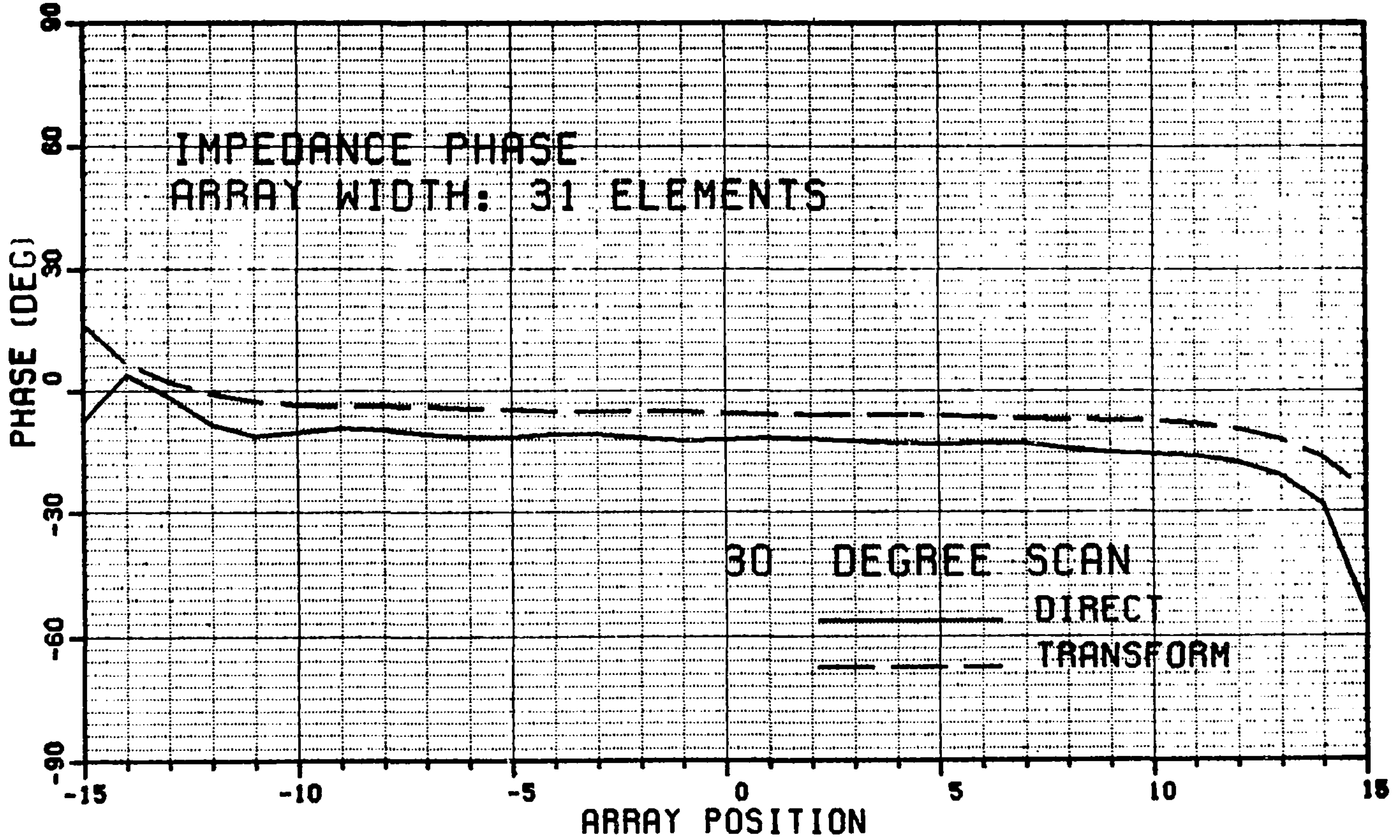

Figure 28. Comparison of impedance phase values between the direct and transform methods for an array 31 elements wide at a 30^{o} scan angle to the right.

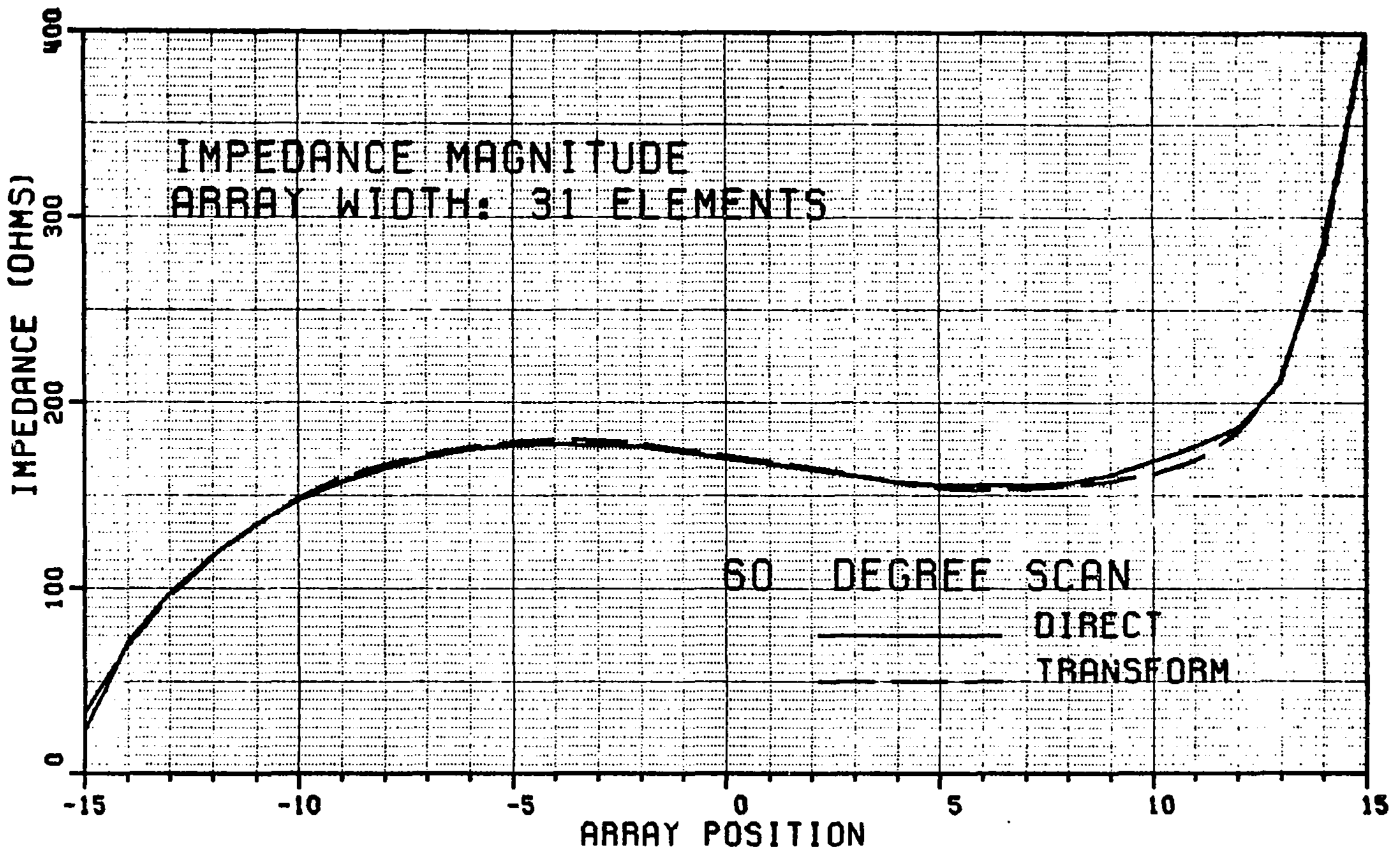

Figure 29. Comparison of impedance magnitude values between the direct and transform methods for an array 31 elements wide at a 60^0 scan angle to the right.

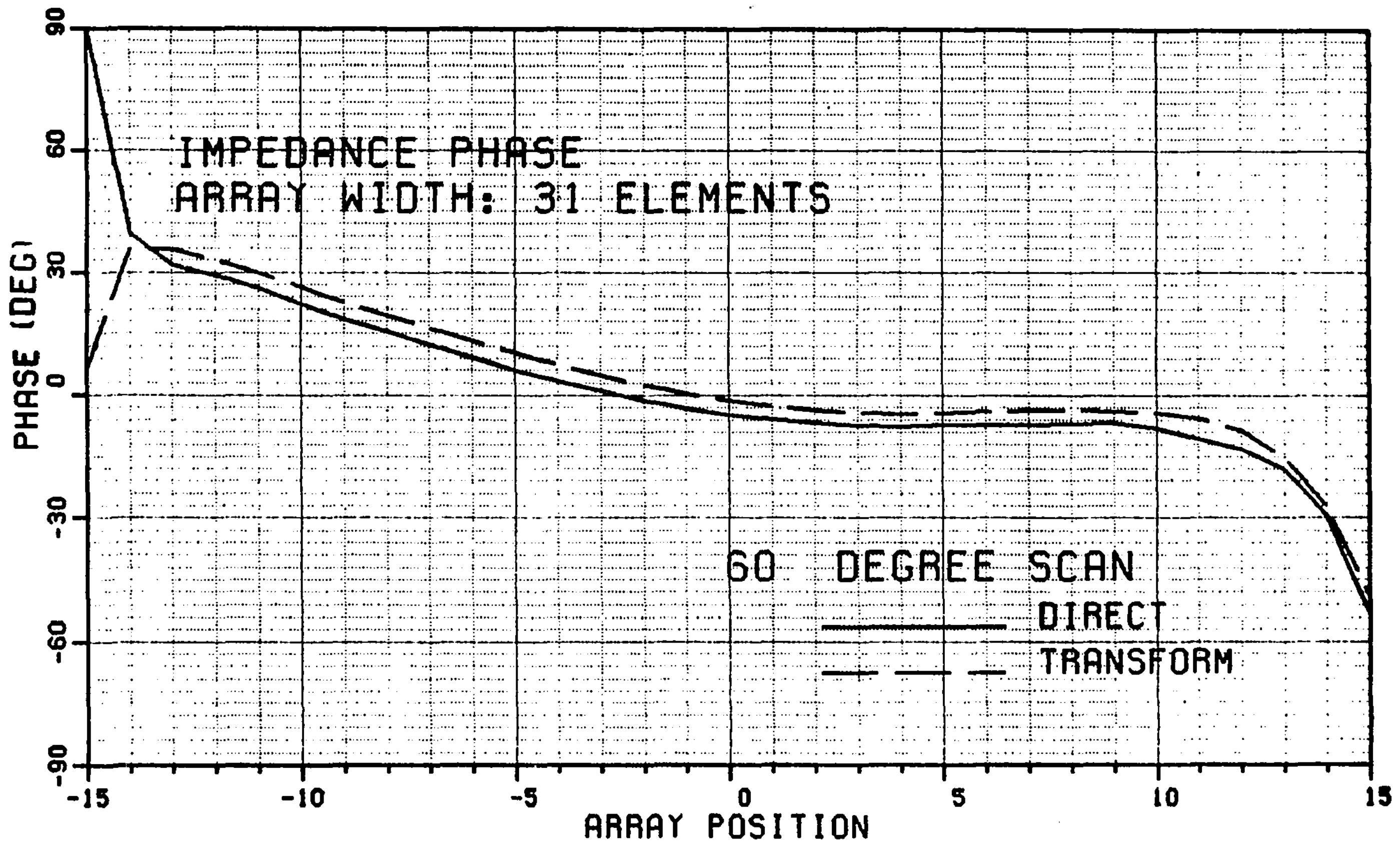

Figure 30. Comparison of impedance phase values between the direct and transform methods for an array 31 elements wide at a 60° scan angle to the right.

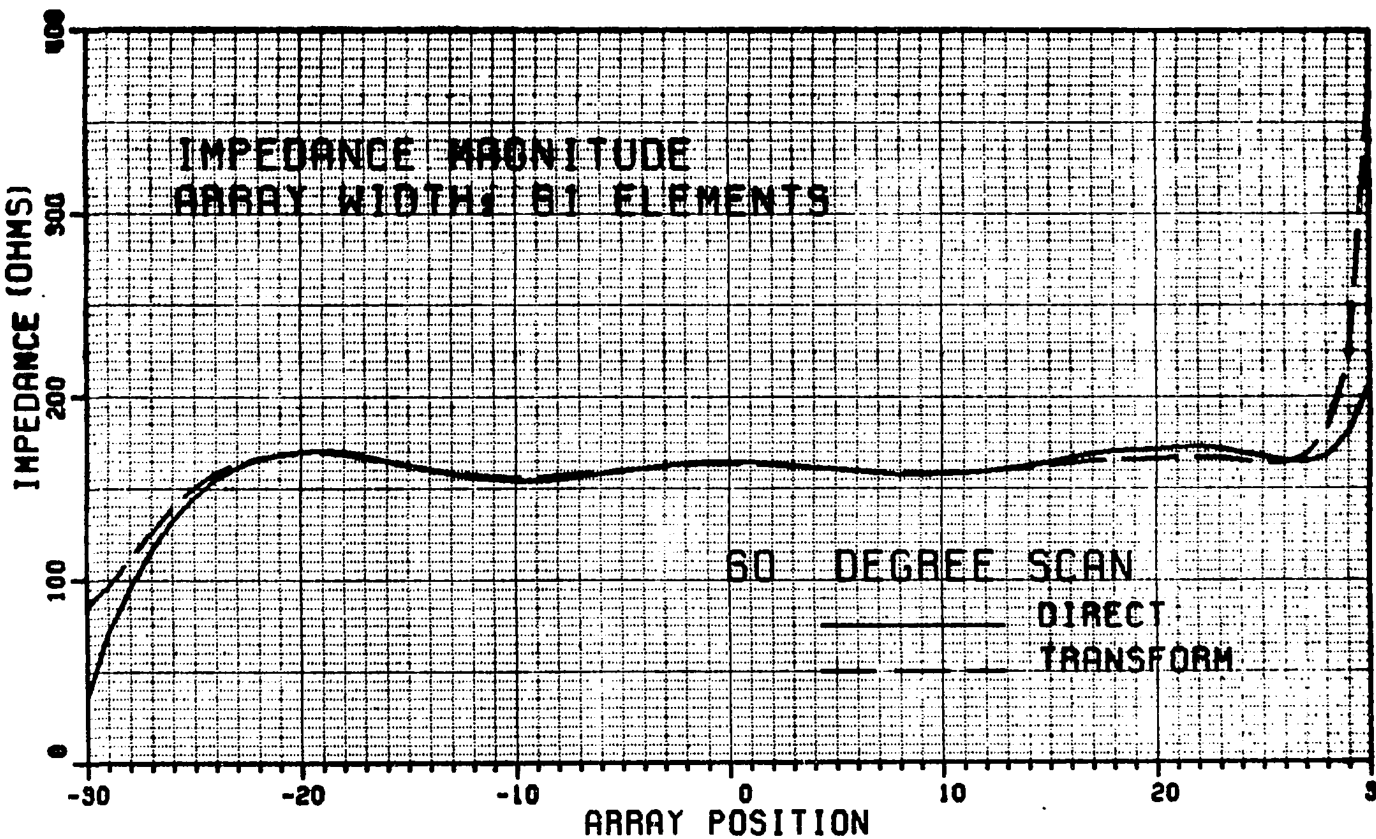

Figure 31. Comparison of impedance magnitude values between the direct and transform methods for an array 61 elements wide at a 60^{0} scan angle to the right.

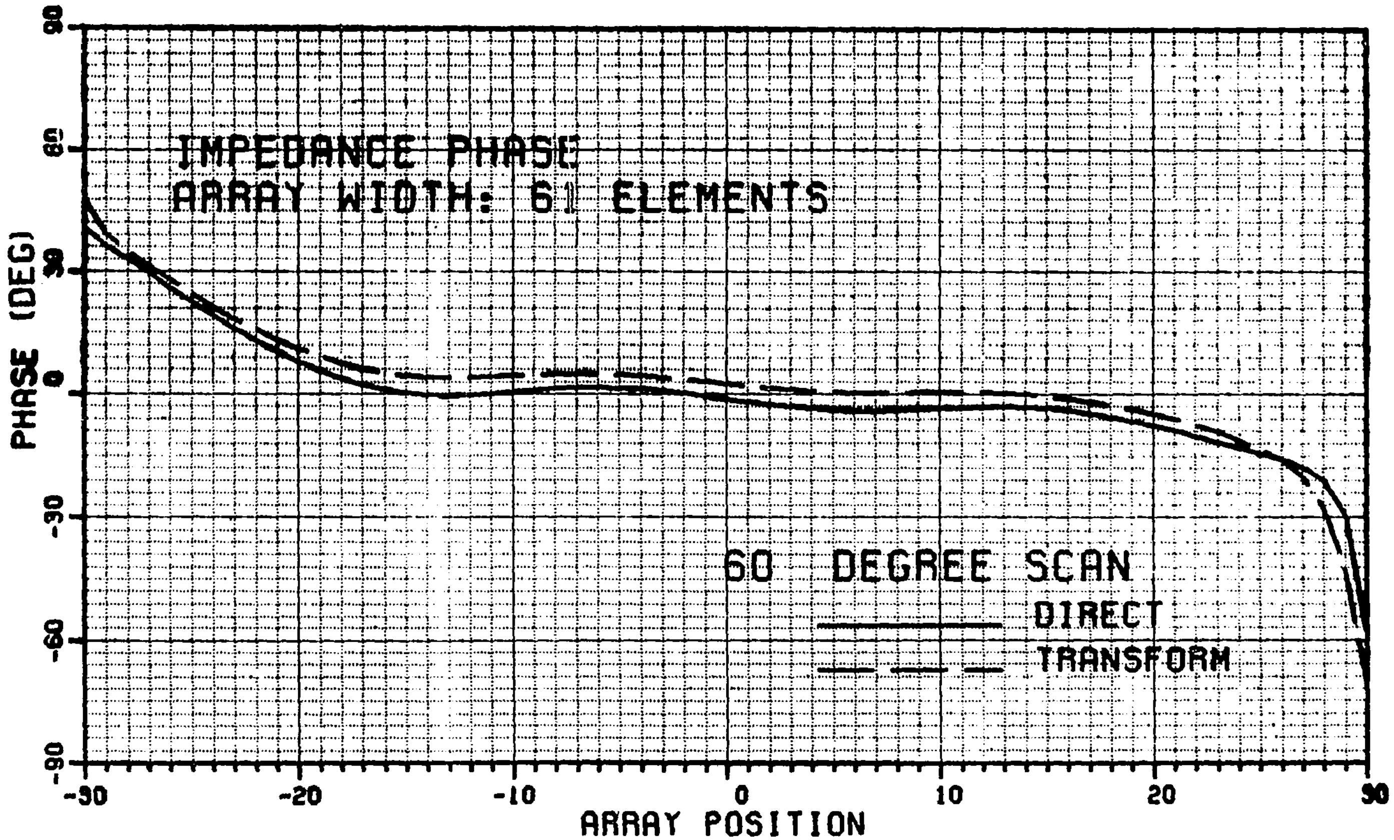

Figure 32. Comparison of impedance phase values between the direct and transform methods for an array 61 elements wide at a 60° scan angle to the right.

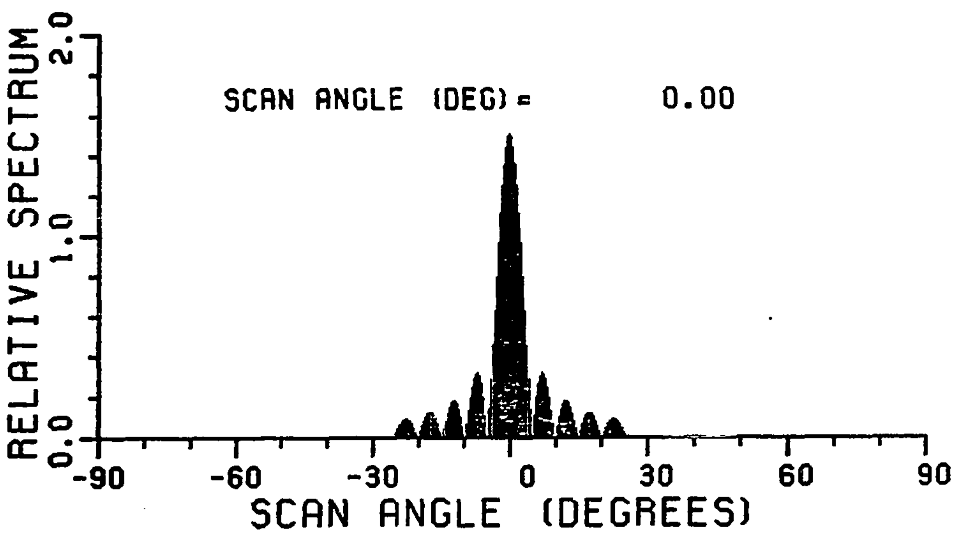

Figure 33. The spectrum of the finite array as a function of scan angle for the trapezoidal aperture scanned at broadside with 60 Fourier terms.

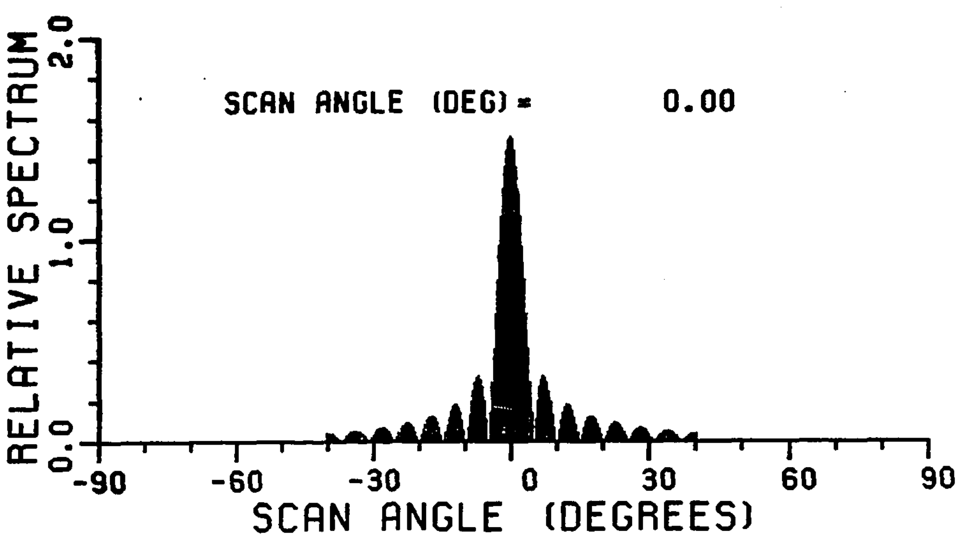

Figure 34. The spectrum of the finite array as a function of scan angle for the trapezoidal aperture scanned at broadside with 60 Fourier terms.

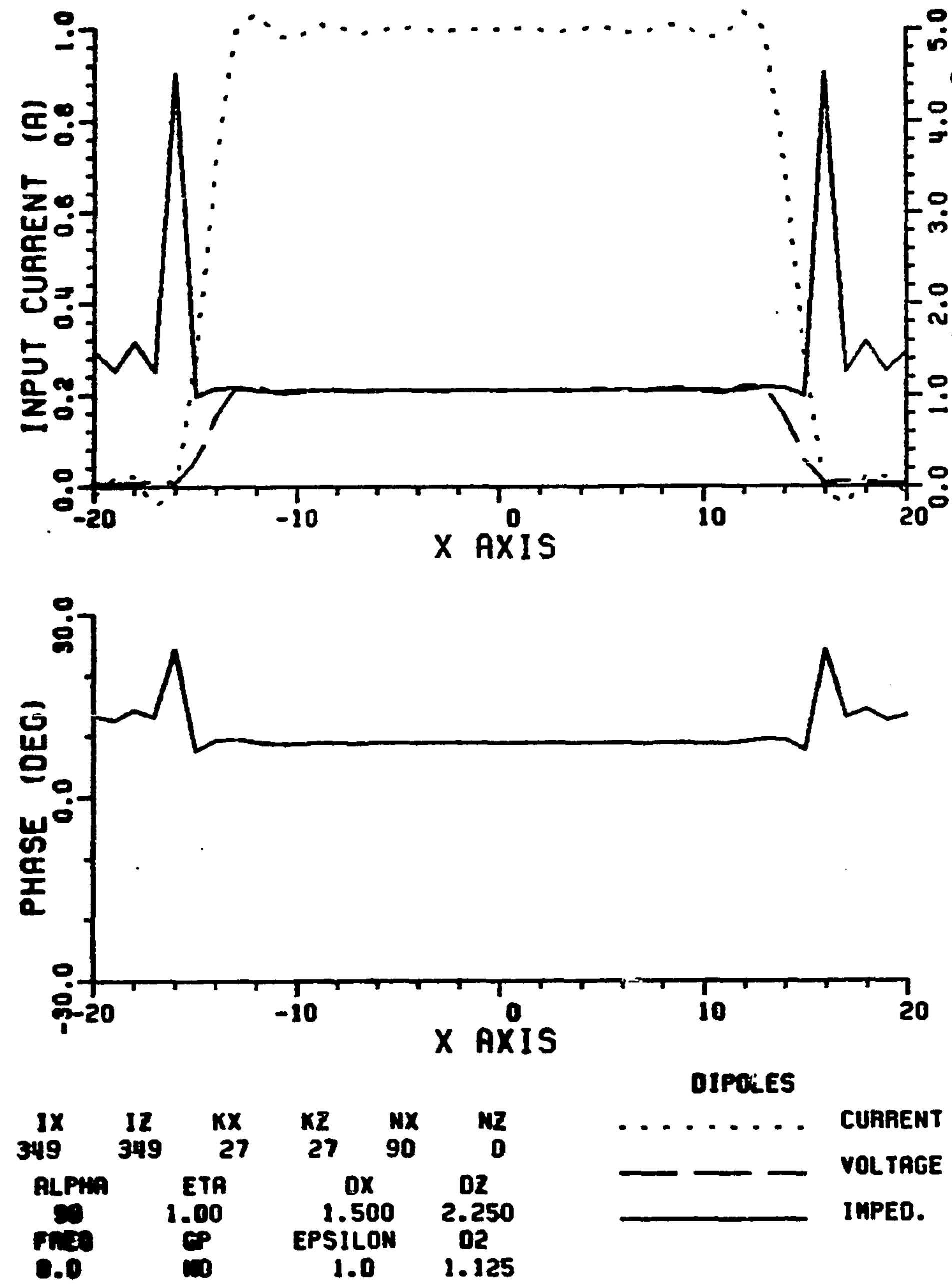

Figure 35. Expanded view of the impedance for array D1 at a broadside scan angle with a trapezoidal distribution of the input current.

the severity of the discontinuity at the edges of the finite aperture. Figure 36 shows array D1 with the aperture scanned at broadside, 30^0, 40^0, and 50^0. Figures 37 and 38 give similar results for array D1 with a difference pattern type aperture. The formulation of the aperture is given in Appendix D by Equation (D15) with the odd symmetry Fourier coefficients given by Equation (D16). No remarkably new result is obtained because this aperture is smoothly tapered with no sharp discontinuities. Its behavior should be much like that of the cosine shaped aperture.

2. Dipole array in a dielectric slab

The present method can also be applied to a dipole array in a dielectric slab. This is done for array D2 with the geometry shown in Figure 39. Equation (77) is applied again to find the impedances of this dipole array using only the μ=0 term to achieve modulation in the x-direction (Equation (82)). $\Omega_{k,n,\nu,0}$ (Equation (75)) will contain the transformation factor as given in Equation (74), in order to treat the dielectric slab. Because the array is centered in the slab, d_2 and d_3 are equal and because free space exists to both sides of the slab, the reflection coefficients are equal. The transformation function is now of the form

$$_{(\perp\parallel)}T_2 = \frac{(1 + {}_{(\perp\parallel)}^{E}\Gamma_{2,1}\, e^{-j2\beta_2 d_2 r_{2y}})^2}{1 - ({}_{(\perp\parallel)}^{E}\Gamma_{2,1})^2 e^{-j4\beta_2 d_2 r_{2y}}} \tag{84}$$

which simplifies to

$$_{(\perp\parallel)}T_2 = \frac{1 + {}_{(\perp\parallel)}^{E}\Gamma_{2,1} e^{-j2\beta_2 d_2 r_{2y}}}{1 - {}_{(\perp\parallel)}^{E}\Gamma_{2,1}\, e^{-j2\beta_2 d_2 r_{2y}}} \tag{85}$$

and because the pattern factor of the array element is again equal to that of the test element Ω is now of the form

$$\Omega_{k,n,\nu,0} = [({}_{\perp}P_2^{(2)t})^2\, {}_{\perp}T_2 + ({}_{\parallel}P_2^{(2)t})^2\, {}_{\parallel}T_2] \tag{86}$$

and the expression for the impedance of the element located at x=qDx is

$$Z_q = \frac{Z_2}{2D_x D_z \sum_{\nu=0}^{\infty} L_\nu^x \cos(2\pi \frac{q\nu}{I_x})}$$

$$\sum_{\nu=-\infty}^{\infty} \frac{L_\nu^x}{\epsilon_\nu} e^{-j2\pi\frac{q\nu}{I_x}} \sum_{k=-\infty}^{\infty} \sum_{n=-\infty}^{\infty} \frac{e^{-j\beta_2 a r_{2y}}}{r_{2y}}\, \Omega_{k,n,\nu,o} \tag{87}$$

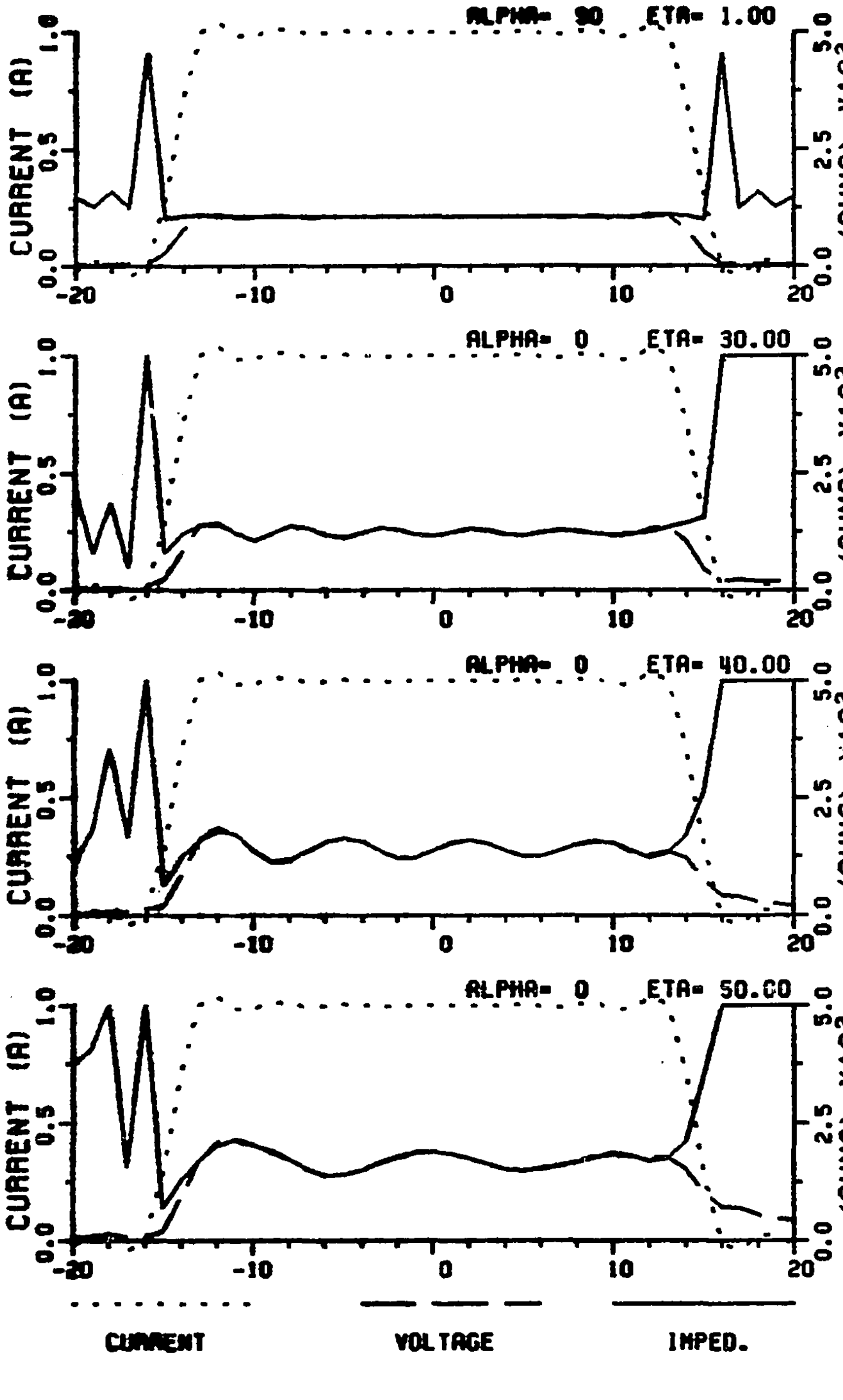

Figure 36. The impedance of array D1 at four scan angles in the x-y plane with a trapezoidal input current. The array scans to the right.

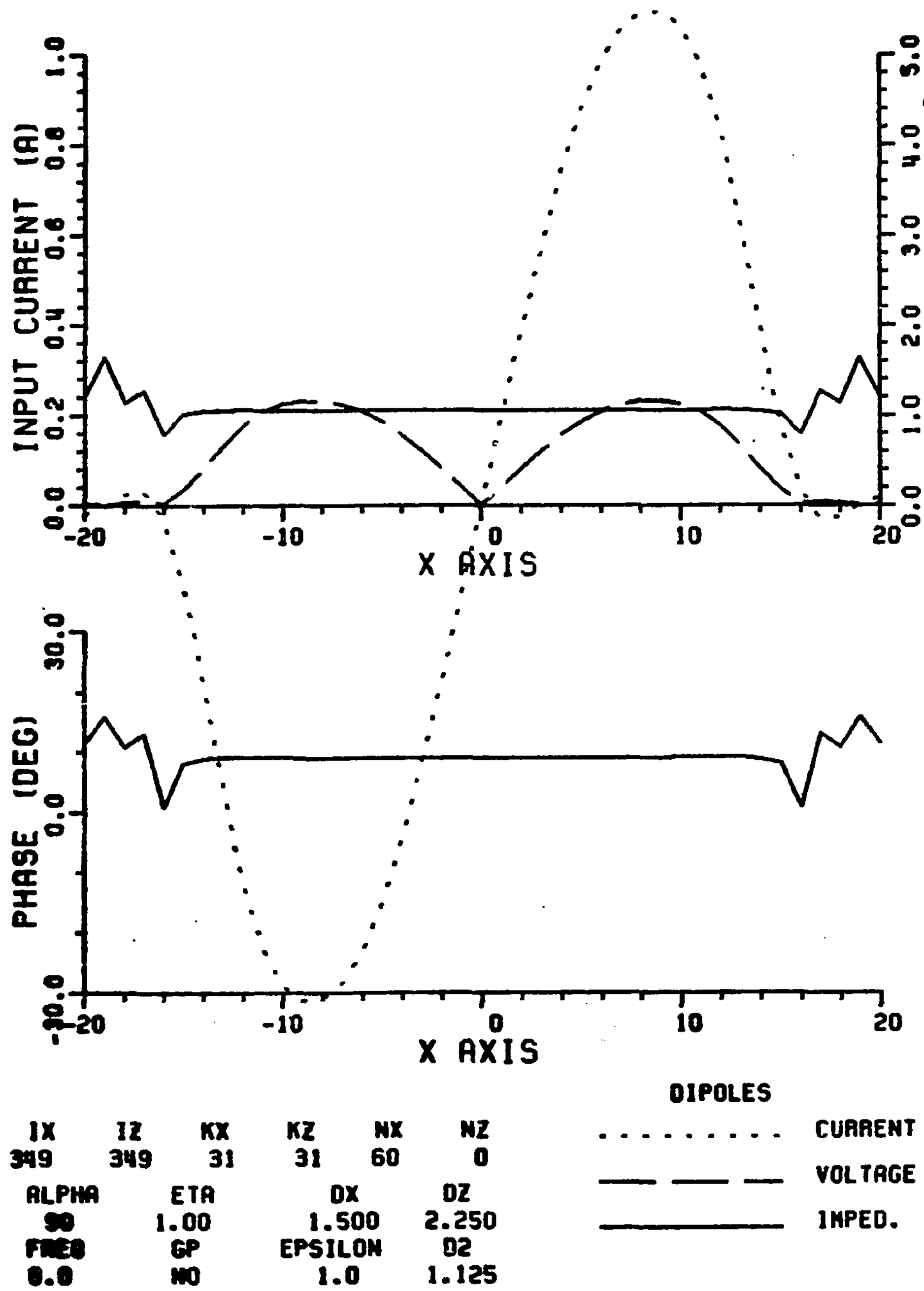

Figure 37. Expanded view of the impedance for array D1 at a broadside scan angle with a difference distribution of the input current.

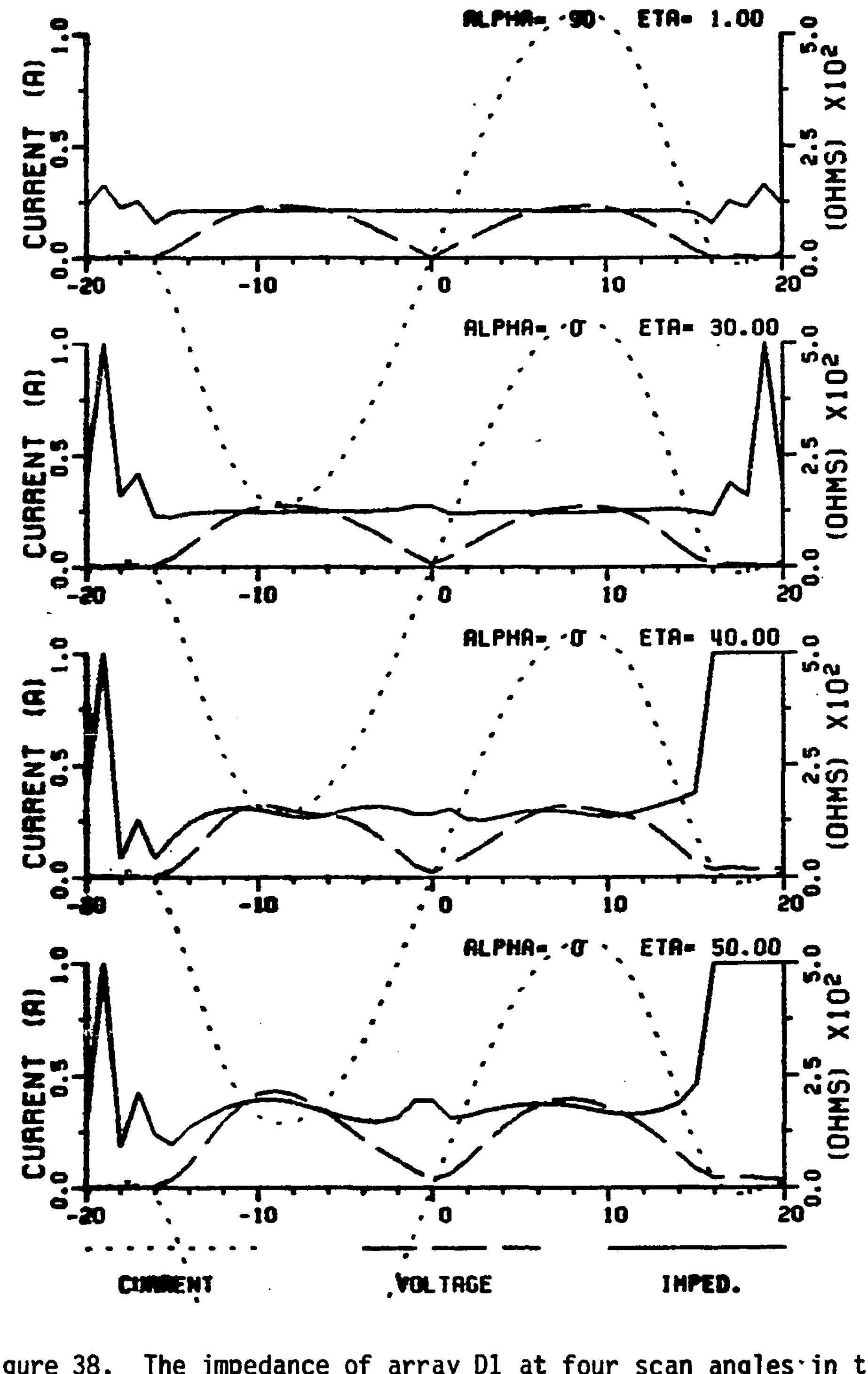

Figure 38. The impedance of array D1 at four scan angles in the x-y plane with a difference distribution input current. The array scans to the right.

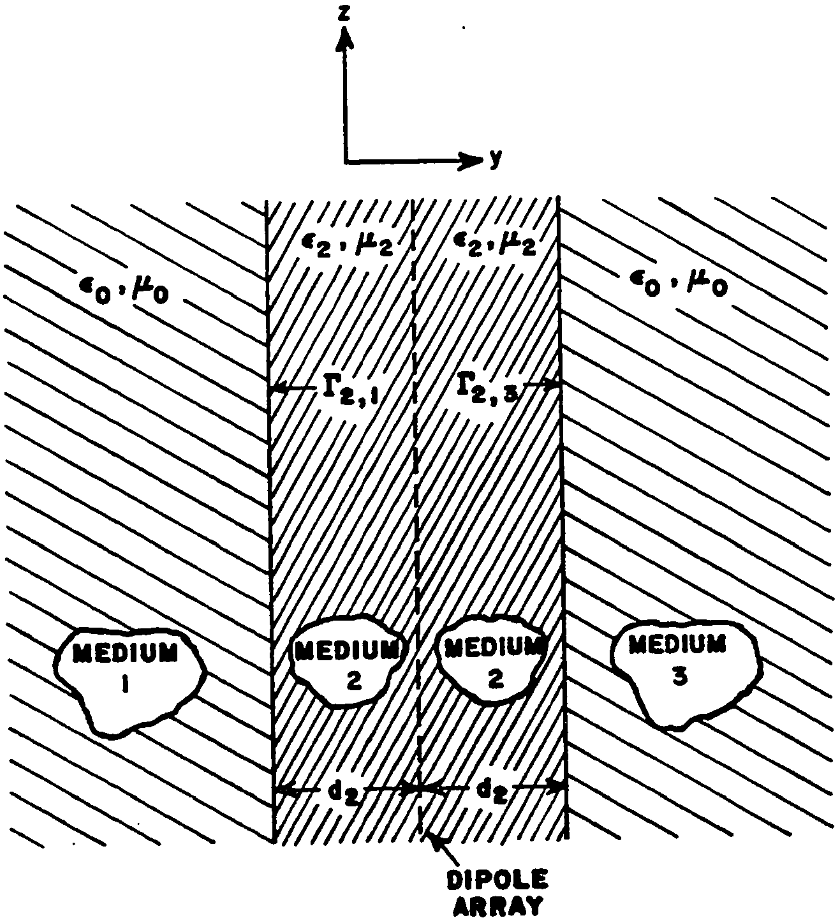

Figure 39. Geometry of array D2. The array is in the center of a dielectric slab with a relative dielectric constant of 1.3. Free space exists to both sides of the dielectric.

Array D2 is modeled at 8 GHz (λ_1 = 3.75 cm) with dipoles of length 1.644 cm ($0.5\lambda_2$), Dx and Dz are 1.31 cm ($0.4\lambda_2$) and 1.974 cm ($0.6\lambda_2$) respectively. The modulation period (i_x) is 349 and 31 elements are excited in the x-direction. The flat dipoles modeled here have width of 0.0877 cm ($0.026667\lambda_2$) and thickness 0.00877 cm ($0.0026667\lambda_2$). The total thickness of the dielectric is 1.974 cm ($0.6\lambda_2$) and its relative dielectric constant is 1.3. Table I summarizes these parameters for all arrays.

Figure 40 shows the admittance plot for array D2 with broadside excitation. The impedance is constant across the extent of the finite aperture (110 ohms), as is the phase (14.3 degrees). Figure 41 shows the magnitude results for broadside, 30°, 40°, and 50° scans. The behavior of the 50° scan data indicates, however, a major problem typical of dielectric coated phased arrays. The enlarged result for the 50° scan is given in Figure 42.

The origin of the problem is traceable to the denominator of the transformation factor of Equation (44). This denominator can go to zero for either the perpendicular or parallel case. It is explained in Appendix F, however, that for this one-dimensional case and straight z-directed elements, the parallel pattern factors of Equation (76) are so small that only the perpendicular transformation factor causes difficulty here. Although the discussion of this singularity below is specific to the present geometry and the perpendicular case, it does apply in general to other situations where the transformation factor goes to zero.

From Appendix F, it is seen that the condition for the denominator of the transformation factor going to zero is

$$\beta_2 d_2 r_{2y} \tan(\beta_2 d_2 r_{2y}) = -\sqrt{(\beta_1 d_2)^2(\varepsilon_2-1)-(\beta_2 d_2 r_{2y})^2} \tag{88}$$

which can be rewritten as

$$u \tan(u) = -\sqrt{(\beta_1 d_2)^2(\varepsilon_2-1)-u^2} \tag{89}$$

where

$$u = \beta_2 d_2 r_{2y} \tag{90}$$

Equation (89) is transcendental, so a graphical method of solution is convenient. Figure 43 (along with a simple computer program) reveals u to be 0.695 for array D2 which leaves r_{2y} as 0.369 for the propagating (k=n=0) mode. Using Equations (71) through 73 (for the present case of no scan in the y-z plane, $r_{z1} = r_{z2}=0$) gives $r_{2x}=0.929$ (68.3° scan), $r_{1x}=1.06$, and $r_{1y}=j0.351$. The interpretation of these numbers is as follows: one of the terms in the Fourier

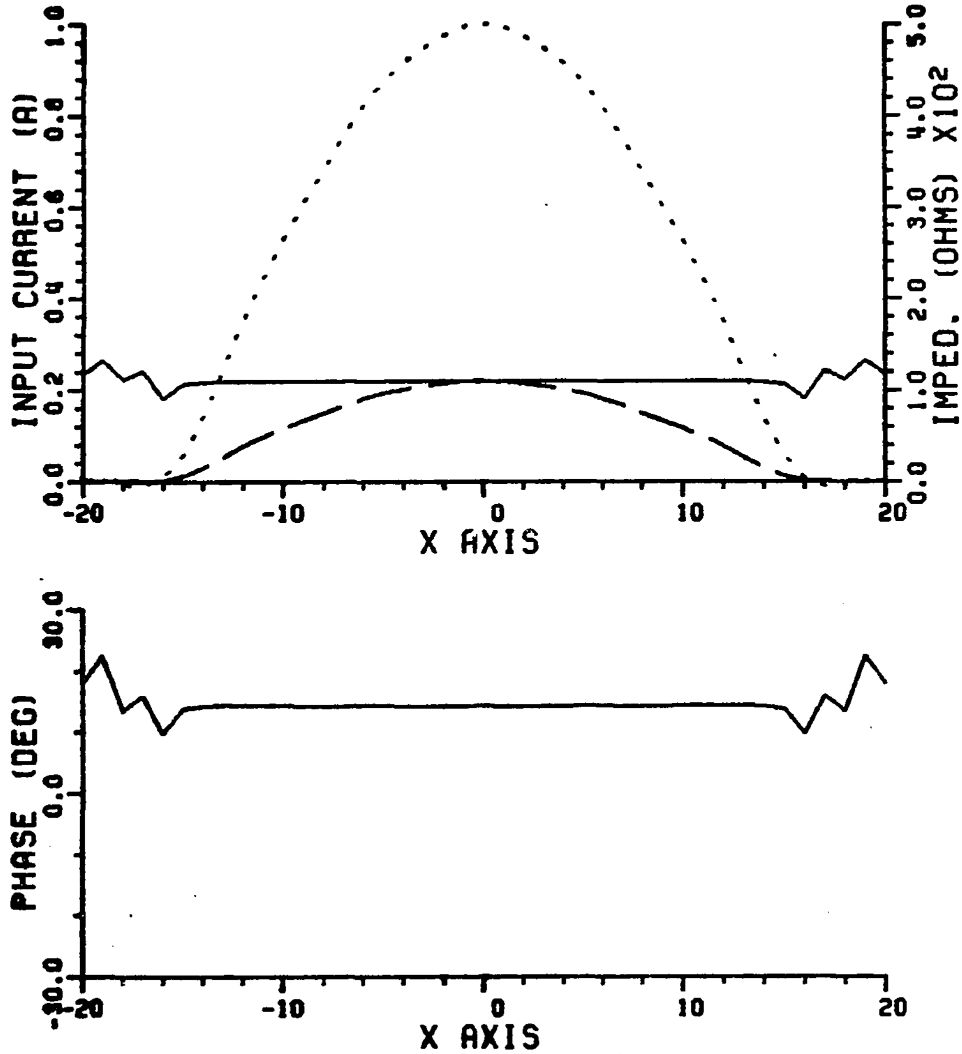

DIPOLES

IX	IZ	KX	KZ	NX	NZ
349	349	31	31	60	0

ALPHA	ETA	DX	DZ
90	1.00	1.316	1.974
FREQ	GP	EPSILON	D2
8.0	NO	1.3	0.987

. . . . CURRENT
— — — — VOLTAGE
———— IMPED.

Figure 40. Expanded view of the impedance for array D2 at a broadside scan angle with a cosine distribution of the input current.

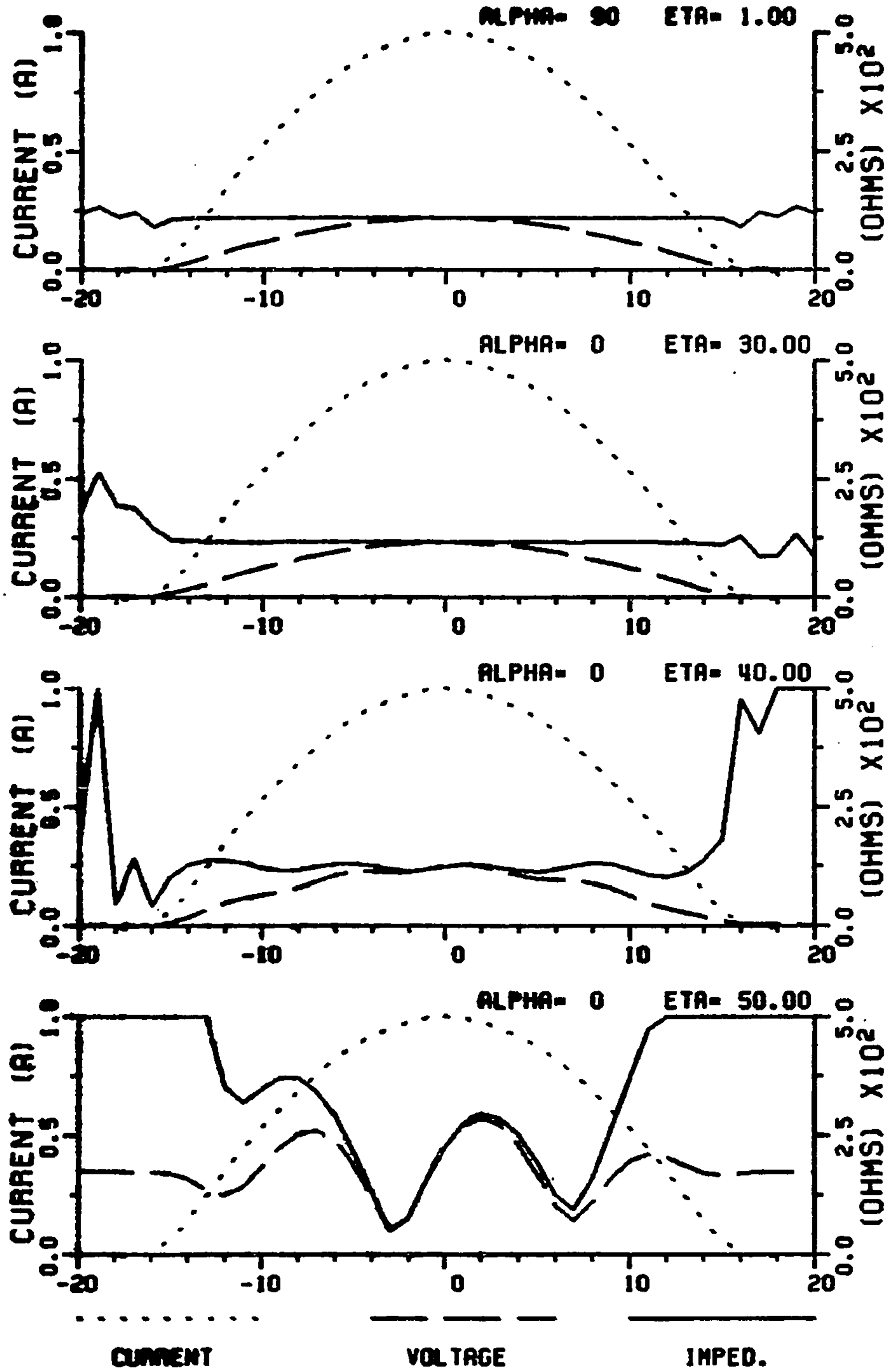

Figure 41. The impedance of array D2 at four scan angles in the x-y plane with a cosine input current. The array scans to the right.

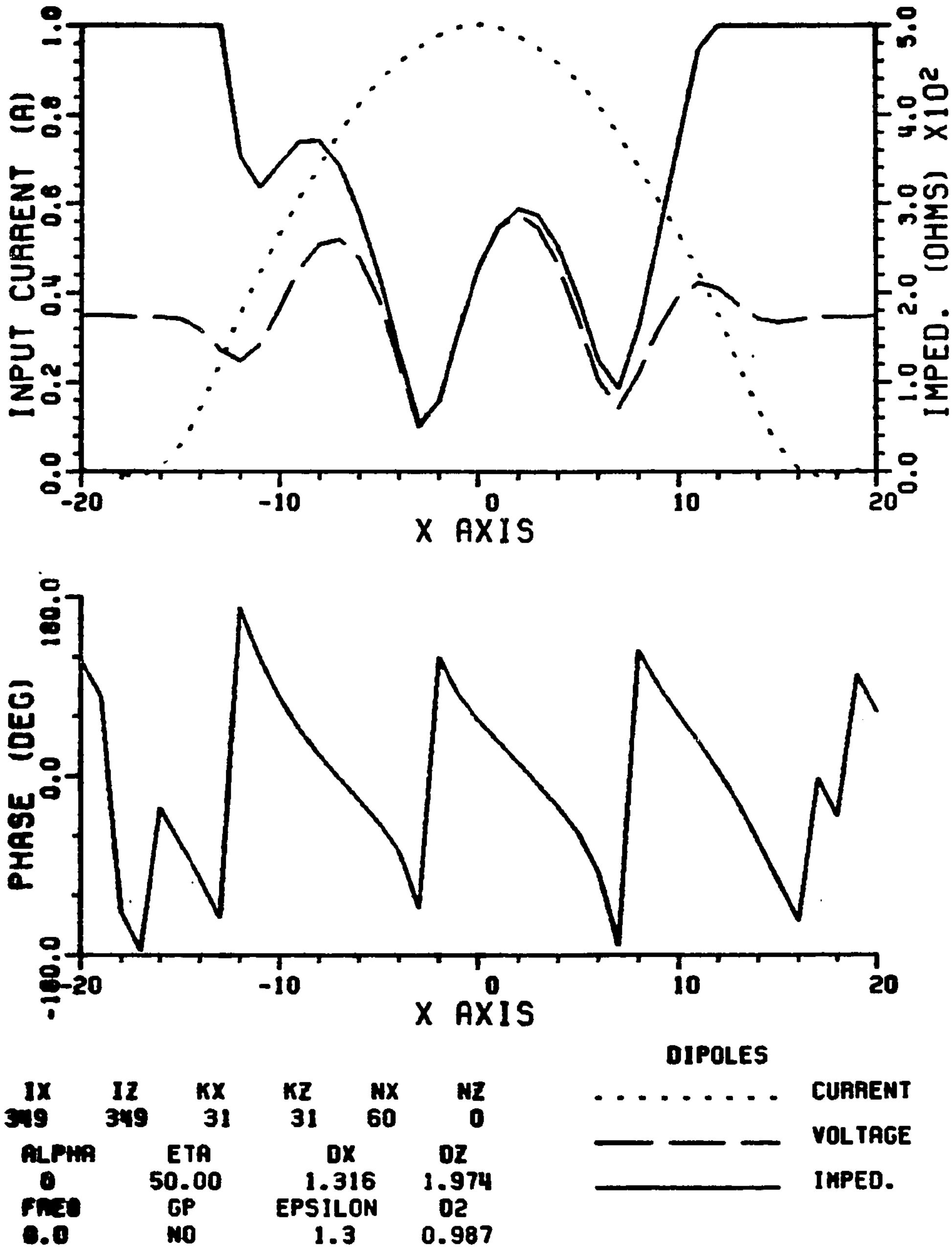

Figure 42. Expanded view of the impedance for array D2 at a 50^{0} scan angle to the right with a cosine distribution of the input current.

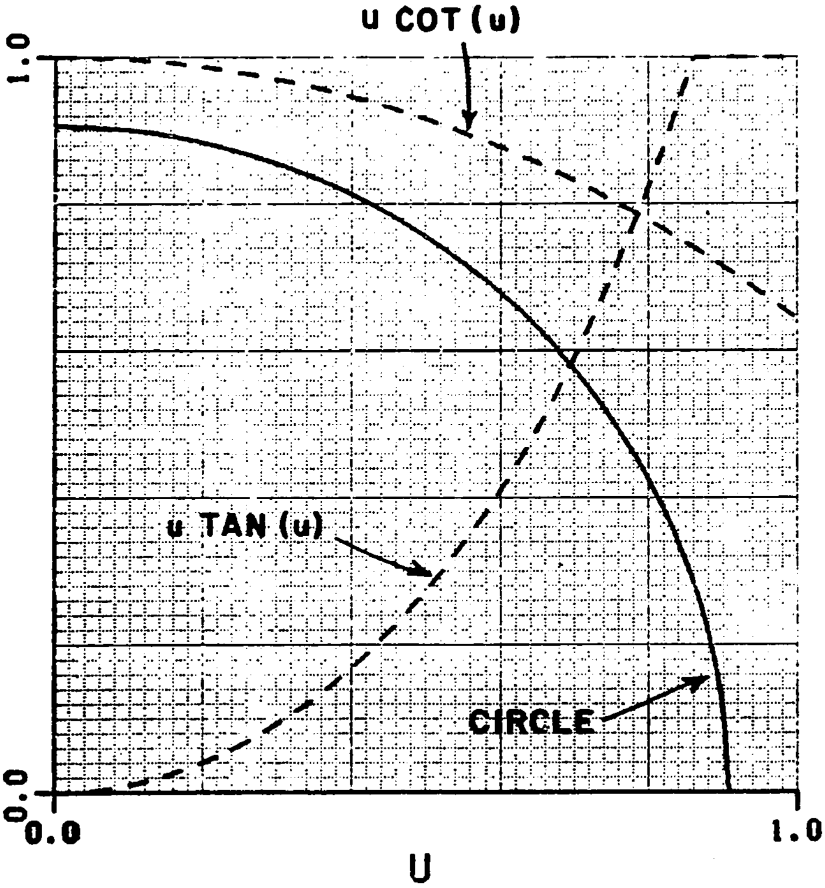

Figure 43. Graphical solution of Equation (88) which reveals u to be approximately 0.695.

Sum corresponds to a scan in real space inside the dielectric at or near the 68.3^o scan indicated above. Because it is intended for the array to be scanning at 50^o, this 68.3^o scan would be a grating lobe. The value of r_{1x} being greater than unity indicates that this wave does not propagate in medium 1 (free space), but in fact corresponds to an attenuating mode. This phenomenon of propagation in the dielectric with an evanescent wave outside the dielectric is referred to as a trapped grating lobe [40]. Physically, it corresponds to a surface wave propagating inside the dielectric. Equation (88) can be recognized as the mode equation for such a wave in a dielectric [41].

Further examination of Equation (89) is informative. Since

$$r_{2y} = \sqrt{1 - (s_{2x} + \frac{\lambda_2}{i_x D_x})^2} \qquad (91)$$

for the k=n=0 propagating mode, it is possible to solve for ν and see that

$$\nu = \frac{f i_x D_x}{30}\left[\sqrt{\epsilon_2 - \left(\frac{30u}{2\pi f d_2}\right)^2} - s_{xo}\right] \qquad (92)$$

where f is in GHz, Dx and d_2 are in cm, and the number 30 is the speed of light in a vacuum in dm/sec. This equation can be used to predict the value of ν, i.e., the term in the Fourier Sum, which represents the scan at 68.3^o. For the 50^o scan and the parameters of array D2, this corresponds to a ν value from Equation (92) of 35.9. This correspondence implies that the 36th term of the Fourier Sum is hitting near the singularity. This fact is confirmed through Figure 44 where the ν=36 term was set to zero and the behavior of the impedance is more like previous examples.

An insight into this difficulty can be achieved by plotting the magnitude of the denominator of the transformation factor as a function of scan angle with the spectrum as a function of angle of the various Fourier terms in the sum, as is done in Figure 45 for a 40^o scan. The abscissa is the scan angle in the dielectric so the spectrum is centered at 40^o divided by the square root of the relative dielectric constant of the dielectric layer. The denominator of the transformation factor goes to zero near 68.3^o as predicted. Figure 46 gives an expanded view of Figure 45 between 60^o and 70^o. The lengths of the spectral lines in the expanded plots are increased in order to ease visibility. Figure 46 reveals why the 40^o scan causes few problems (in Figure 41). Evidently the term which contains the scan near 68.3^o is far enough away and of such small magnitude that it has no noticable effect. Note the position of the critical angle at 61.3^o.

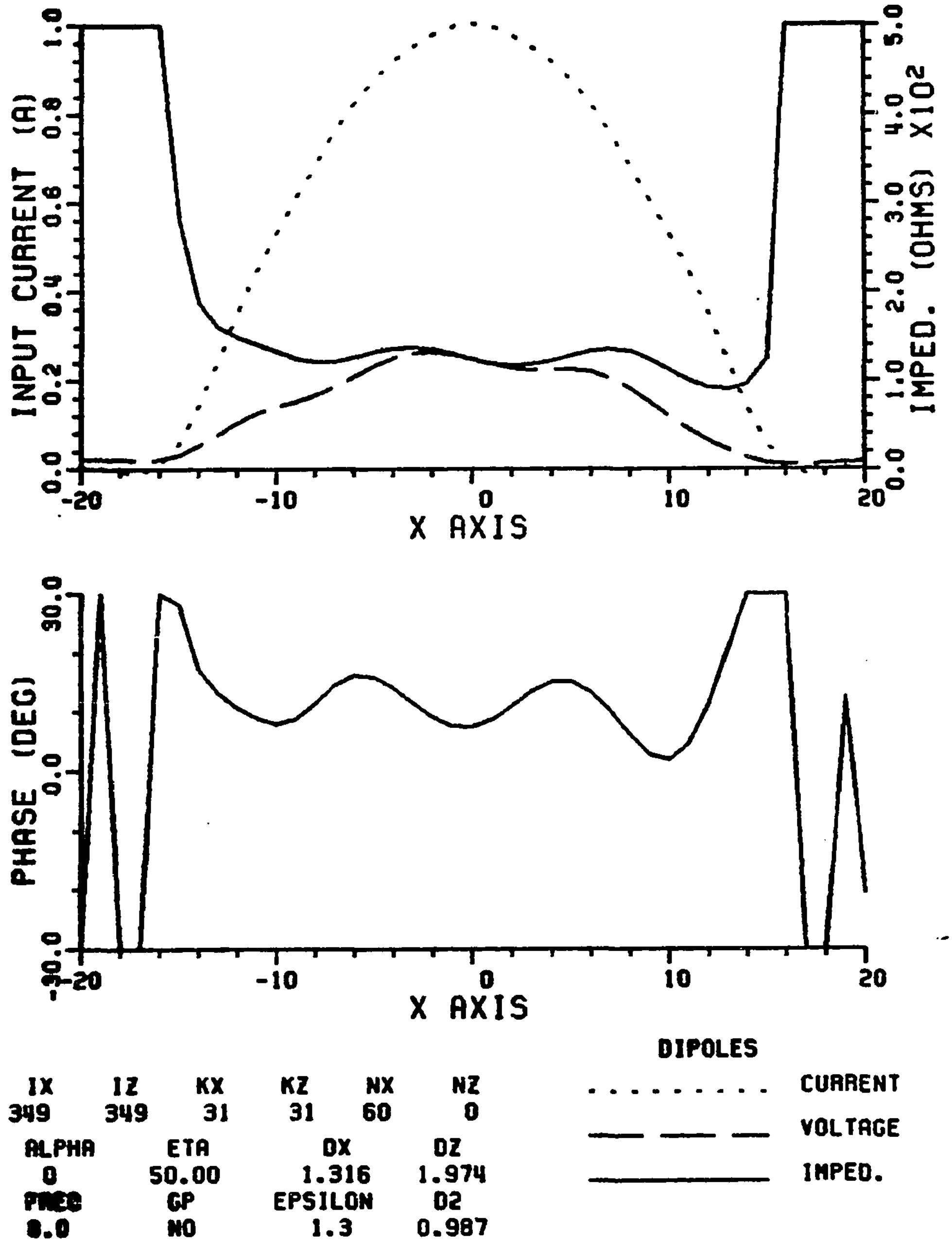

Figure 44. Expanded view of the impedance for array D2 at a 50^{0} scan angle to the right with a cosine input current distribution and the problem causing ν=36 term subtracted.

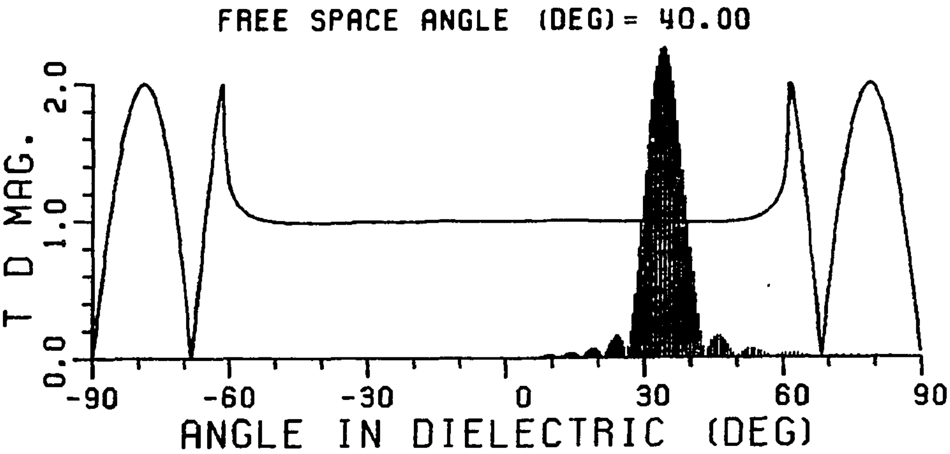

Figure 45. The denominator of the transformation factor plotted with the spectrum of array D2 scanned at 40° as a function of scan angle in the dielectric.

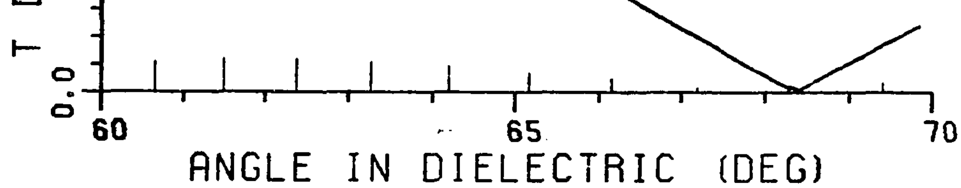

Figure 46. Expanded view of the denominator of the transformation factor plotted with the spectrum of array D2 scanned at 40° as a function of scan angle in the dielectric.

Figures 47 and 48 for the 50^o scan display a considerably different situation. The transformation factor denominator is identical, but the spectrum is changed. In fact, Figure 48 indicates that one of the terms in the sum corresponds very nearly to the angle where the denominator goes to zero. The respective behaviors of Figures 42 and 44 with and without the problem term are not surprising when considered with the information of Figure 48. As Figures 49 and 50 indicate, the 60^o scan should not offer the large variations in impedance, as was the case for the 50^o scan. This notion is confirmed through Figure 51 which shows the impedance to be more nearly constant across the extent of the finite aperture than was the case for the 50^o scan.

Another informative insight can be gained by adjusting the scan angle incrementally near a problem scan angle. Figure 52 gives the plot of the transformation factor denominator with the finite array spectrum between 60^o and 70^o for a 59.5^o scan angle. The Fourier term nearest the singularity is just to the left of it. Figure 53 shows the same plot for a 59.75^o scan where the term seems to coincide with the singularity. Figures 54 and 55 show similar results for 59.9^o and 60.1^o scan respectively. The 59.9^o scan is just to the right of the singularity and the 60.1^o scan is well removed. The impedance plots for these four scan angles are given as Figure 56. The impedance for the 59.75^o angle is completely dominated by the term near the singularity and is so large as to be meaningless. The two scans on either side of it are similar except the relative maximum is displaced to left or right of center. For the 60.1^o scan, the Fourier term is far enough from the singularity that the impedance is nearly constant across the interior of the array.

The question at hand is whether the method itself is the cause of this behavior. This method, as stated above, uses periodically spaced finite arrays and a Fourier sum to calculate impedance values of individual elements in the arrays. Fourier analysis states that in the limit of allowing the period, which here is the inter-array spacing, to go to infinity the Fourier sum becomes a Fourier Integral. This limiting procedure will not be done here, but efforts will be made to make the summation process a closer approximation to the integration procedure and to examine the implications of this approximation.

The first step is to increase the inter-array spacing. Figures 47 and 48 show the spectrum for the 50^o scan of array D2. Increasing the period from the i_x value of 349 used previously in this effort to 1449 will have several effects upon this spectrum. The spectral lines are closer together and the coefficients are in general smaller (see Equations (D5) and (D6) for the cosine distribution coefficients). Because the terms are closer together as a function of the angle in the dielectric in Figure 47, more terms are required to approximate the infinite sum. Figure 57 shows the spectrum for a 50^o scan

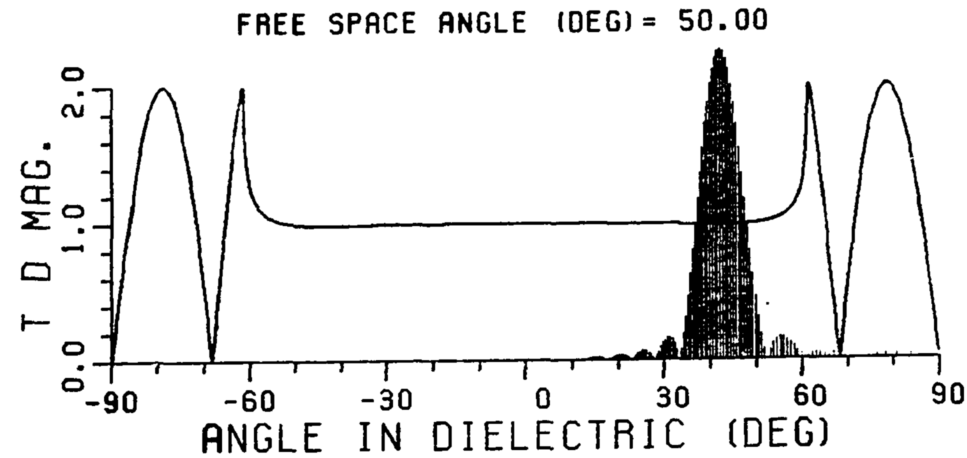

Figure 47. The denominator of the transformation factor plotted with the spectrum of array D2 scanned at 50^{o} as a function of scan angle in the dielectric.

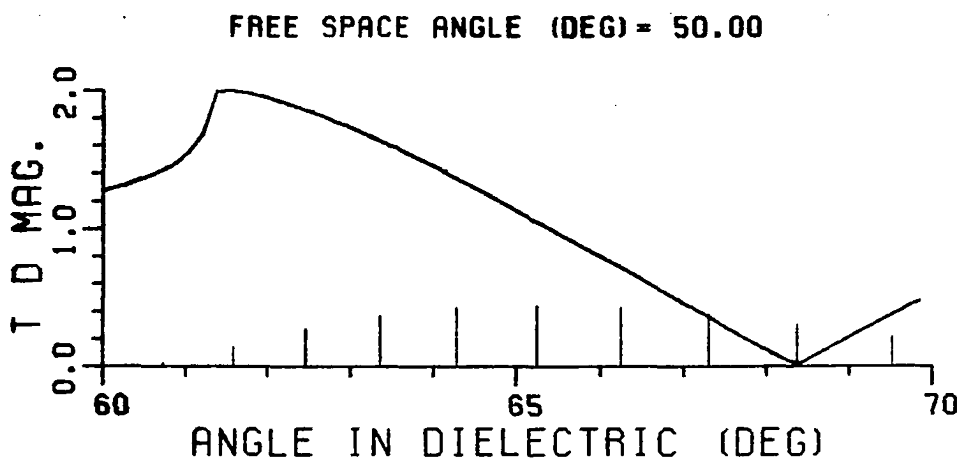

Figure 48. Expanded view of the denominator of the transformation factor plotted with the spectrum of array D2 scanned at 50^{o} as a function of scan angle in the dielectric.

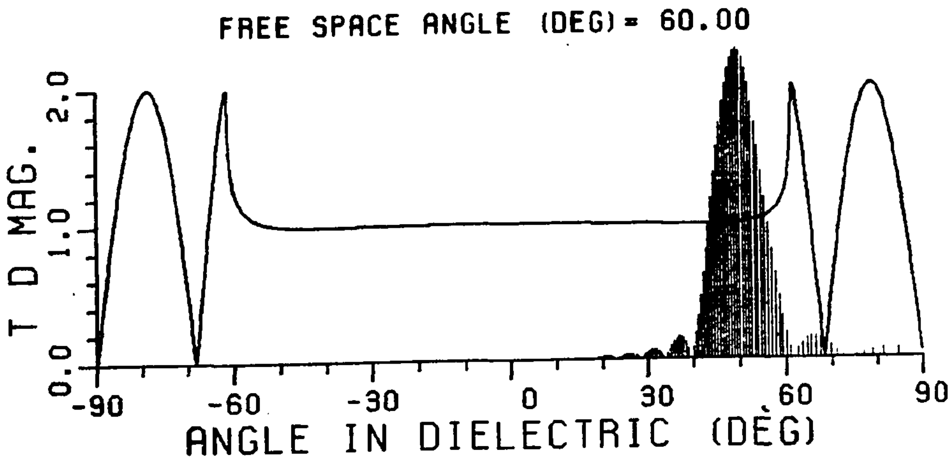

Figure 49. The denominator of the transformation factor plotted with the spectrum of array D2 scanned at 60° as a function of scan angle in the dielectric.

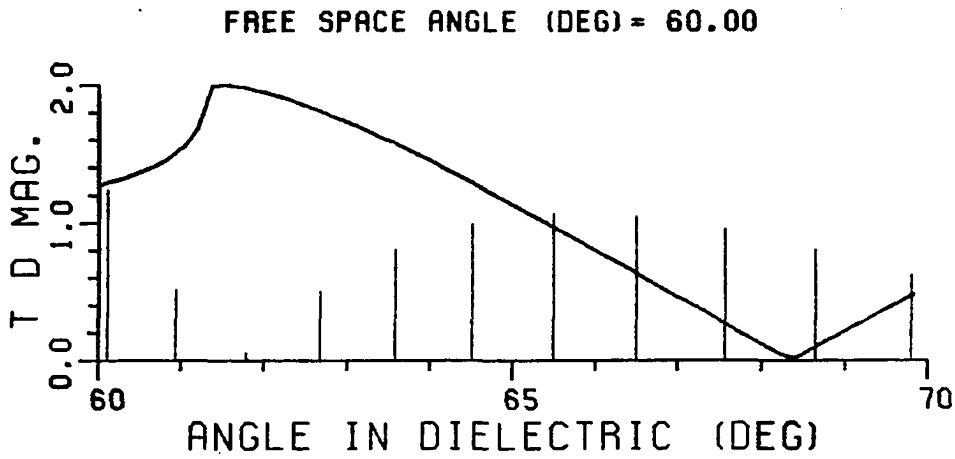

Figure 50. Expanded view of the denominator of the transformation factor plotted with the spectrum of array D2 scanned at 60° as a function of scan angle in the dielectric.

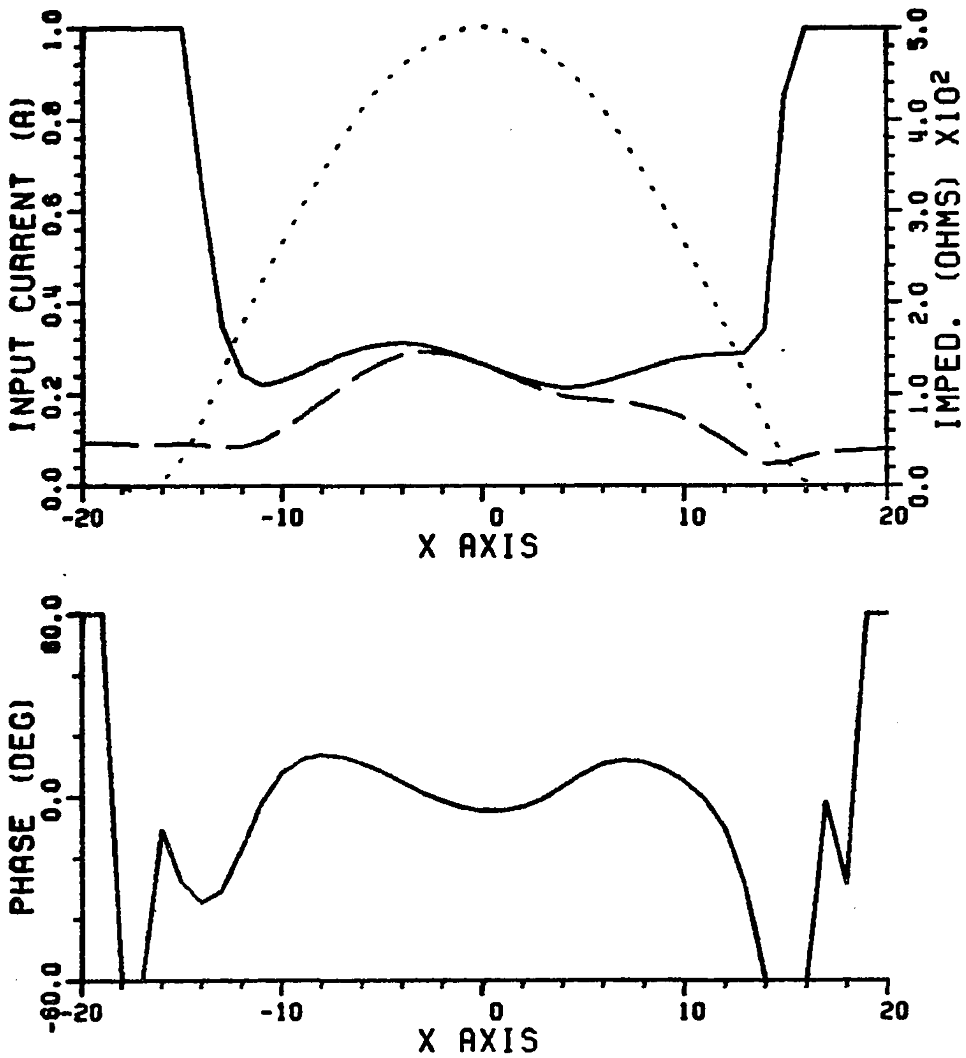

IX	IZ	KX	KZ	NX	NZ
349	349	31	31	60	0

ALPHA	ETA	DX	DZ
0	60.00	1.316	1.974
FREQ	GP	EPSILON	D2
0.0	NO	1.3	0.987

DIPOLES

.... CURRENT

— — — VOLTAGE

——— IMPED.

Figure 51. Expanded view of the impedance for array D2 at a 60^{0} scan angle to the right with a cosine distribution of the input current.

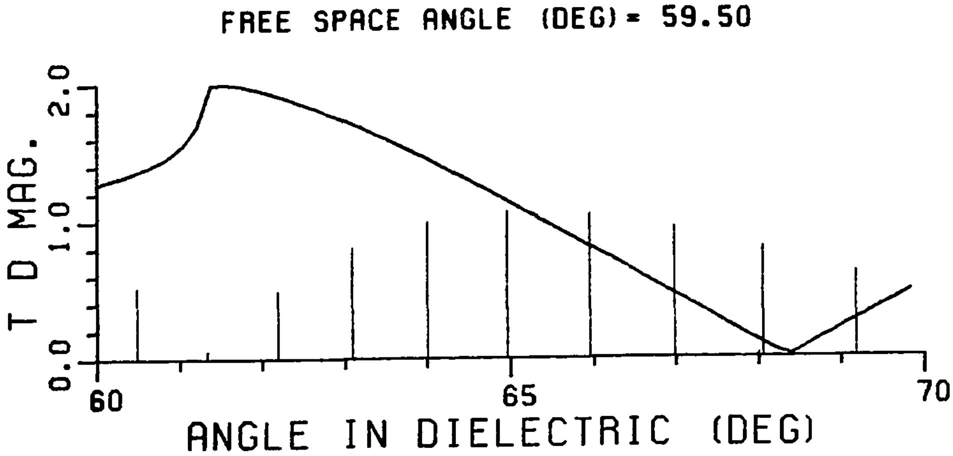

Figure 52. Expanded view of the denominator of the transformation factor plotted with the spectrum of array D2 scanned at 59.50° as a function of scan angle in the dielectric.

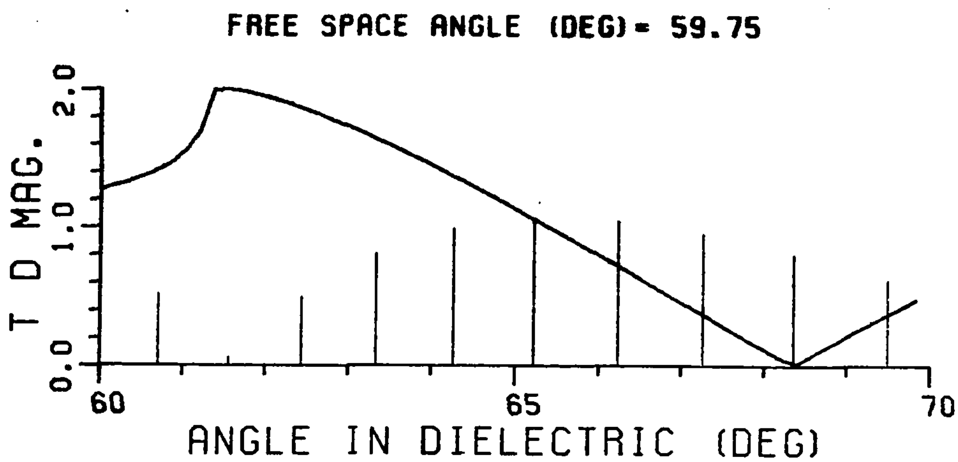

Figure 53. Expanded view of the denominator of the transformation factor plotted with the spectrum of array D2 scanned at 59.75° as a function of scan angle in the dielectric.

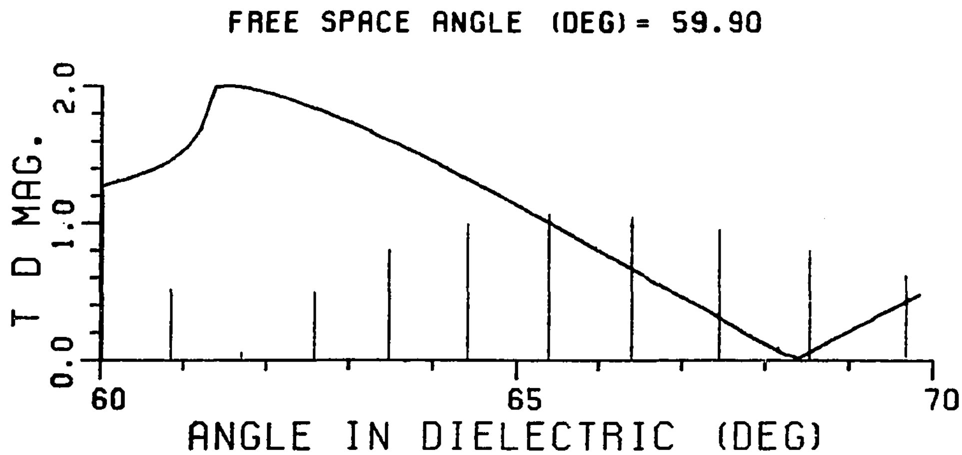

Figure 54. Expanded view of the denominator of the transformation factor plotted with the spectrum of array D2 scanned at 59.9° as a function of scan angle in the dielectric.

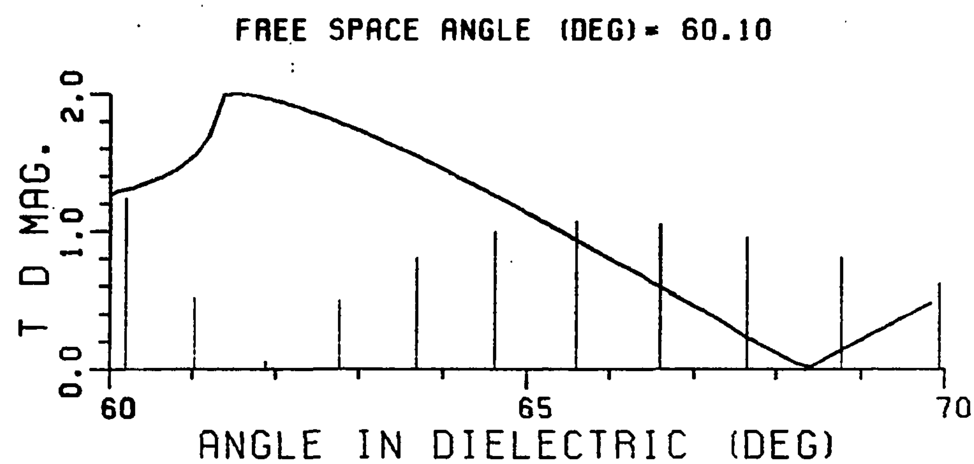

Figure 55. Expanded view of the denominator of the transformation factor plotted with the spectrum of array D2 scanned at 60.1° as a function of scan angle in the dielectric.

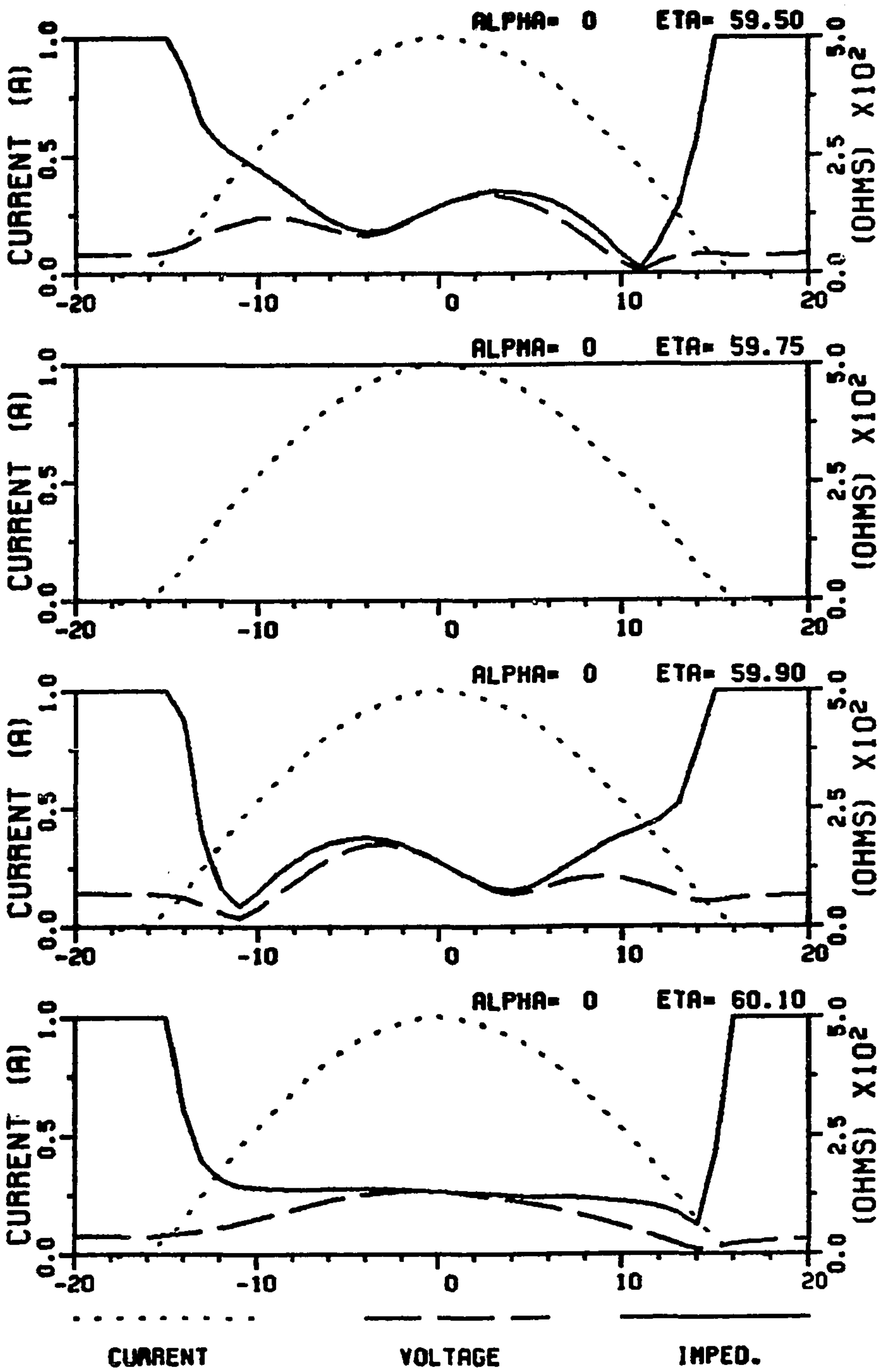

Figure 56. The impedance of array D2 at four scan angles in the x-y plane with a cosine input current. The array scans to the right.

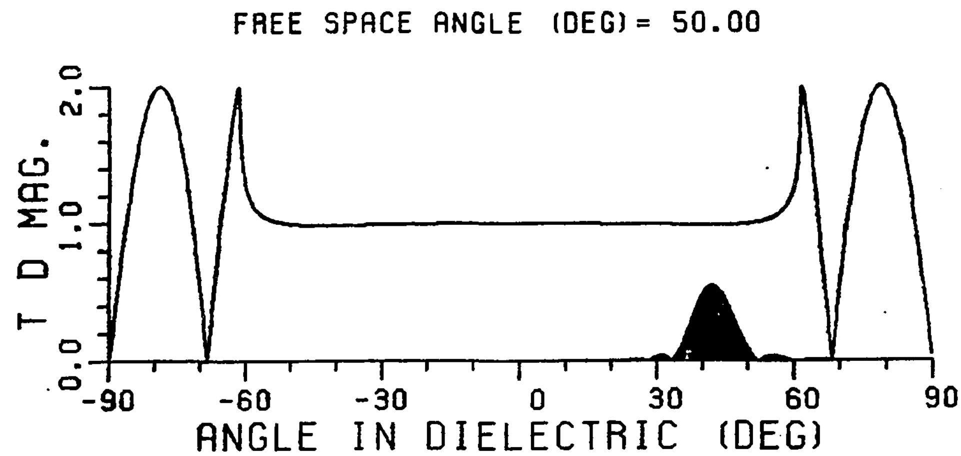

Figure 57. The denominator of the transformation factor plotted with the spectrum of array D2 scanned at 40° as a function of scan angle in the dielectric. The inter-array spacing is 1449 and 180 Fourier terms are used.

with i_x being 1449 and 180 Fourier terms plotted with the denominator of the transformation factor. The expanded view of this plot between 60^o and 70^o is given in Figure 58. It is extremely important that more terms be used in the neighborhood of this singularity. Figures 59 and 60 show the magnitude and phase, respectively, of the entire transformation factor, which again, the position of the critical angle is at 61.3^o. The important point these plots reveal is the 180^o phase change at the singularity. Larger inter-array spacing and more Fourier terms allows more terms just to the left of the singularity and more terms just to the right of it. This closer spacing will allow greater cancellation of the effect of any one single term and allow the impedance to behave as it should as the angle is incrementally changed. Figure 61 gives the impedance plot for the 50^o scan angle. Comparison with Figure 42 shows that this increase in the period is useful in achieving expected behavior. Figure 62 gives impedance results for four scan angles near 50^o.

Figure 63 gives the 60^o results for i_x being 1449 and Figure 64 gives results for four angles near 60^o. The 59.9^o scan angle still has one term very near the singularity so it gives impedance values much larger than they should be. Increasing i_x to 1849 and plotting the results at these four angles, as in Figure 65, eliminates the occurance of one term's being near the singularity and thereby returns expected behavior.

In summary, it is important to have as many terms near the singularity as possible to allow terms to the left of it (-90^o phase) to have cancellation effect upon those of the right of it (90^o phase). This is achieved by increasing the inter-array spacing and number of Fourier terms to much larger values than were necessary in the free space examples presented earlier (which had no transformation factor to deal with). The above results show that expected impedance values can be achieved if none of the Fourier terms correspond to scan angles too near the singularity. If this occurs i_x should be adjusted to separate the singularity from the problem term. In the limit of infinite period size there will be so many terms near the singularity that no single term will dominate.

3. Dipole array in a dielectric slab over a ground plane

The present method can be applied to array D3 and the geometry shown in Figure 66. The transformation factor is taken from Equation (74) with the reflection coefficient at the ground plane set to -1. The transformation factor is now

$$_{(\perp\parallel)}T_2 = \frac{(1-e^{-j2\beta_2 d_2 r_{2y}})(1 + {}_{(\perp\parallel)}^{E}\Gamma_{2,1} e^{-j2\beta_2 d_2 r_{2y}})}{1 + {}_{(\perp\parallel)}^{E}\Gamma_{2,1}\, e^{-j\beta_2 d_2 r_{2y}}} \qquad (93)$$

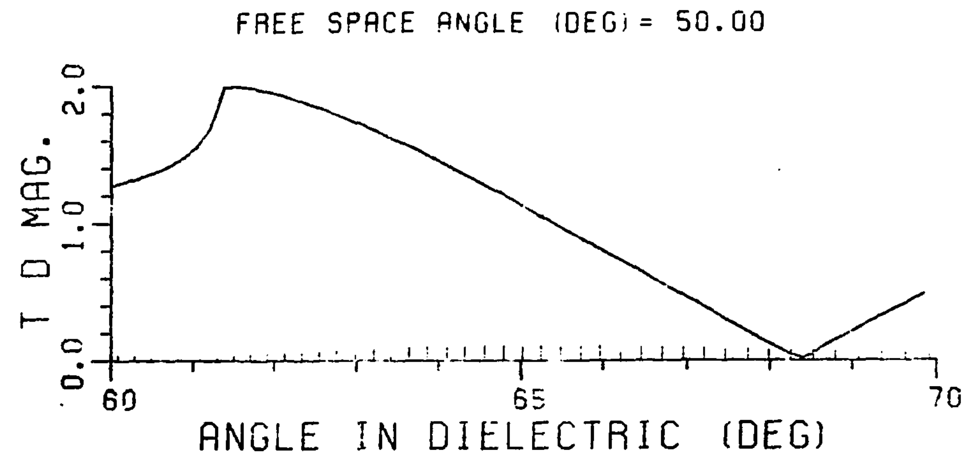

Figure 58. Expanded view of the denominator of the transformation factor plotted with the spectrum of array D2 scanned at 40^{0} as a function of scan angle in the dielectric. The inter-array spacing is 1449 and 180 Fourier terms are used.

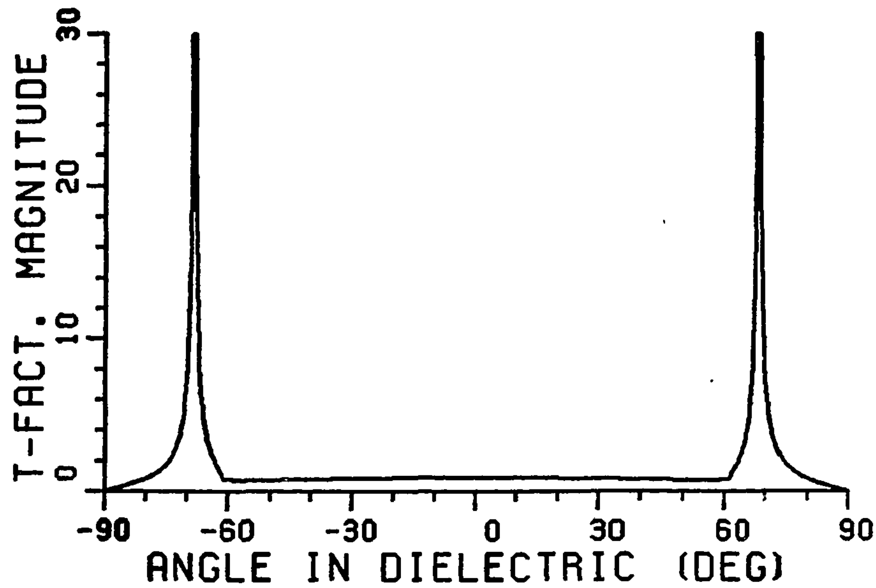

Figure 59. The magnitude of the total transformation factor as a function of scan angle in the dielectric.

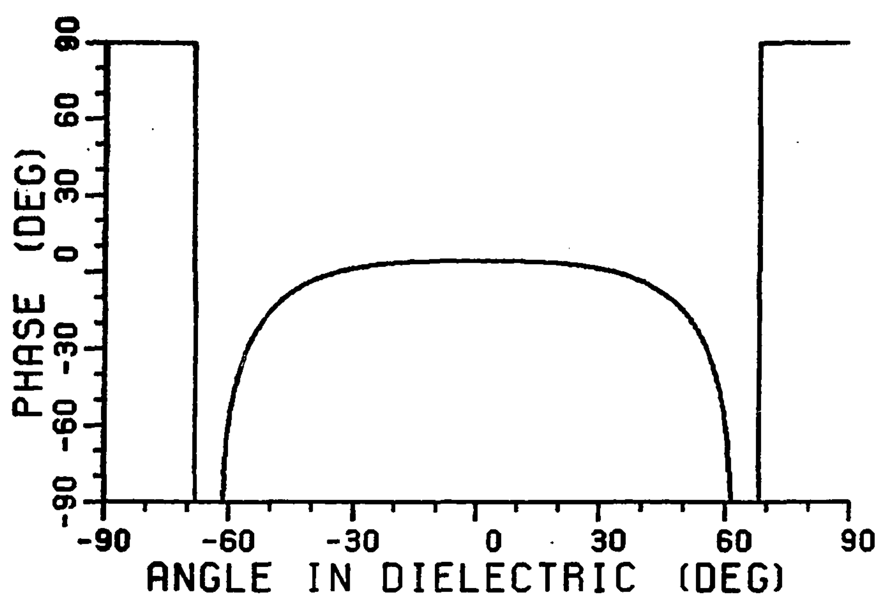

Figure 60. The phase of the total transformation factor as a function of scan angle in the dielectric.

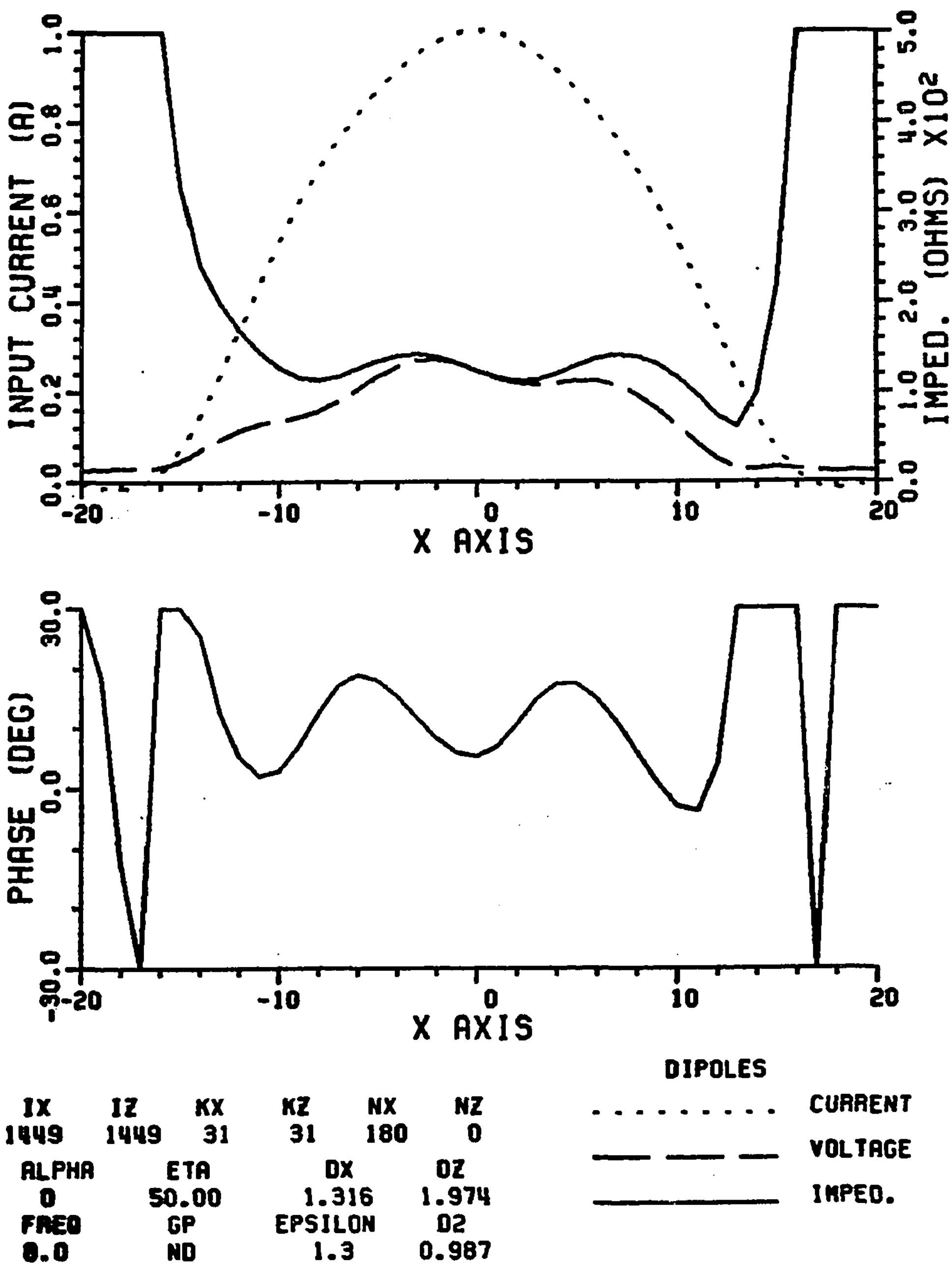

Figure 61. Expanded view of the impedance for array D2 at a 50^{0} scan angle to the right with a cosine distribution of the input current. The inter-array spacing is 1449.

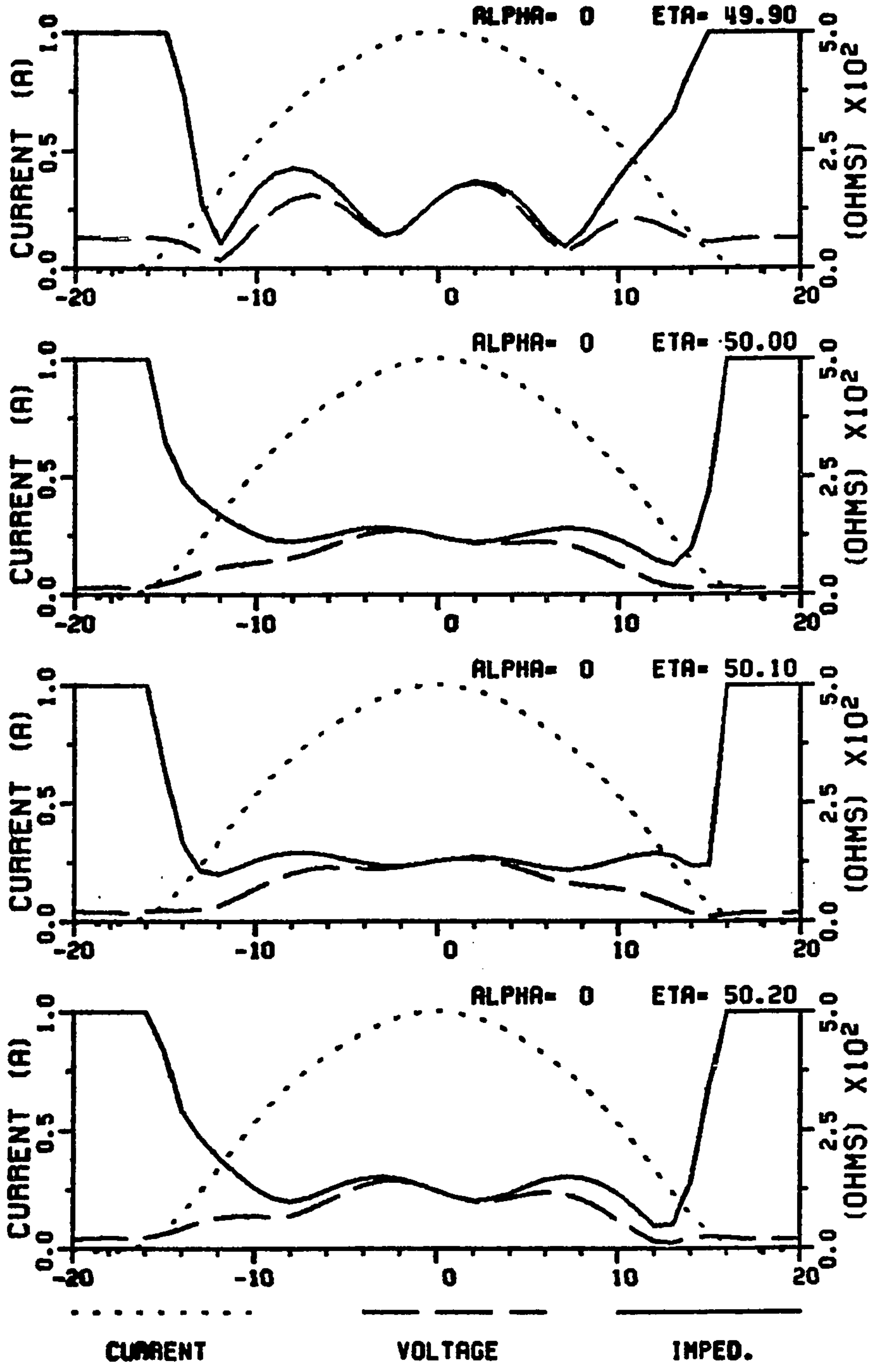

Figure 62. The impedance of array D2 at four scan angles in the x-y plane with a cosine input current. The array scans to the right. The inter-array spacing is 1449.

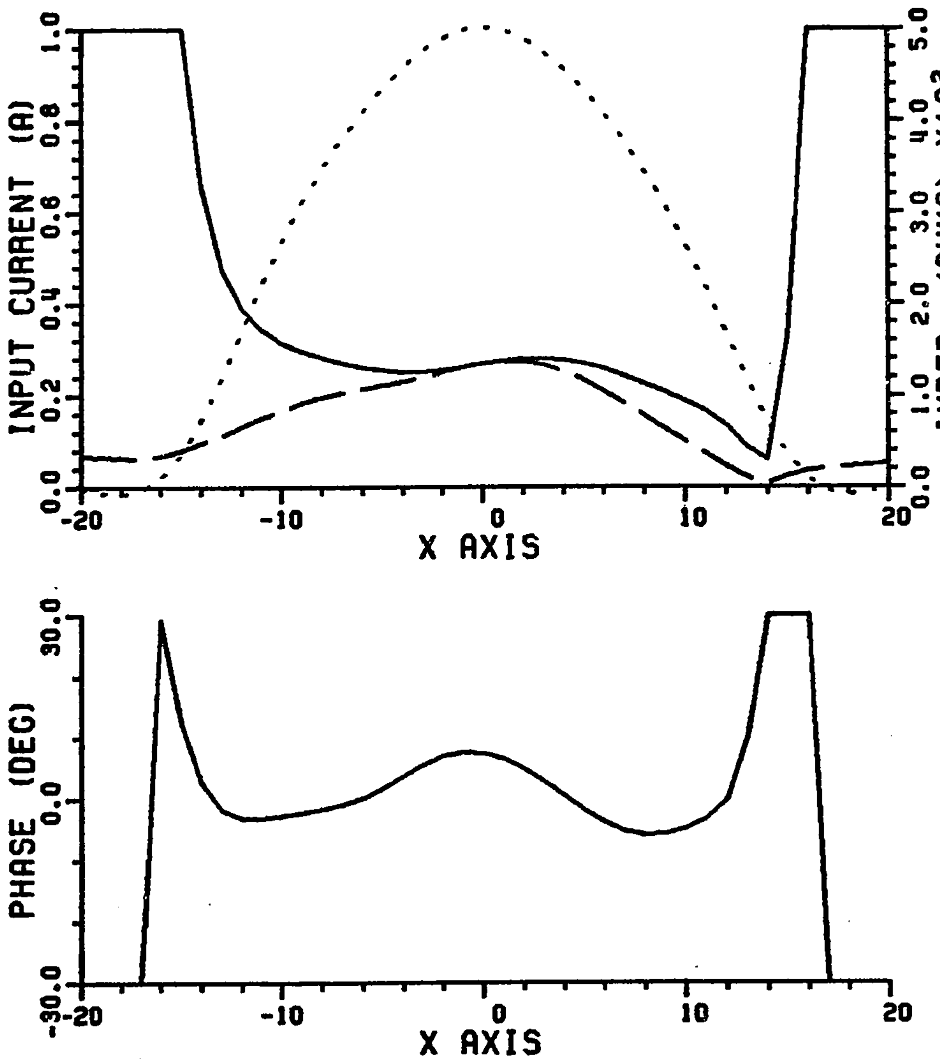

IX	IZ	KX	KZ	NX	NZ
1449	1449	31	31	180	0

ALPHA	ETA	DX	DZ
0	60.00	1.316	1.974
FREQ	GP	EPSILON	D2
8.0	NO	1.3	0.987

DIPOLES

Line	Quantity
. . . .	CURRENT
— — —	VOLTAGE
———	IMPED.

Figure 63. Expanded view of the impedance for array D2 at a 60^{0} scan angle to the right with a cosine distribution of the input current. The inter-array spacing is 1449.

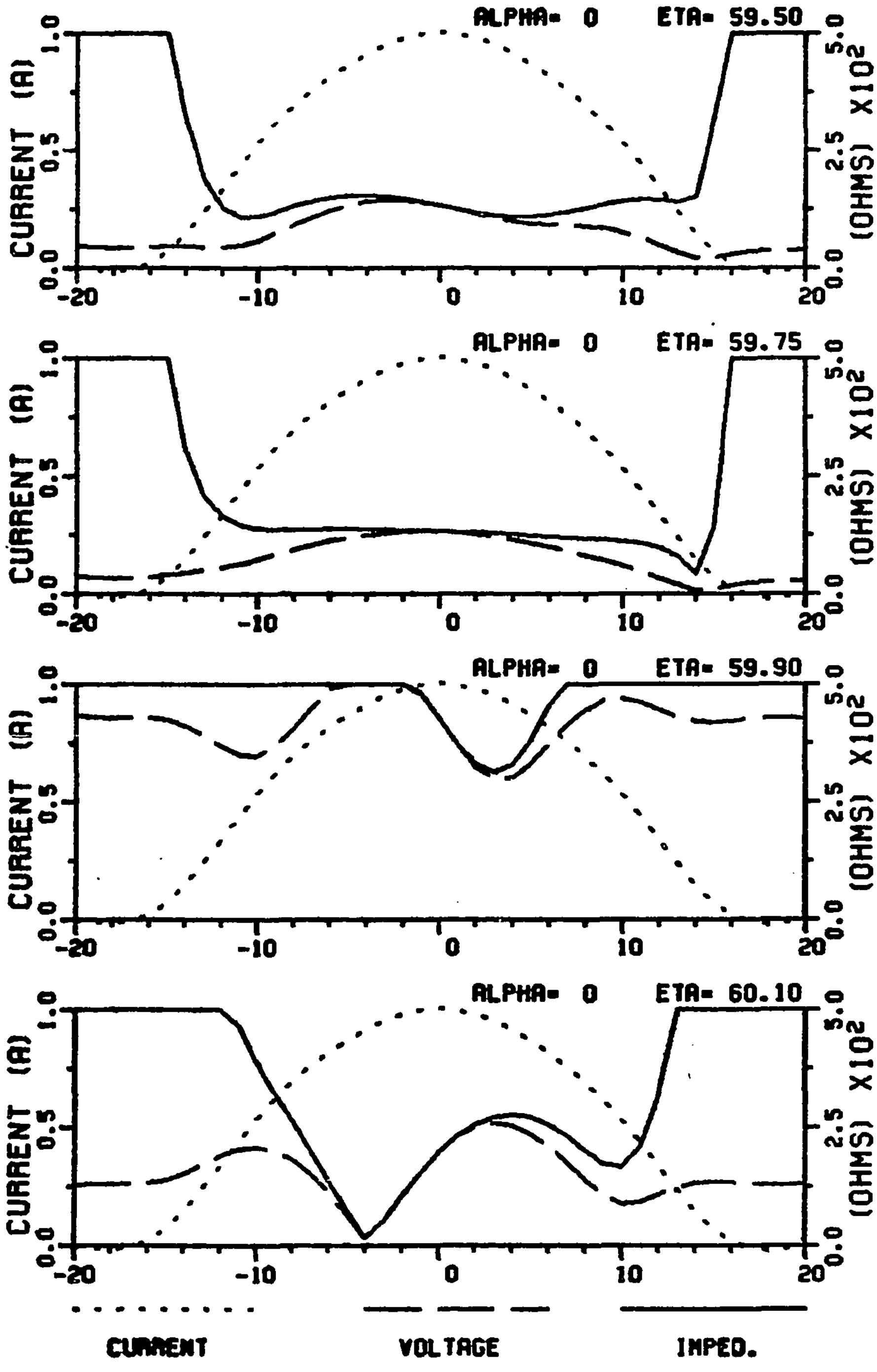

Figure 64. The impedance of array D2 at four scan angles in the x-y plane with a cosine input current. The array scans to the right. The inter-array spacing is 1849.

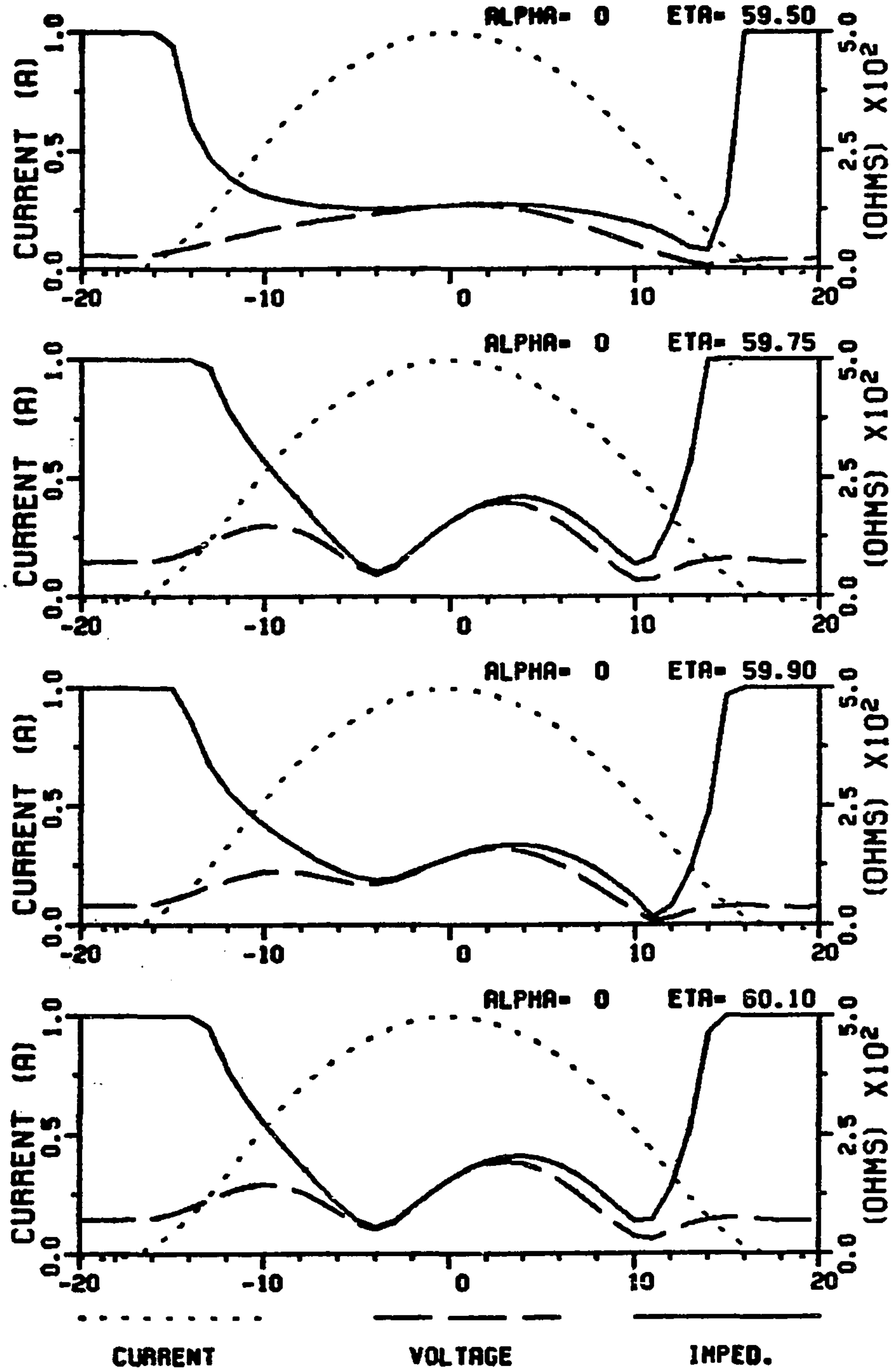

Figure 65. The impedance of array D2 at four scan angles in the x-y plane with a cosine input current. The array scans to the right. The inter-array spacing is 1849.

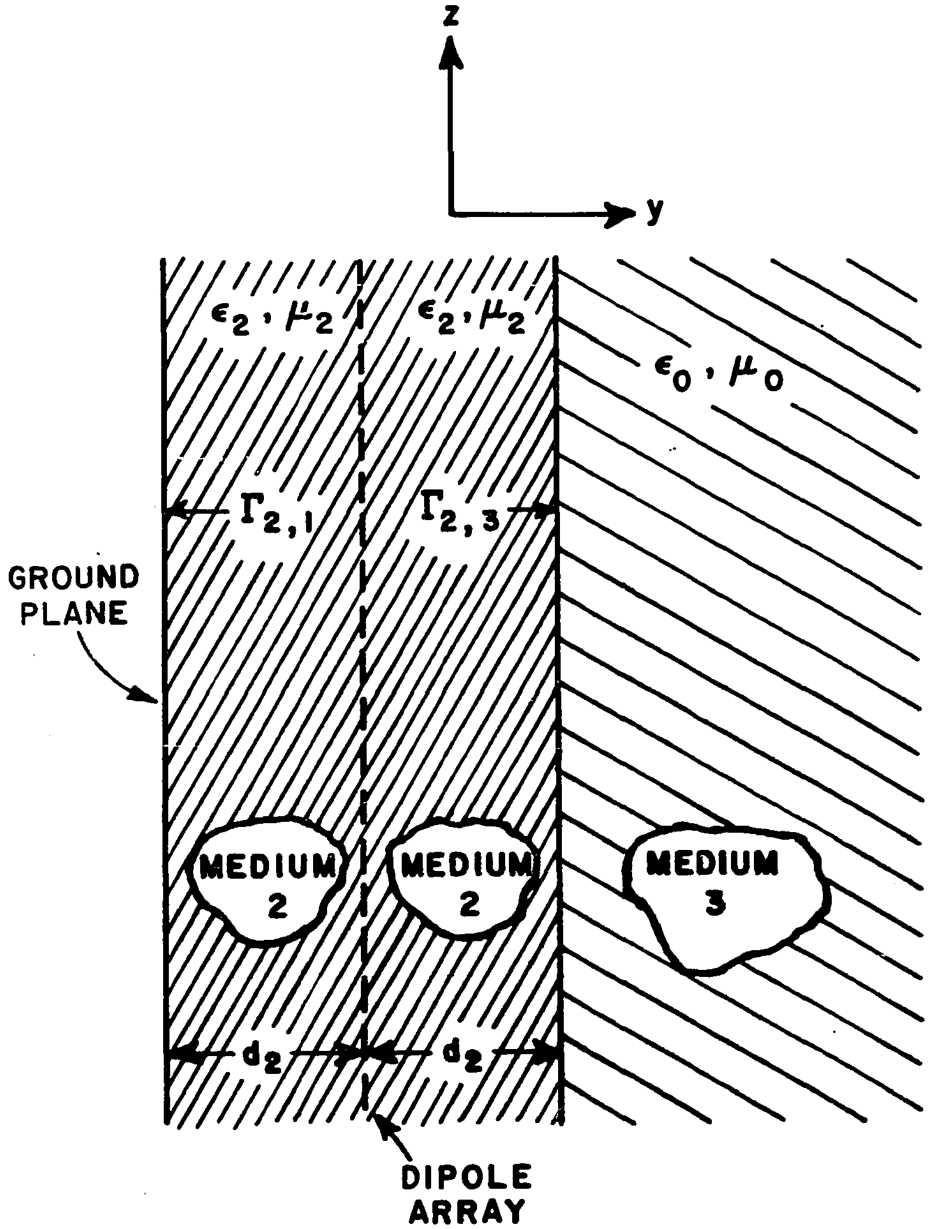

Figure 66. Geometry of array D3. The array is in the center of a dielectric slab with a relative dielectric constant of 1.3. Free space exists to the right of the dielectric slab and a ground plane exists to the left.

Equations (86) and (87) still apply as the expressions for Ω and the impedance at each element. Array D3 is modeled at the same frequency and with the same geometry as array D2. The addition of the ground plane at the edge of the dielectric is the only change. The array parameters are given in Table I.

The impedance at four scan angles is shown in Figure 67. Nothing remarkably different occurs, even at the 50^o scan. Although it appears as if the transformation factor does not have a singularity here, it just happens that none of the Fourier terms are sufficiently near the singularity at these scan angles. Figure 68 shows the transformation factor denominator for this geometry, with the spectrum for a 40^o scan. Figures 69 and 70 give an expanded view of the denominator between 60^o and 70^o for 40^o and 50^o scans, respectively. The data was calculated with i_x being 1049 and 180 Fourier terms and the 50^o data was calculated with i_x of 1449 and 180 Fourier terms so both scan angles would have ample terms in the neighborhood of the singularity. None of the terms for these two scans are sufficiently near the singularity to cause the behavior seen earlier. Even the 50^o data appears to have one Fourier term coincident with the singularity but no unusual behavior is encountered. An attempt was made to find a scan angle with this geometry which would have large variations in its values but none could be found. The singularity for this geometry must be of such a nature that it is much more difficult for the singularity to have effect than for the examples seen earlier of the dielectric coated dipole array with no ground plane to one side.

4. Slot array in a dielectric slab

The present method can be applied to an array of slots in a ground plane as in the geometry of Figure 16. This is the geometry to the right of the array and Equation (80) is the expression for the admittance looking to the right, where Equation (76) is still the expression for Ω and Equation (79) is the new expression for the transformation factor which is

$$_{(\perp'')}T_2 = 2 \times \frac{1 + {}_{(\perp'')}^{H}\Gamma_{2,1}\, e^{-j2\beta_2 d_2 r_{2y}}}{1 - {}_{(\perp'')}^{H}\Gamma_{2,1}\, e^{-j2\beta_2 d_2 r_{2y}}} \tag{94}$$

The admittance is the sum looking to the left and to the right. This one-dimensional slot array, array S1, is modeled at 8 GHz with d_2, the dielectric thickness of each side, being 0.987 cm. The relative dielectric constant is 1.3. The slots are 1.644 cm long, 0.0877 cm wide, and the ground plane is 0.00877 cm thick. Dx and Dz, the inter-element spacings, are 1.316 cm and 1.974 cm, respectively.

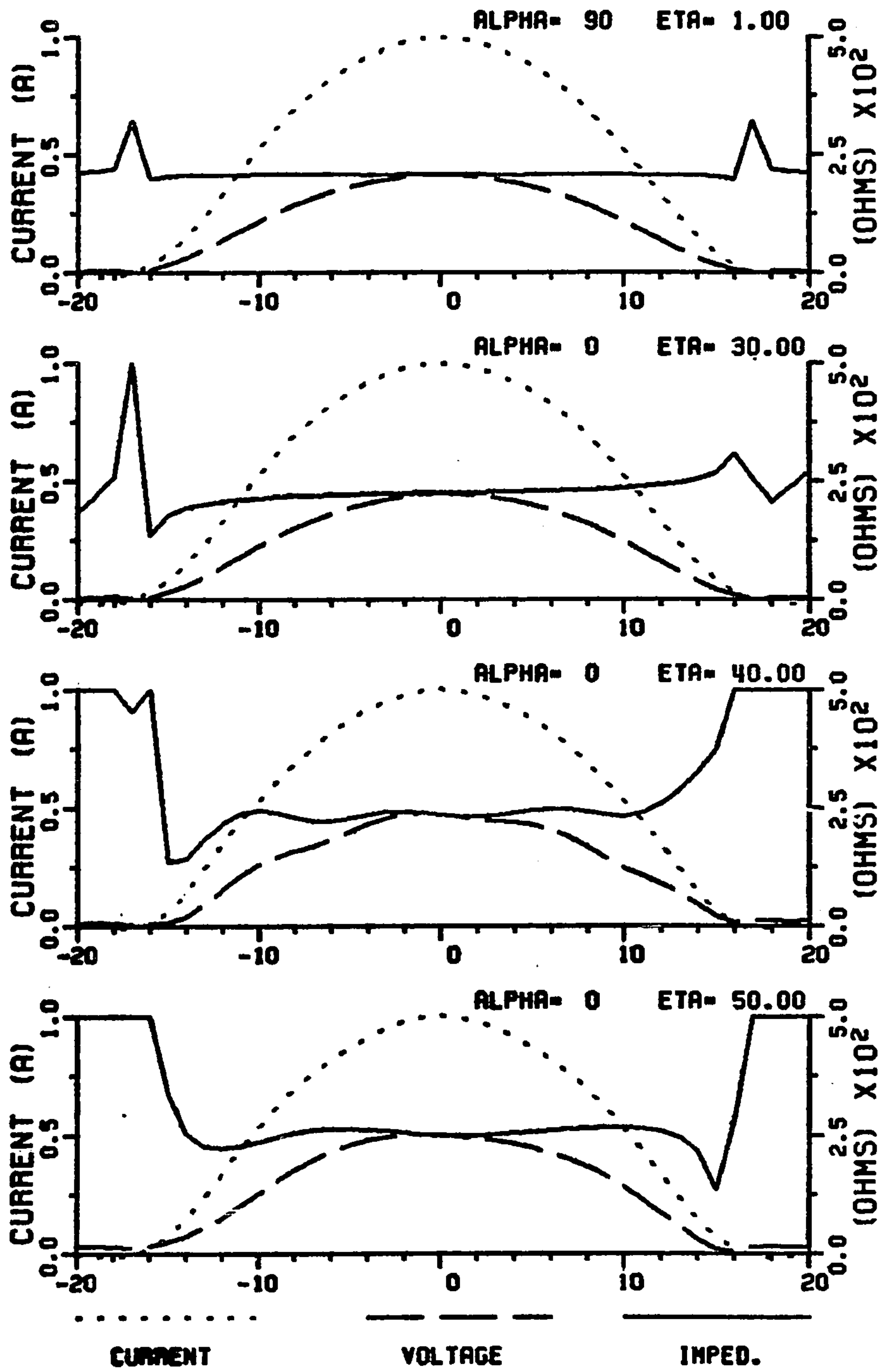

Figure 67. The impedance of array D3 at four scan angles in the x-y plane with a cosine input current. The array scans to the right.

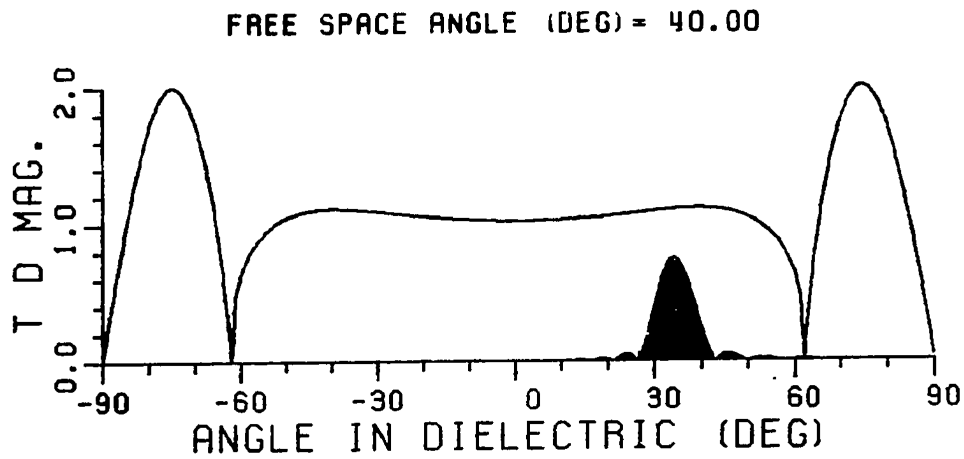

Figure 68. The denominator of the transformation factor plotted with the spectrum of array D3 scanned at 40° as a function of scan angle in the dielectric.

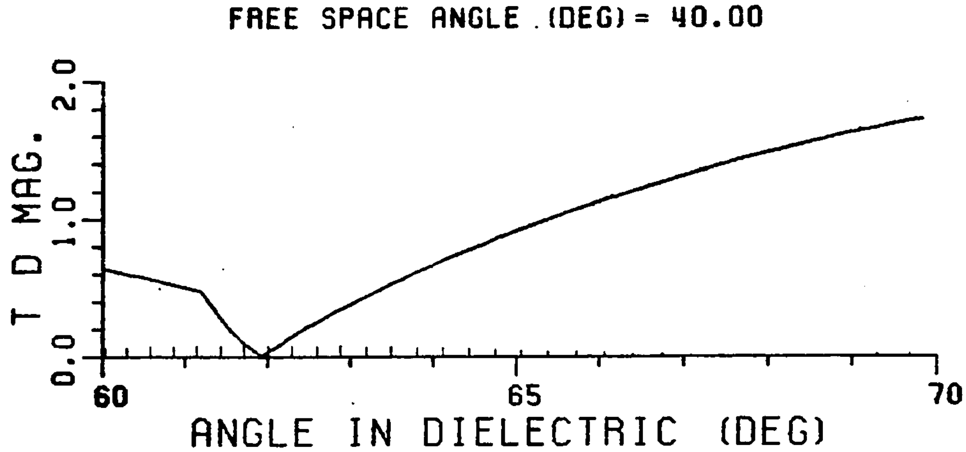

Figure 69. Expanded view of the denominator of the transformation factor plotted with the spectrum of array D3 scanned at 40° as a function of scan angle in the dielectric.

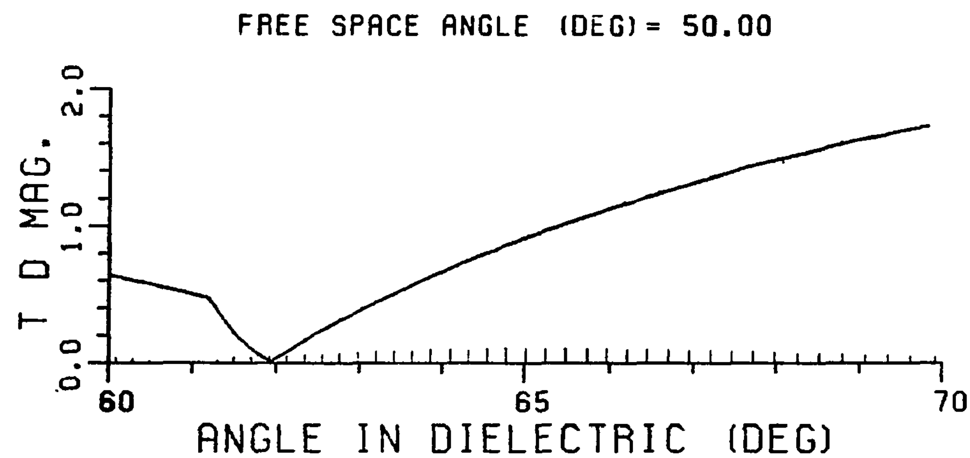

Figure 70. Expanded view of the denominator of the transformation factor plotted with the spectrum of array D3 scanned at 50^{0} as a function of scan angle in the dielectric.

The array parameters are given in Table I. 180 Fourier terms are used and i_x, the inter-array spacing, is 1049 for all scan angles presented here except for the 50^o angle where it is increased to 1449 to insure enough terms being near the singularity of the transformation factor (whose denominator is examined carefully in section 2 of Appendix F).

Figure 71 gives the admittance results for the broadside scan. The voltage input into the slots is given as the dotted line, the resulting current is the dashed line, and the admittance in millimhos is the solid line. Figure 72 shows the admittance at broadside and three other scan angles. Their values are nearly constant across the aperture except for the 40^o case. Figure 73 shows the transformation factor denominator as a function of scan angle in the dielectric and the spectrum for the 40^o scan. Figures 74 and 75 show the expanded plots between 60^o and 70^o (the size of the spectral lines have been increased to aid in visibility). Evidently one of the terms for the 40^o scan is sufficiently near the singularity to cause some problems. Finding a scan angle where the admittance did not behave as expected was difficult but Figure 76 indicates that a 40.28^o angle should cause some problems. Figure 77 indicates that this angle is affected by the singularity. In general, for this geometry, the results are as expected if sufficient terms are used near the transformation factor singularity.

C. Two-dimensional Results

This section extends the results from one to two dimensions and arrays of the geometry of Figure 8. Kx and Kz are both kept at 31 in this section so an array with 961 elements is being modeled. Cosine distributions in both directions are used exclusively to keep Nx and Nz, the number of Fourier terms in each direction, as small as possible. The z-direction inter-array spacing, i_z, is 349 in all examples here. It can be kept small because all examples in this section represent scans in the x-y plane. The x-direction inter-array spacing, i_x, is 649 for broadside and 30^o scans. For 60^o scans it is increased to 1149 to insure that an adequate number of terms are in the vicinity of the transformation factor singularity. It is important to keep i_x and i_z as small as possible (and thereby keep Nx and Nz as small as possible) because (2Nx+1)x(2Nz+1) terms must be calculated. Computation time can become significant for the two-dimensional arrays. For this reason the number of examples presented in this section is kept to a minimum. The results do not behave remarkably different from the one-dimensional results so this limitation is not inappropriate.

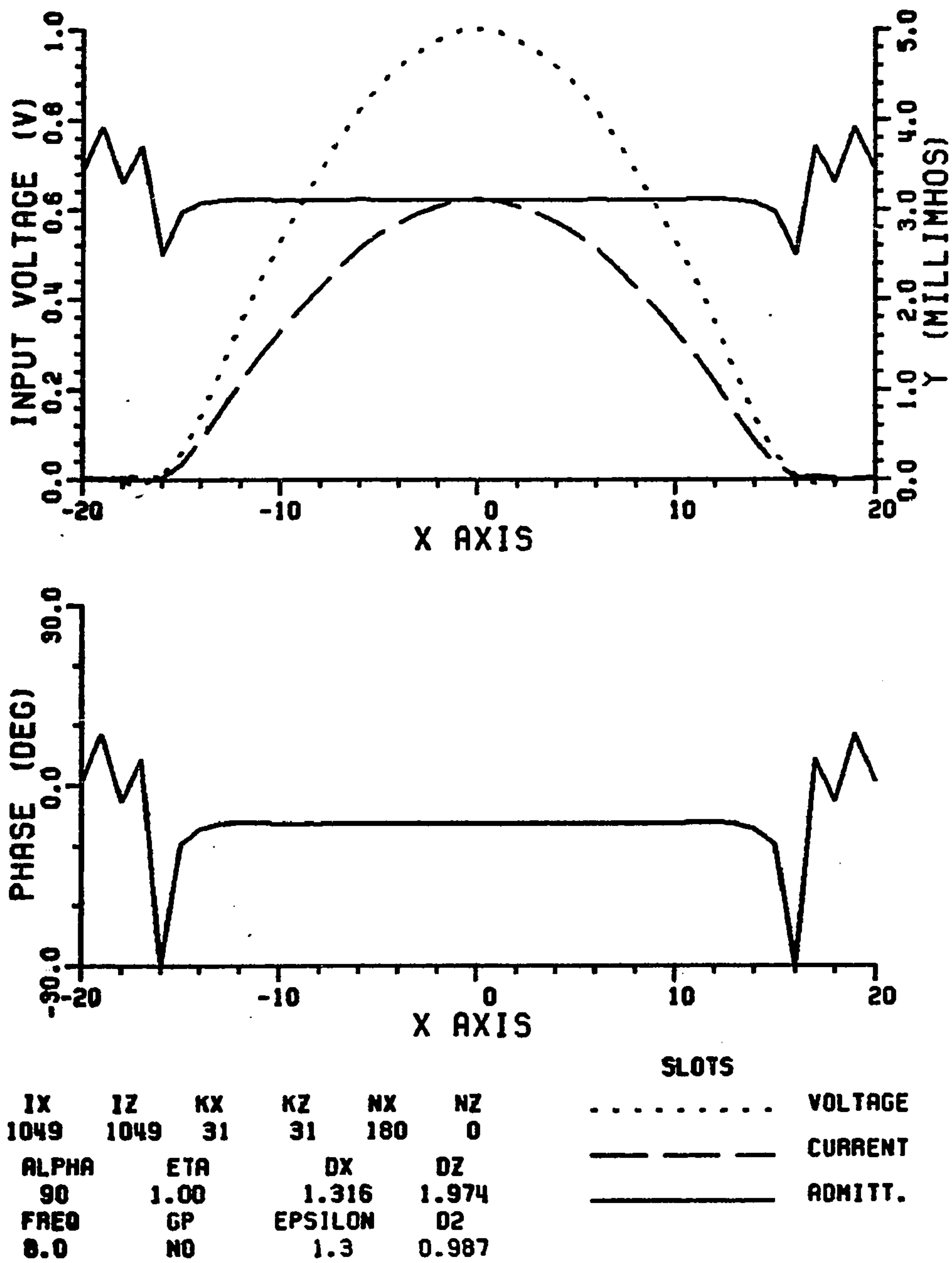

Figure 71. Expanded view of the admittance for array S1 at a broadside scan angle with a cosine distribution of the input voltage.

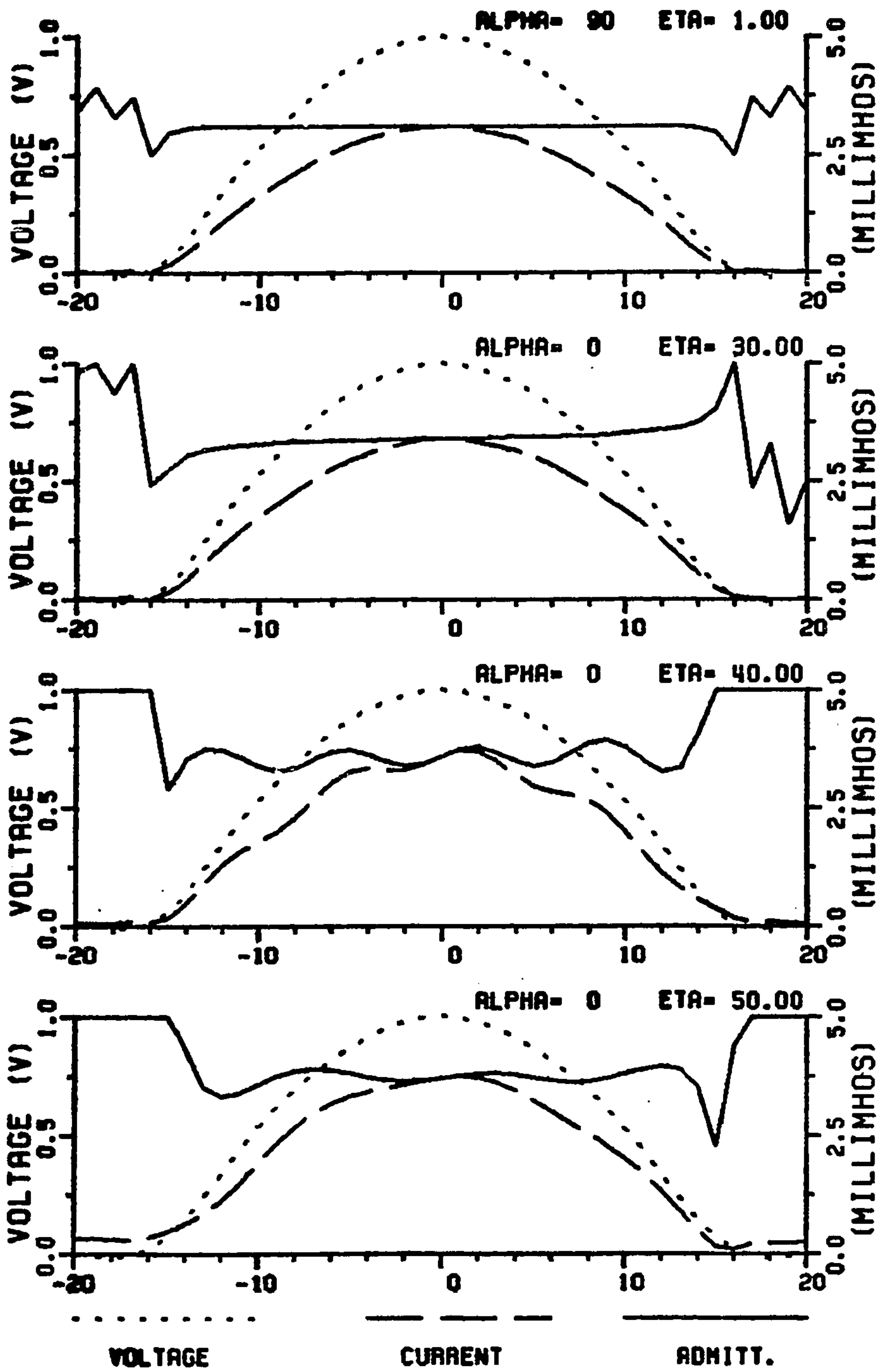

Figure 72. The admittance of array S1 at four angles in the x-y plane with a cosine distribution of the input voltage. The array scans to the right.

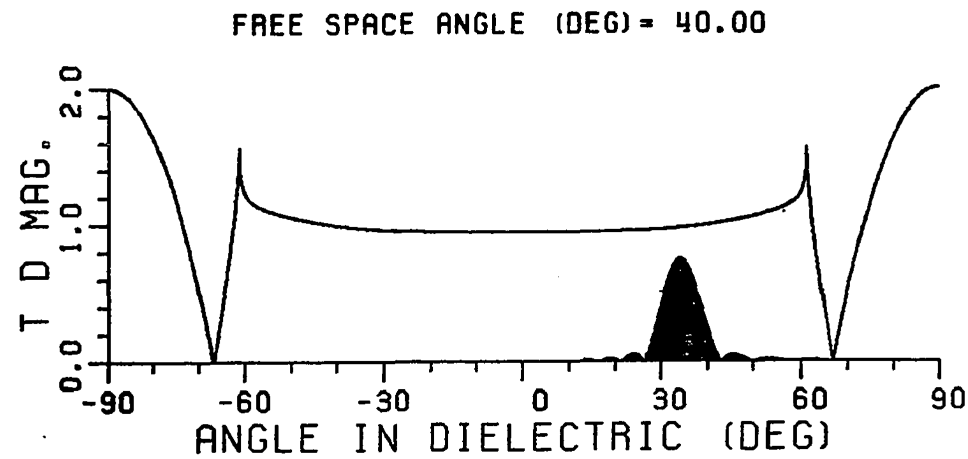

Figure 73. The denominator of the transformation factor plotted with the spectrum of array S1 scanned at 40° as a function of scan angle in the dielectric.

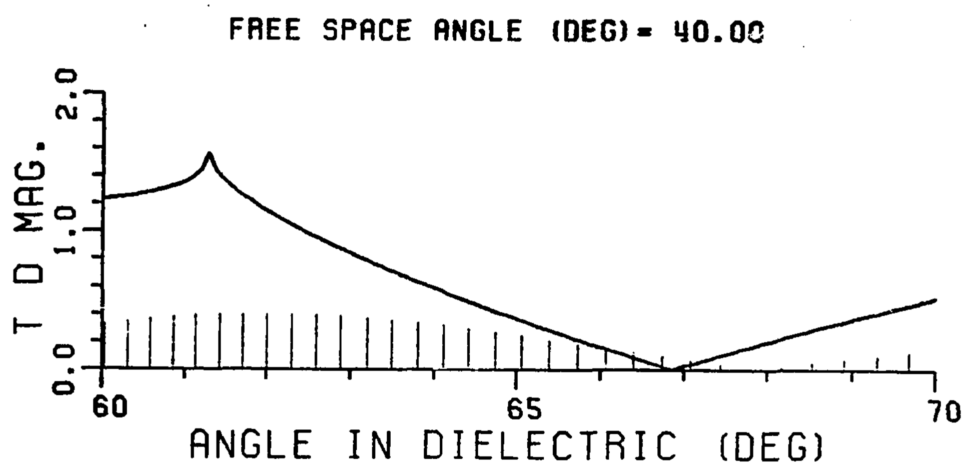

Figure 74. Expanded view of the denominator of the transformation factor plotted with the spectrum of array S1 scanned at 40° as a function of scan angle in the dielectric.

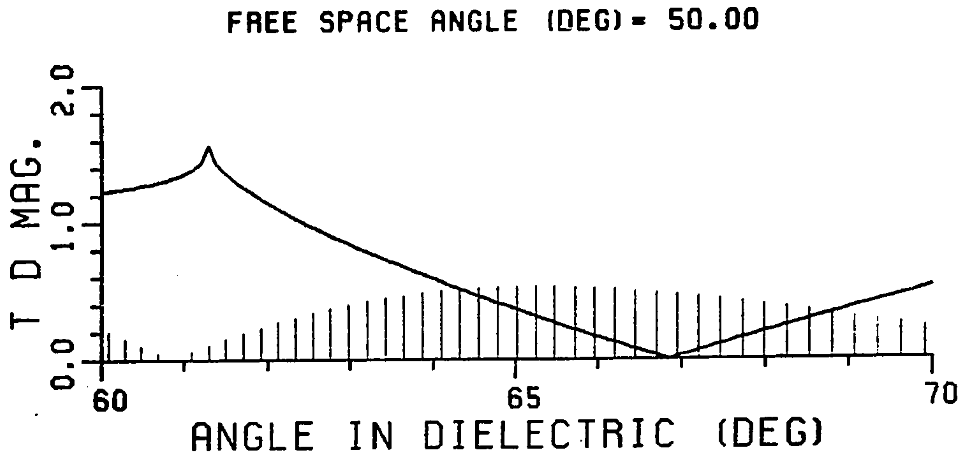

Figure 75. Expanded view of the denominator of the transformation factor plotted with the spectrum of array S1 scanned at 50° as a function of scan angle in the dielectric.

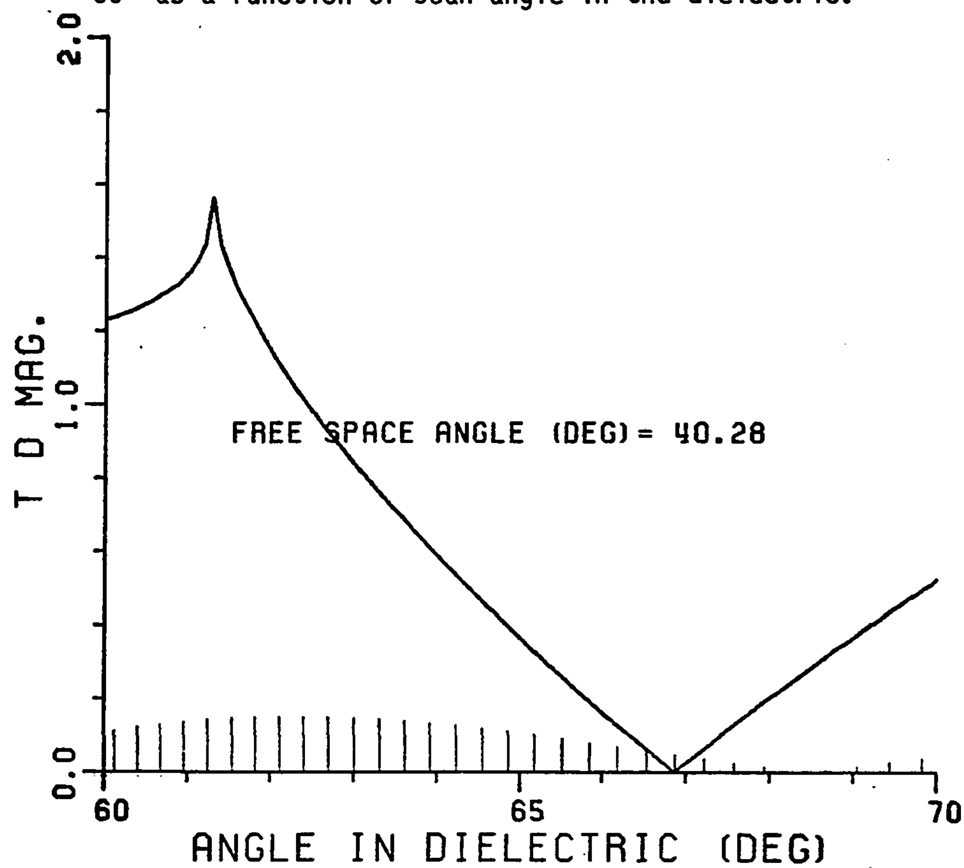

Figure 76. Expanded view of the denominator of the transformation factor plotted with the spectrum of array S1 scanned at 40.28° as a function of scan angle in the dielectric.

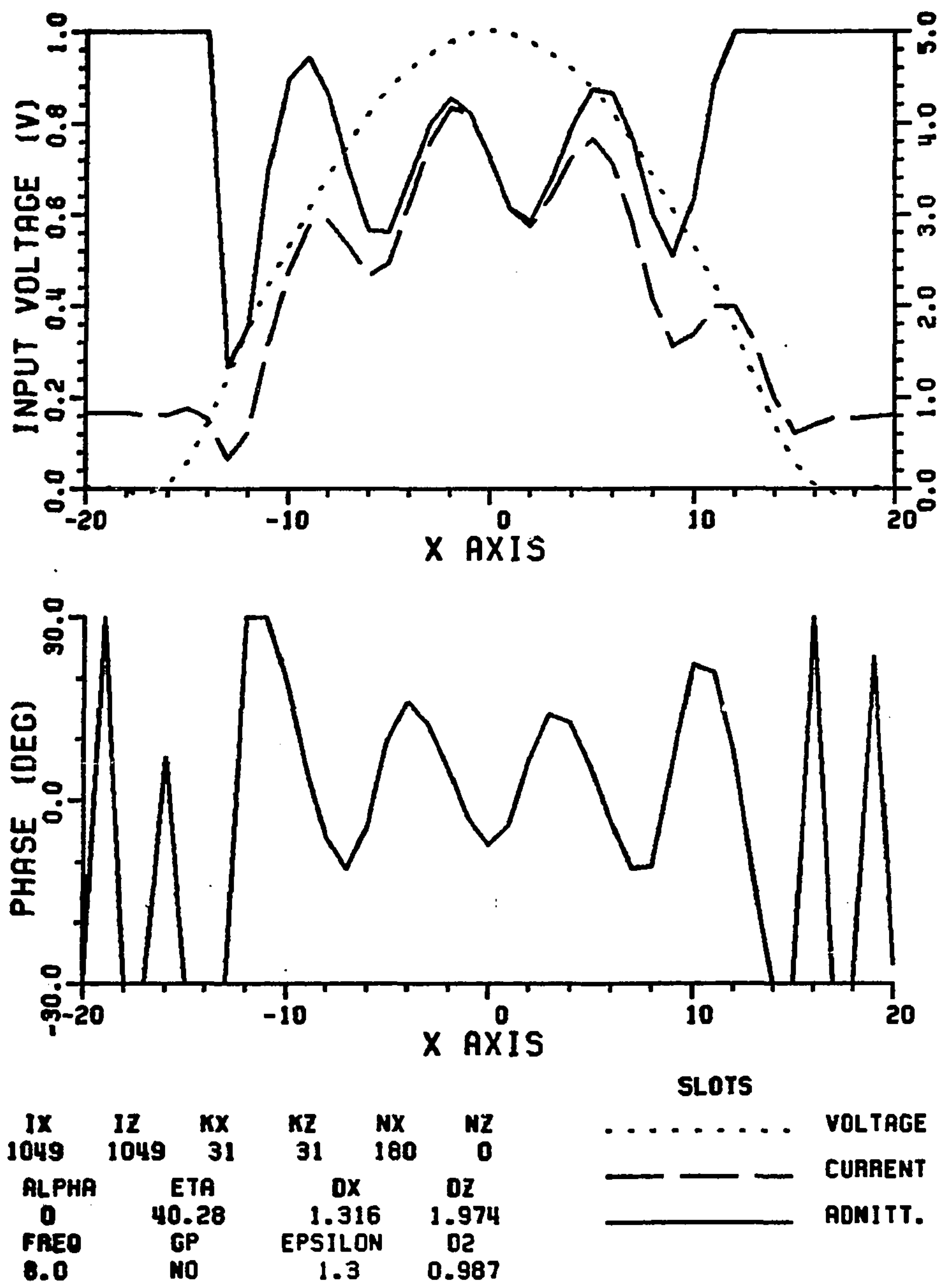

Figure 77. Expanded view of the admittance for array S1 at a 40.28° scan angle with a cosine distribution of the input voltage.

1. Dipole array in a dielectric slab

Array D4 is composed of straight z-directed dipoles in a geometry identical to array D2 (Figure 39) with the exception that array D4 is finite in both the x and z-directions. Table I gives the array parameters. Equation (77) is used to find the impedances at each element with Ω given by Equation (76). The transformation factor is identical to that of array D2, and is given by Equation (85). The array has 31 elements in the x-direction ($-15<q<15$) and 31 elements in the z-direction ($-15<m<15$). Figure 78 shows the ordering of the elements in the x-z plane.

Figure 79 gives the results for broadside scan and the row of elements along the x-axis (n=0,z=0). Figure 80 shows similar results for the rows corresponding to m being 3, 6, 9, and 12. The input current decreases as the two being examined moves along the z-axis, reflecting the cosine input current distribution along the z-axis. Figure 81 shows the impedance plotted along the z-axis (q=0), and Figure 82 shows the impedance plotted along the columns for q being 3, 6, 9, and 12. The impedance is nearly constant for each element in this two-dimensional array at this broadside scan angle.

For the 30° scan angle in the x-y plane Figure 83 gives the impedance for the m=0 row and Figure 84 plots this quantity for m being 3, 6, 9, and 12. Figures 85 and 86 plot along z for q being 0, +6, -6, and -12. Again the impedance has nearly the same value at each element in the array for this 30° scan.

Figure 87 reflects the values of the impedance along the x-axis for a 60° scan in the x-y plane and Figure 88 shows the impedance for rows parallel to the x-axis with m values of 3, 6, 9, and 12. Figure 89 gives the impedance along the z-axis. Examination of Figure 87 reveals large changes in the impedance for the elements from position -14 to -8. This corresponds to q values from -14 to -8. Figure 90 plots the impedances along these columns parallel to z for a values of -14, -12, -10, and -8. The plots are symmetrical with respect to the x-axis (the 0 position on the abscissa) as they should be with scan in the x-y plane. For this larger scan at 60° the impedance is no longer nearly constant over the extent of the two-dimensional array. Figure 91 plots the impedance at four columns parallel to the z-axis at q values of 6, 8, 10, and 12. This 60° data shows the way the impedance can change in a finite array at large scan angles even in directions at which the array is not scanning (i.e., Figure 90 shows variation in the z-direction even when the array is scanning in the x-y plane).

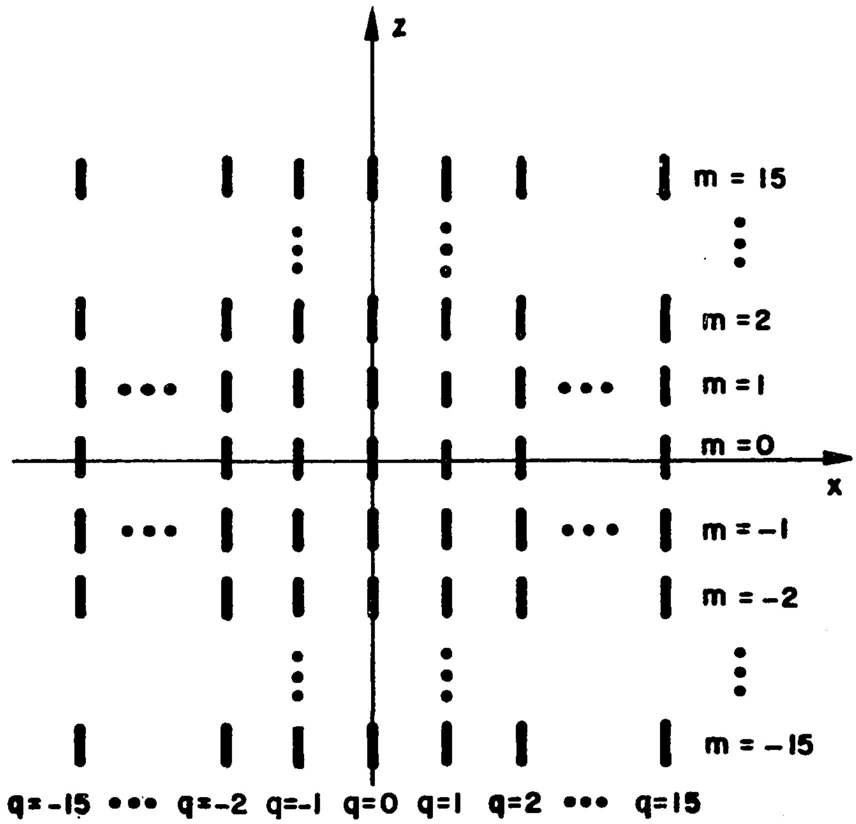

Figure 78. Representation of the finite two-dimensional array showing the ordering of rows parallel to the x-axis $(-15<m<15)$ and columns parallel to the z-axis $(-15<q<15)$.

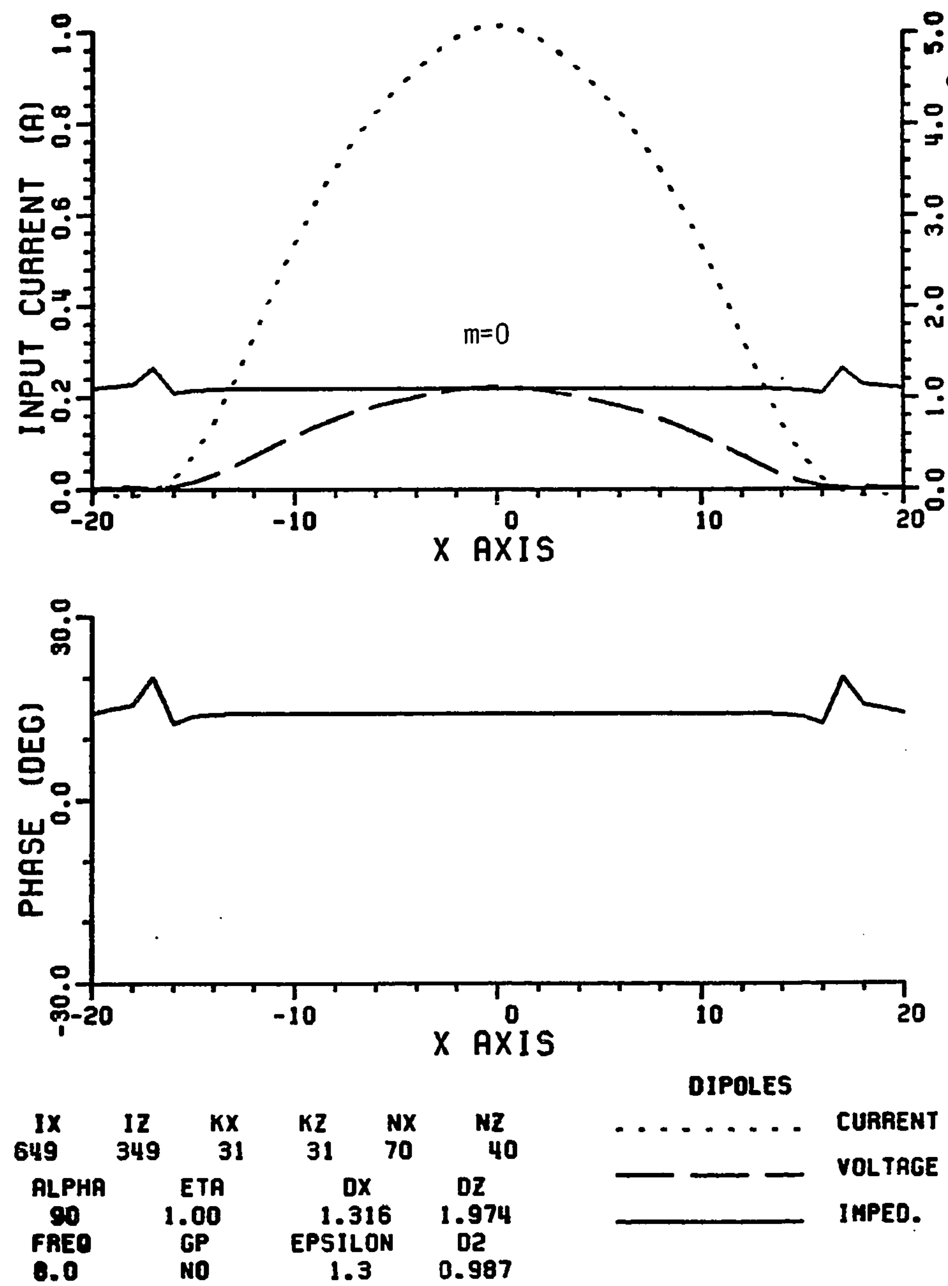

Figure 79. Expanded view of the impedance of array D4 for the m=0 row and a cosine distribution of the input current at a broadside scan angle.

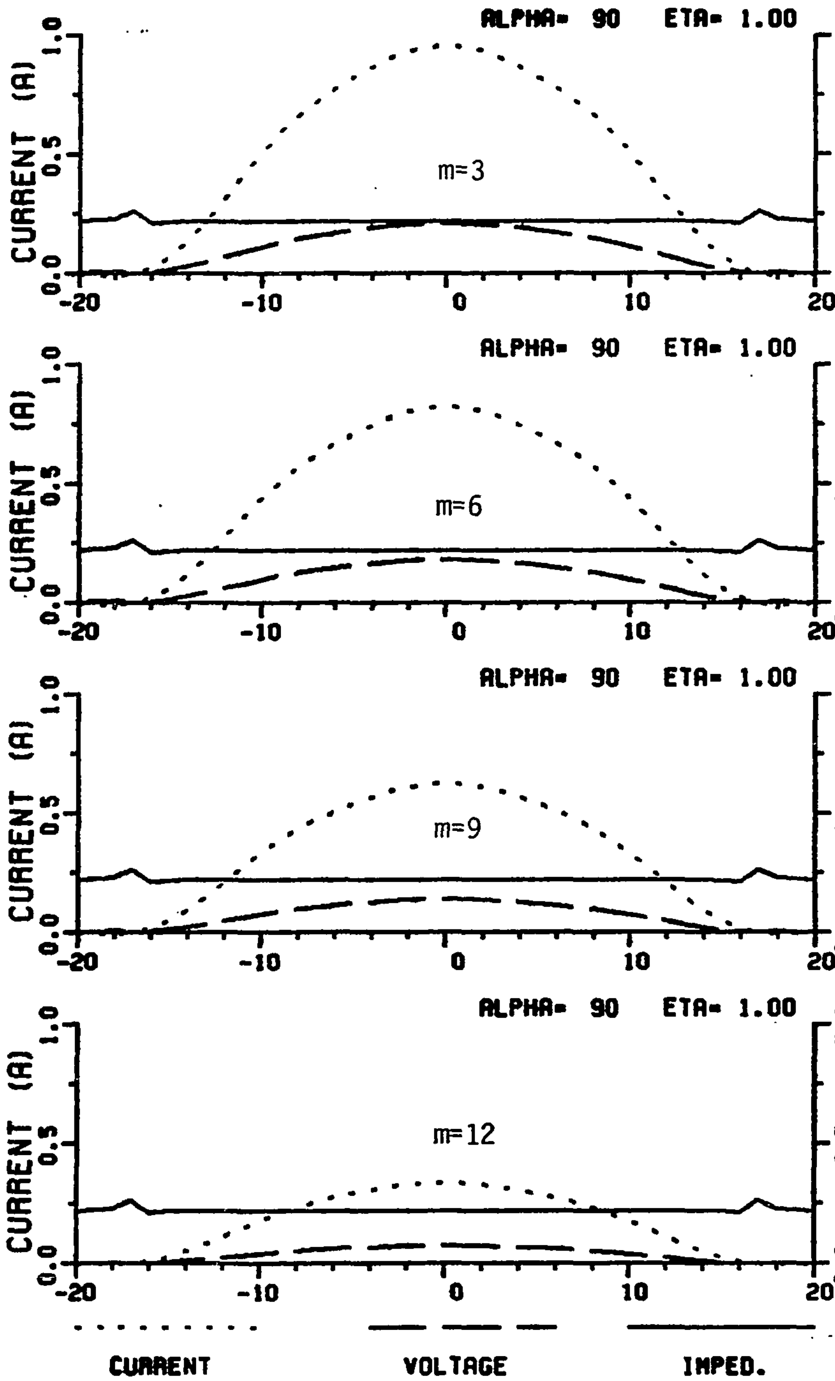

Figure 80. The impedance of array D4 for four rows parallel to the x-axis (m=3,6,9,12) at a broadside scan angle.

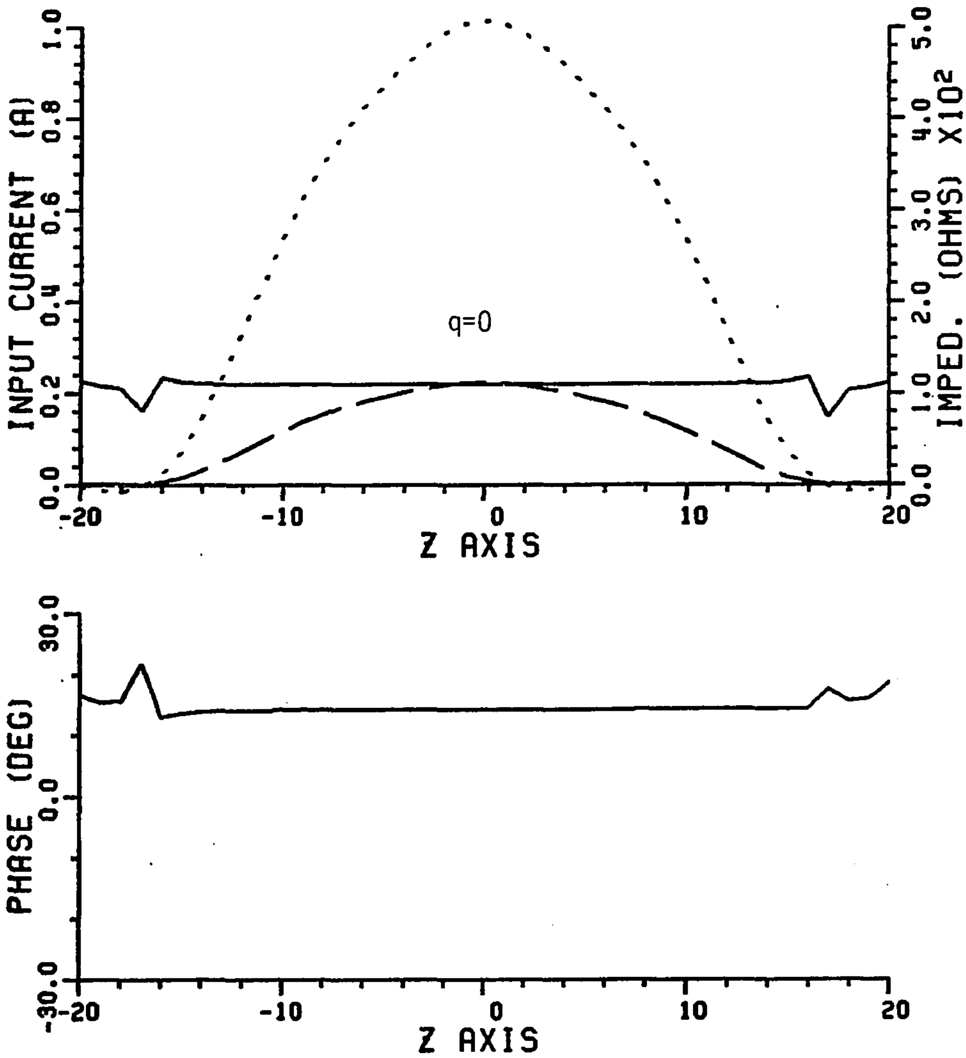

IX	IZ	KX	KZ	NX	NZ
649	349	31	31	70	40

ALPHA	ETA	DX	DZ
90	1.00	1.316	1.974
FREQ	GP	EPSILON	D2
8.0	NO	1.3	0.987

DIPOLES

. . . . CURRENT

— — — VOLTAGE

——— IMPED.

Figure 81. Expanded view of the impedance of array D4 for the q=0 column and a cosine distribution of the input current at a broadside scan angle.

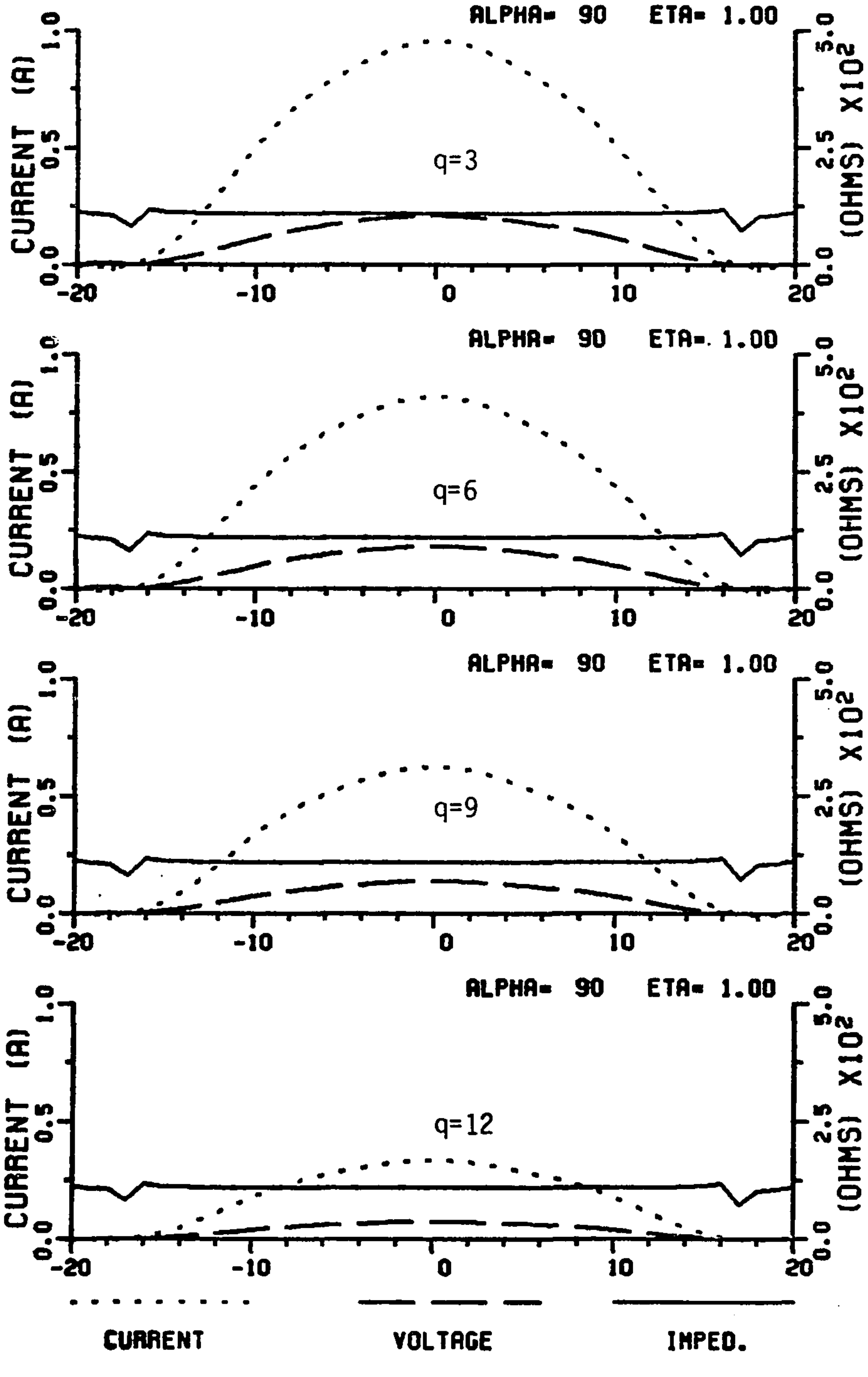

Figure 82. The impedance of array D4 for four columns parallel to the z-axis (q=3,6,9,12) at a broadside scan angle.

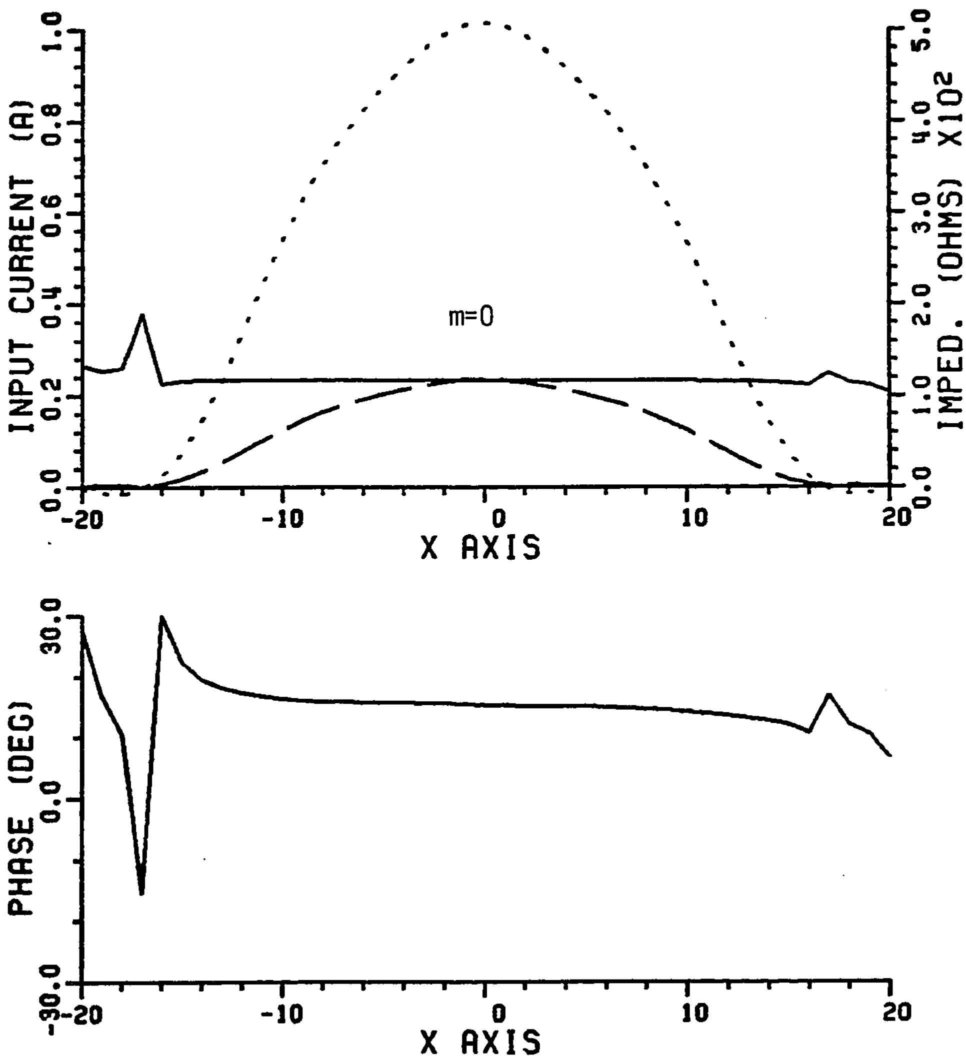

IX	IZ	KX	KZ	NX	NZ
649	349	31	31	70	40

ALPHA	ETA	DX	DZ
0	30.00	1.316	1.974
FREQ	GP	EPSILON	D2
8.0	NO	1.3	0.987

DIPOLES

. . . . CURRENT

— — — — VOLTAGE

———————— IMPED.

Figure 83. Expanded view of the impedance of array D4 for the m=0 row and a cosine distribution of the input current at a 30° scan angle to the right.

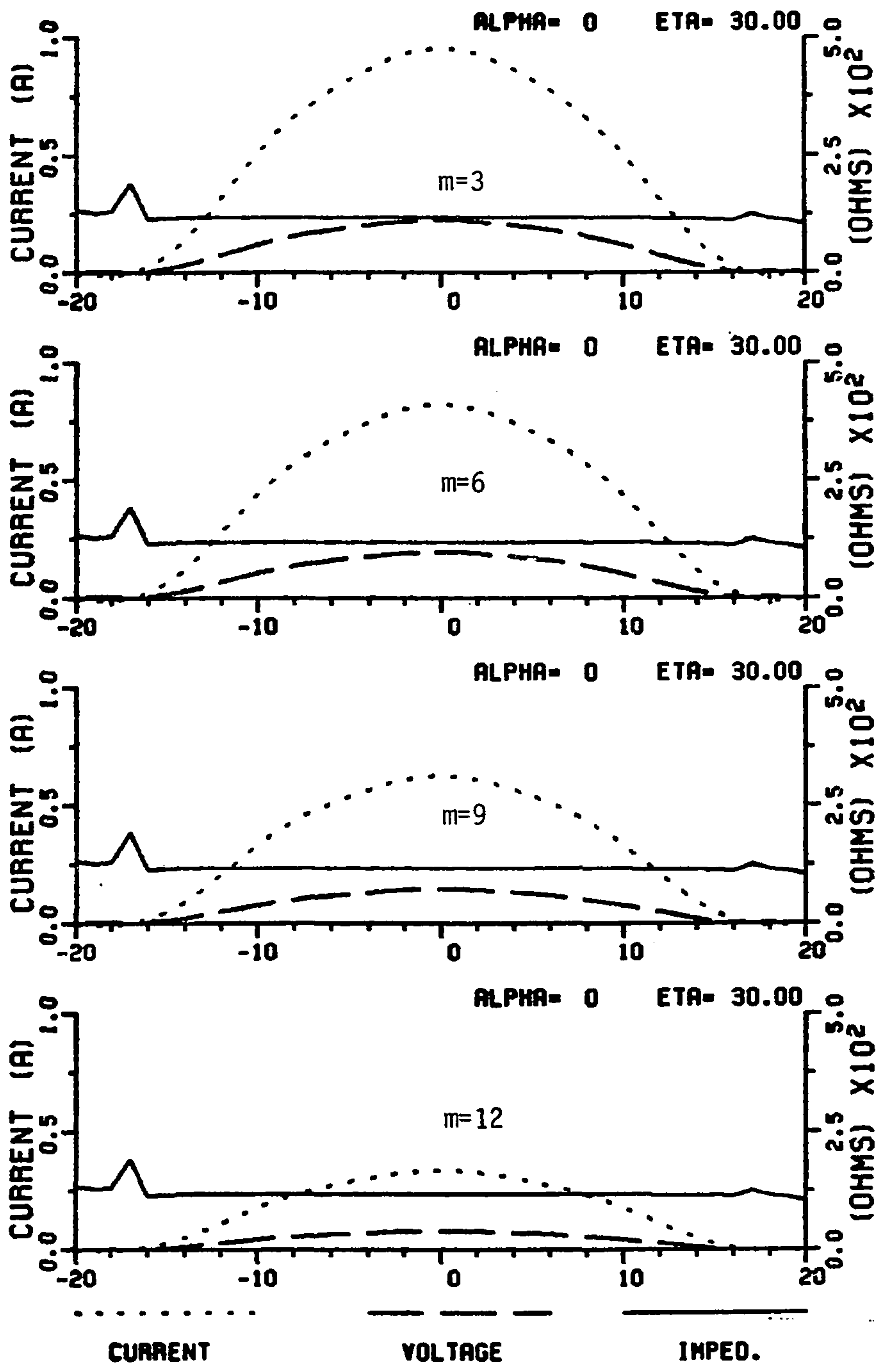

Figure 84. The impedance of array D4 for four rows parallel to the x-axis (m=3,6,9,12) at a 30° scan angle to the right.

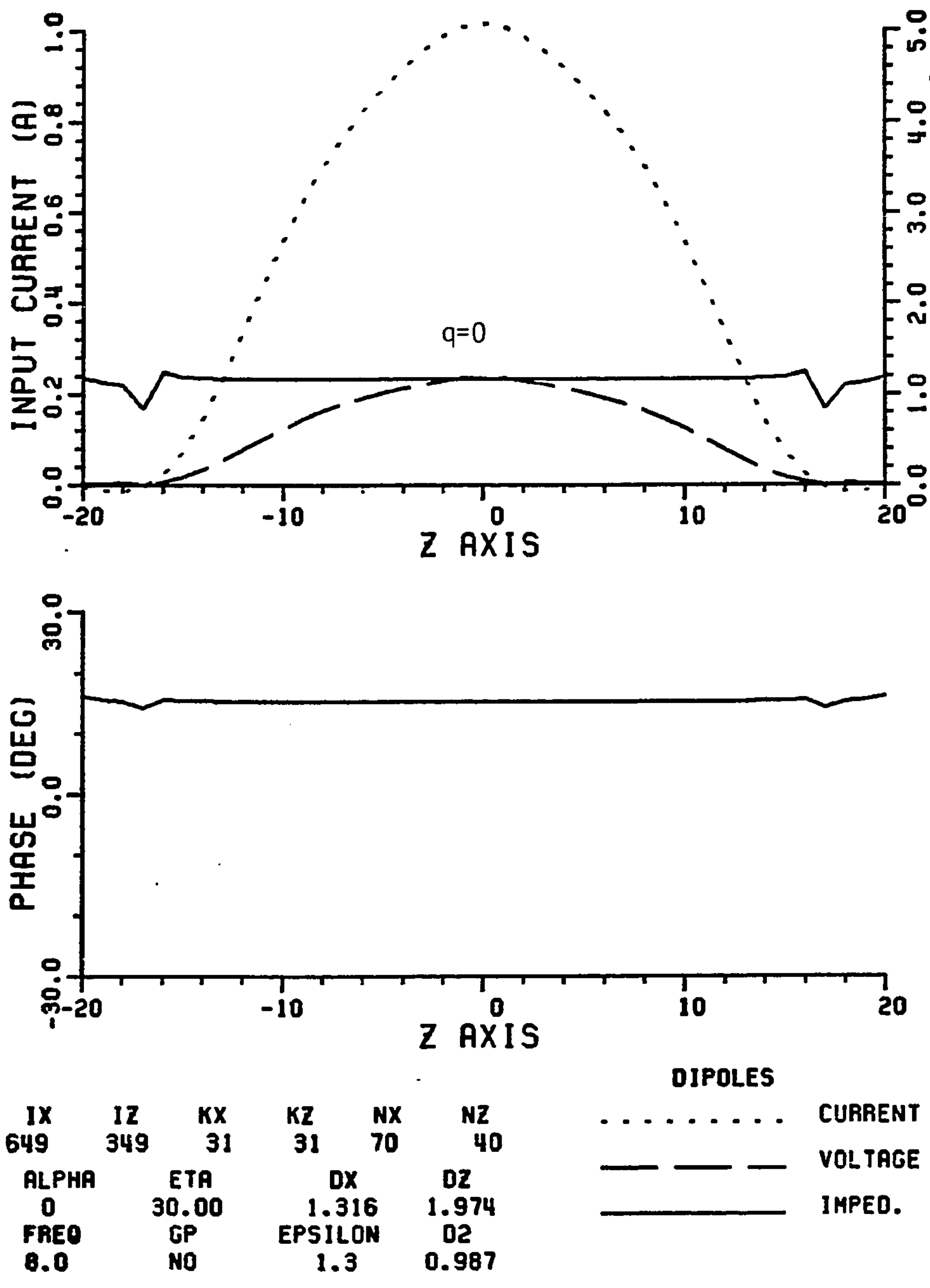

Figure 85. Expanded view of the impedance of array D4 for the q=0 column and a cosine distribution of the input current at a 30° scan angle out of the plot (in the x-y plane).

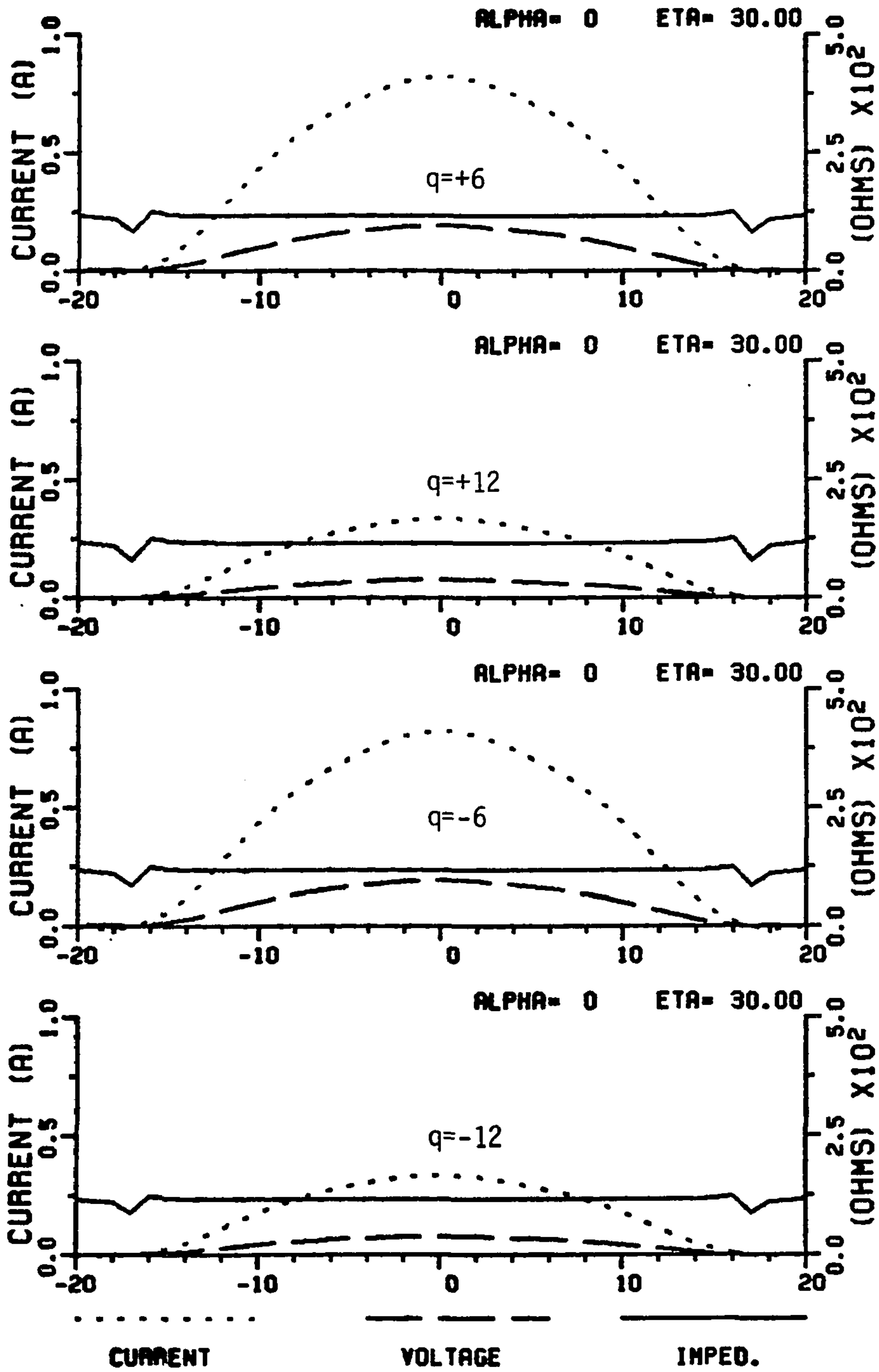

Figure 86. The impedance of array D4 for four columns parallel to the z-axis (q=-6,+12,-6,-12) at a 30° scan angle out of the plot (in the x-y plane).

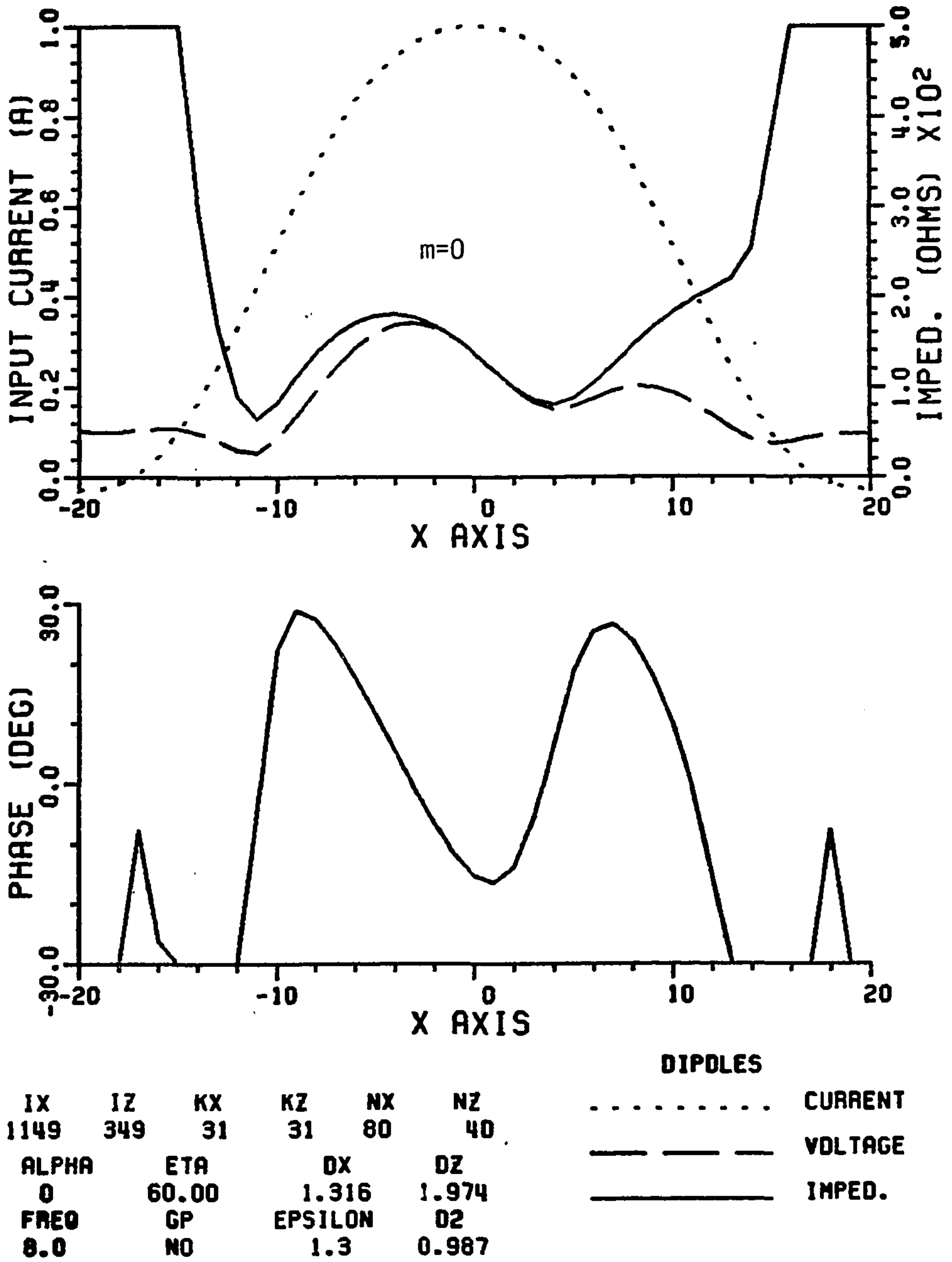

Figure 87. Expanded view of the impedance of array D4 for the m=0 row and a cosine distribution of the input current at a 60° scan angle to the right.

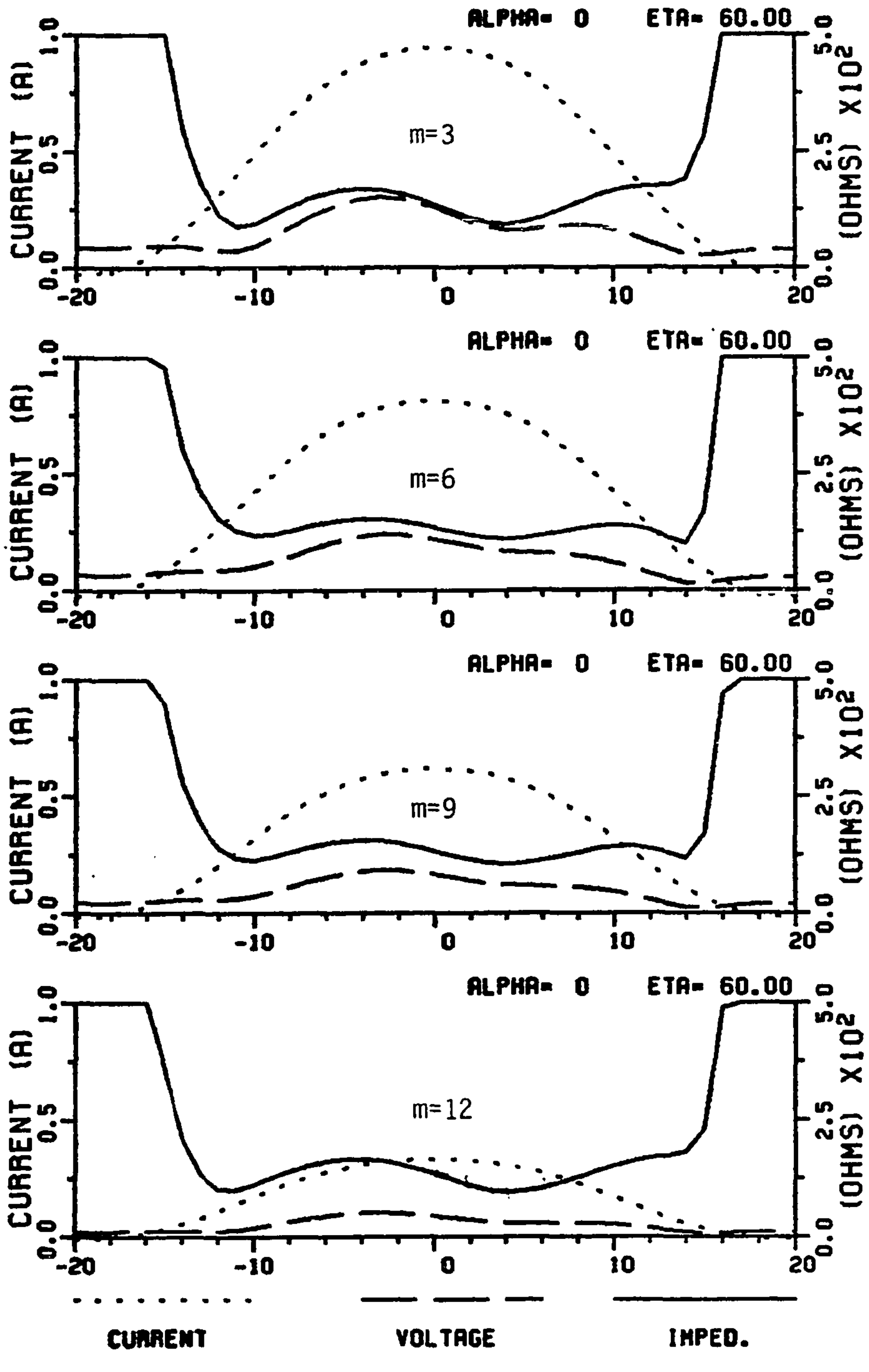

Figure 88. The impedance of array D4 for four rows parallel to the x-axis (m=3,6,9,12) at a 60° scan angle to the right.

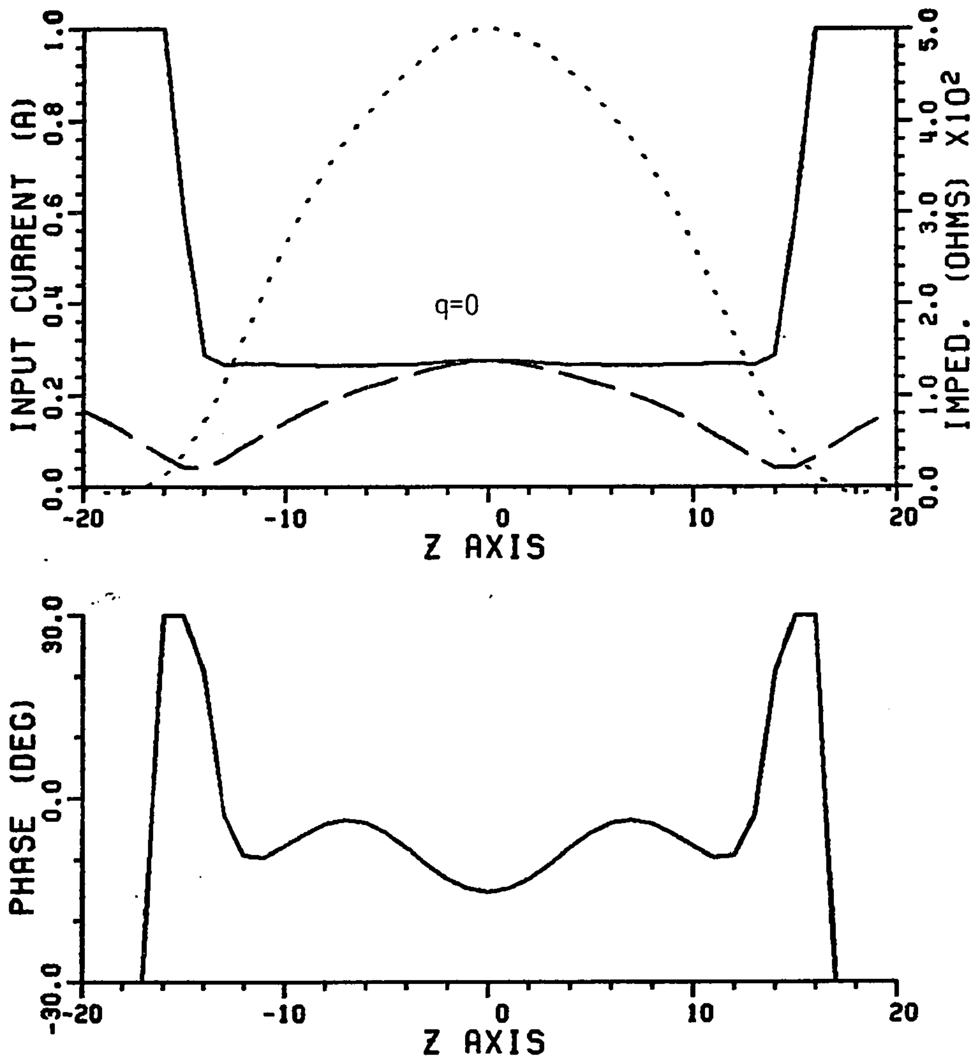

IX	IZ	KX	KZ	NX	NZ
1149	349	31	31	80	40

ALPHA	ETA	DX	DZ
0	60.00	1.316	1.974
FREQ	GP	EPSILON	D2
8.0	NO	1.3	0.987

DIPOLES

. . . . CURRENT

—— —— —— VOLTAGE

———————— IMPED.

Figure 89. Expanded view of the impedance of array D4 for the q=0 column and a cosine distribution of the input current at a 60^{0} scan angle out of the plot (in the x-y plane)..

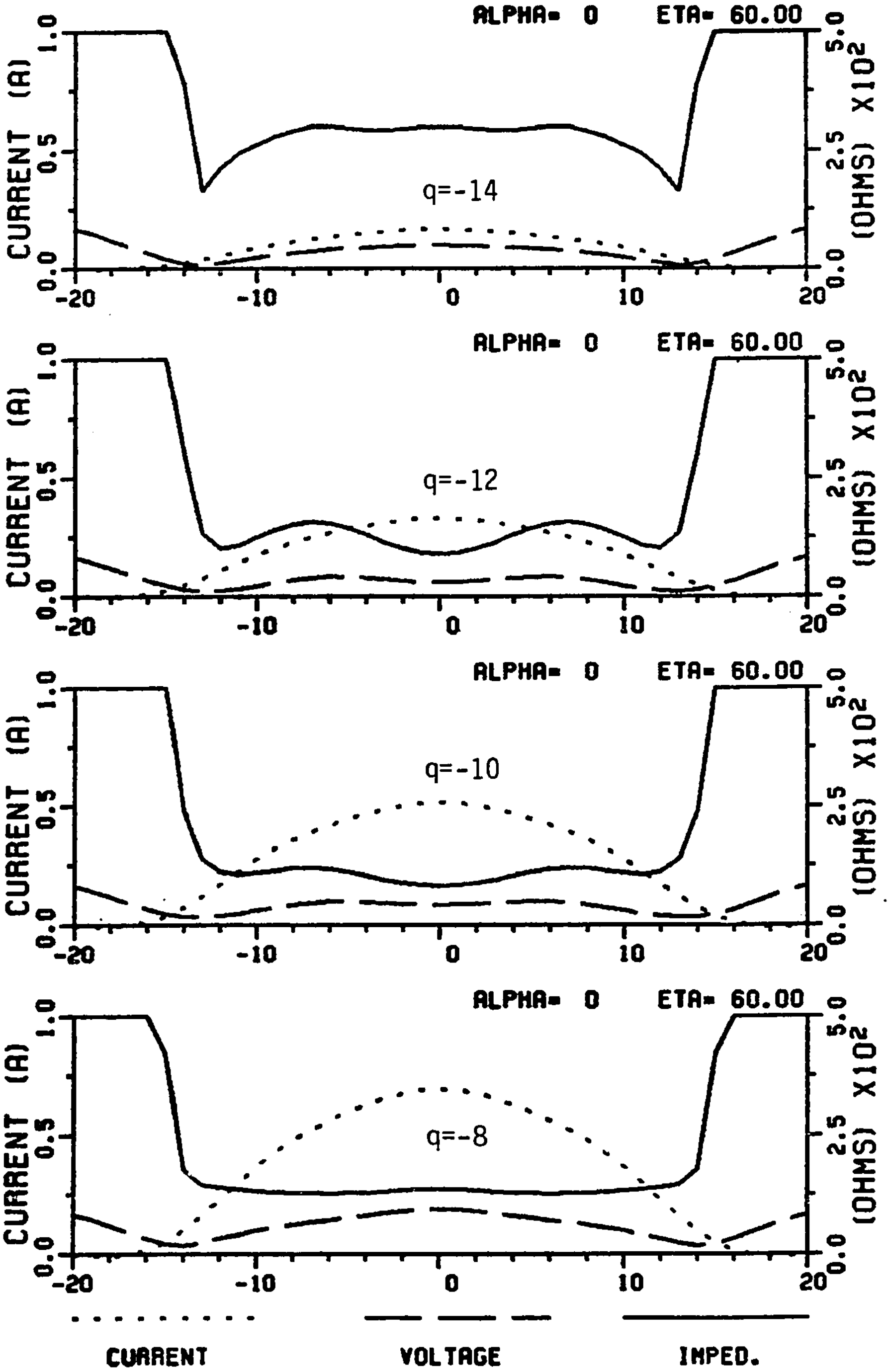

Figure 90. The impedance of array D4 for four columns parallel to the z-axis (q=-14,-12,-10,-8) at a 60^0 scan angle out of the plot (in the x-y plane).

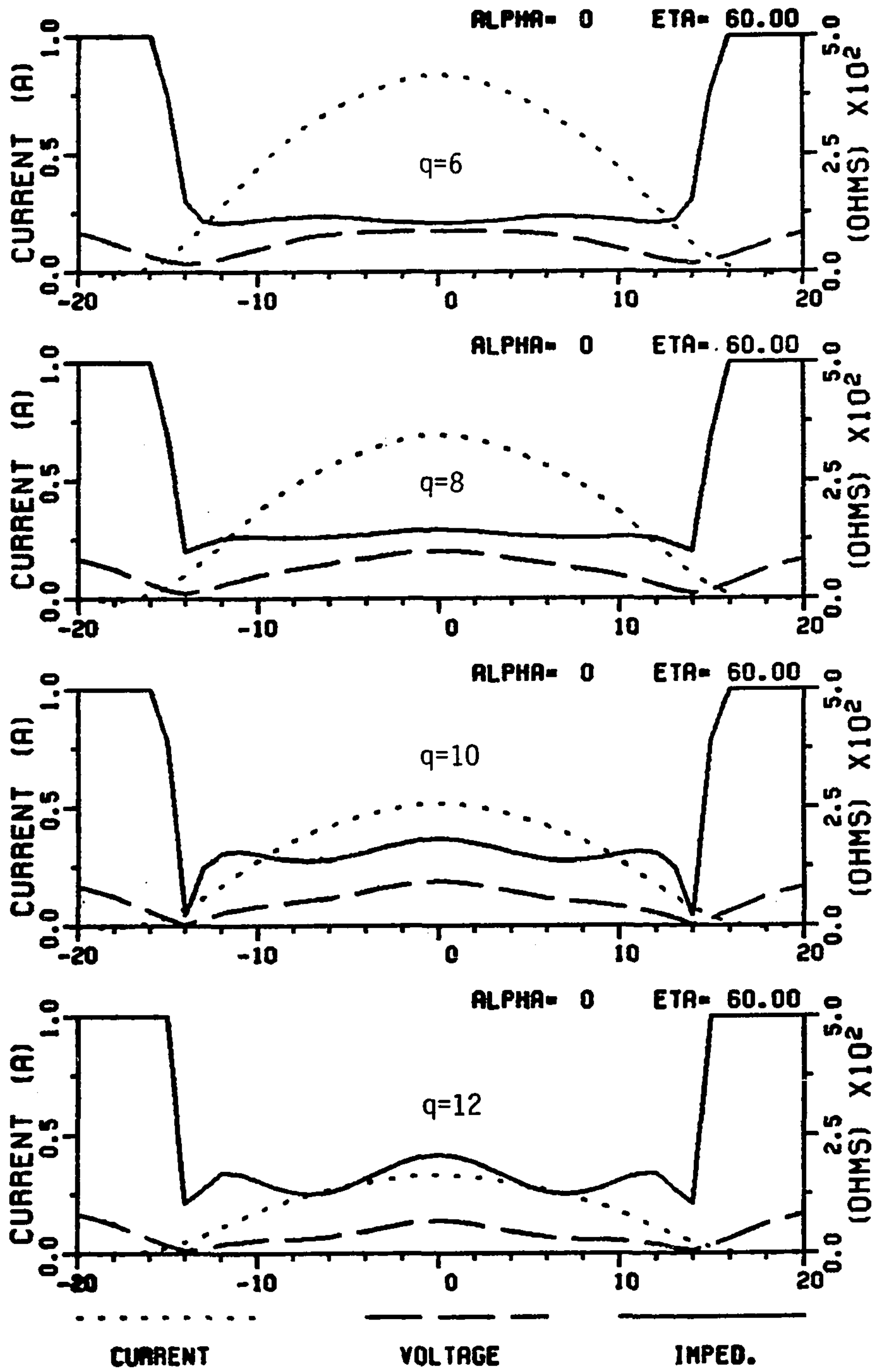

Figure 91. The impedance of array D4 for four columns parallel to the z-axis (q=6,8,10,12) at a 60° scan angle out of the plot (in the x-y plane).

2. Slot array in a dielectric slab

Array S2 is composed of straight z-directed slots in a ground plane in a geometry identical to array S1 (Figure 16) with the exception that array S2 is finite in both the x and z-directions. Table I gives the array parameters. Equation (80) is used to find the admittances of each element with Ω given by Equation (76). The transformation factor is identical to that of array S1 and is given by Equation (94). The array has cosine distributions in both the x and z-directions with 31 elements in each direction. The labeling of the elements in the array is given by Figure 78.

Figures 92 through 95 give the results for the broadside scan and elements plotted along rows parallel to the x and z-axes. As in the case with dipole array D4 in two-dimensions the impedance is nearly constant across the entire extent of the array.

Figures 96 through 99 give the results for array S2 scanned at 30^o in the x-y plane. Figures 96 and 97 show the slight variation in admittance across the array in the x-direction which is typical of results presented here for scans at 30^o in the x-y plane.

Scanning array S2 to 60^o caused some difficulties as seen in Figure 100 where the admittance is plotted along the x-axis for m=0. The maximum on the admittance plots is 15 millimhos for the 60^o scan results while it was 5 millimhos on the broadside and 30^o results. Obviously, one of the Fourier terms nearly coincides with the transformation factor singularity, which is surprising in light of Figure 101 which plots the transformation factor denominator with the term locations. It appears as if none of the terms are sufficiently near the singularity to cause problems. The format of this Figure, while useful in the one-dimensional case, is somewhat misleading here. While Equation (F26) in Appendix F still gives the approrpiate transcendental equation for the slot geometry and Equation (90) is still the correct expression for r_{2y} in terms of the solution to the transcendental equation (u=0.740), the expression for r_{2y} has changed because r_{2z} is no longer necessarily zero. From Equations (34) through (36) for the k=n=0 case and scan in the x-y plane, r_{2y} is now

$$r_{2y} = \sqrt{1 - \left(s_{2x} + \nu \frac{\lambda_2}{i_x d_x}\right)^2 - \left(\mu \frac{\lambda_2}{i_z d_z}\right)^2} \tag{95}$$

which leaves the expression for the problem causing ν term to be (in analogy to Equation (92))

$$\nu = \frac{i_x D_x f}{30}\left[\sqrt{\varepsilon_2 - \left(\frac{30u}{2\pi f d_2}\right)^2 - \mu^2\left(\frac{30}{i_z D_z f}\right)^2} - s_{x1}\right] \tag{96}$$

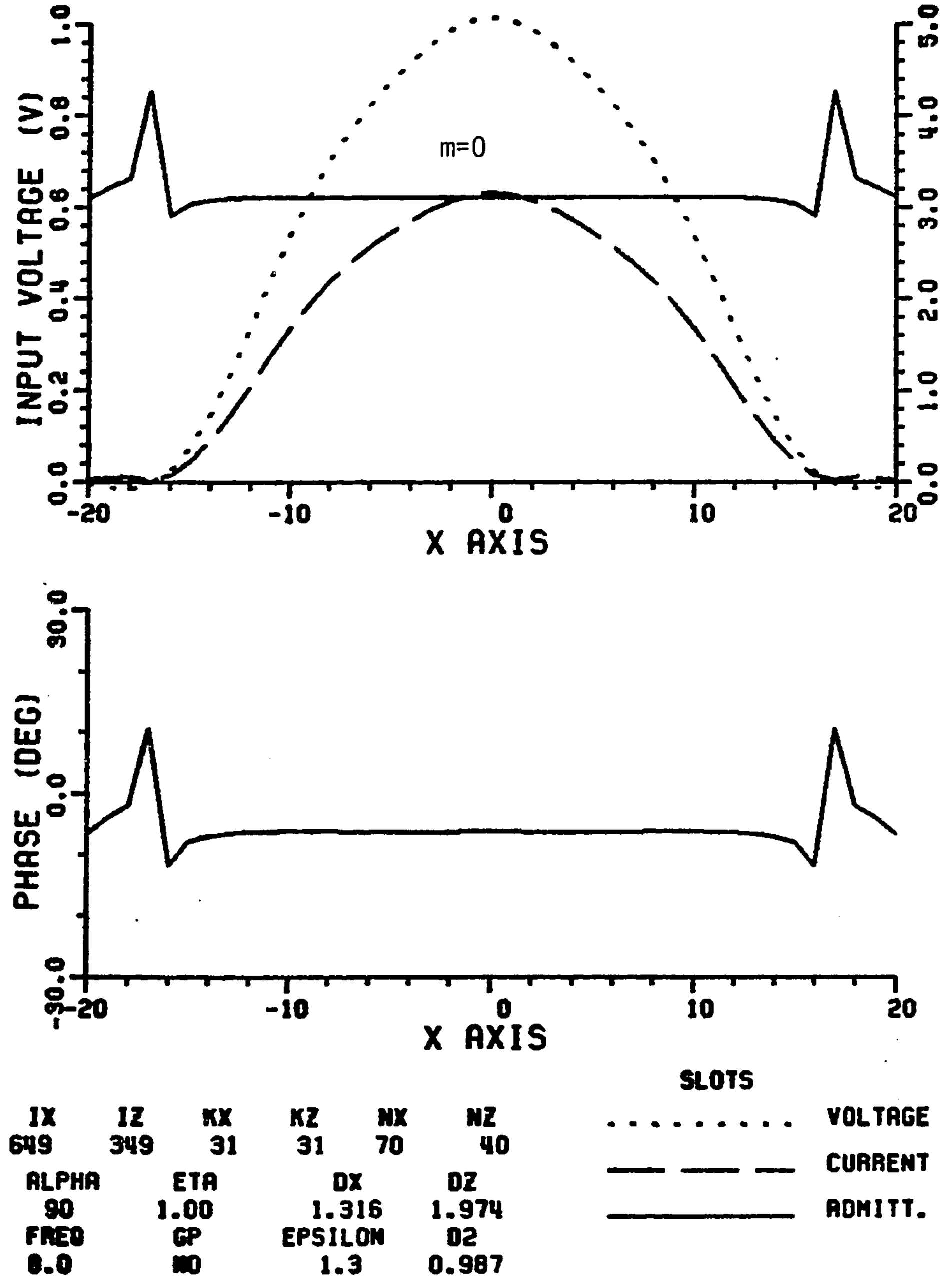

Figure 92. Expanded view of the admittance of array S2 for the m=0 row and a cosine distribution of the input current at a broadside scan angle.

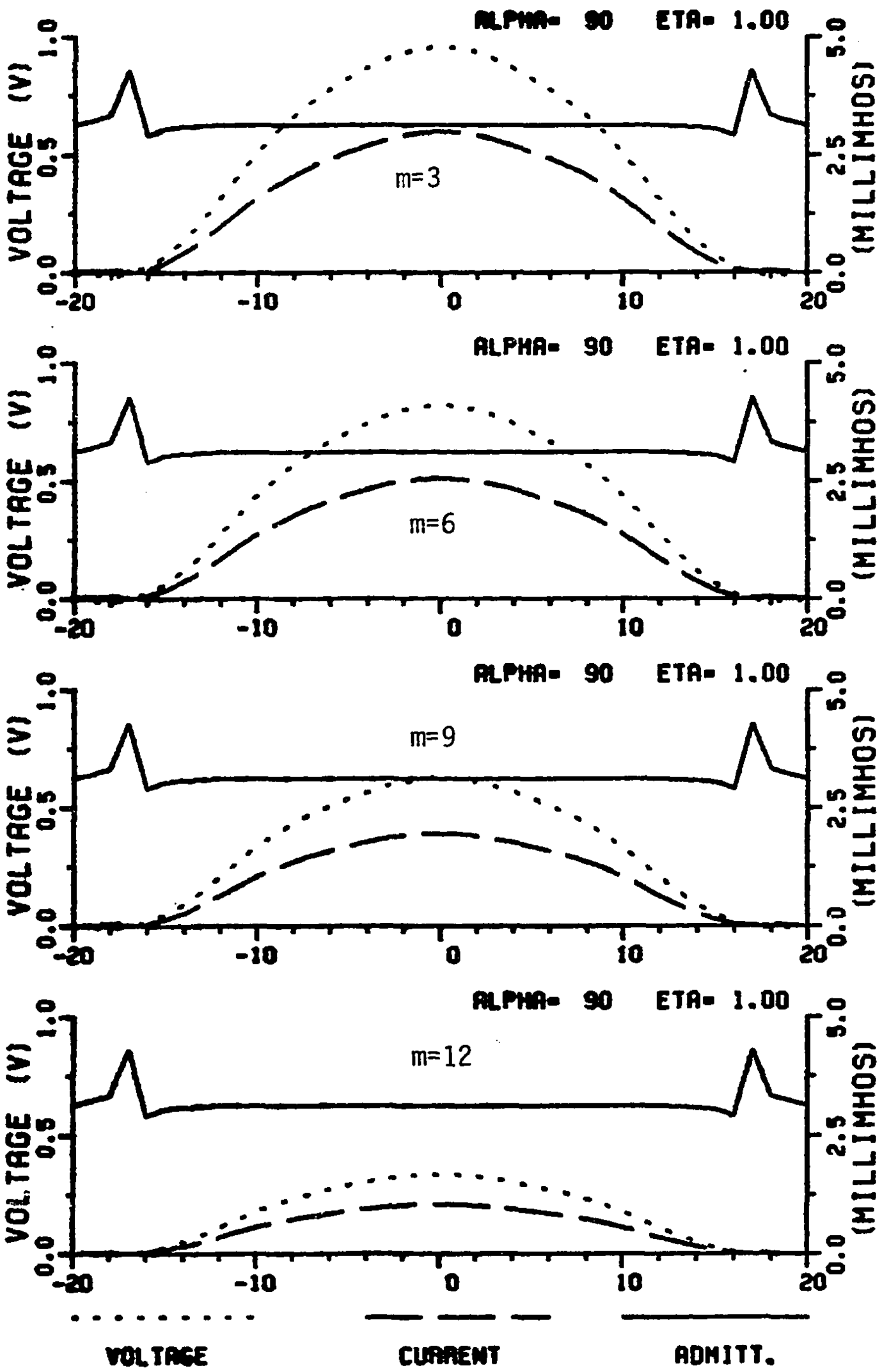

Figure 93. The admittance of array S2 for four rows parallel to the x-axis (m=3,6,9,12) at a broadside scan angle.

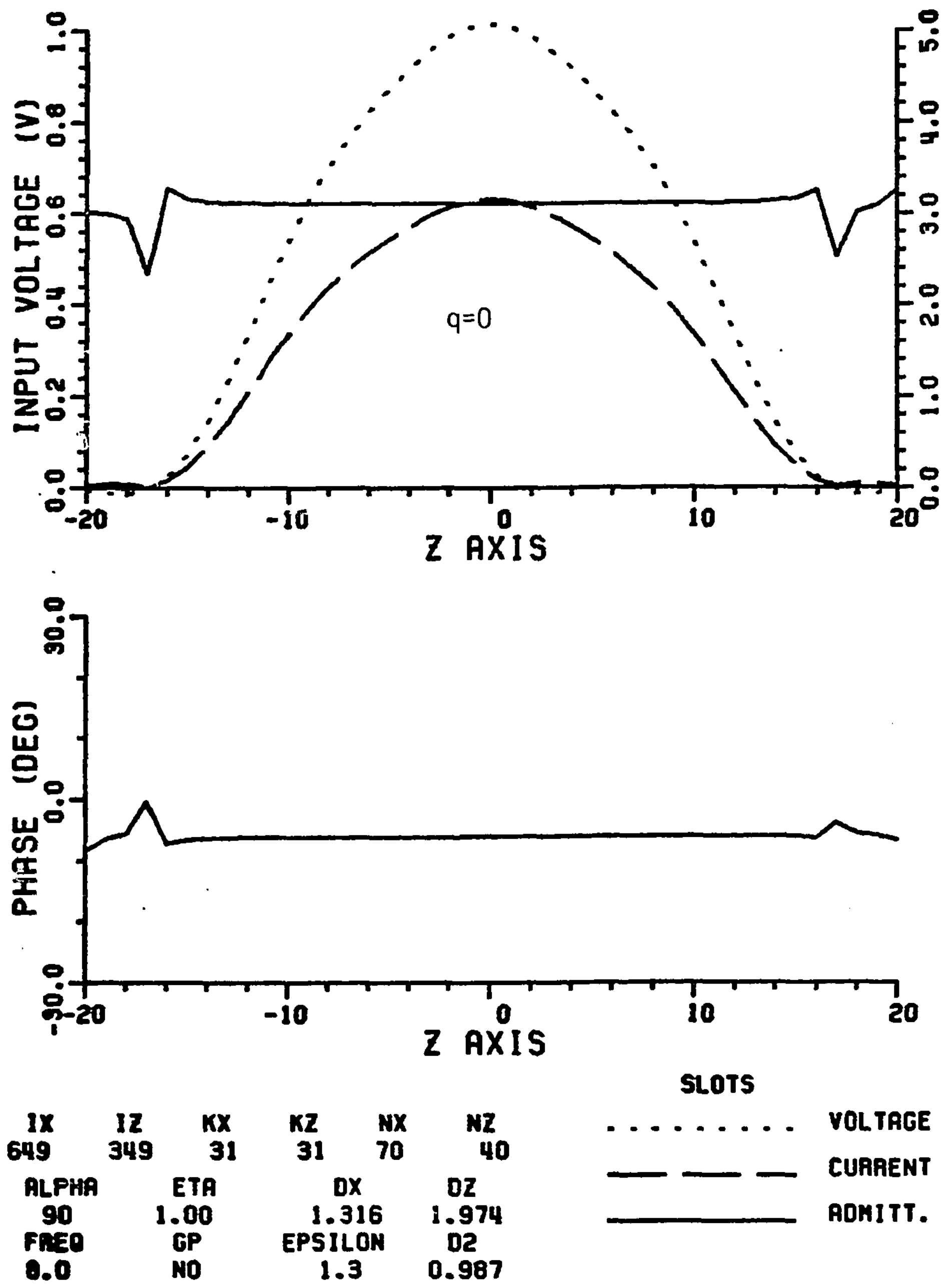

Figure 94. Expanded view of the admittance of array S2 for the q=0 column and a cosine distribution of the input current at a broadside scan angle.

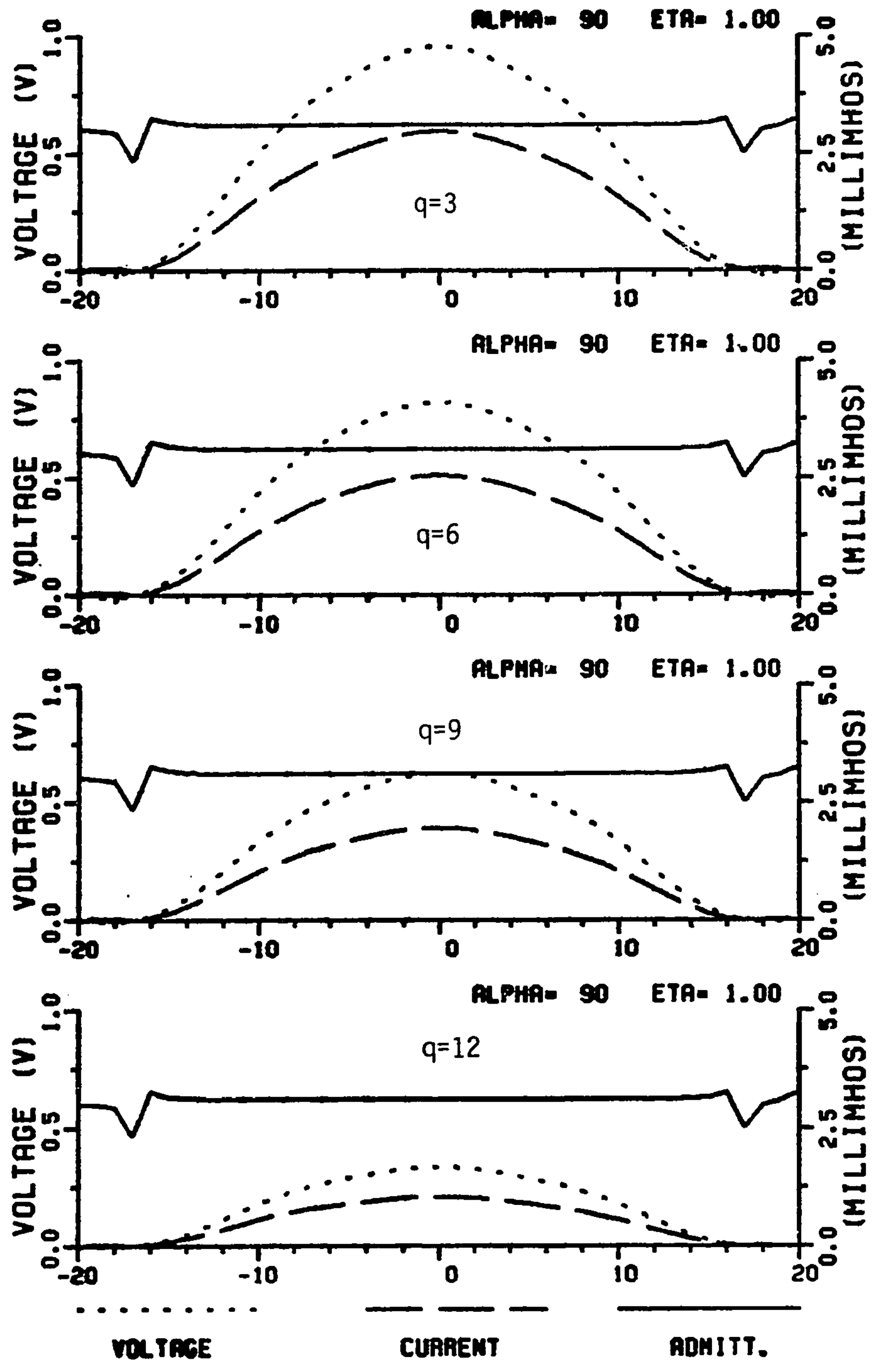

Figure 95. The admittance of array S2 for four columns parallel to the z-axis (q=3,6,9,12) at a broadside scan angle.

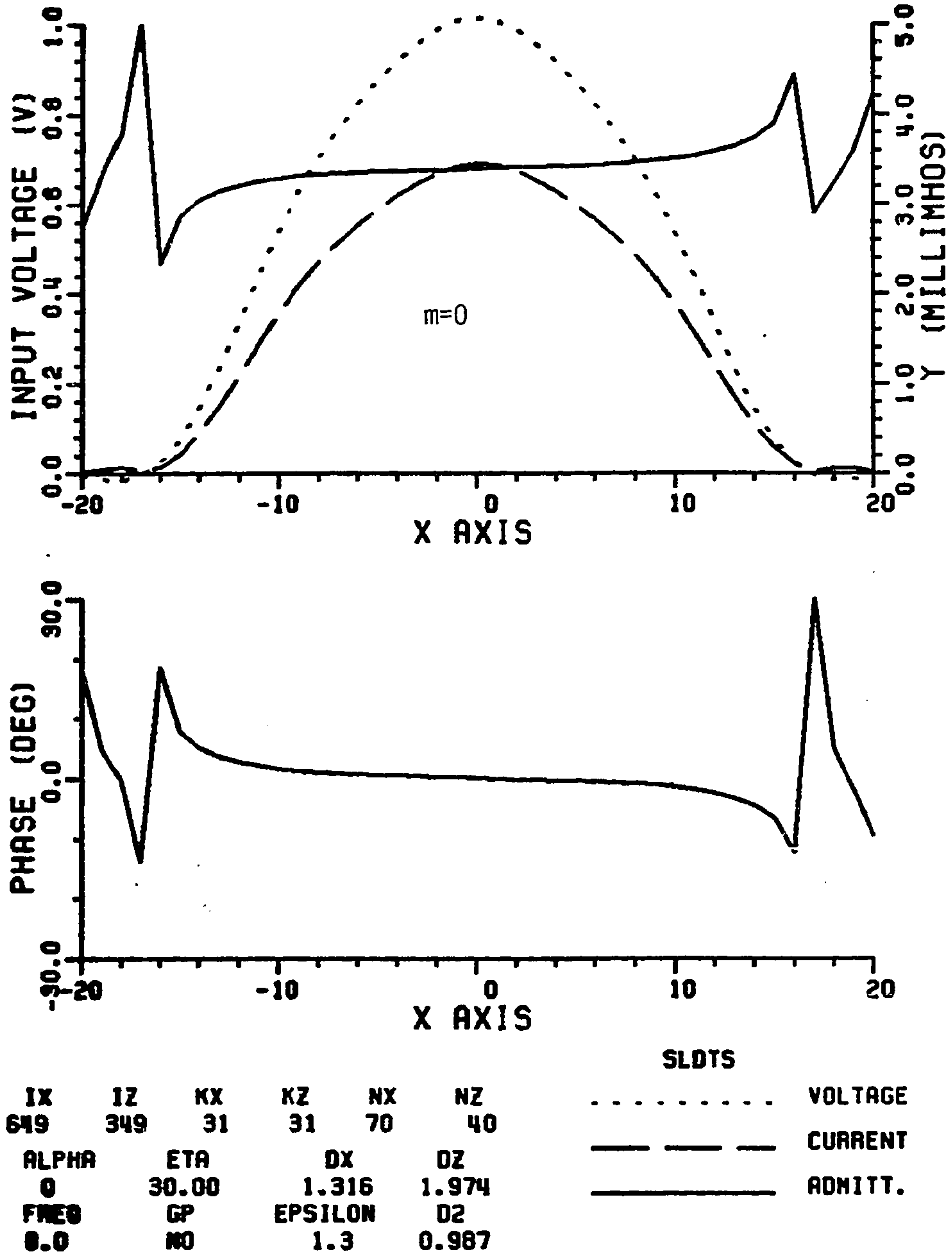

Figure 96. Expanded view of the admittance of array S2 for the m=0 row and a cosine distribution of the input current at a 30^{0} scan angle to the right.

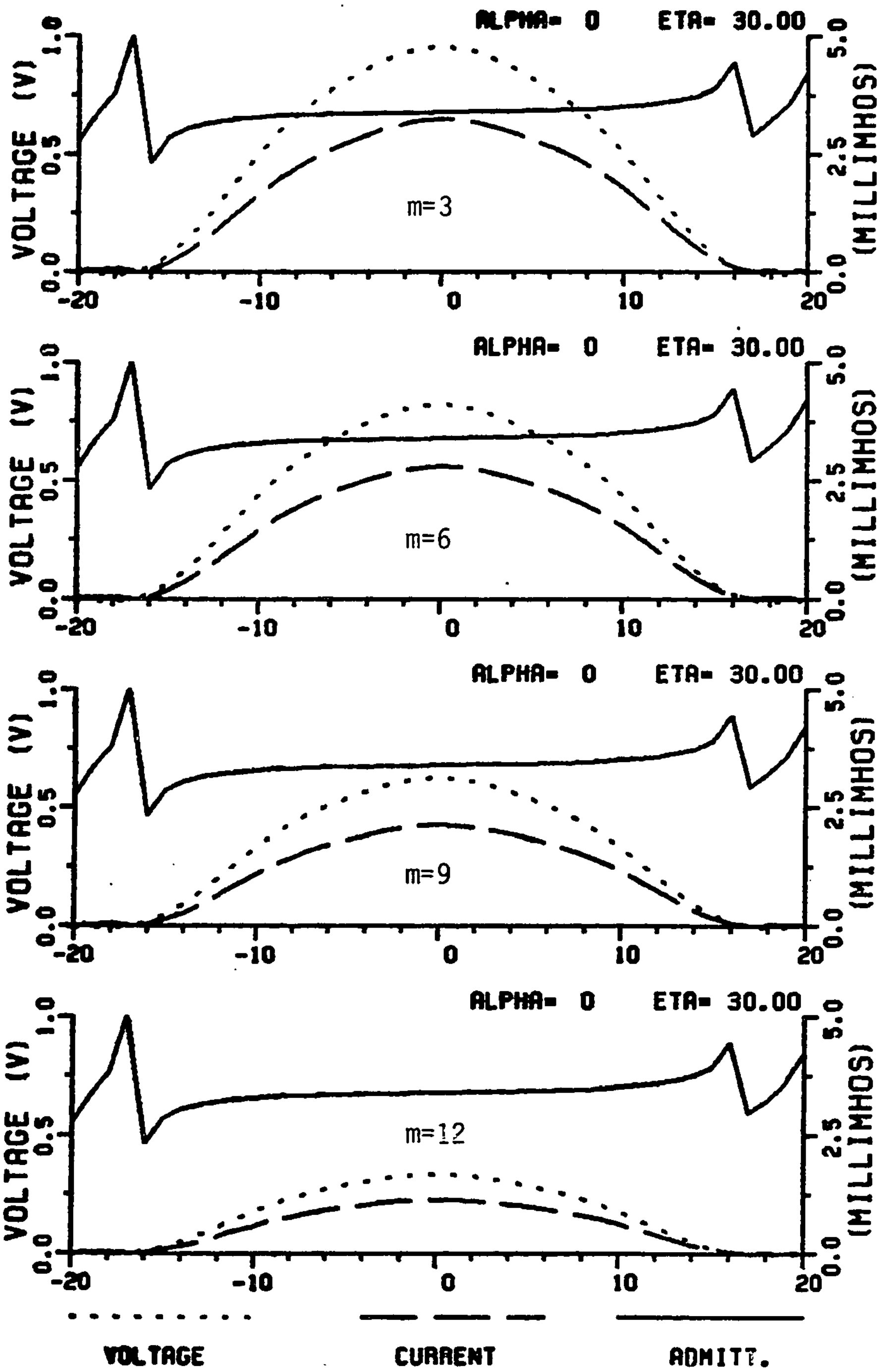

Figure 97. The admittance of array S2 for four rows parallel to the x-axis (m=3,6,9,12) at a 30^{o} scan angle to the right.

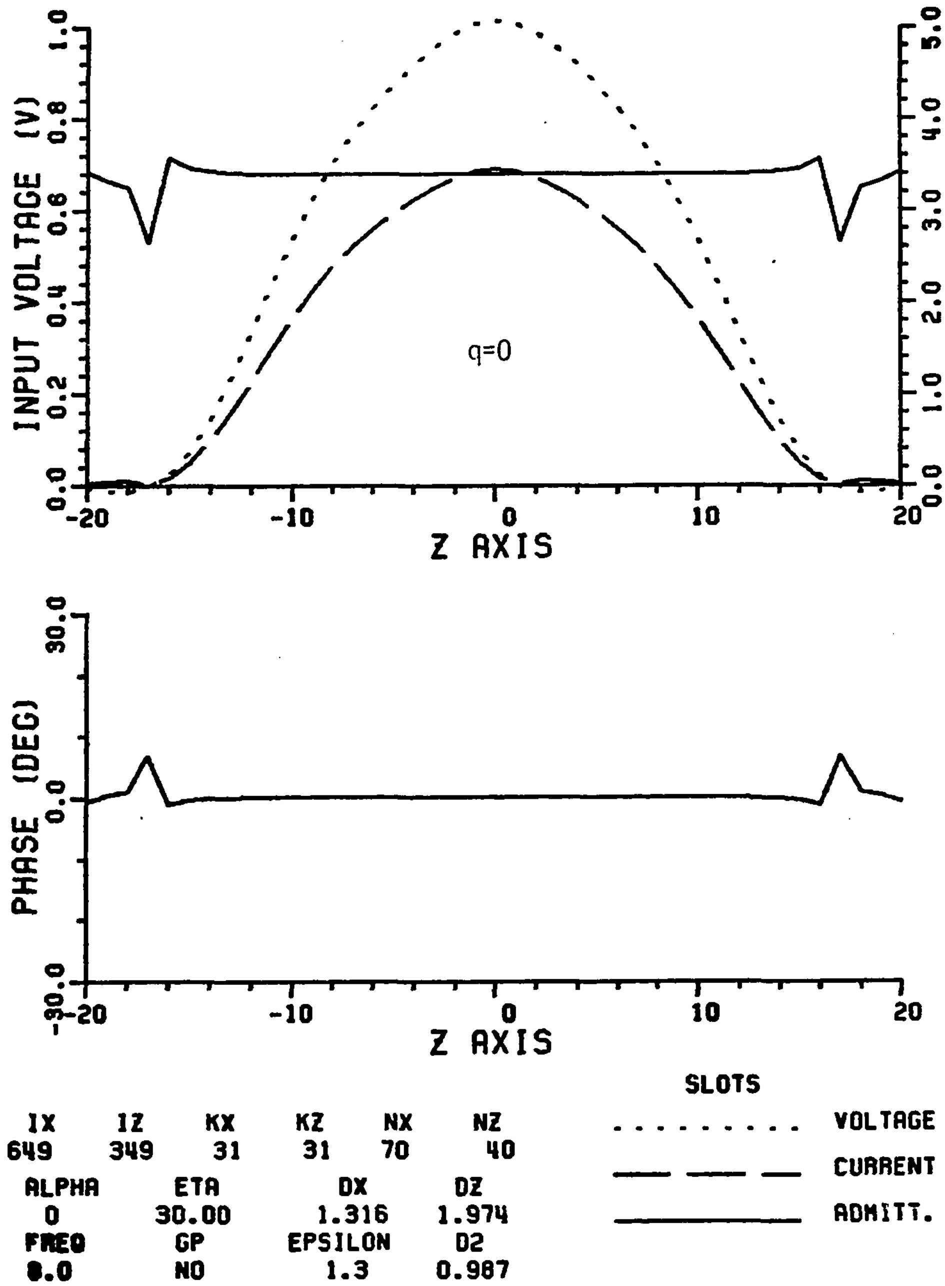

Figure 98. Expanded view of the admittance of array S2 for the q=0 column and a cosine distribution of the input current at a 30° scan angle out of the plot (in the x-y plane).

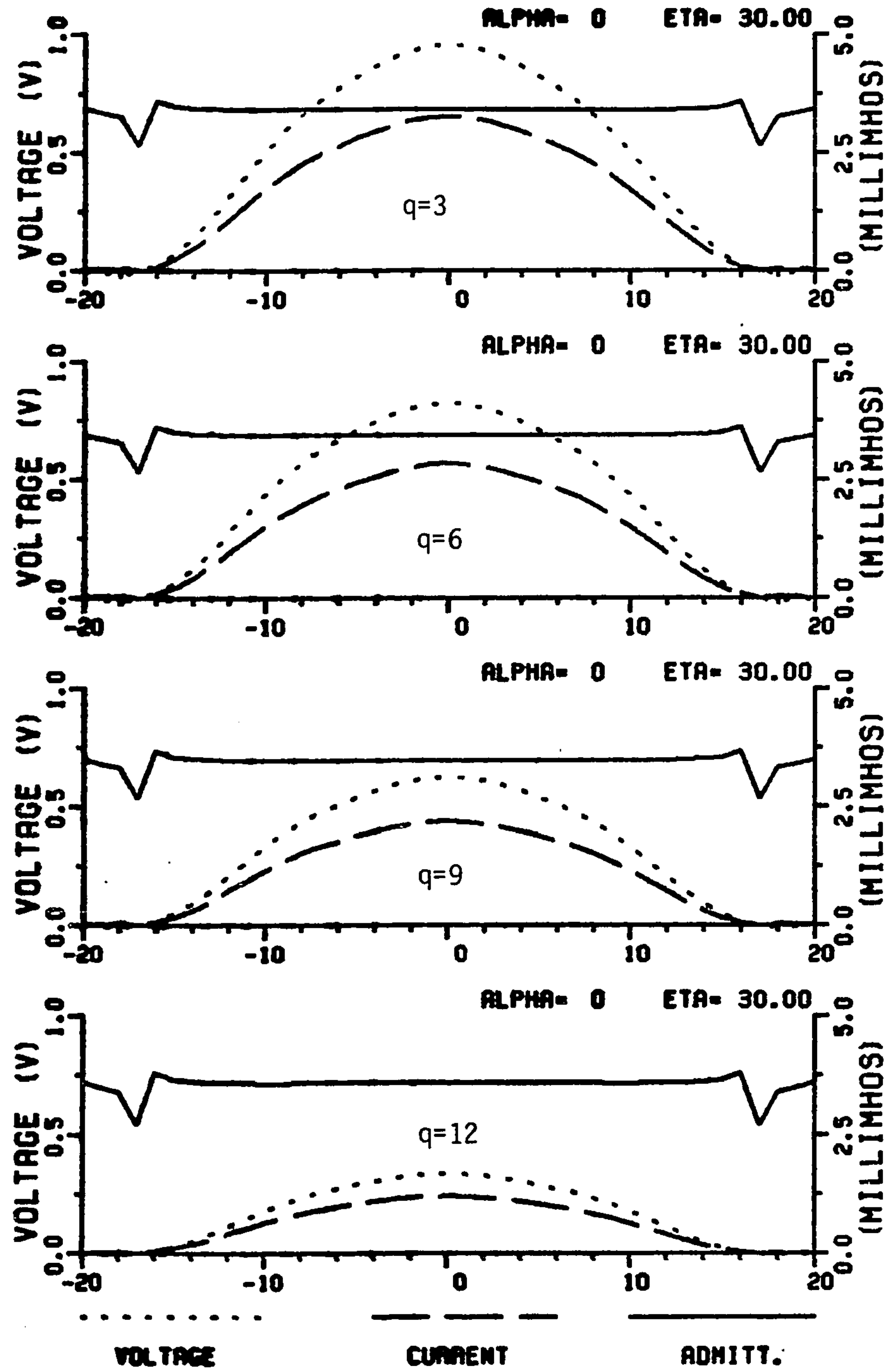

Figure 99. The admittance of array S2 for four columns parallel to the z-axis (q=3,6,9,12) at a 30^0 scan angle out of the plot (in the x-y plane).

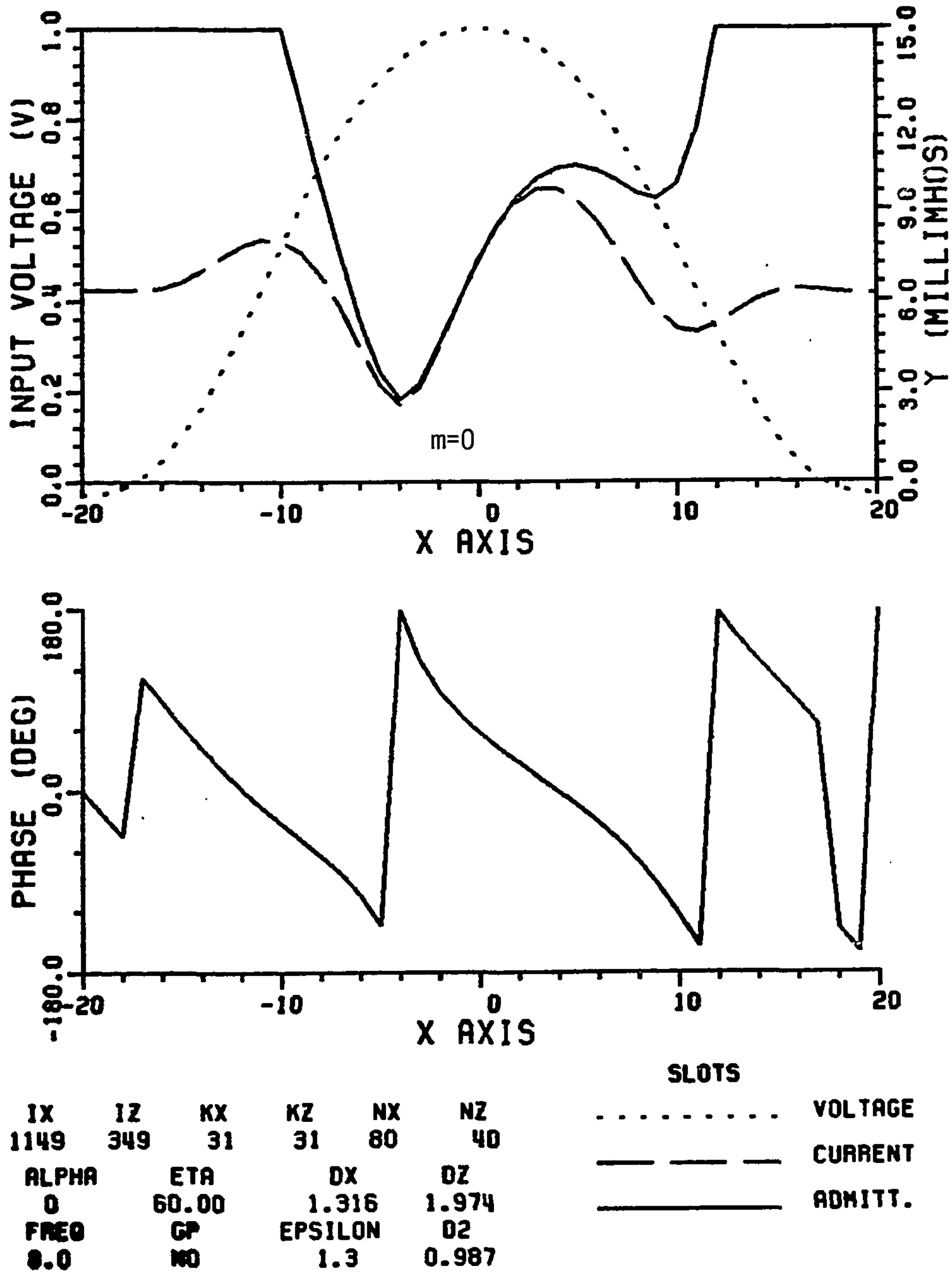

Figure 100. Expanded view of the admittance of array S2 for the m=0 row and a cosine distribution of the input current when the array scans 60° to the right and the inter-array spacing is 1149.

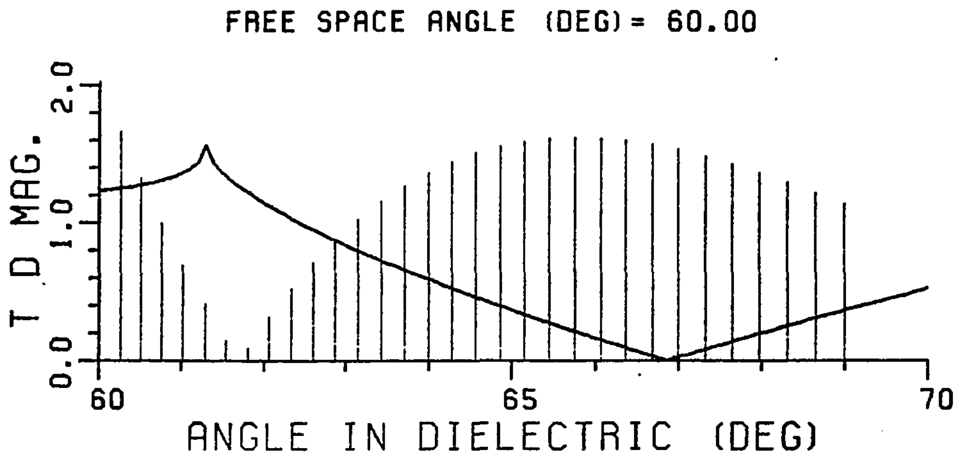

Figure 101. Expanded view of the denominator of the transformation function plotted with the spectrum at 60^{o} to the right for array S2 and an inter-array spacing of 1149.

When $\mu = 0$, Equation (96) is the same as Equation (92). This new equation implies that a plot, such as Figure 101, could be made for each value of μ in the two-dimensional case, Equation (96) implies, in general, that many more Fourier terms are necessary to insure sufficient coverage near the transformation factor singularity and that greater care must be used to assure that no one term coincides with the singularity.

In order to obtain more meaningful results for the 60^0 scan of array S2, the x-direction inter-element spacing, i_x, was changed to 1069. Figures 102 through 105 give the resulting admittance plots. Figures 102 and 103 give the admittance along four rows parallel to the x-axis and Figures 104 and 105 give the results for four columns parallel to the z-axis. Behavior is similar to the 60^0 scan results for the two-dimensional dipole array D4.

D. Discussion

This chapter has presented computer generated plots of immittances for finite phased arrays in several geometrical configurations, including those with adjacent dielectric layers. It has confirmed those results for the free space geometry through comparison to another analytic technique. And it has examined one feature of the method which describes the physical situation encountered when dielectric is used with a finite array. Two more topics are mentioned in this section. The first is an interesting and perhaps useful feature which may be unique to this particular method. The second is an example of how the physical interpretation which this method initiates explains a phenomenon present in finite arrays of any geometry.

No mention has been made in this work of the far-field pattern which the arrays mentioned here would generate. The primary reason for this is the fact that once the matching or immittance properties of an array are understood, pattern calculation is straightforward. The problem of synthesis, that is finding the aperture distribution and matching properties for a prescribed far-field pattern, is not as trivial, however. Figure 22 suggests a way in which this new transform method could be useful. This figure shows the magnitudes and positions of the Fourier coefficients for a cosine distribution of the one-dimensional aperture. Because the far-field pattern is also the Fourier Transform of the aperture distribution [42], Figure 22 also shows the far-field pattern of the array with the cosine aperture distribution. This suggests that if some far-field pattern is desired, the Fourier coefficients required by the transform method could be found simply by analyzing the far-field pattern. The shape of the aperture distribution itself can then be ignored.

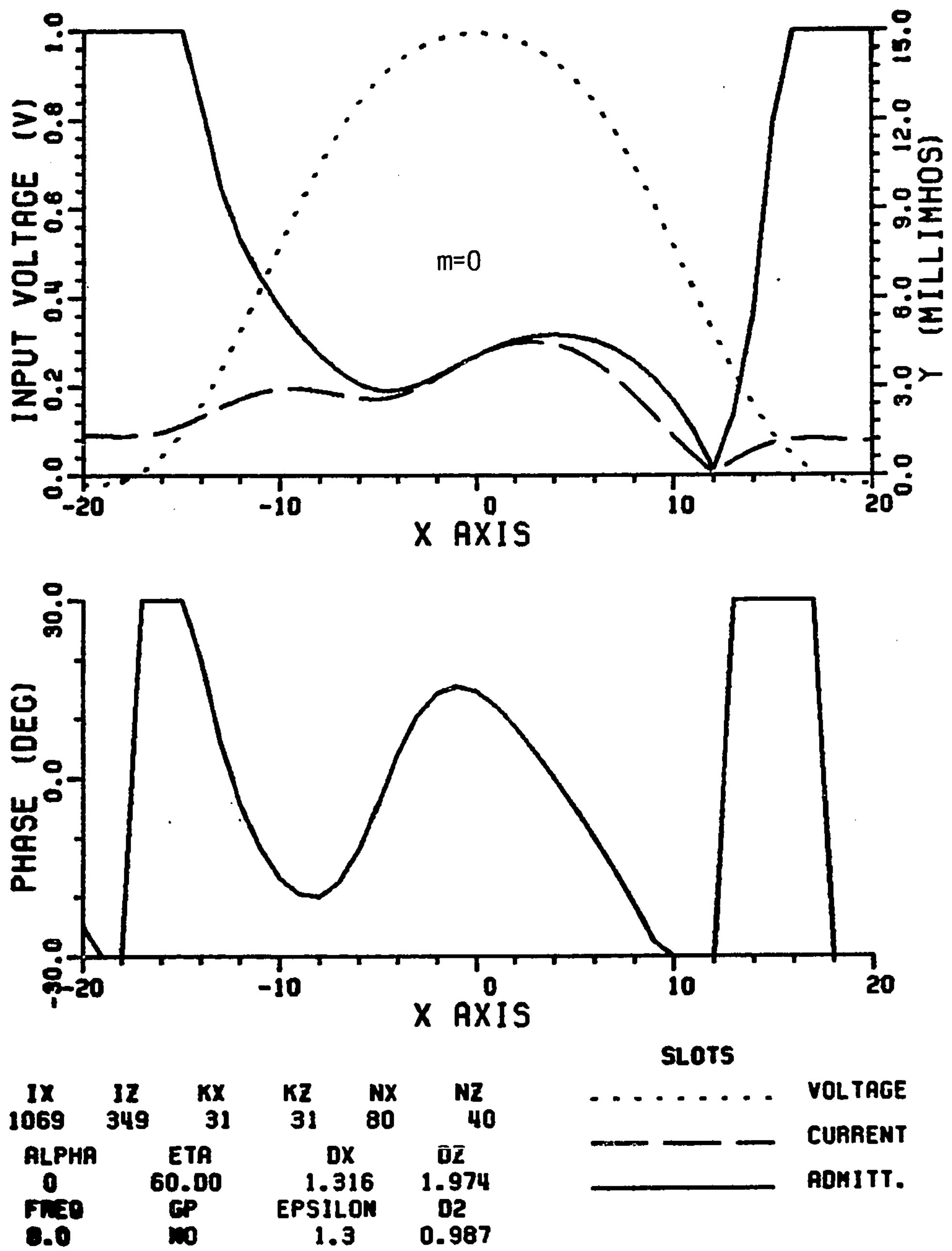

Figure 102. Expanded view of the admittance of array S2 for the m=0 row and a cosine distribution of the input current when the array scans 60^{o} to the right and the inter-array spacing is 1069.

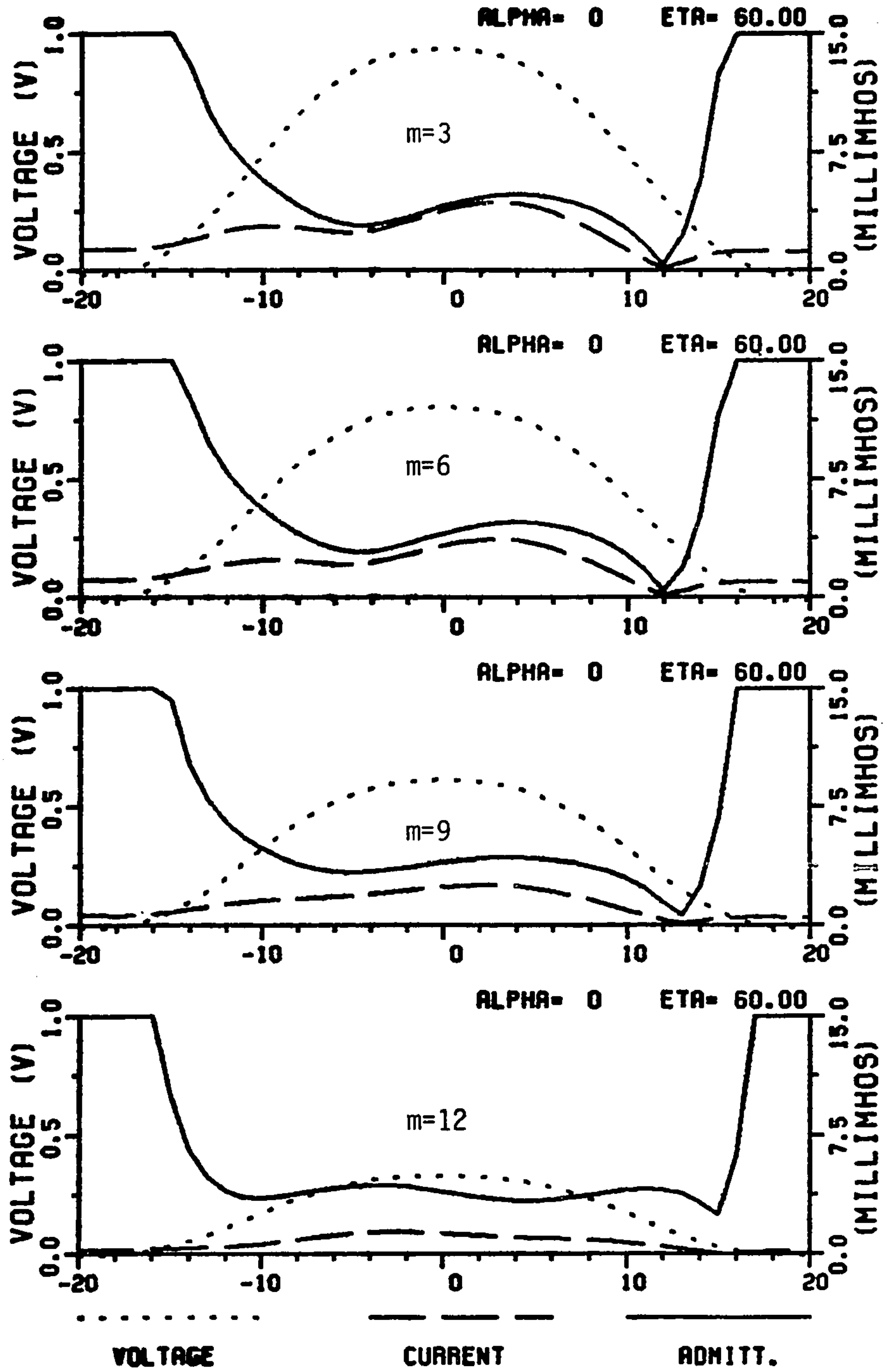

Figure 103. The admittance of array S2 when scanned 60° to the right along four rows parallel to the x-axis (m=3,6,9,12). The inter-array spacing is 1069.

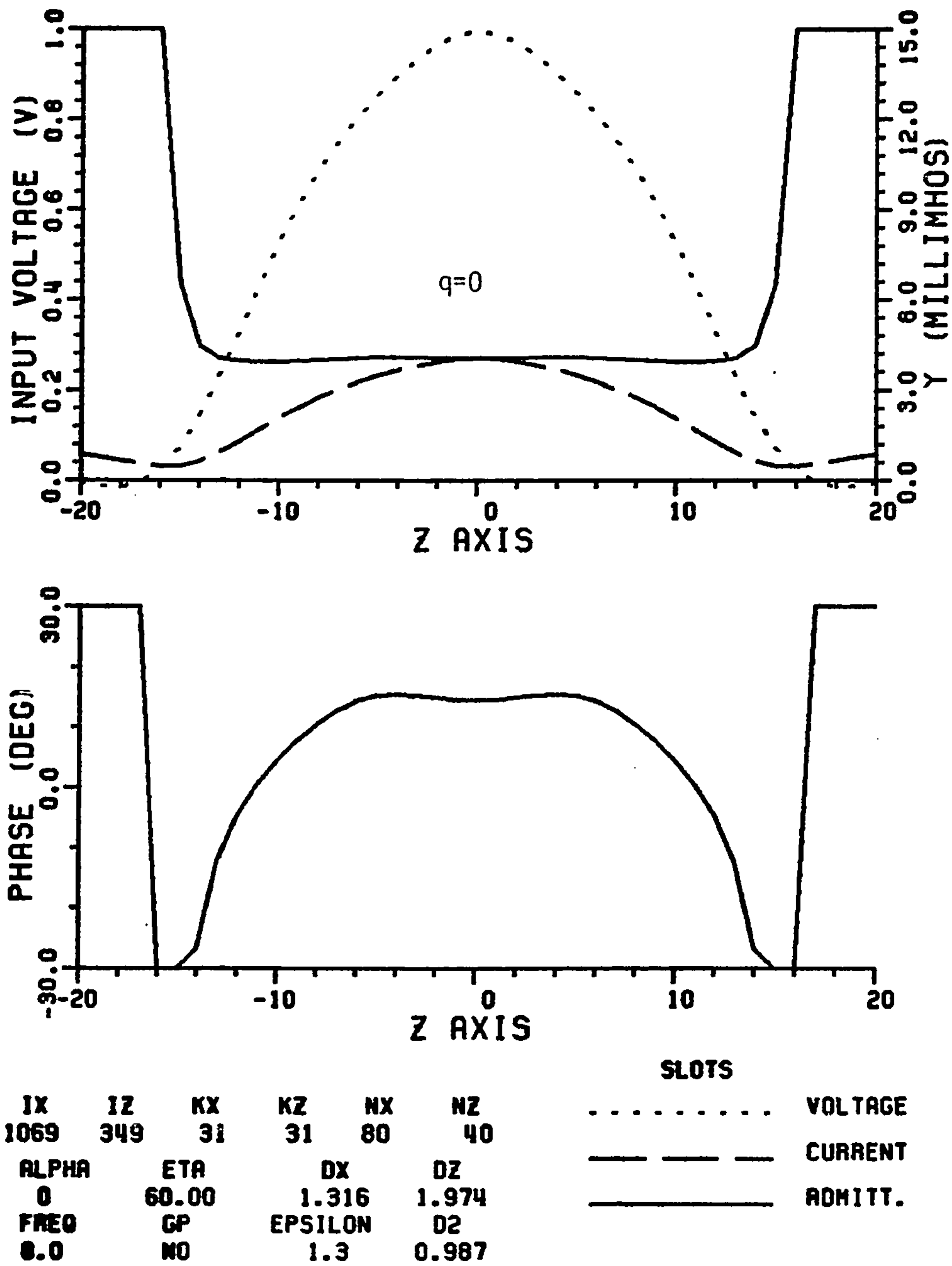

Figure 104. Expanded view of the admittance of array S2 for the q=0 row and a cosine distribution of the input current when the array scans 60^{0} out of the plot (in the x-y plane) and the inter-array spacing is 1069.

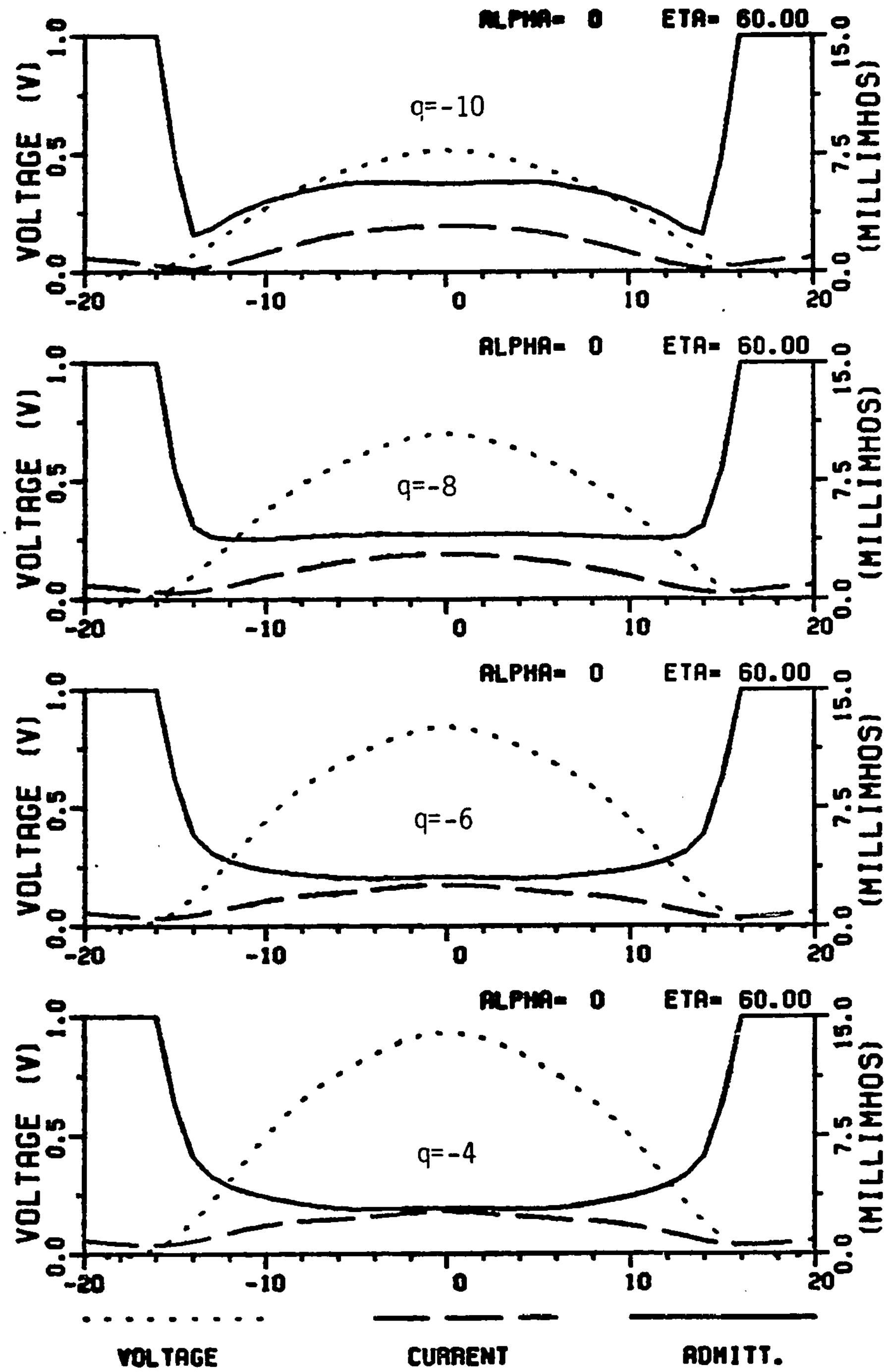

Figure 105. The admittance of array S2 when scanned 60^{0} out of the plot along four rows parallel to the z-axis (q=-10,-8,-6,-4). The inter-array spacing is 1069.

It is also interesting to note the behavior of the free space one-dimensional dipole array when the trapezoidal current distribution is examined (Figure 36). What might be labeled "ripples" appear in the 30^o, 40^o, and 50^o scans. It is appropriate to consider whether these ripples occur in all finite arrays or whether they occur because of the method itself. The interpretation of a finite array scanning at, for example, 40^o having propagating modes in all directions suggests a solution. Because the ripples appear as if interference between two waves may be taking place, it is useful to consider the component of the ray in the direction of scan and the ray which goes down the x-axis directly from one element to the next. For array D1, the electrical spacing, βDx, is 144^o. For the 40^o scan, the component of the ray in the scan direction has a phase shift from element to element of $\beta Dx \cdot s_x$ or 92.6^o. The wave along the x-axis would have a phase shift of $\beta Dx \sin(90^o)$ or 144^o. The phase difference between these two is 51.4^o. In other words the standing wave caused by their interference has a phase shift of 51.4^o between any two elements so a full period should be $360^o/51.40^o$ or 7 spacings. This turns out to be the case as one maximum occurs at element -5 and the next at +2. For the 60^o example the phase difference is 33.7^o which indicates a full period every 11.6 spaces. The difference between the relative maxima in the 60 plot of Figure 36 is 11. The ripples do not appear visibly in the tapered distributions of this study because the magnitude of the wave in the scan direction is much larger than the magnitude of the wave along the array is for those distributions. This discussion not only indicates that the ripples will appear and are not a peculiarity of the method, but that the physical description inherent in the transform method is useful in its own right in finite array analysis.

CHAPTER V
CONCLUSIONS

The objective of this dissertation was to establish a new method, referred to here as the transform method, which was capable of calculating the element by element immittances of large finite phased arrays. This objective was reached using a method for calculating immittances of infinite arrays which exploits a plane wave spectrum approach and allows the treatment of dielectric slabs adjacent to the array. This infinite array approach is, of itself, extremely useful, but it cannot predict behavior near the edge of a finite array nor can it predict fluctuations in immittance values from element to element as the array is scanned.

The results from the finite arrays modeled here do reflect these behaviors. The effects at the edges as well as the variation across the aperture due to scan and interaction with the dielectric surfaces are given. Admittedly, truncation of the Fourier sums will be noticed at the edges most, even for the tapered aperture distributions. The addition of more Fourier terms (and computer time) will lessen this problem. Results can be obtained which are of value in actual implementation of a finite array where general behavior rather than actual numerical values is desired. The addition of dielectric layers is most useful in situations where a phased array must be covered by some dielectric protective cover or where the properties gained by the presence of the dielectric are required. Analysis of antennas in the presence of such dielectric layers is difficult but it has been put into manageable terms for the finite arrays discussed here. The singularity which causes problems for large scan angles in the dielectric covered arrays has been examined closely and some meaningful results have been obtained which require more Fourier terms and more computer time. A slightly different analysis using integration and the Principle Value Theorem [43] near this well behaved singularity could be useful.

A future extension of this work could be made in examining the possibility of using a round aperture shape and distributions characteristic of that shape. A possible method for this analysis does exist [44] but some aspects of the theory will be sufficiently different to warrant the inclusion of that material elsewhere.

APPENDIX A
TRANSFORMATION FROM SPHERICAL TO PLANE WAVES

This appendix gives the process of starting with the simple sum of spherical wave vector potentials from all the elements in the array and going to the spectrum of plane waves expression for the electric field. This derivation is given here for convenient reference because of its importance, even though it has appeared elsewhere [45]. As Figure 9 shows, (repeated here as Figure (A1)) all elements are Hertizian dipoles in the x-z plane with orientation p and separation in the x and z directions D_x and D_z respectively. In this appendix, the reference element is located at the origin. Its position in space is generalized in the text of Chapter 2.

All sums in this appendix go from $-\infty$ to ∞. This dependence may not be given explicitly for the sake of convenience.

From Harrington [46] but using the definition

$$\overline{B} = \nabla \times \overline{A} \tag{A1}$$

the vector potential for the Hertzian dipole located at $x=qD_x$, $z=mD_z$ is

$$d\overline{A}_{q,m} = \hat{p}\,\frac{\mu_c\, I_{q,m}\, d\ell}{4\pi}\;\frac{e^{-j\beta R_{qm}}}{R_{qm}} \tag{A2}$$

where

$$R_{qm}^2 = a^2 + (mD_z-z)^2 \tag{A3}$$

$$a^2 = y^2 + (qD_x-x)^2 \tag{A4}$$

Substituting the magnitude of the modulated current from Equation (25) and summing over all the elements in the plane yields

$$d\overline{A} = \frac{\hat{p}\mu_c}{4\pi} \sum_{\nu=-\infty}^{\infty}\sum_{\mu=-\infty}^{\infty} \frac{I_x^{(\nu)} I_z^{(\mu)} d\ell}{\varepsilon_\nu \varepsilon_\mu} \sum_{q=-\infty}^{\infty}\sum_{m=-\infty}^{\infty}$$

$$\times\, e^{-j\beta q D_x s_x^\nu}\; e^{-j\beta m D_z s_z^\mu}\; \frac{e^{-j\beta R_{qm}}}{R_{qm}} \tag{A5}$$

The first step in the transformation is to deal with the sum on m. Isolating terms which depend on m yields

$$d\overline{A} = \frac{\hat{p}\mu_c}{4\pi} \sum_\nu \sum_\mu \frac{I_x^{(\nu)} I_z^{(\mu)} d\ell}{\varepsilon_\nu \varepsilon_\mu} \sum_q e^{-j\beta q D_x s_x^\nu} A_q \tag{A6}$$

where

$$A_q = \sum_m e^{-j\beta m D_z s_z^\mu} \frac{e^{-j\beta R_{qm}}}{R_{qm}} . \tag{A7}$$

Using the Poisson Sum Formula [47]

$$\sum_{m=-\infty}^{\infty} e^{jm\omega_o t} F(m\omega_o) = T \sum_{n=-\infty}^{\infty} f(t+nT) \tag{A8}$$

where $f(t)$ and $F(\omega)$ form a Fourier Transform pair and

$$T = \frac{2\pi}{\omega_o} \tag{A9}$$

the following transform pair from Bateman [48] can be used

$$\frac{e^{-j\beta\sqrt{a^2+\omega^2}}}{\sqrt{a^2+\omega^2}} \longleftrightarrow \frac{1}{2j} H_o^{(2)}(a\sqrt{\beta^2-t^2}) . \tag{A10}$$

A note of explanation should be given with this formula. It is formula 42 on p. 56. It appears in the table with two errors but the correct form should be,

$$(x^2+a^2)^{-1/2\nu}\ H_\nu^{(2)}\ [b(a^2+x^2)^{1/2}] \longleftrightarrow$$

Re $\nu > -1/2$

$a,b > 0$

$$\begin{cases} (1/2\pi a)^{1/2}(ab)^{-\nu}(b^2-u^2)^{1/2\nu-1/4}H_{\nu-1/2}^{(2)}[a(b^2-y^2)^{1/2}] & 0<y<b \\ \\ j(2a/\pi)^{1/2}(ab)^{-\nu}(y^2-b^2)^{1/2\nu-1/4}K_{\nu-1/2}[a(y^2-b^2)^{1/2}] & b<y<\infty \end{cases} \tag{A11}$$

Equation (A10) utilizes $\nu=1/2$ and the form for $0<y<b$. The left side of (A11) can be shown to be equal to the left side of (A10) using reference [49], specifically relations in sections 10.1.1, 10.1.11, and 10.1.12 of that reference.

Using the frequency shifting theorem

$$e^{j\omega_1 t} f(t) \leftrightarrow F(\omega-\omega_1) \tag{A12}$$

Equation (A9) becomes

$$\frac{e^{-j\beta\sqrt{a^2+(\omega-\omega_1)^2}}}{\sqrt{a^2+(\omega-\omega_1)^2}} \longleftrightarrow \frac{e^{j\omega_1 t}}{2j} H_0^{(2)}(a\sqrt{\beta^2-t^2}) \tag{A13}$$

Comparison of Equations (A7), (A8), and (A13) reveal the appropriate substitutions to be

$$\omega_o=D_z,\ T = \frac{2\pi}{\omega_o} = \frac{2\pi}{D_z},\ t = -\ \beta s_z^\mu,\ \omega_1 = z \tag{A14}$$

and Equation (A7) becomes

$$A_q = \frac{\pi}{jD_z} \sum_{n=-\infty}^{\infty} e^{-jz(\beta s_z^{\mu} + n \frac{2\pi}{D_z})} H_0^{(2)}(a\sqrt{\beta^2-(\beta s_z^{\mu} + n \frac{2\pi}{D_z})^2})$$

$$A_q = \frac{\pi}{jD_z} \sum_{n=-\infty}^{\infty} e^{-j\beta z(s_z^{\mu} + n \frac{\lambda}{D_z})} H_0^{(2)}(\beta r_\rho a) \tag{A15}$$

where

$$r_\rho = \sqrt{1 - (s_z^{\mu} + n \frac{\lambda}{D_z})^2} \tag{A16}$$

The next step is to substitute Equation (A15) into (A6) and separate all terms which depend on q. This leaves

$$d\overline{A} = \hat{p} \frac{\mu_c I d\ell}{4j D_z} \sum_{\nu} \sum_{\mu} \frac{I_x^{(\nu)} I_z^{(\mu)}}{\varepsilon_\nu \varepsilon_\mu} \sum_{n=-\infty}^{\infty} e^{-j\beta z(s_z^{\mu} + n \frac{\lambda}{D_z})}$$

$$\times \sum_{q=-\infty}^{\infty} e^{-j\beta q D_x s_x} H_0^{(2)}(\beta r_\rho a) \tag{A17}$$

Equation (A11) for ν=0 becomes

$$H_0^{(2)}(\beta r_\rho \; y^2+\omega^2) \longleftrightarrow \frac{e^{-jy\sqrt{(\beta r_\rho)^2-t^2}}}{\pi\sqrt{(\beta r_\rho)^2-t^2}} \tag{A18}$$

for

$$\omega_{\;0}=D_x, \quad T = \frac{2\pi}{D_x}, \quad t = -\beta s_x \quad . \tag{A19}$$

Applying the frequency shift theorem yields

$$H_0^{(2)}(\beta r_\rho \; y^2+(\omega-\omega_1)^2) \longleftrightarrow e^{j\omega_2 t} \frac{e^{-jy\sqrt{(\beta r_\rho)^2-t^2}}}{\pi\sqrt{(\beta r_\rho)^2-t^2}} \tag{A20}$$

Substituting ω_2=x and applying (A20) to (A17) and (A8) gives

$$d\bar{A} = \hat{p}\,\frac{\mu_c}{2j\beta D_x D_z}\sum_{\nu}\sum_{\mu}\frac{I_x^{(\nu)} I_z^{(\mu)} d\ell}{\varepsilon_\nu \varepsilon_\mu}\sum_{k}\sum_{n}\frac{e^{-j\beta\bar{R}.\hat{r}}}{r_y} \tag{A21}$$

where

$$\bar{R} = \hat{x}x + \hat{y}y + \hat{z}z \tag{A22}$$

$$\hat{r} = \hat{x}r_x \pm \hat{y}r_y + \hat{z}r_z \qquad y \gtrless 0 \tag{A23}$$

$$r_x = s_x^\nu + k\frac{\lambda}{D_x} = s_x + k\frac{\lambda}{D_x} + \nu\,\frac{\lambda}{1_x D_x} \tag{A24}$$

$$r_z = s_z^\mu + n\frac{\lambda}{D_z} = s_z + n\frac{\lambda}{D_z} + \mu\,\frac{\lambda}{1_z D_z} \tag{A25}$$

$$r_y = \sqrt{1 - r_x^2 - r_z^2} \tag{A26}$$

In Equation (A21) the -j value is taken for r_y to insure attenuation of the evanescent waves as their distance from the array increases.

To obtain the electric field, it is appropriate to first find $d\bar{H}$ from [50]

$$d\bar{H}(\bar{R}) = \frac{1}{\mu_c}\ \nabla x d\bar{A}(\bar{R}) \tag{A27}$$

with

$$\nabla x(\bar{A}\phi) = \phi\nabla\ x\bar{A} - \bar{A}x\ \nabla\phi \tag{A28}$$

and obtain

$$d\bar{H}(\bar{R}) = \frac{1}{2D_x D_z}\sum_{\nu}\sum_{\mu}\frac{I_x^{(\nu)} I_z^{(\mu)} d\ell}{\varepsilon_\nu \varepsilon_\mu}\sum_{k}\sum_{n}\frac{e^{-j\beta\bar{R}.\hat{r}}}{r_y}\ \hat{p} \times \hat{r} \tag{A29}$$

Substituting $d\bar{H}$ into

$$\bar{E} = \frac{1}{j\omega\varepsilon_c}\ \nabla x\bar{H} \tag{A30}$$

yields

$$d\overline{E}(\overline{R}) = \sum_{\nu}\sum_{\mu} \frac{I_x^{(\nu)} I_z^{(\mu)} d\ell Z_c}{\varepsilon_\nu \varepsilon_\mu 2D_x D_z} \sum_k \sum_n \frac{e^{-j\beta\overline{R}.\hat{r}}}{r_y} (\hat{p} \times \hat{r}) \times \hat{r} \tag{A31}$$

which is the desired expression for the electric field from an array of Hertzian dipoles with the reference located at the origin.

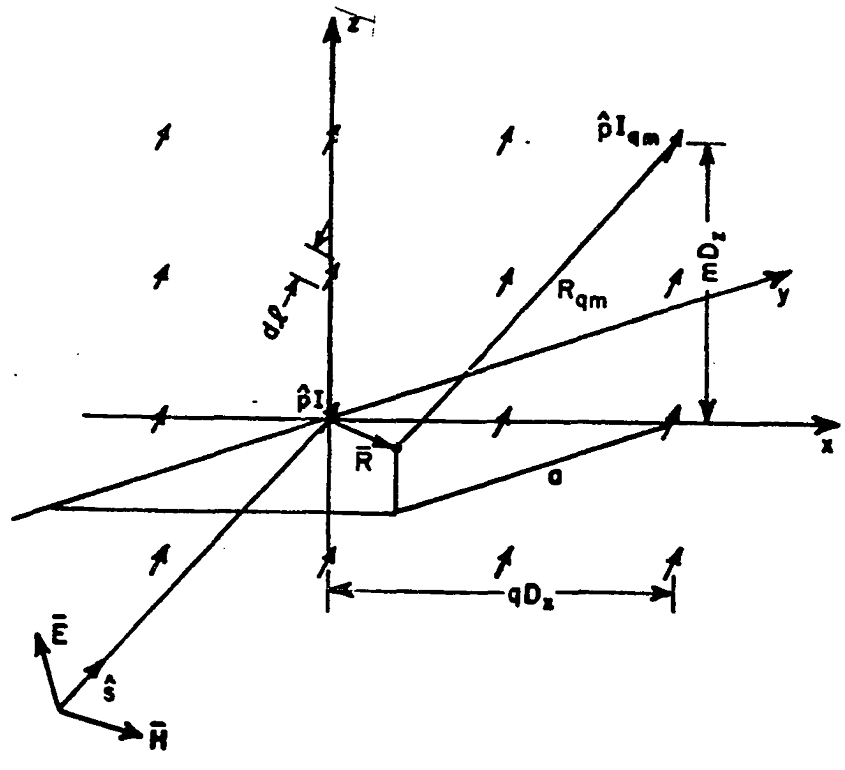

Figure A1. The field at $\overline{R}(x,y,z)$ from an infinite array.

APPENDIX B
PLANE WAVE REFLECTION COEFFICIENTS

This Appendix tabulates the plane wave reflection coefficients for the E and H fields when both are perpendicular or parallel to the plane of incidence. These formulas apply to a plane wave traveling in the direction $\hat{r}_1$ in semi-infinite medium (ε_1,μ_1) into semi-infinite medium 2 (ε_2,μ_2) where its direction becomes $\hat{r}_2$. The relationship between $\hat{r}_1$ and $\hat{r}_2$ is Snell's Law, which is given in the text as Equations (71) through (73). This list of the reflection coefficients is identical to [51] in form, with a generalization. The reflection coefficients are now given in terms of the intrinsic impedances and the intrinsic admittances of the two media, and r_{iy}, the y-component of the vector direction. This generalization allows for the two media to have different permeabilities as well as the case of complex permitivities and permeabilities, as the description of lossy media requires.

<u>Reference to the E-field</u>

$$ {}^{E}_{\perp}\Gamma_{1,2} = \frac{Z_2 r_{1y} - Z_1 r_{2y}}{Z_2 r_{1y} + Z_2 r_{2y}} \tag{B1} $$

$$ {}^{E}_{\parallel}\Gamma_{1,2} = \frac{Z_2 r_{2y} - Z_1 r_{1y}}{Z_2 r_{2y} + Z_1 r_{1y}} \tag{B2} $$

<u>Reference to the H-field</u>

$$ {}^{H}_{\perp}\Gamma_{1,2} = \frac{Y_2 r_{1y} - Y_1 r_{2y}}{Y_2 r_{1y} + Y_1 r_{2y}} \tag{B3} $$

$$ {}^{H}_{\parallel}\Gamma_{1,2} = \frac{Y_2 r_{2y} - Y_1 r_{1y}}{Y_2 r_{2y} + Y_1 r_{1y}} \tag{B4} $$

<u>Relationship between ^{E} and ^{H}</u>

$$ {}^{E}_{\perp}\Gamma_{1,2} = - {}^{E}_{\perp}\Gamma_{2,1} = - {}^{H}_{\parallel}\Gamma_{1,2} = {}^{H}_{\parallel}\Gamma_{2,1} \tag{B5} $$

$$ {}^{E}_{\parallel}\Gamma_{1,2} = - {}^{E}_{\parallel}\Gamma_{2,1} = - {}^{H}_{\perp}\Gamma_{1,2} = {}^{H}_{\perp}\Gamma_{2,1} \tag{B6} $$

APPENDIX C
THE PATTERN FACTOR

This appendix gives the derivation for the pattern factor of Equations (50) and (56) for straight z-directed elements. An expression for the pattern factor, directly translatable into computer code is presented here with the operation which finds the parallel and perpendicular components of the pattern factor, ${}_{\parallel}P_2^{(1)}$ and ${}_{\perp}P_2^{(1)}$ of Equation (76), respectively.

The two equations of interest are repeated here for convenience. The first, Equation (50), the pattern factor of the array reference element, is

$$P_2^{(1)} = \frac{1}{I^{(1)}(\bar{R}^{(1)})} \int_a^b I^{(1)}(\ell) \; e^{j\beta\ell\hat{p}^{(1)}\cdot\hat{r}} \, d\ell. \tag{C1}$$

The second, Equation (56), the pattern factor of the test element under transmitting conditions, is

$$P_2^{(2)t} = \frac{1}{I^{(2)t}(\bar{R}^{(2)})} \int_a^b I^{(2)t}(\ell) \; e^{-j\beta\ell\hat{p}^{(2)}\cdot\hat{s}} \, d\ell. \tag{C2}$$

Both equations represent a current times an appropriate phase factor integrated over the length of the element, divided by the terminal current. Requiring the test and array elements to be identical straight z-directed dipoles near resonance allows the current to be written as

$$I(\ell) = \sin[\beta_d(\ell_e-|\ell|)] \tag{C3}$$

where ℓ is the variable of integration over the length of the element which extends from -z' to z', $_d$ is the effective propagation constant along the element, and ℓ_e is the effective (half) length of the element which takes into account the actual (half) length and the capacitance effects near the ends of the slots or flat dipoles. z', the actual (half) length, is less than ℓ_e, the effective (half) length. The current is plotted in Figure C1. In this study where slots are used as elements, β_d was calculated using

$$\beta_d = \sqrt{\frac{\beta_L^2 + \beta_R^2}{2}} \tag{C4}$$

where β_L and β_R are the propagation constants in the media to the left and to the right of the slot, respectively [52]. For the flat dipoles, β_d was set to the value of β in the medium containing the dipoles. The effective length for slots and flat dipoles was calculated using Reference [53] with one correction found recently [54]. When the incremental length change was first formulated, it contained two correction terms. One term accounted for the fringe field close to the end of the dipole. The other was concerned with capacitance effects due to the finite thickness of the dipole. When this formulation was applied to slots in a ground plane with finite thickness, it was discovered that the resonance frequency was predicted incorrectly. It turns out that the second term becomes an inductance for slots and should be subtracted rather than added as it was in the dipole case. The first term is unchanged. This does not violate Babinet's Principle, which says that the dipole and slot situations are complementary (as stated at the end of Chapter III). Babinet's Principle applies exactly only to infinitesimally thin flat dipoles or ground planes, in which case the second term is zero and the corrections to both situations are identical.

Because $\hat{s}$ in Equation (C2) represents a plane wave's "propagating" direction, which in this study is $\hat{r}$, and because all elements are straight and z-directed (i.e., $\hat{p}^{(1)} = \hat{p}^{(2)} = \hat{z}$) the phase terms in Equations (C1) and (C2) can be written as

$$e^{-jt\beta_d \ell \hat{z}\cdot\hat{r}} = e^{-jt\beta\ell r_z} \tag{C5}$$

where

$$t = \begin{cases} +1 & \text{transmitting case} \\ -1 & \text{non-transmitting case.} \end{cases} \tag{C6}$$

The above notation can be used to rewrite the pattern factor equations as

$$P_2 = \frac{1}{\sin(\beta_d \ell_e)} \int_{-z'}^{z'} \sin \beta_d(\ell_e - |\ell|)\, e^{-jt\beta\ell r_z} d\ell \tag{C7}$$

Performing the integration yields

$$P_2 = \frac{1}{\sin(\beta_d \ell_e)} \left[\frac{1}{\beta_d + t\beta r_z} \left\{ \cos[\beta_d(\ell_e - z') - t\beta r_z z'] - \cos(\beta_d \ell_e) \right\} + \frac{1}{\beta_d - t\beta r_z} \left\{ \cos[\beta_d(\ell_e - z') + t\beta r_z z'] - \cos(\beta_d \ell_e) \right\} \right] \tag{C8}$$

Since the above expression is independent of the allowed values of $t(\pm 1)$, the final expression for the pattern factor of both the array elements and the test element is

$$P_2^{(1)} = P_2^{(2)t} = P_2 = \frac{1}{\sin(\beta_d \ell_e)} \times$$

$$\times \left[\frac{1}{\beta_d + \beta r_z} \left\{ \cos[\beta_d(\ell_e - z') - \beta r_z z'] - \cos(\beta_d \ell_e) \right\} \right.$$

$$\left. + \frac{1}{\beta_d - \beta r_z} \left\{ \cos[\beta_d(\ell_e - z') + \beta r_z z'] - \cos(\beta_d \ell_e) \right\} \right] \qquad \text{(C9)}$$

Reference [55] defines that the parallel (perpendicular) component of the pattern factor is equal to the pattern factor times the component of the unit vector of the array element direction in the direction of the unit vector palallel (perpendicular) to the plane of incidence, or

$$_{(\perp\parallel)}P_2^{(1)} = P_2^{(1)} \hat{p}^{(1)} \cdot {}_{(\perp\parallel)}\hat{n}_2 \qquad \text{(C10)}$$

For straight z-directed elements $\hat{p}^{(1)}$ is $\hat{z}$ and

$$_{\perp}\hat{n}_2 = \frac{-\hat{x}\, r_{2z} + \hat{z}\, r_{2x}}{\sqrt{r_{2x}^2 + r_{2z}^2}} \qquad \text{(C11)}$$

$$_{\parallel}\hat{n}_2 = \frac{1}{\sqrt{r_{2x}^2 + r_{2z}^2}} \left[-\hat{x}\, r_{2x} r_{2y} + \hat{y}(r_{2x}^2 + r_{2z}^2) - \hat{z}\, r_{2y} r_{2z} \right] \qquad \text{(C12)}$$

which gives

$$_{\perp}P_2^{(1)} = P_2^{(1)} \frac{r_{2x}}{\sqrt{r_{2x}^2 + r_{2z}^2}} \qquad \text{(C13)}$$

$$_{\parallel}P_2^{(1)} = P_2^{(1)} \frac{-r_{2y} r_{2z}}{\sqrt{r_{2x}^2 + r_{2z}^2}} \qquad \text{(C14)}$$

These last two expressions are the ones used in Ω in Equation (76).

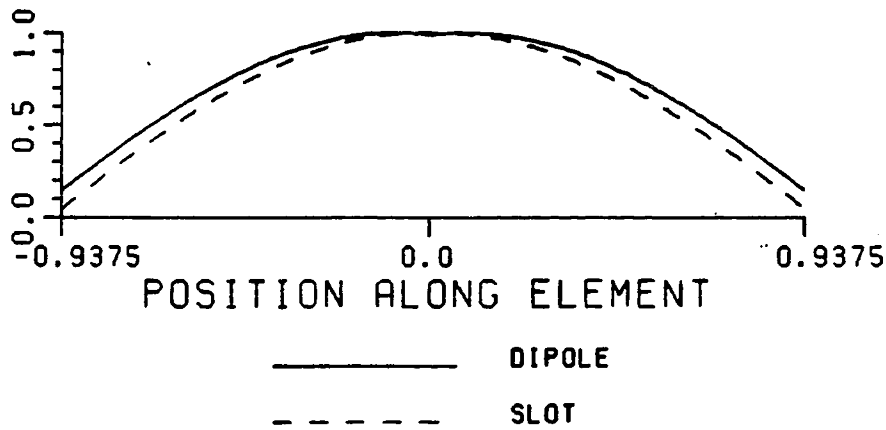

Figure C1. The currents on the slot and dipole elements used in this study.

APPENDIX D
FOURIER COEFFICIENTS

This Appendix gives the Fourier Coefficients for the aperture distributions used in this study. Coefficients of four even distributions which yield sum patterns are given with one odd distribution which yields a difference pattern.

The geometry for the Coefficient calculation in one dimension (along x) is given as Figure D1. For all of the following distributions K_x is the width of the finite aperture, D_x is the interelement spacing, and $(i_x D_x)$ is the modulation period, i.e., the spacing between the centers of the finite apertures. Because the aperture distributions are chosen to be separable in x and z (as shown in Chapter II), these coefficients for the different distributions apply to the z-direction also and can be used in any combinations along x and z.

For the even distributions the form of the Fourier Sum is

$$f_s(x) = \sum_{n=0}^{\infty} a_n \cos\left(\frac{2n\pi}{T} x\right) \tag{D1}$$

with the coefficients, a_n, being given by

$$a_o = \frac{2}{T} \int_0^{\frac{T}{2}} f(x)dx \tag{D2}$$

$$a_n = \frac{4}{T} \int_0^{\frac{T}{2}} f(x)\cos\left(\frac{2n\pi}{T} x\right) dx, \quad n\neq 0 \tag{D3}$$

Since the value of f_s is of interest only at element locations (x=qDx) and since the period, T, is $i_x D_x$, Equation (D1) can be written as

$$f_s(qDx) = \sum_{n=0}^{\infty} a_n \cos\left(\frac{2n\pi}{ix} q\right) \tag{D4}$$

For the cosine distribution of Figure D1, f(x) is given by $\cos\left(\frac{\pi}{K_x} x\right)$ and the Fourier Coefficients of Equations (D2) and (D3) become

$$a_o = \frac{2K_x}{i_x \pi} \tag{D5}$$

$$a_n = a_o \left[\frac{\sin \frac{\pi}{2} \left(\frac{i_x - 2nK_x}{i_x} \right)}{\frac{i_x - 2nK_x}{i_x}} + \frac{\sin \frac{\pi}{2} \left(\frac{i_x + 2nK_x}{i_x} \right)}{\frac{i_x + 2nK_x}{i_x}} \right] , \quad n \neq 0 \tag{D6}$$

The coefficients for the rectangular pulse of Figure D2 are

$$a_o = \frac{K_x}{i_x} \tag{D7}$$

$$a_n = \frac{2}{n\pi} \sin \left(\frac{n\pi K_x}{i_x} \right) , \quad n \neq 0 \tag{D8}$$

The coefficients for the trapezoidal pulse of Figure D3 are

$$a_o = \frac{G_x + 2K_x}{2i_x} \tag{D9}$$

$$a_n = \frac{2i_x}{G_x n^2 \pi^2} \left[\cos \left(n\pi \frac{K_x}{i_x} \right) - \cos \left(n\pi \frac{K_x + G_x}{i_x} \right) \right] , \quad n \neq 0 \tag{D10}$$

The coefficients for the rectangular pulse sum of Figure D4 are

$$a_o = \frac{1}{i_x} \left[(C-B)G_x + (B-A)F_x + A \cdot K_x \right] \tag{D11}$$

$$a_n = \frac{2}{n\pi} \left[(C-B)\sin \left(n\pi \frac{G_x}{i_x} \right) + (B-A)\sin \left(n\pi \frac{F_x}{i_x} \right) + A \cdot \sin \left(n\pi \frac{K_x}{i_x} \right) \right] , \quad n \neq 0 \tag{D12}$$

For odd distributions the appropriate form of the Fourier Sum is

$$f_s(qD_x) = \sum_{n=1}^{\infty} b_n \sin\left(\frac{2n\pi}{i_x}\, q,\right) \tag{D13}$$

where

$$b_n = \frac{4}{i_x} \int_0^{\frac{ix}{2}} f(x)\sin\left(\frac{2n\pi}{i_x}\, x\right)dx \tag{D14}$$

The only such difference distribution employed in this study is shown in Figure D5. It is taken from [50] and given analytically for $x>0$ by

$$f(x) = \begin{cases} 2x\, \cos\left(\frac{\pi}{K_x}\, x\right) & 0 \leq x \leq \frac{K_x}{2} \\ 0 & \frac{K_x}{2} \leq x \leq \frac{i_x}{2} \end{cases} \tag{D15}$$

The Fourier Coefficients for this distribution are

$$b_n = -\frac{8}{i_x}\left\{\frac{K_x}{4}\left[\frac{\cos(B-A)\,\frac{K_x}{2}}{B-A} + \frac{\cos(B+A)\,\frac{K_x}{2}}{B+A}\right] - \frac{1}{2(B-A)^2}\sin(B-A)\,\frac{K_x}{2} - \frac{1}{2(B+A)^2}\sin(B+A)\,\frac{K_x}{2}\right\} \tag{D16}$$

where

$$A = \frac{\pi}{K_x} \tag{D17}$$

and

$$B = \frac{2n\pi}{i_x} \tag{D18}$$

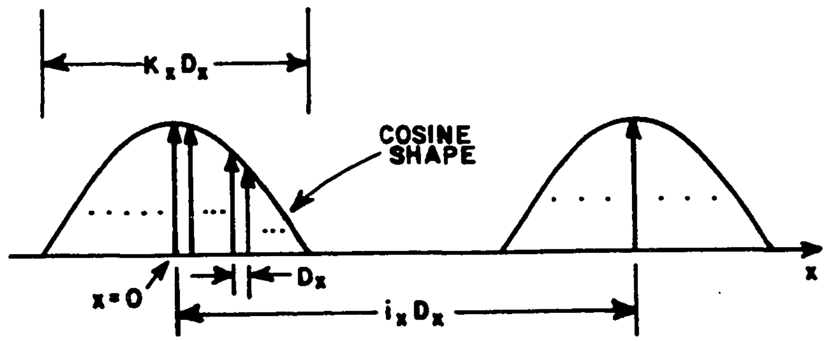

Figure D1. The parameters used in calculating the Fourier coefficients for the cosine aperture distribution.

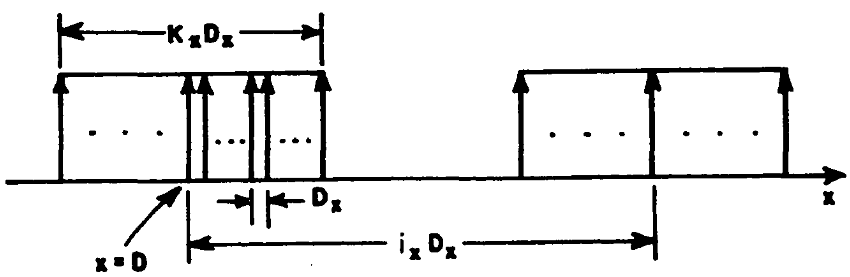

Figure D2. The parameters used in calculating the Fourier coefficients for the pulse aperture distribution.

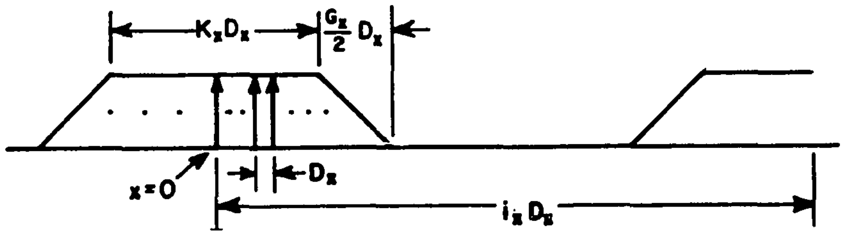

Figure D3. The parameters used in calculating the Fourier coefficients for the trapezoidal aperture distribution.

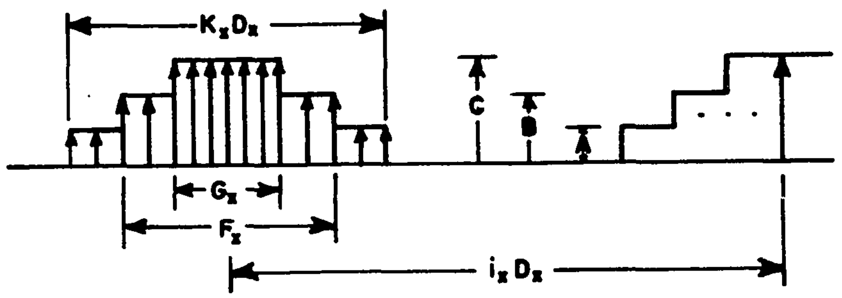

Figure D4. The parameters used in calculating the Fourier coefficients for the step aperture distribution.

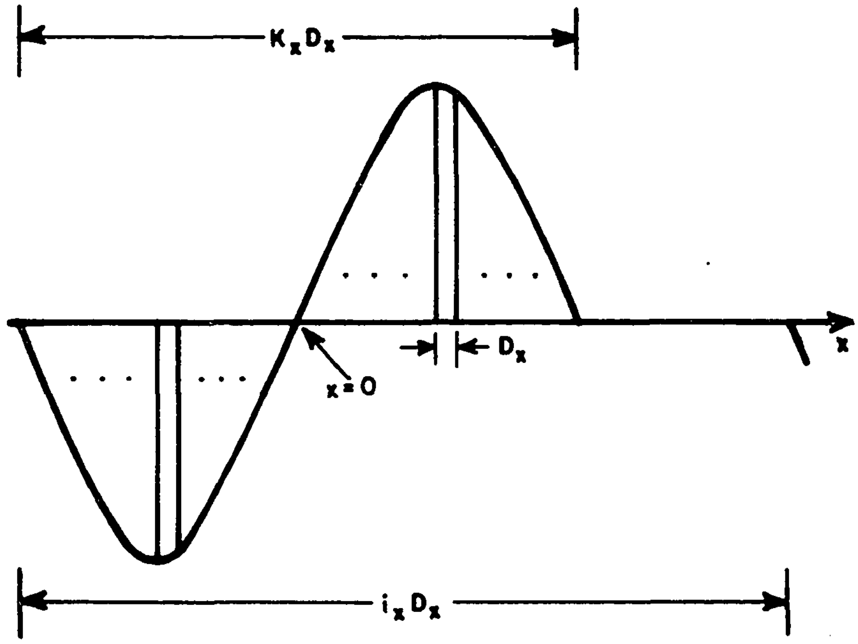

Figure D5. The parameters used in calculating the Fourier coefficients for the odd difference pattern aperture distribution.

APPENDIX E
COMPARISON OF THE PRESENT METHOD WITH
THE MUTUAL IMPEDANCE METHOD

Since the methods of this study are new, it was desired to find a confirmation of results through a different method of calculation. Although it may have been possible to find a similar goal of calculating the element by element immittance of a large finite phased array in the general literature, it was decided to use the mutual impedance method programs of J. H. Richmond [57] (labeled the direct method in the rest of this Appendix) to simulate a large finite two-dimensional array of dipoles which closely resembles a geometry modeled using the methods of this study (labeled the transform method in the rest of this Appendix).

The geometry employed is depicted in Figure E1. The direct method models K_x x K_z linear z-directed thin, half-wave, single mode and dipoles with interelement spacings D_x and D_z. The transform method models a similar array of z-directed dipoles which is finite in the x-direction. The medium surrounding both arrays is free space. This condition is necessary because the direct method cannot be applied to a dielectric covered array. Currents are identical for any elements in a given column in the direct method which corresponds roughly to the one-dimensional array in the transform method. A cosine distribution was used for both methods in the x-direction. To closer simulate the transform example, the direct method used the actual input currents of the transform method which include the slight errors due to Fourier truncation.

A thorough description of the mutual impedance method is not given here but a brief explanation of the technique for finding the impedance of an individual element is. Figure E2 gives an example. The currents along any column are identical, as will be the resulting voltages and impedances. The voltages can be written as functions of the currents and mutual impedances as

$$I_1(Z_{11}+Z_{14}+Z_{17}) + I_2(Z_{12}+Z_{15}+Z_{18}) + I_3(Z_{13}+Z_{16}+Z_{19}) = V_1 \qquad \text{(E1)}$$

$$I_1(Z_{12}+Z_{24}+Z_{27}) + I_2(Z_{22}+Z_{25}+Z_{28}) + I_3(Z_{23}+Z_{26}+Z_{29}) = V_2 \qquad \text{(E2)}$$

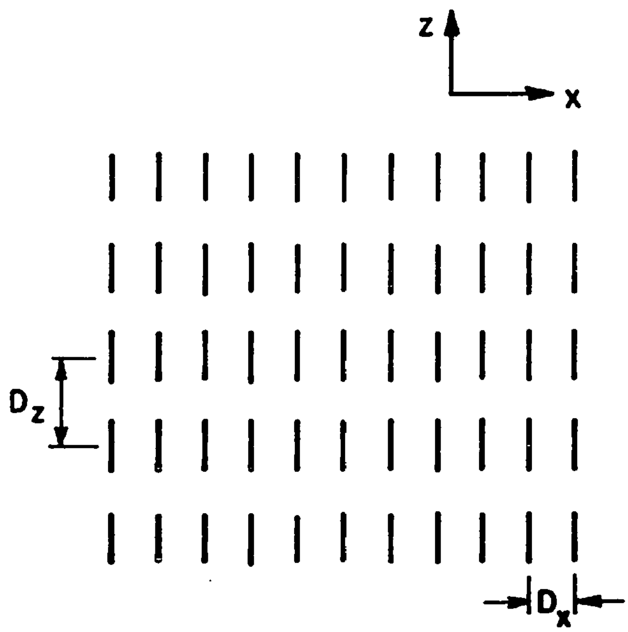

Figure E1. The geometry of the array used in the direct method.

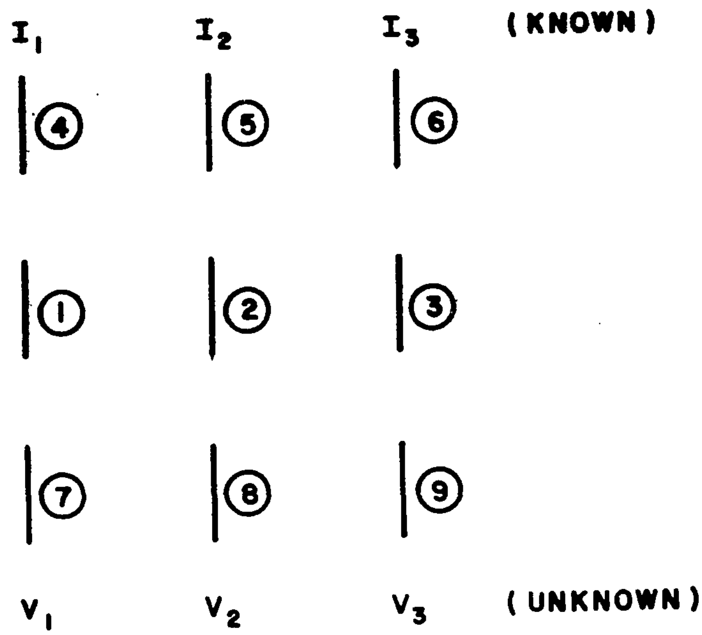

Figure E2. The array used as an example explaining the approach of the direct method.

$$I_1(Z_{13}+Z_{34}+Z_{37}) + I_2(Z_{32}+Z_{35}+Z_{38})$$
$$+ I_3(Z_{33}+Z_{36}+Z_{39}) = V_3 \tag{E3}$$

Since the center row is an axis of symmetry any impedance associated with an element in the first row is equal to the corresponding impedance associated with the third row. Equations (E1) through (E3) can then be written as

$$\begin{pmatrix} Z_{11}+2Z_{14} & Z_{12}+2Z_{15} & Z_{13}+2Z_{16} \\ Z_{12}+2Z_{24} & Z_{22}+2Z_{25} & Z_{23}+2Z_{26} \\ Z_{13}+2Z_{34} & Z_{32}+2Z_{35} & Z_{33}+2Z_{36} \end{pmatrix} \begin{pmatrix} I_1 \\ I_2 \\ I_3 \end{pmatrix} = \begin{pmatrix} V_1 \\ V_2 \\ V_3 \end{pmatrix} \tag{E4}$$

Examination of the diagonal elements of the impedance matrix reveals these elements to be equal. Each is the self-impedance of a center-row element added to the mutual impedances of the elements above and below it. Similar geometrical symmetries reveal

$$Z_{15} = Z_{24} = Z_{26} = Z_{35} \tag{E5}$$

$$Z_{16} = Z_{34} \tag{E6}$$

which shows the impedance matrix to be symmetric and Toeplitz, i.e., of the form

$$\begin{pmatrix} Z(1) & Z(2) & Z(3) \\ Z(2) & Z(1) & Z(2) \\ Z(3) & Z(2) & Z(1) \end{pmatrix} \begin{pmatrix} I_1 \\ I_2 \\ I_3 \end{pmatrix} = \begin{pmatrix} V_1 \\ V_2 \\ V_3 \end{pmatrix} \tag{E7}$$

This analysis shortens computation time. Professor Richmond's mutual impedance routines are used to calculate Z(1), Z(2), and Z(3). Performing the multiplication of Equation (E7) yields the voltages. Subsequent division by the associated current results in the impedance of the desired center-row element (and thereby all elements).

One further note on the transform method in this comparison is necessary. As stated in Appendix C, for the slot or flat dipole half-wave element case in this study, an incremental length was added to the actual element length to allow for capacitance effects near the ends. Since no similar theory was readily available for dipoles, the increment was set to zero in the examples of this Appendix.

For the examples presented here, the lengths of the elements are 0.5λ, the spacing in the z-direction, D_z, is 0.6λ and the arrays have either 31 or 61 elements in the x-direction. For the transform method, i_x is 349. The direct method, which is finite in the z-direction, has 41 elements along z. Making this number larger or slightly smaller had little effect on the results. Because the currents are equal on elements in any column along z, the finiteness along z is still considered to be a good model for an array which is infinite in the z direction.

The first comparison is shown in Figures E3 and E4 for arrays with 31 elements in the x-direction scanned at broadside. The magnitude and phase values are remarkably similar for the two methods Some disagreement, which could be attributed to many factors, does exist. The current shapes on individual elements are not exactly the same. This variation could easily be responsible for the slight disagreement in the values. Considering the significant differences in the two methods, the results compare favorably.

Figures E5 and E6 compare magnitude and phase results for a 50° scan and an array width of 31 elements. Again, agreement is excellent in the interior of the array with elements near the edge disagreeing to a larger extent.

One further experiment was performed, namely, the width of the array in the x-direction was increased to 61 elements. The results for this effort are presented in Figures E7 and E8. The magnitude and phase are more nearly constant in the interior of this large array than in the smaller array, as would be expected. A further example of this large array comparison is given in Chapter IV with Figures 29 through 32 for a 60° scan.

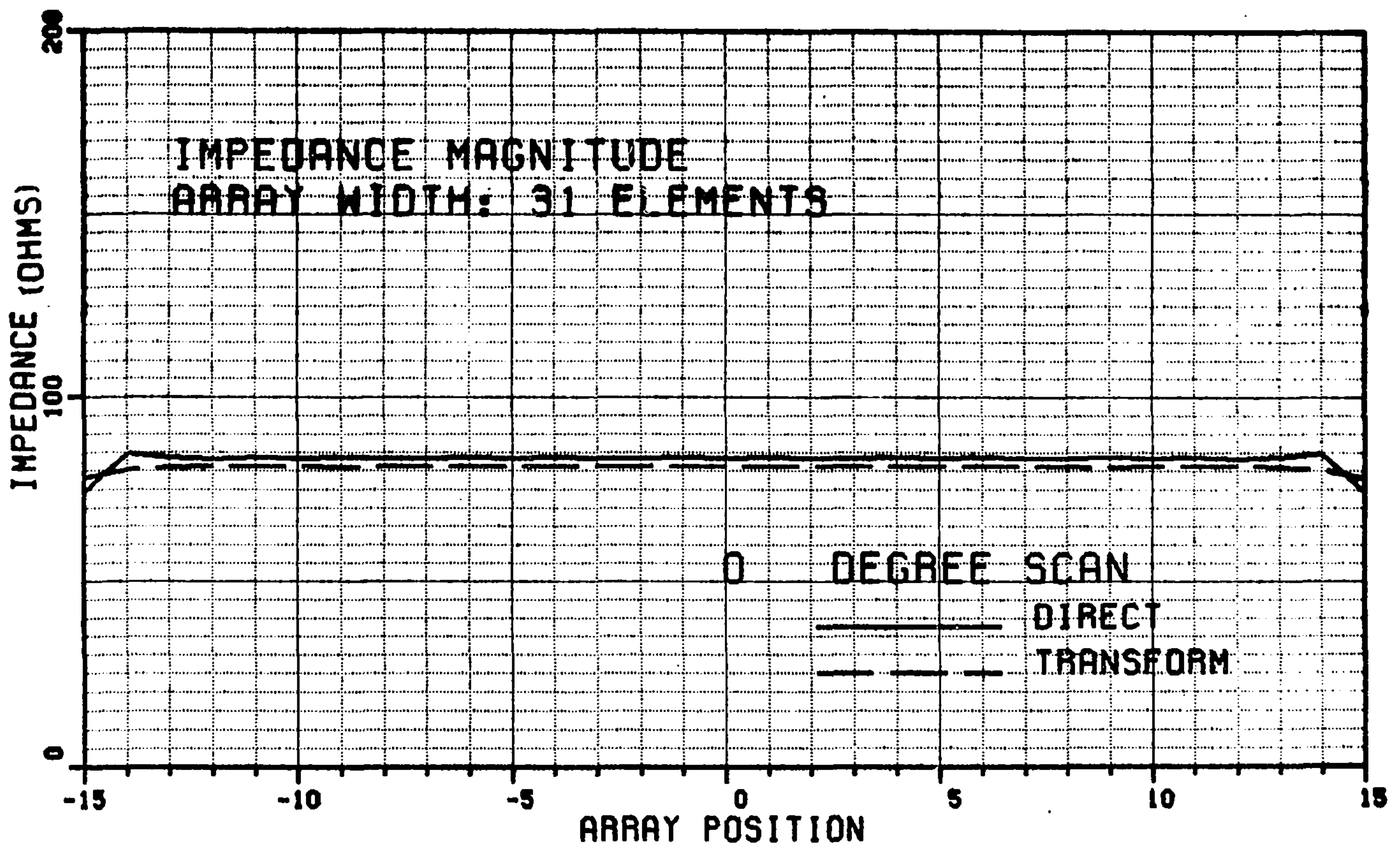

Figure E3. Comparison of impedance magnitude values between the direct and transform methods for an array 31 elements wide at a broadside scan angle.

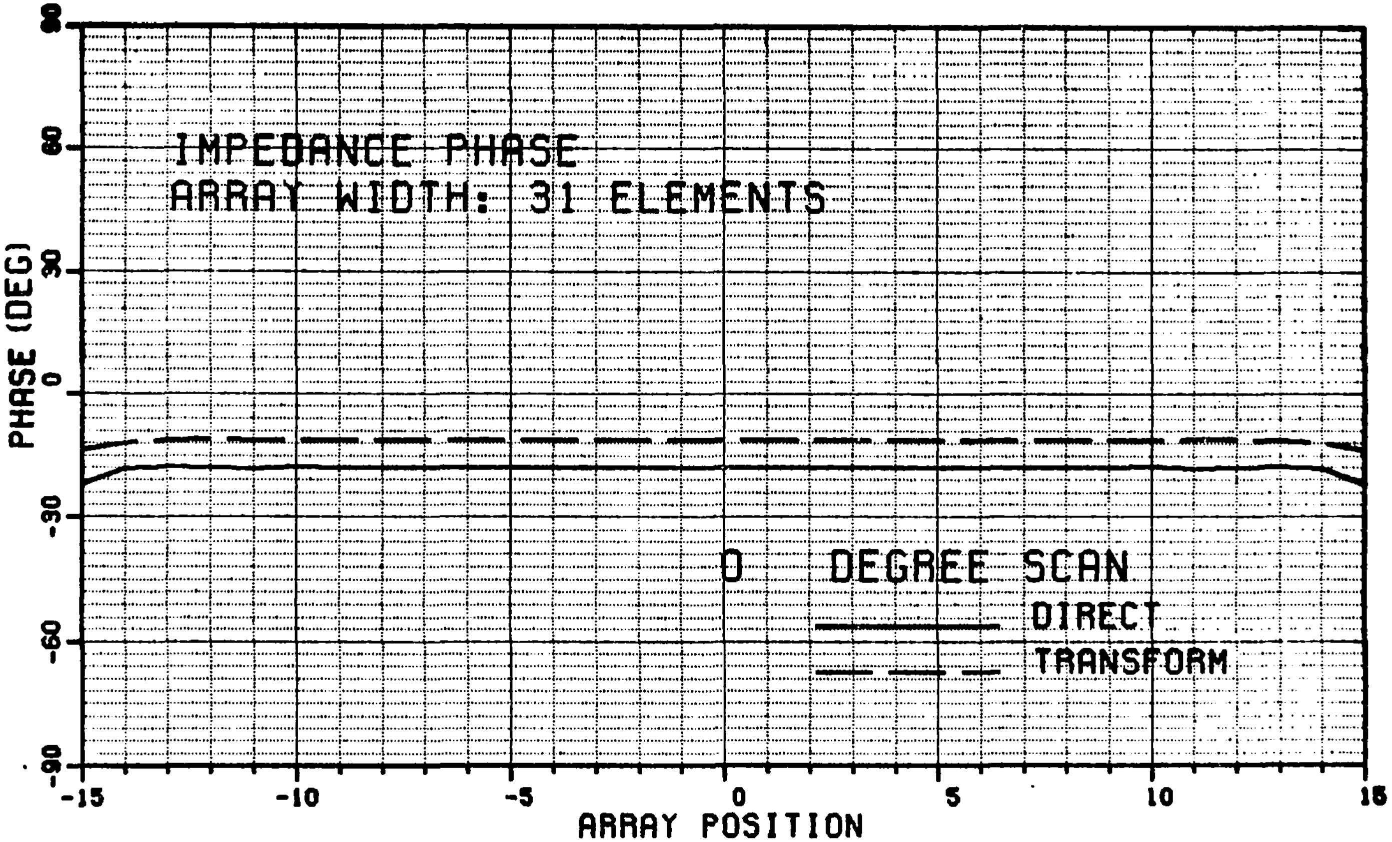

Figure E4. Comparison of impedance phase values between the direct and transform methods for an array 31 elements wide at a broadside scan angle.

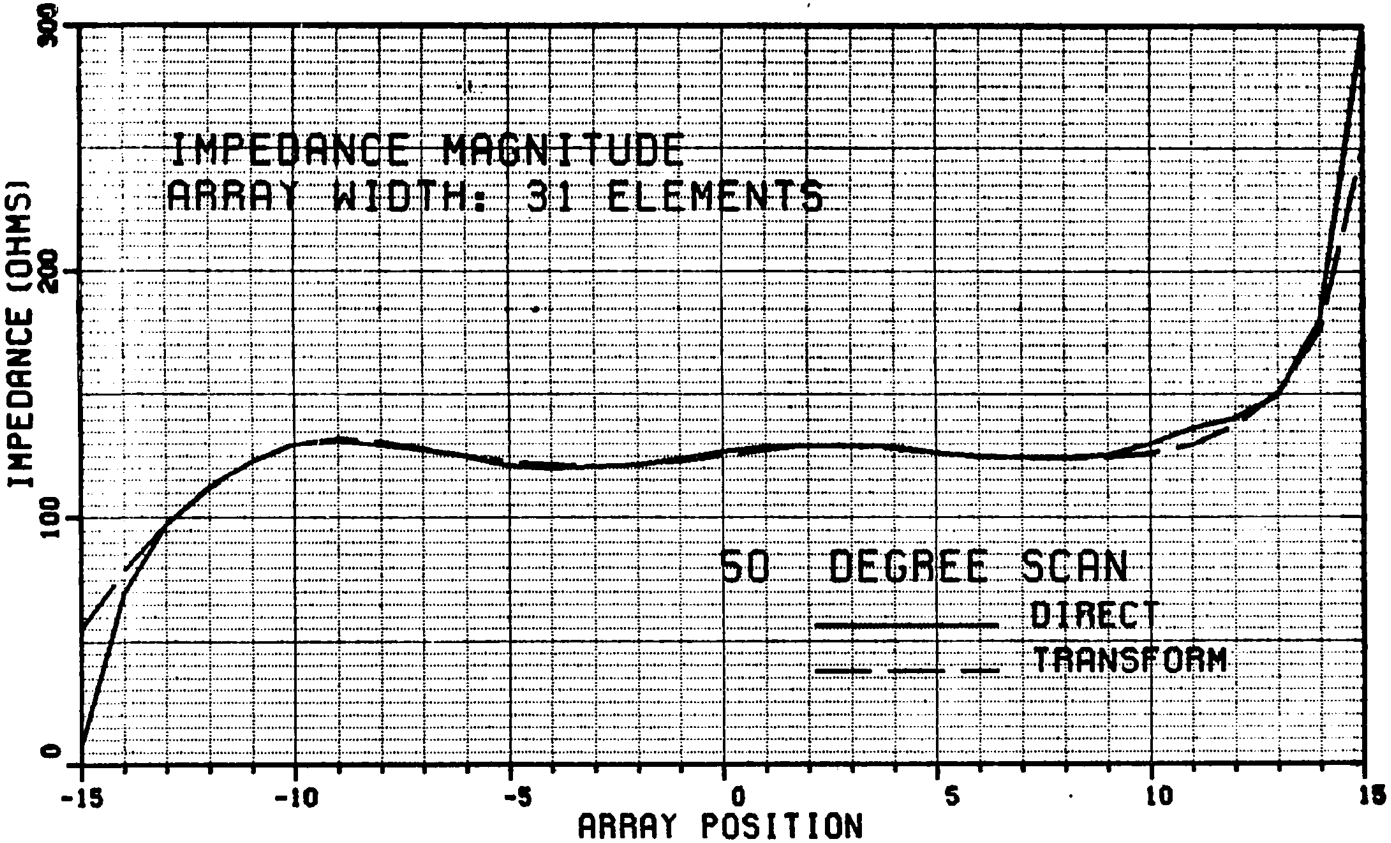

Figure E5. Comparison of impedance magnitude values between the direct and transform methods for an array 31 elements wide at a 50° scan angle to the right.

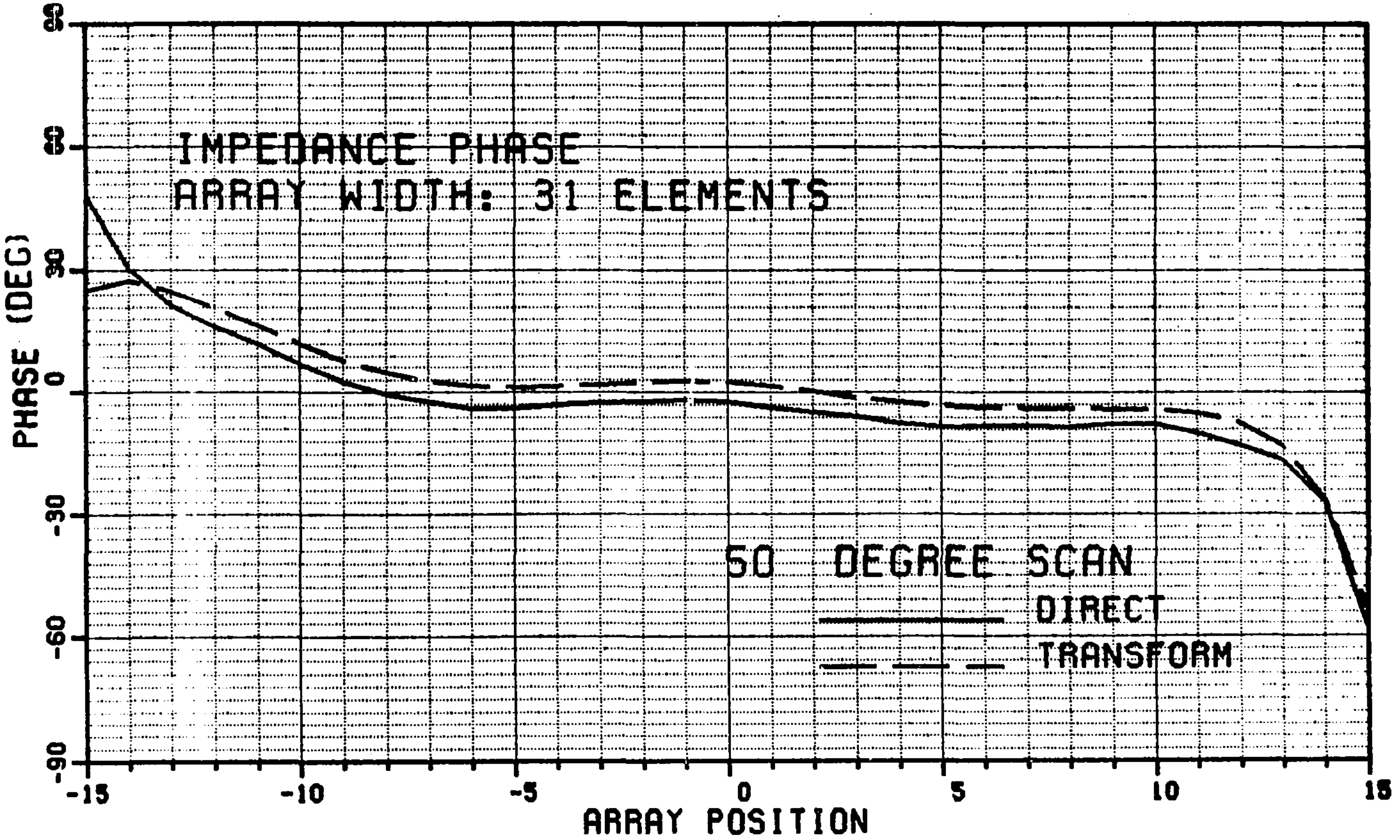

Figure E6. Comparison of impedance phase values between the direct and transform methods for an array 31 elements wide at a 50^{o} scan angle to the right.

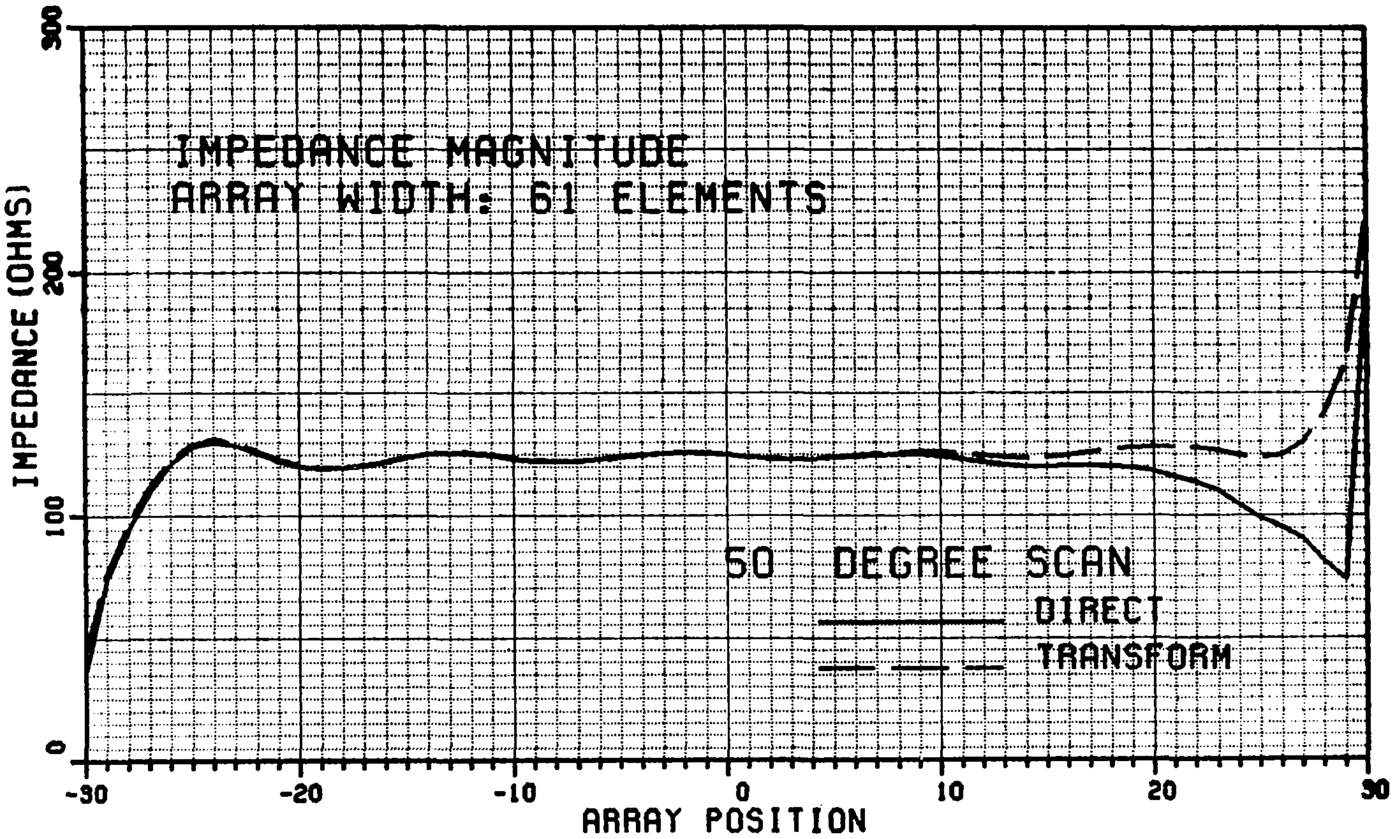

Figure E7. Comparison of impedance magnitude values between the direct and transform methods for an array 61 elements wide at a 50^{0} scan angle to the right.

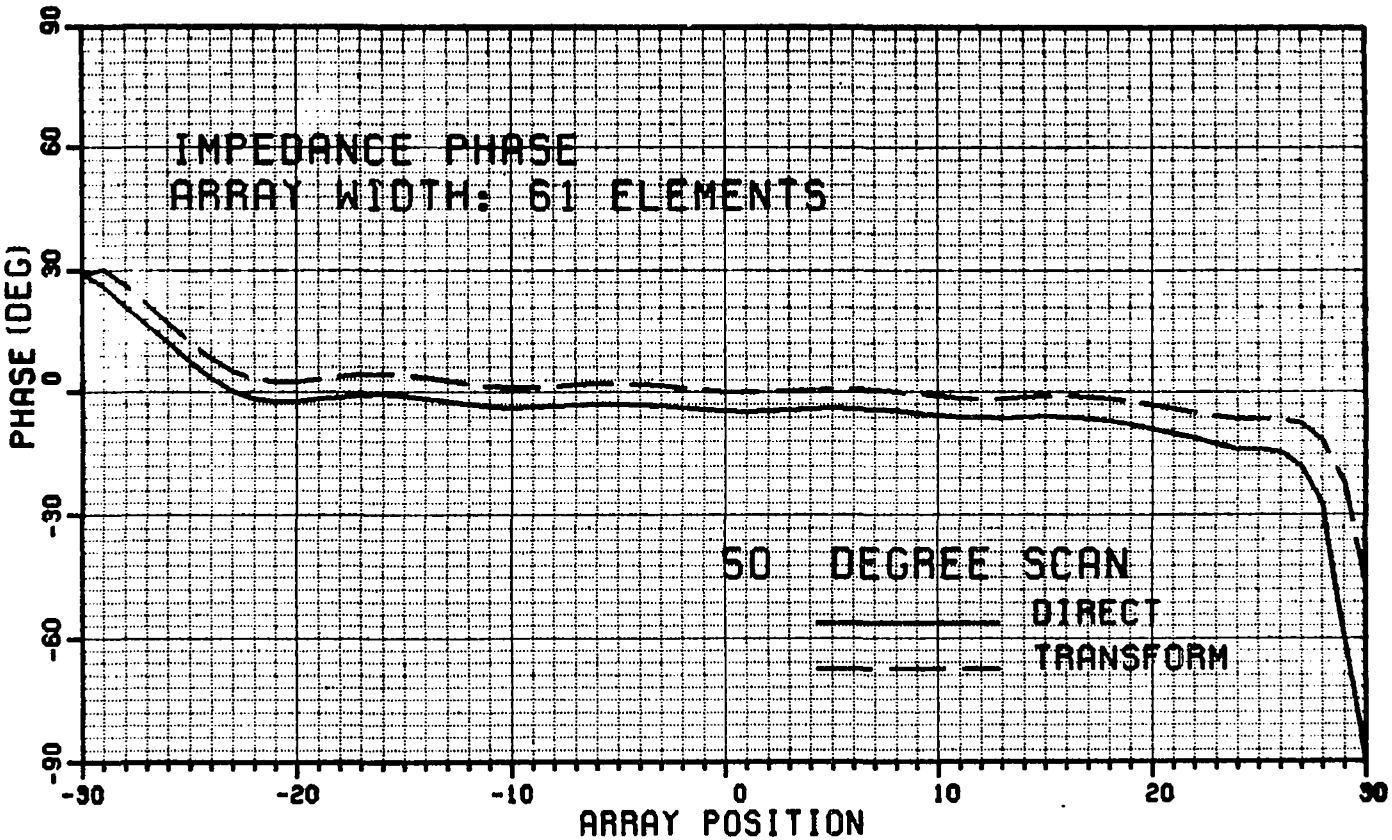

Figure E8. Comparison of impedance phase values between the direct and transform methods for an array 61 elements wide at a 50° scan angle to the right.

APPENDIX F
TRANSFORMATION FACTOR DENOMINATOR

In addition to grating lobes which can occur in any phased array (and can be eliminated by keeping the interelement spacing small enough) another phenomenon known as trapped grating lobes can occur in dielectric covered phased arrays. If the array is immersed in a dielectric which has a permittivity higher than that outside the dielectric (which is usually the case where free space exists outside the dielectric), any attempt to scan the array past the critical angle will result in a wave being guided inside the dielectric with no radiation outside the dielectric into free space, only evanescent modes there. Although it would not normally be prudent to scan past the critical angle, the method presented in this effort uses terms which correspond to scans in many directions, one or more of which may cause some difficulty. Isolating this problem in the present formulation is possible by stating the conditions for a scan direction which allows a propagating wave in the dielectric (r_{2y} is real) with an evanescent wave in free space (r_{1y} is imaginary) and realizing that the transformation factor of Equation (74) (in the text) treats the effects of the dielectric slab. The most obvious aspect of this expression which may cause problems is the possibility of the denominator of the transformation factor going to zero. This condition is examined in this appendix for three geometries; 1) dipole array in the center of a dielectric slab, 2) slot array in the center of a dielectric slab, and 3) dipole array in the center of a dielectric slab with one boundary of the slab being a perfectly conducting ground plane.

1. Dipole Array in a Dielectric Slab

The equation of interest for the geometry of Figure 39 is the general transformation factor expression of Equation (74) specialized to Equation (85) for this case. The condition for the denominator being zero is

$$ {}_{(\perp\shortparallel)}^{E}\Gamma_{2,1}\, e^{-j2\beta_2 d_2 r_{2y}} = 1 = e^{j2n\pi} \quad , n=0,\pm1,\pm2,\ \ldots \qquad \text{(F1)}$$

where d_2 is the half-width of the dielectric, β_2 is its propagation constant, r_{2y} is the magnitude of the y-component of the vector direction of propagation in the dielectric, and ${}_{(\perp\shortparallel)}^{E}\Gamma_{2,1}$ is the perpendicular or parallel electric field reflection coefficient inside the dielectric as given in Appendix B. The perpendicular and parallel cases are examined separately below. For all examples in this appendix the permeabilities of all media are equal to that of free space and the permittivity of medium 1 is that of free space so that its relative dielectric constant is unity.

A. Perpendicular case - dipoles

The reflection coefficient for this case can be found from Appendix B. It is

$$ {}^{E}_{\perp}\Gamma_{2,1} = \frac{\sqrt{\varepsilon_2}\, r_{2y} - \sqrt{\varepsilon_1}\, r_{1y}}{\sqrt{\varepsilon_2}\, r_{2y} + \sqrt{\varepsilon_1}\, r_{1y}} = \frac{\sqrt{\varepsilon_2} r_{2y} - r_{1y}}{\sqrt{\varepsilon_2} r_{2y} + r_{1y}} \tag{F2} $$

To show that r_{2y} must be pure real and that r_{1y} must be pure imaginary, it is useful to examine Equation (F1) carefully. The reflection coefficient must have magnitude less than or equal to unity on physical grounds. Therefore, the exponential term must have unity or greater magnitude which implies that r_{2y} is pure real (the exponential term being larger than one is ruled out as that would imply a field growing in magnitude as it leaves the source). If r_{1y} were pure real, Equation (F2) would indicate the reflection coefficient to be pure real and less than one. The condition of Equation (F1) could not be realized so r_{1y} must be pure imaginary or

$$ {}^{E}_{\perp}\Gamma_{2,1} = \frac{\sqrt{\varepsilon_2} r_{2y} - j|r_{1y}|}{\sqrt{\varepsilon_2} r_{2y} + j|r_{1y}|} = e^{-j2\tan^{-1}\left(\frac{|r_{1y}|}{\sqrt{\varepsilon_2} r_{2y}}\right)} \tag{F3} $$

Equation (F1) becomes

$$ e^{-j2\tan^{-1}\left(\frac{|r_{1y}|}{\sqrt{\varepsilon_2} r_{2y}}\right)} e^{-j2\beta d_2 r_{2y}} = e^{j2n\pi} \tag{F4} $$

or

$$ \tan^{-1}\left(\frac{|r_{1y}|}{\sqrt{\varepsilon_2} r_{2y}}\right) + \beta_2 d_2 r_{2y} = -n\pi \tag{F5} $$

which can be written as

$$ \frac{|r_{1y}|}{\sqrt{\varepsilon_2} r_{2y}} = \tan\left(-\beta_2 d_2 r_{2y} - n\pi\right) \tag{F6} $$

Only two values of n need be examined;

<u>n=0</u> $$\frac{|r_{1y}|}{\sqrt{\varepsilon_2}\, r_{2y}} = -\tan(\beta_2 d_2 r_{2y}) \tag{F7}$$

<u>n=1</u> $$\frac{|r_{1y}|}{\sqrt{\varepsilon_2}\, r_{2y}} = -\tan(\beta_2 d_2 r_{2y}) \tag{F8}$$

Of these two possible solutions, only n=0 is unique. Matters are further simplified when r_{1y} is written in terms of r_{2y}. For the case of scan only in the x-y plane and the one-dimensional array (μ=0), Equation (36) relates r_{1y} to r_{1x} as

$$r_{1y} = \sqrt{1-r_{1x}^2} \tag{F9}$$

while Equation (71) related r_{1x} to r_{2x} as

$$\beta_1 r_{1x} = \beta_2 r_{2x} \tag{F10}$$

or

$$\sqrt{\varepsilon_1}\, r_{1x} = \sqrt{\varepsilon_2}\, r_{2x} \tag{F11}$$

so

$$r_{1y} = \sqrt{1-\varepsilon_2(1-r_{2y}^2)} = \sqrt{1-\varepsilon_2+\varepsilon_2 r_{2y}^2} \tag{F12}$$

Because r_{1y} is pure imaginary here, its magnitude, as required by Equation (F7) is

$$|r_{1y}| = \sqrt{\varepsilon_2 - 1 - \varepsilon_2 r_{2y}^2} \tag{F13}$$

Substituting Equation (G13) into Equation (F7) yields

$$\beta_2 d_2 r_{2y} \tan(\beta_2 d_2 r_{2y}) = -\sqrt{(\beta_1 d_2)^2(\varepsilon_2-1)-(\beta_2 d_2 r_{2y})^2} \tag{F14}$$

Substituting u for $\beta_2 d_2 r_{2y}$ yields

$$-u\tan(u) = \sqrt{(\beta_1 d_2)^2(\varepsilon_2-1)-u^2} \tag{F15}$$

The right hand sides of Equation (F15) is seen to be a circle of radius $\beta_1 d_2 (\varepsilon_2-1)$, so the negative sign on Equation (F15) is immaterial as far as finding the abscissa of the intersection is concerned. Quadrant I is shown plotted for the parameters of arrav D2 in Figure F1. It is interesting to note at this point that Equation (F14) is the mode equation for a wave propagating in a dielectric slab [58]. This condition indicates that the phenomenon present in the dielectric covered phased dipole array is that of a guided wave in the dielectric with an evanescent mode outside the slab.

The computer program which plotted Figure F1 found the value of u for the intersection to be approximately 0.695. It is useful to find which scan angle causes the denominator to go to zero. If the discussion concerned the infinite dielectric coated dipole array (which can be modeled here with the $\nu=\mu=0$ term) it is seen that

$$u = \beta_2 d_2 r_{2y} = \frac{2\pi d_2}{\lambda_1} \sqrt{\varepsilon_2} \sqrt{1 - r_{2x}^2} \tag{F16}$$

Solving for $_{1x}$, the direction of scan as defined in Figure 2

$$s_{1x} = \sqrt{\varepsilon_2 - \left(\frac{30u}{2\pi f d_2}\right)^2} \tag{F17}$$

where f is in GHz, d_2 is in cm and 30 is the speed of light in a vacuum in dm/s. For the parameters of this array r_{1x} is equal to 1.06. This corresponds to a scan in imaginary space, as early arguments indicated it would. Scan in this direction could be achieved through a grating lobe in the traditional sense, as the name trapped grating lobe implies. However, for the infinite array, this phenomenon can be avoided by keeping the interelement spacing small enough. In the dielectric r_{2x} is 0.93 which corresponds to an angle of 68.3°.

The problem this singularity creates in the present modeling of an infinite number of finite arrays is more profound. In the infinite array situation, a problem exists at one scan angle. In the finite model, the problem exists, theoretically, at all scan angles. Even broadside scan is modeled by a Fourier sum which is composed of terms, each of which represent a scan in a certain direction. Figure F2 plots the denominator of the transformation factor as a function of the scan angle in the dielectric. The singularity exists at 68.3° as predicted. Also plotted is the spectrum of Fourier terms, each corresponding to scan in the indicated direction, for a finite array scanning at a 40° free space angle. Figure F3 gives the same information for a 50° scan. The array impedance values will have the erratic behavior whenever one of these terms

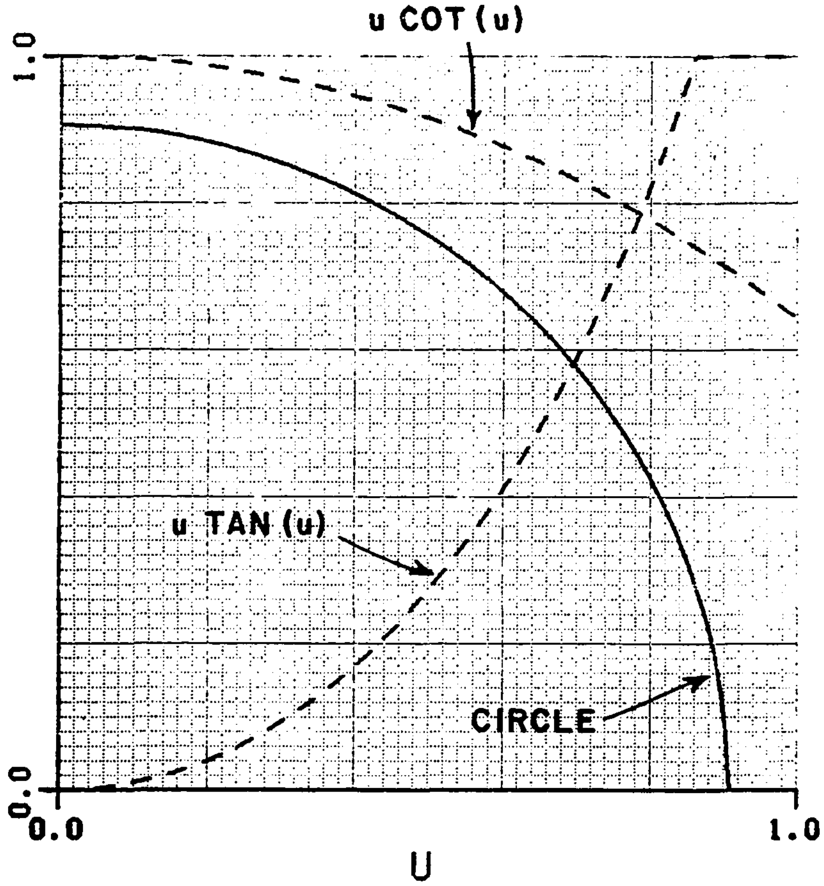

Figure F1. Plot showing the solution to the transcendental equation, 40° angle.

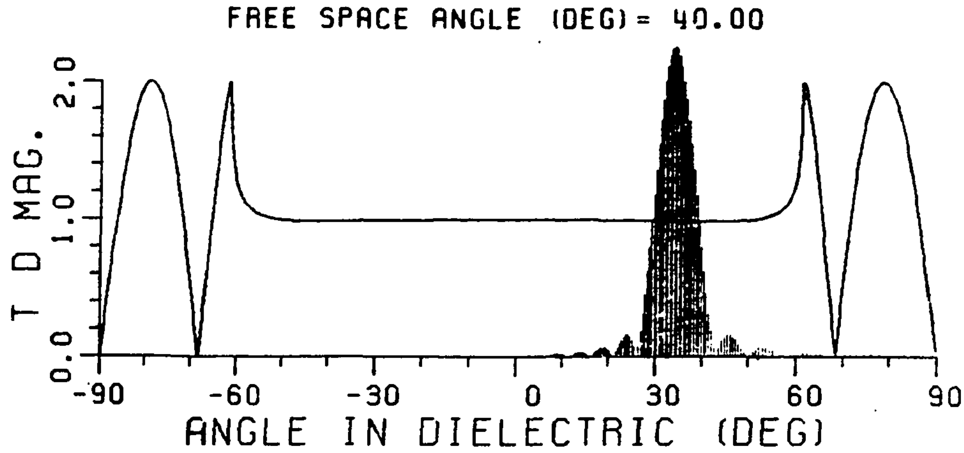

Figure F2. The denominator of the transformation function and the spectrum for a cosine distribution scanning at a 40^{0} angle.

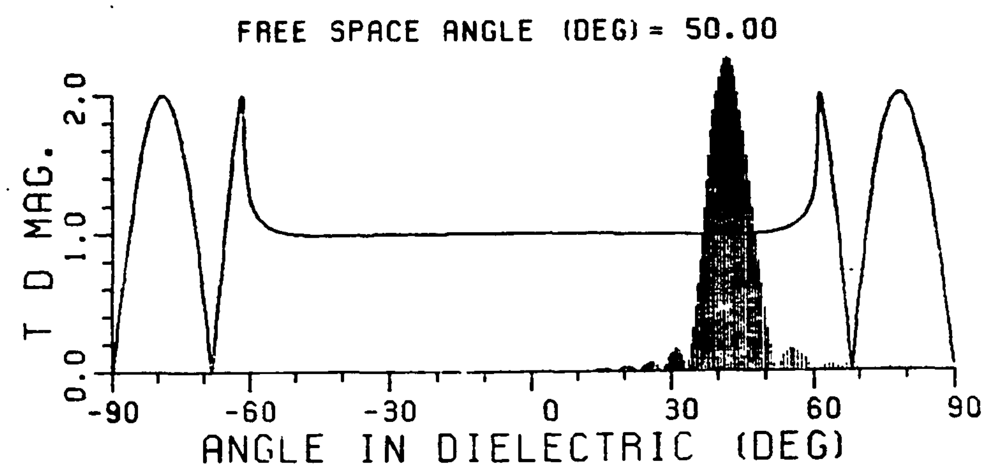

Figure F3. The denominator of the transformation function and the spectrum for a cosine distribution scanning at a 50^{0} angle.

(or terms in the sum) come close to the direction of the trapped wave. In the limit of having an infinite spacing between finite arrays and the Fourier sum becoming a Fourier integral, a continuum of scan angles is employed which must include the problem direction r_{2x}.

The Fourier term which causes the singularity can be identified from Equation (F17) when it is written as

$$u = \frac{2\pi d_2}{\lambda_1}\sqrt{\varepsilon_2}\sqrt{1 - (s_{2x} + \nu \frac{\lambda_2}{i_x D_x})^2} \tag{F18}$$

where s_{2x} is the direction of scan in the dielectric. Solving for yields

$$\nu = \frac{f i_x D_x}{30}\left[\sqrt{\varepsilon_2 - \left(\frac{30u}{2\pi f d_2}\right)^2} - s_{1x}\right] \tag{F19}$$

For example, with a 40° scan s_{1x} is the arc sine of 40° and ν is 51.10. This indicates that if the finite array is scanned at 40°, the 51st term in the Fourier sum is very near this singularity.

B. <u>Parallel case - Dipoles</u>

The reflection coefficient for this case, ${}^{E}_{\shortparallel}\Gamma_{2,1}$, can be found in Appendix B and rewritten for the conditions r_{2y} real and r_{1y} imaginary as

$${}^{E}_{\shortparallel}\Gamma_{2,1} = -e^{-j2\tan^{-1}\left(\frac{\varepsilon_2 |r_{1y}|}{r_{2y}}\right)} \tag{F20}$$

similar to the perpendicular case of Equation (F3). Substituting the expression into Equation (F1), the condition for the denominator of the transformation factor being zero and manipulating the results as for the perpendicular case yields the solution

$$\frac{1}{\varepsilon_2}\,\beta_2 d_2 r_{2y}\tan(\beta_2 d_2 r_{2y}) = \sqrt{(\beta_1 d_2)^2(\varepsilon_2 - 1) - (\beta_2 d_2 r_{2y})^2} \tag{F21}$$

Setting $\beta_2 d_2 r_{2y}$ equal to u and plotting this expression in Figure F4 indicates the solution to this equation. For the parameters of array D2 the solution is 0.740. Because u is still $\beta_2 d_2 r_{2y}$, Equation (F19) can be used to indicate the values of ν for a given scan angle which will cause problems. For the 40^{o} scan example, ν is 53.472.

This singularity in the parallel transformation factor is not as significant as it is for the perpendicular case and the one-dimensional array with the straight z-directed elements of this study. Equation (75) in the text indicates the parallel transformation factor is multiplied times two identical parallel polarization components of the pattern factors. For scan in the x-y plane of these straight z-directed elements, the parallel components of the pattern factors are very small. For other scans and other array elements this would not be the case. The discussion in the text of the problems caused by the perpendicular case singularity applies to the parallel case also, in general, even if the parallel case caused few problems in this study.

2. Slot array in a dielectric slab

The equation of interest for the geometry of Figure 16 is the general transformation factor of Equation (74) specialized to Equation (94) for this geometry. The condition for the denominator being zero is

$$ {}_{(\perp\shortparallel)}^{H}\Gamma_{2,1}\, e^{-j2\beta_2 d_2 r_{2y}} = e^{jn2\pi}, \quad n=0,\pm1,\pm2\ \dots \tag{F22}$$

where d_2 is the distance from the plane containing the array to the free space interface. ${}_{(\perp\shortparallel)}^{H}\Gamma_{2,1}$ is the perpendicular or othgononal reflection coefficient inside the dielectric as given by Appendix B.

a. Perpendicular case - slots

Rewriting the perpendicular H-field reflection coefficient for r_{2y} real and r_{1y} imaginary yields

$$ {}_{\perp}^{H}\Gamma_{2,1} = e^{-j2\tan^{-1}\left(\frac{\sqrt{\varepsilon_2}\,|r_{1y}|}{r_{2y}}\right)} \tag{F23}$$

Combining Equations (F22) and (F23) yields

$$ e^{-j2\tan^{-1}\left(\frac{\sqrt{\varepsilon_2}\,|r_{1y}|}{r_{2y}}\right)}\, e^{-j2\beta_2 d_2 r_{2y}} = e^{jn2\pi} \tag{F24}$$

or

$$\frac{\sqrt{\varepsilon_2}|r_{1y}|}{r_{2y}} = \tan(-\beta_2 d_2 r_{2y} - n\pi) \qquad \text{(F25)}$$

using Equation (F13) for $|r_{1y}|$ yields

$$\frac{1}{\varepsilon_2}\beta_2 d_2 r_{2y}\tan(\beta_2 d_2 r_{2y}) = \sqrt{(\beta_1 d_2)^2(\varepsilon_2-1)-(\beta_2 d_2 r_{2y})^2} \qquad \text{(F26)}$$

which is the same as Equation (F21) for the parallel case of the dipole geometry. Only the n=0 condition of Equation (F24) is unique. The $1/\varepsilon_2$ u tan u curve of Figure F4 reveals that u here is 0.740.

b. Parallel case - slots

The appropriate reflection coefficient is

$$^{H}_{\parallel}\Gamma_{1,2} = \frac{r_{1y} - \sqrt{\varepsilon_2}r_{2y}}{r_{1y} + \sqrt{\varepsilon_2}r_{2y}} = -e^{-j2\tan^{-1}\left(\frac{|r_{1y}|}{\sqrt{\varepsilon_2}r_{2y}}\right)} \qquad \text{(F27)}$$

Substituting Equation (F27) into (F22) yields

$$e^{-j2\tan^{-1}\left(\frac{|r_{1y}|}{\sqrt{\varepsilon_2}r_{2y}}\right)} e^{-j2\beta_2 d_2 r_{2y}} = e^{j(2n+1)\pi} \qquad \text{(F28)}$$

or

$$\frac{|r_{1y}|}{\sqrt{\varepsilon_2}r_{2y}} = \tan(-\beta_2 d_2 r_{2y} - \pi) \qquad \text{(F29)}$$

Using Equation (F13) for $|r_{1y}|$ yields

$$\beta_2 d_2 r_{2y}\cot(\beta_2 d_2 r_{2y}) = -\sqrt{(\beta_1 d_2)^2(\varepsilon_2-1)-(\beta_2 d_2 r_{2y})^2} \qquad \text{(F30)}$$

Figure F1 indicates, for the u cot(u) curve, there is no intersection and subsequently the parallel transformation factor does not have a singularity for the parameters of this array.

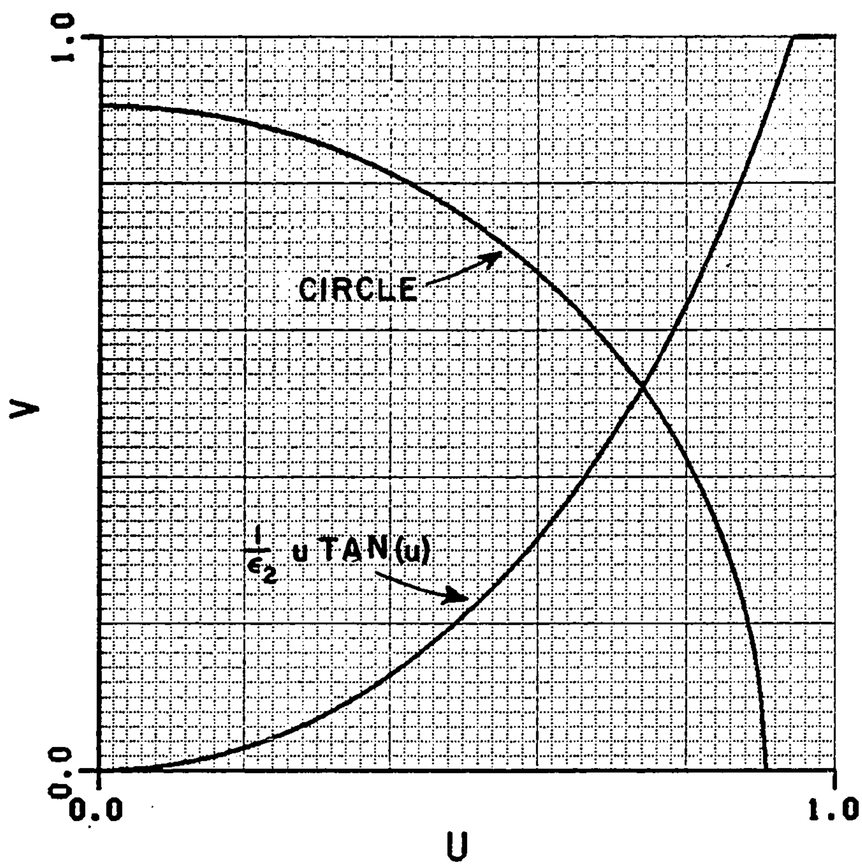

Figure F4. Plot showing the solution to the transcendental equation, Equation (F26).

3. Dipole Array in a Dielectric Slab with a Ground Plane at One Interface

The equation of interest for the geometry of Figure 66 is the general transformation factor of Equation (74) specialized to Equation (93) for this geometry. The condition for the denominator being zero is

$$({\perp}\,\|)\,{}^{E}\Gamma_{2,1}\, e^{-j4\beta_2 d_2 r_{2y}} = -e^{jn2\pi},\ n=0,\pm1,\pm2,\ \ldots \tag{F31}$$

where d_2 is the half-width of the dielectric slab.

A. Perpendicular case - dipoles with ground plane

Rewriting the perpendicular H-field reflection coefficient for r_{2y} real and r_{1y} imaginary yields

$$ {}^{E}_{\perp}\Gamma_{2,1} = e^{-j2\tan^{-1}\left(\frac{|r_{1y}|}{\sqrt{\epsilon_2}\, r_{2y}}\right)} \tag{F32}$$

Combining Equations (F31) and (F32) gives

$$e^{-j2\tan^{-1}\left(\frac{|r_{1y}|}{\sqrt{\epsilon_2}\, r_{2y}}\right)}\ e^{-j4\beta_2 d_2 r_{2y}} = e^{j(2n+1)\pi} \tag{F33}$$

or

$$\frac{|r_{1y}|}{\sqrt{\epsilon_2}\, r_{2y}} = \tan\left(-\beta_2 d_2 r_{2y} + (2n+1)\frac{\pi}{2}\right) \tag{F34}$$

which is the same as

$$\frac{|r_{1y}|}{\sqrt{\epsilon_2}\, r_{2y}} = \cot(2\beta_2 d_2 r_{2y}) \tag{F35}$$

Note the new factor of two in the cotangent agrument. Using Equation (F13) for $|r_{1y}|$ yields

$$2\beta_2 d_2 r_{2y} \cot(2\beta_2 d_2 r_{2y}) = \sqrt{(2\beta_1 d_2)^2(\epsilon_2-1)-(2\beta_2 d_2 r_{2y})^2} \tag{F36}$$

The right side of the equation is now an ellipse rather than a circle. The appropriate curves are plotted as Figure F5. The value of u for the intersection is 0.887. The negative of the left side of Equation (F43) is plotted to show the intersection in quadrant I.

b. Parallel case - dipoles with ground plane

The appropriate reflection coefficient is

$$\Gamma^{E}_{\parallel 2,1} = -e^{-j2\tan^{-1}\left(\frac{\sqrt{\varepsilon_2}\,|r_{1y}|}{r_{2y}}\right)} \quad \text{(F37)}$$

Substituting this equation into Equation (F31) yields

$$e^{-j2\tan^{-1}\left(\frac{\sqrt{\varepsilon_2}\,|r_{1y}|}{r_{2y}}\right)}\, e^{-j4\beta_2 d_2 r_{2y}} = e^{+jn2\pi} \quad \text{(F38)}$$

or

$$\frac{\sqrt{\varepsilon_2}\,|r_{1y}|}{r_{2y}} = -\tan(2\beta_2 d_2 r_{2y}) \quad \text{(F39)}$$

Using Equation (F13) for $|r_{1y}|$ yields

$$\frac{1}{\varepsilon_2}\, 2\beta_2 d_2 r_{2y} \tan(2\beta_2 d_2 r_{2y}) = -\sqrt{(2\beta_1 d_2)^2(\varepsilon_2 - 1) - (2\beta_2 d_2 r_{2y})^2} \quad \text{(F40)}$$

Figure F6 indicates the value of u is 0.608.

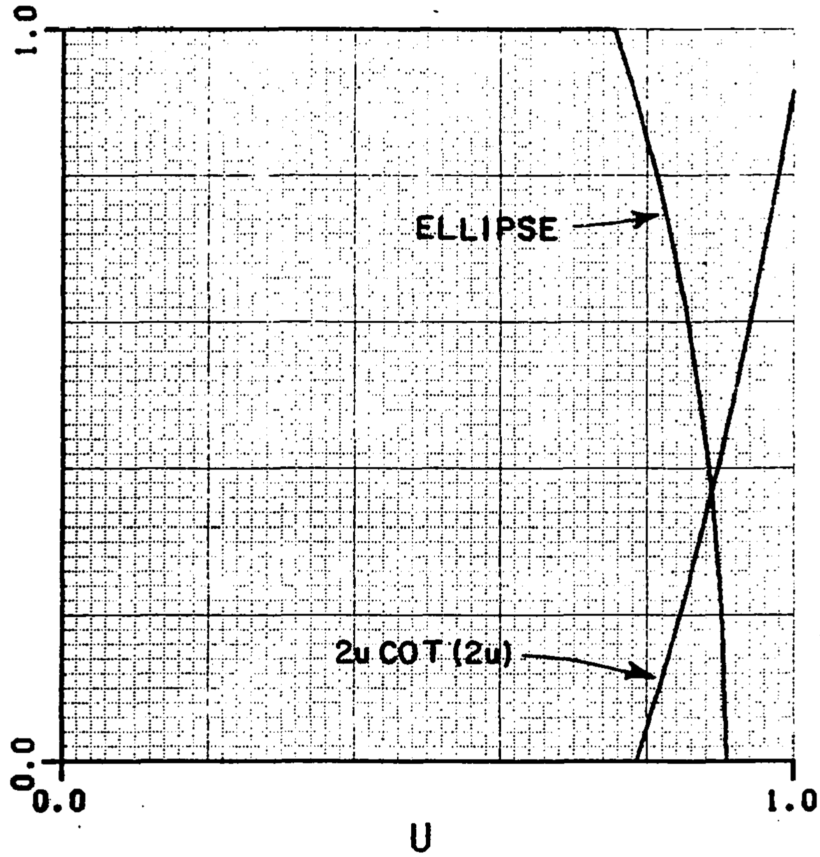

Figure F5. Plot showing the solution to the transcendental equation, Equation (F36).

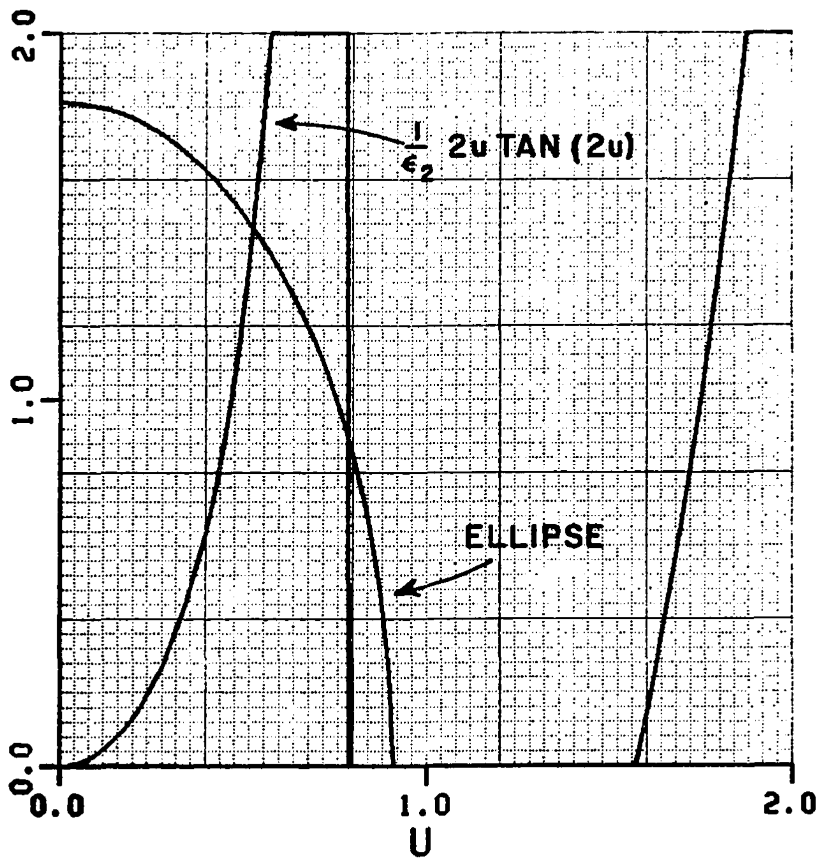

Figure F6. Plot showing the solution to the transcendental equation, Equation (F40).

APPENDIX G
PROGRAMMING CONSIDERATIONS

Although Equations (77) and (80) allow calculation of the self-immittances of all elements of a potentially large finite array of dipoles or slots in a ground plane without matrix inversion, the presence of four infinite sums makes the equation appear formidable. In this section a careful examination of Equation (80), the slot case, will reveal the technique of this study for dealing with this expression and obtaining meaningful results.

The initial consideration must be the limits for the sums on ν and μ. Since these sums are Fourier Series sums, they can be truncated so $-N_x<\nu<N_x$, and $-N_z<\mu<N_z$. There is, however, no straightforward method of knowing when to truncate. The number of terms required is related to modulated aperture size, modulation periods (i_x, i_z), and the shape of the aperture's distribution (i.e., a smooth cosine shaped aperture distribution requires fewer terms than a square pulse shaped aperture distribution does.) To compound the difficulty with this double sum, the values N_x and N_z must be set initially. In general, for the tapered distributions of this study, no major problem was encountered concerning the truncations of ν and μ.

Careful analysis of Equation (80) for the purpose of efficient programming requires isolating particular variables or parameters upon which the various terms of the expression depend. Equation (80) claims to be an expression for $Y_{q,m}$ while in fact it is an expression for

$$Y(q,n,\alpha,\eta,i_x,i_z,f,D_x,D_z,N_x,N_z,G) \quad \text{(G1)}$$

where the arguments inside the parentheses imply Y to be a function of

$$\alpha,\eta = \text{scan angles defined by Figure 4} \quad \text{(G2)}$$

$$i_x,i_z = \text{period of current modulation defined by Figure 8} \quad \text{(G3)}$$

$$f = \text{frequency} \quad \text{(G4)}$$

D_x, D_z = interelement spacing (G5)

N_x, N_z = number of Fourier terms (G6)

G = general term specified by geometry which includes $d_2, \varepsilon_2, \varepsilon_3$ of Figure 16 (G7)

Additionally, terms on the right hand side of Equation (80) may also depend upon ν, μ, k, and n. For brevity, the dependence upon f, D_x, D_z, N_x, N_z, and G will not be explicitly included below. Changing any of these parameters requires the computation of Y to be done again.

Using the above notation, Equation (80) could be rewritten as

$$Y(q,m,\alpha,\eta,i_x,i_z) = \frac{C}{I^x(q,i_x)I^z(m,i_z)}$$

$$\times \sum_{\nu=-N_x}^{N_x} \sum_{\mu=-N_z}^{N_z} D(\nu,\mu,q,m,i_x,i_z)$$

$$\times \sum_{k=-\infty}^{\infty} \sum_{n=-\infty}^{\infty} E(k,n,\nu,\mu,\alpha,\eta,i_x,i_z) \cdot \Omega(k,n,\nu,\mu,\alpha,\eta,i_x,i_z) \qquad \text{(G8)}$$

or

$$Y(q,m,\alpha,\eta,i_x,i_z) = \frac{C}{I^x(q,i_x)I^z(m,i_z)} \times$$

$$\sum_{\nu=-N_x}^{N_x} \sum_{\mu=-N_z}^{N_z} D(\nu,\mu,q,m,i_x,i_z)F(\nu,\mu,\alpha,\eta,i_x,i_z) \qquad \text{(G9)}$$

where

$$F(\nu,\mu,\alpha,\eta,i_x,i_z) = \sum_{k=-\infty}^{\infty} \sum_{n=-\infty}^{\infty} E(k,n,\nu,\mu,\alpha,\eta,i_x,i_z)$$

$$\times \Omega(k,n,\nu,\mu,\alpha,\eta,i_x,i_z) \qquad \text{(G10)}$$

This isolation of F in Equation (G9) is extremely important because it reveals F not to be a function of position as specified by q and m. This allows, for fixed scan angle (α,η) and fixed modulation periods (i_x,i_z), $F(\nu,\mu)$ to be considered a data base which is calculated once to compute Y at any value of q and m, if the sums on ν and μ are finite. Since these sums are truncated so $-N_x<\nu<N_x$ and $-N_z<\mu<N_z$, $F(\nu,\mu)$ is a matrix of size $(2N_x + 1) \cdot (2N_z + 1)$. Once $F(\nu,\mu)$ is calculated, the admittance Y for any element in the plane can be computed.

F itself, as defined by Equations (G10) and (80), has two infinite summations. This double sum, for each ν and μ, was previously considered and programmed [59]. The subroutine which handles the summations on k and n is SUMZT which is included in Appendix H. This subroutine calculates a convergence number and, for example, sums on n for a given value of k. When three consecutive values below the convergence number are found, the sum along n is terminated and the next value of k is employed. In this manner, the two dimensional sum is completed.

One additional constraint on this study of modeling finite arrays helped in shortening the computation times. Although the theory of Chapters II and III are general in the orientation of the linear array element will, at some point, take part in a dot product with the direction vector of the other element, only z-components of the field are non-zero. Additionally, the derivation of the pattern factor in Appendix C reveals the pattern under transmitting conditions to be equal to the pattern under non-transmitting conditions, which reduces computation time by reducing Ω of Equation (76) to

$$\Omega_{m,n,\nu,\mu} = ({}_{\perp}P_2^{(1)})^2 \; {}_{\perp}T_2 + ({}_{\parallel}P_2^{(1)})^2 \; {}_{\parallel}T_2 \tag{G11}$$

Any reduction of the form of Ω is important since it is inside all four infinite summations. The pattern factor is also a function of r_z only, which depends on n and not k. This dependence saves time by allowing the computation of the z-component of the pattern to be done outside the sum of k, i.e., only once for each value of n. This can be represented by rewriting Equation (G10) as

$$F(\nu,\mu) = \sum_{n=-\infty}^{\infty}{}^{*} \sum_{k=-\infty}^{\infty} \frac{e^{-j\beta_2 a r_{2y}}}{r_{2y}} \; \Omega_{k,n,\nu,\mu} \tag{G12}$$

The order of summation has been reversed and the (*) indicates where the calculation of the z-component of the pattern is performed. Although the x-component of the pattern is zero, Equation (G11) employs the parallel and perpendicular components which are a function of ν,μ,n, and k. Therefore $({}_{\perp\parallel}P_2^{(1)})$ cannot be taken outside the k summation, The appearance of the expression is not altered, but significant computation time is saved.

A mention should be made at this time concerning the treatment of the explicit phase term in Equation (80). According to Chapter III, when the test dipole is located one radius from an array element, the mutual impedance between the two is the self-impedance of the array element. Actually, this is merely a good approximation. The procedure outlined in Schelkunoff [60] consists of moving the test dipole to all angles in the x-z plane one radius from the element and finding the mutual impedance at each point. The self-impedance is the average of those values. The greatest difference between the multi-position method and the single position method employed here is, for the k=n=0 propagating mode, or any other propagating mode if grating lobes exist, the single position method yields a phase term which is not pure real. To correct this problem, the phase is set to zero wherever r_y is real. Since r_y is pure real or pure imaginary, the explicit phase term can be rewritten as

$$e^{-j\beta a r_{2y}} = e^{-\beta a \mathrm{Im}\{r_{2y}\}} \tag{G13}$$

This yields the correct phase when r_y is pure imaginary and if r_y is pure real, the term becomes unity.

The actual coding of Equation (G9) in FORTRAN involves two computer programs. The first calculates F of Equation (G10), and can be considered a data base generator. Its inputs are the scan angle, the modulation periods i_x and i_z, the frequency, the geometry (G of Equation (G7), and N_x and N_z which specify the number of Fourier terms used. Its output is a large matrix, $CF(\nu,\mu)$; $-N_x<\nu<N_x$, $-N_z<\mu<N_z$, which contains the value of F for each value of ν and μ. This program, SLOT, is documented and listed in Appendix H with program DIPOLE. Both programs use the same subroutines, which are listed, with one exception. In subroutine QUANZT, the call to TFACTD must be made and for the slot case subroutine TFACT must be used.

The second program is an operator interactive data processing program. It uses the matrix $CF(\nu,\mu)$ as input as well as instructions from the operator via the computer terminal. It calculates the Fourier coefficients for the desired size and shape of the finite aperture and completes the calculation of Y of Equation (G9) for operator specified values of q and n. The output of the program takes the form of listings of the admittance values or computer generated plots. This program is named CMPLOT and is listed and documented in Appendix I.

APPENDIX H
COMPUTER PROGRAMS DIPOLE AND SLOT

All computer results in this work were obtained with the aid of a Digital Equipment Corporation VAX 11/780. The FORTRAN 4 PLUS compiler was used. Most features of this compiler are the same as other compilers with some exceptions. This compiler ignores exclamation points (!) and any characters following them on the same line. A dollar sign ($) at the end of a FORMAT statement inhibits a carriage return and line feed which occurs on a default basis if the FORMAT statement is involved in output to the terminal. "IF THEN ELSE" statements are used in addition to "IF GO TO" statements. The most important statement exploited here is the "INCLUDE" statement. It has the format

```
INCLUDE 'FILENAME'
```

and has the function of inserting whatever statements are in the indicated file into the computer code at the point of the "INCLUDE" statement. In the programs given here, the specified file contains COMMON, COMPLEX, DIMENSION, and DATA statements as seen in Figure H1. Because the main program and all the subroutines share these statements exactly, the statements need be listed here only once. An additional feature includes the fact that any change in these statements need be done only once and not done for the main program and each subroutine. Other I/O statements such as OPEN and CLOSE statements may be unique to this system. They open and close files.

Two main programs DIPOLE and SLOT are listed in this Appendix. Their use is indicated by the type of element in the array. Both programs use the same input file format as shown in Figure H2 and the same INCLUDE file, 'COMMON.CMN', as shown in Figure H1. They also share the same subroutines with one important exception. Subroutine QUANZT must use either line 4000 and call TFACTD (dipole case), or line 4600 and call TFACT (slot case). Only one of these calls can be made. Erroneous results will occur if the wrong call is made.

The main programs read the input file and set up the geometry (including calculating the effective lengths of the elements described in Appendix C). The main programs then call SUMZT for each value of NU and MU. SUMZT handles the double summation on k and n. It calls QUANZT, for each value of k and n, which calculates Q of line 5300 in QUANZT. The main programs then output the sum of k and n for each value of NU and MU. This input quantity is F as described by Equation (G10) in Appendix G.

SLOT has the additional feature of allowing conducting walls between the slot array and some ground plane. This feature was not used in this effort. Further documentation on it can be found in the References [61,62].

In the listings, program DIPOLE is given, followed by SLOT and all the subroutines used by them. The following is a short explanation of the subroutines:

SUBROUTINE SUMZT
: Manages the double summation on k and n. Its output, DSUM, is the sum on k and n for that particular value of NU and MU.

SUBROUTINE RZN
: Calculates the value of RZKN for each NU, MU, and n.

SUBROUTINE QUANZT
: Calls the other subroutines to calculate the value inside the double sum on k and n.

SUBROUTINE DIRECT
: Calculates RXKN and RYKN for each value of NU, MU, k, and n.

SUBROUTINE COMPAT
: Calculates the pattern factors in the x and z directions for each value of NU, MU, and n. It is independent of k and x. Its derivation for straight z-directed elements is given in Appendix C.

SUBROUTINE OPCOMP
: Calculates the parallel and perpendicular components of the z-component of the pattern factor.

SUBROUTINE TFACTD
: Calculates the transformation factor for dipole arrays.

FUNCTION TEXP
: Function called in TFACTD.

SUBROUTINE EGAMMA

Subroutine called in TFACTD to calculate the E-field reflection coefficients as given in Appendix B.

SUBROUTINE TFACT

Calculates the transformation factor for slot arrays.

FUNCTION HGAMMA

Subroutine called in TFACT to calculate the H-field reflection coefficients given in Appendix B.

SUBROUTINE DELL

Calculates the incremental length to be added to a slot or flat wire dipole.

SUBROUTINE SICI

Called in DELL. Calculates the sine and cosine integrals.

```
      COMPLEX CJ,CO,C1,RYKN(11),ZIMP(9),YADM(9)
      COMMON END(11,9),ELEMX(10,9),ELEMZ(10,9)
     1    ,RLAMDA(11),BETA(11),SX(11),SZ(11),RXKN(11),RZKN(11)
     1    ,ER(11),D(11),ISTR(11),SRER(9),EFFL(9),NLEG(9)
     1    ,RYKN,DX,DZ,DXH,DZH,FREQ,AEFF,REFXX,REFZZ
     1    ,NLAY,NARR,ITYP,IMED,ISYM,ID1,ID2
     1    ,NU,MU,VETO,TVETO,LRY(9),ZIMP,YADM,TZO
      DATA CJ,CO,C1/(0.0,1.0), (0.0,0.0), (1.0,0.0)/
      DATA TPI,RPD/6.28318531, 0.0174532925/
```

Figure H1. The contents of the file COMMON.CMN which contains the COMMON in each program unit along with specification statements each unit used.

```
DZERO
60,0,.005,90.,1.          !NX,NZ,VETO,ALPHA,ETA
349,349                   !IX,IZ
8. 0.                     !FREQUENCY,GROUND PLANE INDICATOR
3                         !NUMBER OF DIELECTRIC LAYERS
.987  .987  1.            !THICKNESS OF DIELECTRIC LAYERS
1.3    1.3  1.3           !REL. DIELECT. CONSTANTS OF LAYERS
1.316  1.974              !DX,DZ
.0877  .00877             !ELEM. WIDTH, ELEM. THICKNESS
0. 0.                     !LINE IMP., SHORT LENGTH
2                         !NUMBER OF LEGS OF AN ELEMENT
-.822  0.  .822           !END PTS OF LEGS
0.,1.                     !LEG DIRECTIONS X,Z
0.,1.                     !LEG DIRECTIONS X,Z
0 0. 0.                   !ISTR(3),DXH,DZH
50,50,100                 !NNXO,NNZO USED IN ADTERMS.FOR
```

Figure H2. Typical input file to program DIPOLE. The first line is name of the output file. The corrresponding output plot is Figure 40.

```
CZZZZZZZZZZZZZZZZZZZZZZZZZZZZZZZZZZZZZZZZZZZZZZZZZZZZZZZZZZZZZZZ
C
C                          PROGRAM DIPOLE
C
C  VERSION WHICH USES ONE DIPOLE ARRAY BETWEEN MEDIA 2 AND 3.
C  MEDIA 1 AND 4 ARE FREE SPACE UNLESS ITYP=1, THEN A GROUND
C  PLANE EXISTS AT THE INTERFACE OF MEDIA 1 AND 2.
C
C  LINK WITH SUM,SUB,DRA0:[GRP11LIB]LIB/LIB
C
C  COMMON STATEMENTS IN FILE 'COMMON.CMN'
C
C  ALLOWS DIELECTRIC TO THE LEFT AND RIGHT OF THE SINGLE
C  ARRAY WITH A GROUND PLANE TO THE RIGHT.
CZZZZZZZZZZZZZZZZZZZZZZZZZZZZZZZZZZZZZZZZZZZZZZZZZZZZZZZZZZZZZZZ
C
        COMPLEX Y(9,9),H(2,2),YL(9),P(2),TF(2),CUR(2),VN(2)
        1   ,YP,YLEFT,YRITE,PX,PZ,DETN,PHASE,DET,EX,PH
        COMPLEX SUMKN(201),CTP,YKS
        CHARACTER*40 FILENM
        DIMENSION REFX(9),REFZ(9),DUM(10)
        1   ,HLENG(9),WIDTH(9),THICK(9),ZC(9),SLENG(9)
        1   ,ITMA1(3),ITMA2(3),ITMA3(3)
        REAL K2DIPI
        INTEGER TNNZP1
        EQUIVALENCE (GPLI,DUM(2)),(TVETO,DUM(8))
        EQUIVALENCE (DIPOLE,DUM(9))
        INCLUDE 'COMMON.CMN'
        DATA LRY/9*0/
        DATA ISTR/11*0/
        DATA TZ0/5.305E-3/
        CALL CPU_TIME_LIM(180)  !TIME LIMIT FOR EXECUTION
        PI=3.1415926535         !PROGRAM ABORTS IF MORE
        PID2=PI/2.              !THAN SPECIFIED MINUTES
C                               !ARE USED BY CPU
        DIPOLE=1.                   !INDICATES DIPOLE DATA
        OPEN(UNIT=16,NAME='DPOLIN.DAT',TYPE='OLD')
89      FORMAT(A30)
        READ(16,89) FILENM
        OPEN(UNIT=10,NAME=FILENM,TYPE='NEW',FORM='UNFORMATTED')
        READ(16,*) NNX,NNZ,VETO,ALPHA,ETA
        READ(16,*) IIX,IIZ
        READ(16,*) FREQ,GPLI            !GPLI=1=GROUND PLANE
        READ(16,*) NLAY                 !NUMBER OF LAYERS
        READ(16,*) (D(I+1),I=1,NLAY)    !LAYER THICKNESS
        ER(1)=1.                        !REGION 1 FREE SPACE
        READ(16,*) (ER(I+1),I=1,NLAY)   !REL. DIEL. CONSTANTS
C  ER(2)=ER(3) FOR DIPOLE CASE
        ER(3)=ER(2)
        READ(16,*) DX,DZ                !INTERELEMENT SPACING
```

```
      N=1                               !ONLY ONE ARRAY
      READ(16,*) WIDTH(N),THICK(N)      !OF SLOT ELEMENTS
      READ(16,*) ZC(N),SLENG(N)    !LINE IMP.,SHORT LENGTH
      READ(16,*) NL                     !NUMBER OF LEGS
      NLP=NL+1
      READ(16,*) (END(I,N),I=1,NLP)     !ENDPTS OF LEGS
      NLEG(N)=NL
      DO 150 I=1,NL
      READ(16,*) X,Z
      ISX=0
      IF(X.NE.0.) ISX=1
      U=SQRT(X*X+Z*Z)
      ELEMX(I,N)=X/U
      ELEMZ(I,N)=Z/U
150   CONTINUE
      READ(16,*) ISTR(3),DXH,DZH
      READ(16,*) XDUM,YDUM,TVETO
      IF(GPLI.EQ.0 .AND. ISTR(3).NE.0) GO TO 300
      HLENG(N)=END(NLP,N)      !HALF LENGTH OF ELEMENTS
      CLOSE(UNIT=16)                    !CLOSE INPUT FILE
      IF(ER(2).NE.ER(3)) GO TO 300      !CHECK SYMMETRY
      IF(D(2).NE.D(3)) GO TO 300        !CHECK SYMMETRY
      MNNX=-NNX
      MNNZ=-NNZ
      TNNZP1=(2*NNZ)+1
      NARR=1
C
C*** SET UP CONSTANTS ***
C
      DO 205 I=1,NARR
      SRER(I)=SQRT((ER(I+1)+ER(I+2))/2.0)
205   CONTINUE
C
C SET UP ARRAYS BASED ON ER & FREQ
      DO 210 L=1,NLAY
      ZIMP(L)=SQRT(1./ER(L))*120.*PI
      YADM(L)=1./ZIMP(L)
      RLAMDA(L)=30.0/(FREQ*SQRT(ER(L)))
210   BETA(L)=TPI/RLAMDA(L)
C
C*** FIND EFFECTIVE LENGTHS & LOAD ADMITTANCES ***
C
      DO 215 L=1,NARR
      CALL DELL(HLENG(L),WIDTH(L),THICK(L),RLAMDA(1),
     1                SRER(L),DL)
      EFFL(L)=HLENG(L)+DL
215   YL(L)=CJ*14.09E-6*ZC(L)*SRER(L)*TAN(BETA(1)*SRER(L)
     1                                  *SLENG(L))
C
C*** DETERMINE THE SCAN ANGLE ***
```

```
C
        SINE=SIN(ETA*RPD)
        SXX=SINE*COS(ALPHA*RPD)
        IF(ALPHA.EQ.90.) SXX=0.
        SZZ=SINE*SIN(ALPHA*RPD)
        FL2DXA=RLAMDA(1)/(FLOAT(IIX)*DX)
        FL2DZA=RLAMDA(1)/(FLOAT(IIZ)*DZ)
C
        WRITE(10) ALPHA,ETA               !WRITE
        WRITE(10) NNX,NNZ,IIX,IIZ,VETO    !TO THE OUTFILE
        WRITE(10) FREQ,ISC,D(3),ER(2),ER(3)
        WRITE(10) DX,DZ,WIDTH(1),THICK(1),END(1,1),END(3,1)
        WRITE(10) DUM                     !IN SEQUENTIAL I/O
C
C
        ITYP=0
        IF(GPLI.EQ.1.) ITYP=1             !ITYP=1 =>GRND PLANE
C
        LNU=0
        DO 702 NU=MNNX,NNX                !LOOP FOR EACH VALUE
        LMU=0                             !OF NU
        LNU=LNU+1
        DO 700 MU=MNNZ,NNZ                !LOOP FOR EACH VALUE
        LMU=LMU+1                         !OF MU
        DO 701 L=1,NLAY
        SX(L)=(SXX+NU*FL2DXA)/SQRT(ER(L))
        SZ(L)=(SZZ+MU*FL2DZA)/SQRT(ER(L))
701     CONTINUE
        N=1
        ID1=1
        ID2=1
        IMED=2
        AEFF=WIDTH(ID1)/4.
        CALL SUMZT(YLEFT)
        SUMKN(LMU)=YLEFT
700     CONTINUE
        WRITE(10) (SUMKN(LD),LD=1,TNNZP1)   !TO UNFORMATTED
702     CONTINUE                            !OUTPUT FILE
C
C*** END OF RUN ***
C
        CLOSE(UNIT=10)                    !CLOSE OUTPUT FILE
        CALL EXIT
300     TYPE 301
301     FORMAT(2X,'*** NON-SYMMETRIC INPUT ER OR D ***')
        CALL EXIT
        END
```

```
CZZZZZZZZZZZZZZZZZZZZZZZZZZZZZZZZZZZZZZZZZZZZZZZZZZZZZZZZZZZZZZ
C
C                       PROGRAM SLOT
C
C
C  LINK WITH SUM,SUB,[GRP11LIB]LIB/LIB
C
C  ALLOWS DIELECTRIC TO THE LEFT AND RIGHT OF THE SINGLE
C  ARRAY WITH A GROUND PLANE TO THE RIGHT.
CZZZZZZZZZZZZZZZZZZZZZZZZZZZZZZZZZZZZZZZZZZZZZZZZZZZZZZZZZZZZZZ
C  MODIFICATIONS FOR CENTER LAYER CONDUCTING WALL
C  STRUCTURE MADE MAY 2, 1980.
CZZZZZZZZZZZZZZZZZZZZZZZZZZZZZZZZZZZZZZZZZZZZZZZZZZZZZZZZZZZZZZ
C
        COMPLEX Y(9,9),H(2,2),YL(9),P(2),TF(2),CUR(2),VN(2)
        1   ,YP,YLEFT,YRITE,PX,PZ,DETN,PHASE,DET,EX,PH
        COMPLEX SUMKN(201),CTP,YKS
        CHARACTER*40 FILENM
        DIMENSION REFX(9),REFZ(9),DUM(10)
        1   ,HLENG(9),WIDTH(9),THICK(9),ZC(9),SLENG(9)
        1   ,ITMA1(3),ITMA2(3),ITMA3(3)
        REAL K2DIPI
        INTEGER TNNZP1
        EQUIVALENCE (GPLI,DUM(2)),(TVETO,DUM(8))
        EQUIVALENCE (DIPOLE,DSUM(9))
        INCLUDE 'COMMON.CMN'
        DATA LRY/9*0/
        DATA ISTR/11*0/
        DATA TZ0/753.4/
CZZZZZZZZZZZZZZZZZZZZZZZZZZZZZZZZZZZZZZZZZZZZZZZZZZZZZZZZZZZZZZ
C
C       ISTR(3) INDICATES THE CONDUCTING WALL STRUCTURE BETWEEN
C       THE ARRAY AND THE GROUND PLANE FOR THE FOLLOWING
C       STRUCTURES
C
C               ISTR(3)=0       NO CONDUCTING WALLS
C
C               ISTR(3)=1       PARALLEL CONDUCTING WALLS
C
C               ISTR(3)=2       ORTHOGONAL CONDUCTING WALLS
C
C               ISTR(3)=3       HONEYCOMB STRUCTURE
C                               (PARALEL AND ORTH. WALLS)
C
CZZZZZZZZZZZZZZZZZZZZZZZZZZZZZZZZZZZZZZZZZZZZZZZZZZZZZZZZZZZZZZ
        CALL CPU_TIME_LIM(180)  !TIME LIMIT FOR EXECUTION
        PI=3.1415926535         !PROGRAM ABORTS IF MORE
        PID2=PI/2.              !THAN SPECIFIED MINUTES
C                               !ARE USED BY CPU
        DIPOLE=0.                       !INDICATES SLOT DATA
```

```
      OPEN(UNIT=16,NAME='SLOTIN.DAT',TYPE='OLD')
89    FORMAT(A30)
      READ(16,89) FILENM
      OPEN(UNIT=10,NAME=FILENM,TYPE='NEW',FORM='UNFORMATTED')
      READ(16,*) NNX,NNZ,VETO,ALPHA,ETA
      READ(16,*) IIX,IIZ
      READ(16,*) FREQ,GPLI              !GPLI=1=GROUND PLANE
      READ(16,*) NLAY                   !NUMBER OF LAYERS
      READ(16,*) (D(I+1),I=1,NLAY)      !LAYER THICKNESS
      ER(1)=1.                          !REGION 1 FREE SPACE
      READ(16,*) (ER(I+1),I=1,NLAY)     !REL. DIEL. CONSTANTS
      READ(16,*) DX,DZ                  !INTERELEMENT SPACING
      N=1                               !ONLY ONE ARRAY
      READ(16,*) WIDTH(N),THICK(N)      !OF SLOT ELEMENTS
      READ(16,*) ZC(N),SLENG(N)     !LINE IMP.,SHORT LENGTH
      READ(16,*) NL                     !NUMBER OF LEGS
      NLP=NL+1
      READ(16,*) (END(I,N),I=1,NLP)     !ENDPTS OF LEGS
      NLEG(N)=NL
      DO 150 I=1,NL
      READ(16,*) X,Z
      ISX=0
      IF(X.NE.0.) ISX=1
      U=SQRT(X*X+Z*Z)
      ELEMX(I,N)=X/U
      ELEMZ(I,N)=Z/U
150   CONTINUE
      READ(16,*) ISTR(3),DXH,DZH
      READ(16,*) XDUM,YDUM,TVETO
      IF(GPLI.EQ.0 .AND. ISTR(3).NE.0) GO TO 300
      HLENG(N)=END(NLP,N)           !HALF LENGTH OF ELEMENTS
      CLOSE(UNIT=16)                    !CLOSE INPUT FILE
      IF(ER(2).NE.ER(3)) GO TO 300      !CHECK SYMMETRY
      IF(D(2).NE.D(3)) GO TO 300        !CHECK SYMMETRY
      MNNX=-NNX
      MNNZ=-NNZ
      TNNZP1=(2*NNZ)+1
      NARR=1
C
C*** SET UP CONSTANTS ***
C
      DO 205 I=1,NARR
      SRER(I)=SQRT((ER(I+1)+ER(I+2))/2.0)
205   CONTINUE
C
C SET UP ARRAYS BASED ON ER & FREQ
      DO 210 L=1,NLAY
      ZIMP(L)=SQRT(1./ER(L))*120.*PI
      YADM(L)=1./ZIMP(L)
      RLAMDA(L)=30.0/(FREQ*SQRT(ER(L)))
```

```
210     BETA(L)=TPI/RLAMDA(L)
C
C*** FIND EFFECTIVE LENGTHS & LOAD ADMITTANCES ***
C
        DO 215 L=1,NARR
        CALL DELL(-HLENG(L),WIDTH(L),THICK(L),RLAMDA(1)
        1                                         ,SRER(L),DL)
        EFFL(L)=HLENG(L)+DL
215     YL(L)=CJ*14.09E-6*ZC(L)*SRER(L)*TAN(BETA(1)*SRER(L)
        1                                         *SLENG(L))
C
C*** DETERMINE THE SCAN ANGLE ***
C
        SINE=SIN(ETA*RPD)
        SXX=SINE*COS(ALPHA*RPD)
        IF(ALPHA.EQ.90.) SXX=0.
        SZZ=SINE*SIN(ALPHA*RPD)
        FL2DXA=RLAMDA(1)/(FLOAT(IIX)*DX)
        FL2DZA=RLAMDA(1)/(FLOAT(IIZ)*DZ)
C
        WRITE(10) ALPHA,ETA               !WRITE
        WRITE(10) NNX,NNZ,IIX,IIZ,VETO    !TO THE OUTFILE
        WRITE(10) FREQ,ISC,D(3),ER(2),ER(3)
        WRITE(10) DX,DZ,WIDTH(1),THICK(1),END(1,1),END(3,1)
        WRITE(10) DUM                     !IN SEQUENTIAL I/O
C
C
        LNU=0
        DO 702 NU=MNNX,NNX                !LOOP FOR EACH VALUE
        LMU=0                             !OF NU
        LNU=LNU+1
        DO 700 MU=MNNZ,NNZ                !LOOP FOR EACH VALUE
        LMU=LMU+1                         !OF MU
        DO 701 L=1,NLAY
        SX(L)=(SXX+NU*FL2DXA)/SQRT(ER(L))
        SZ(L)=(SZZ+MU*FL2DZA)/SQRT(ER(L))
701     CONTINUE
        N=1
        ID1=1
        ID2=1
        ITYP=-1                           !-1= LEFT NO GP
        IMED=2                            !MEDIUM 2 LEFT OF
        AEFF=WIDTH(ID1)/4.                !ARRAY
        CALL SUMZT(YLEFT)                 !ADMITTANCE TO LEFT
        IF(GPLI.NE.1.) THEN
                YRITE=YLEFT
                GO TO 699
        END IF
        ITYP=1                            !+1= RIGHT TO GP
        IMED=3                            !MEDIUM 3 RIGHT OF
```

```
C                                               !ARRAY
        CALL SUMZT(YRITE)                       !ADMITTANCE TO RIGHT
CZZZZZZZZZZZZZZZZZZZZZZZZZZZZZZZZZZZZZZZ
C  FOR THE FREE SPACE GEOMETRY OR IF
C  LAYERS TO THE LEFT ARE THE SAME AS
C  THOSE TO THE RIGHT (SYMMETRIC CASE)
C  THEN YRITE=YLEFT.  IF THERE IS NO SYMMETRY
C  THEN A CALL TO SUM MUST BE MADE FOR
C  THE RIGHT ALSO.
CZZZZZZZZZZZZZZZZZZZZZZZZZZZZZZZZZZZZZZZ
699     CONTINUE
        SUMKN(LMU)=YLEFT+YRITE
700     CONTINUE
        WRITE(10) (SUMKN(LD),LD=1,TNNZP1)   !TO UNFORMATTED
702     CONTINUE                                !OUTPUT FILE
C
C*** END OF RUN ***
C
        CLOSE(UNIT=10)                          !CLOSE OUTPUT FILE
        CALL EXIT
300     TYPE 301
301     FORMAT(2X,'*** NON-SYMMETRIC INPUT ER OR D ***')
        CALL EXIT
        END
```

```
CZZZZZZZZZZZZZZZZZZZZZZZZZZZZZZZZZZZZZZZZZZZZZZZZZZZZZZZZZZZZZZ
C  CHANGES MADE JULY 1979 BY K. SHUBERT FOR
C  STRAIGHT Z-DIRECTED ELEMENTS.  TAKES ADVANTAGE
C  OF THE FACT THAT THE PATTERN IS A FUNCTION
C  OF N ONLY AND NOT OF K.  RZKN AND PZ (THE
C  PATTERN) ARE THEREFORE CALCULATED IN SUMZ FOR
C  A GIVEN VALUE OF N ONLY ONCE.  THE ADVANTAGE
C  IS IN SAVING CPU TIME.
CZZZZZZZZZZZZZZZZZZZZZZZZZZZZZZZZZZZZZZZZZZZZZZZZZZZZZZZZZZZZZZ
C
C$$$$$$$$$$$$$$$$$$$$$$$$$$$$$$$$$$$$$$$$$$$$$$$$$$$$$$$$$$$$$$
C
        SUBROUTINE SUMZT(DSUM)
C
C THIS SUBROUTINE MANAGES THE DOUBLE SUMMATION IN THE POISSON
C SUM FORMULA AND CHECKS FOR CONVERGENCE.
C
C.DAT CONVG :CONVERGENCE NUMBER SELECTED BY EXPERIMENT
C.OUT DSUM  :THE FINAL VALUE OF THE DOUBLE SUMMATION
C
        COMPLEX DSUM,Y,Y1,Y2,Y3,Y4,Y5,Y6,Y7,Y8,Y9
        COMPLEX PX,PZ
C
        INTEGER TEST,TEST1
C
        INCLUDE 'COMMON.CMN'
        DATA CONVG /1.0E+3/
C
        NAR=ID1
        MED=IMED
C
        COMP=0.0
        DO 100 I=1,3
        N=I-2
        CALL RZN(N)
        CALL COMPAT(MED,NAR,1,PX,PZ)
        DO 100 M=1,3
        K=M-2
        CALL QUANZT(N,K,PZ,Y)
100     COMP=COMP+ABS(AIMAG(Y))
        COMP=COMP/CONVG
C
C*** K=N=0 TERM ***
C
        CALL RZN(0)
        CALL COMPAT(MED,NAR,1,PX,PZ)
        CALL QUANZT(0,0,PZ,Y1)
C
C*** SUM ALONG +K AXIS ***
C
```

```
      TEST=0
      Y2=C0
      DO 220 K=1,200
      CALL QUANZT(0,K,PZ,Y)
      Y2=Y2+Y
      IF(ABS(AIMAG(Y)).GE.COMP) TEST=-1
      TEST=TEST+1
      IF(TEST.EQ.3) GOTO 300
220   CONTINUE
C
C*** SUM ALONG -K AXIS ***
C
300   Y3=Y2
      TEST=0
      Y3=C0
      DO 320 K=1,200
      CALL QUANZT(0,-K,PZ,Y)
      Y3=Y3+Y
      IF(ABS(AIMAG(Y)).GE.COMP) TEST=-1
      TEST=TEST+1
      IF(TEST.EQ.3) GOTO 400
320   CONTINUE
C
C*** SUM ALONG +N AXIS ***
C
400   TEST=0
      Y4=C0
      DO 420 N=1,200
      CALL RZN(N)
      CALL COMPAT(MED,NAR,1,PX,PZ)
      CALL QUANZT(N,0,PZ,Y)
      Y4=Y4+Y
      IF(ABS(AIMAG(Y)).GE.COMP) TEST=-1
      TEST=TEST+1
      IF(TEST.EQ.3) GOTO 500
420   CONTINUE
C
C*** SUM ALONG -N AXIS ***
C
500   Y5=Y4
      TEST=0
      Y5=C0
      DO 520 N=1,200
      CALL RZN(-N)
      CALL COMPAT(MED,NAR,1,PX,PZ)
      CALL QUANZT(-N,0,PZ,Y)
      Y5=Y5+Y
      IF(ABS(AIMAG(Y)).GE.COMP) TEST=-1
      TEST=TEST+1
      IF(TEST.EQ.3) GOTO 600
```

```
520     CONTINUE
C
C*** SUM IN FIRST QUAD K(+) N(+) ***
C
600     TEST1=0
        Y6=C0
        DO 650 N=1,200
        CALL RZN(N)
        CALL COMPAT(MED,NAR,1,PX,PZ)
        CALL QUANZT(N,1,PZ,Y)
        Y6=Y6+Y
        IF(ABS(AIMAG(Y)).GE.COMP) TEST1=-1
        TEST1=TEST1+1
        IF(TEST1.EQ.3) GOTO 700
        TEST=0
        DO 640 K=2,200
        CALL QUANZT(N,K,PZ,Y)
        Y6=Y6+Y
        IF(ABS(AIMAG(Y)).GE.COMP) TEST=-1
        TEST=TEST+1
        IF(TEST.EQ.3) GOTO 650
640     CONTINUE
650     CONTINUE
C
C*** SUM IN SECOND QUAD K(-) N(+) ***
C
700     Y7=Y6
        Y8=Y6
        Y9=Y6
        TEST1=0
        Y7=C0
        DO 750 N=1,200
        CALL RZN(N)
        CALL COMPAT(MED,NAR,1,PX,PZ)
        CALL QUANZT(N,-1,PZ,Y)
        Y7=Y7+Y
        IF(ABS(AIMAG(Y)).GE.COMP) TEST1=-1
        TEST1=TEST1+1
        IF(TEST1.EQ.3) GOTO 760
        TEST=0
        DO 740 K=2,200
        CALL QUANZT(N,-K,PZ,Y)
        Y7=Y7+Y
        IF(ABS(AIMAG(Y)).GE.COMP) TEST=-1
        TEST=TEST+1
        IF(TEST.EQ.3) GOTO 750
740     CONTINUE
750     CONTINUE
760     Y8=Y7
C
```

```
C*** SUM IN THIRD QUAD K(-) N(-) ***
C
800     CONTINUE
        TEST1=0
        Y8=CO
        DO 850 N=1,200
        CALL RZN(-N)
        CALL COMPAT(MED,NAR,1,PX,PZ)
        CALL QUANZT(-N,-1,PZ,Y)
        Y8=Y8+Y
        IF(ABS(AIMAG(Y)).GE.COMP) TEST1=-1
        TEST1=TEST1+1
        IF(TEST1.EQ.3) GOTO 900
        TEST=0
        DO 840 K=2,200
        CALL QUANZT(-N,-K,PZ,Y)
        Y8=Y8+Y
        IF(ABS(AIMAG(Y)).GE.COMP) TEST=-1
        TEST=TEST+1
        IF(TEST.EQ.3) GOTO 850
840     CONTINUE
850     CONTINUE
C
C*** SUM IN FOURTH QUAD K(+) N(-) ***
C
900     Y9=Y8
        TEST1=0
        Y9=CO
        DO 950 N=1,200
        CALL RZN(-N)
        CALL COMPAT(MED,NAR,1,PX,PZ)
        CALL QUANZT(-N,1,PZ,Y)
        Y9=Y9+Y
        IF(ABS(AIMAG(Y)).GE.COMP) TEST1=-1
        TEST1=TEST1+1
        IF(TEST1.EQ.3) GOTO 990
        TEST=0
        DO 940 K=2,200
        CALL QUANZT(-N,K,PZ,Y)
        Y9=Y9+Y
        IF(ABS(AIMAG(Y)).GE.COMP) TEST=-1
        TEST=TEST+1
        IF(TEST.EQ.3) GOTO 950
940     CONTINUE
950     CONTINUE
C
C*** SUM ALL OF THE AXES & QUADRANTS ***
C
990     DSUM=Y1+Y2+Y3+Y4+Y5+Y6+Y7+Y8+Y9
        DSUM=DSUM*SQRT(ER(IMED))/(TZO*DX*DZ)
```

```
      RETURN
      END
C$$$$$$$$$$$$$$$$$$$$$$$$$$$$$$$$$$$$$$$$$$$$$$$$$$$$$$$$$$$$$$
C
      SUBROUTINE RZN(N)
      INCLUDE 'COMMON.CMN'
      DO 1 L=1,NLAY
      IF((ISTR(L).AND.2).NE.0) THEN
              RZKN(L)=-(FLOAT(N) + .5)*RLAMDA(L)/DZH
      ELSE
              RZKN(L)=SZ(L) + N*RLAMDA(L)/DZ
      END IF
1     CONTINUE
      RETURN
      END
```

```
C$$$$$$$$$$$$$$$$$$$$$$$$$$$$$$$$$$$$$$$$$$$$$$$$$$$$$$$$$$$$$$$$$$
        SUBROUTINE QUANZT(N,K,PZ,Q)
C
C CALCULATION OF QUANITY INSIDE THE DOUBLE SUM
C.IN  K & N :SUMMATION INDICIES
C.COM ID1   :FIRST INDEX OF ADMITTANCE IDENITY
C.COM ID2   :SECOND INDEX OF ADMITTANCE IDENITY
C.OUT Q :THE VALUE OF THE QUANITY
C
        COMPLEX Q,PX,PZ,POT,PPT,PO,PP,TFO,TFP,PHASE,PH,TCM
        INCLUDE 'COMMON.CMN'
        CALL DIRECT(K,N)                !GET RXKN,RYKN
        MED=IMED                        !RZKN FOUND IN
C PATTERN; TRANSMITTING                 !RZN
        NAR=ID1
C       CALL COMPAT(MED,NAR,1,PX,PZ)    !CALLED IN SUMZT
C                                       !PX=0, PZ A FUNCTION
C                                       !OF N ONLY
C CALCULATE PARALLEL AND ORTHOGONAL
C COMPONENTS OF PATTERN
        CALL OPCOMP(MED,CO,CO,PZ,POT,PPT)
C PATTERN; NON-TRANSMITTING
        PO=POT
        PP=PPT
C       NAR=ID2                         !FOR STRAIGHT
C       CALL COMPAT(MED,NAR,-1,PX,PZ)   !Z-DIRECTED
C       CALL OPCOMP(MED,PX,CO,PZ,PO,PP) !ELEMENTS,TRANSMIT
C                                       !PATTERN
C T FACTOR                              !NON-TRANSMIT
C____________________________________________________________
C
C  TO FIND IMPEDANCES OF DIPOLES SUBROUTINE TFACTD MUST BE
C  CALLED.  TO FIND ADMITTANCES OF SLOTS ROUTINE TFACT MUST
C  BE CALLED.  BOTH ARE NOT USED WITH A LOGICAL OPERATION
C  TO SAVE CPU TIME WHICH CAN BE LARGE BECAUSE SUBROUTINE
C  QUANZT IS CALLED FOR EACH K,N,NU,MU.
C
C
C        DIPOLES
        CALL TFACTD(MED,TFO,TFP,K,N)    !T-FACTOR FOR DIPOLES
C        DIPOLES
C
C
C
C        SLOTS
C       CALL TFACT(MED,TFO,TFP,K,N)     !T-FACTOR FOR SLOTS
C        SLOTS
C
C____________________________________________________________
C PHASE TERM
```

```
        TCM=CMPLX(BETA(MED)*AEFF*AIMAG(RYKN(MED)),0.)
        PHASE=CEXP(TCM)
150     Q=((POT*PO*TFO) + (PPT*PP*TFP))*PHASE/RYKN(MED)
        RETURN
        END
C$$$$$$$$$$$$$$$$$$$$$$$$$$$$$$$$$$$$$$$$$$$$$$$$$$$$$$$$$$$$$$$$$
        SUBROUTINE DIRECT(IKK,INN)
C
C DETERMINES WAVE DIRECTION RXKN,RYKN
C.IN  IKK,INN  :INDICIES K & N
C
        INCLUDE 'COMMON.CMN'
        DO 100 L=1,NLAY
        IF((ISTR(L).AND.1).NE.0) THEN
                RXKN(L)=IKK*RLAMDA(L)/DXH
        ELSE
                RXKN(L)=SX(L) + IKK*RLAMDA(L)/DX
        END IF
        YR=1.0-RXKN(L)**2-RZKN(L)**2
        IF(YR.LT.0.) THEN
                RYKN(L)=CMPLX(0.,-SQRT(-YR))
        ELSE
                RYKN(L)=CMPLX(SQRT(YR),0.)
        END IF
100     CONTINUE
        RETURN
        END
C$$$$$$$$$$$$$$$$$$$$$$$$$$$$$$$$$$$$$$$$$$$$$$$$$$$$$$$$$$$$$$$$$
        SUBROUTINE COMPAT(MED,NAR,ITR,PATX,PATZ)
C
C CALCULATES THE PATTERN FUNCTION OF DIPOLE OR SLOT
C CONFIGURATIONS ASSUMING SINUSOIDAL CURRENT DISTRIBUTION
C IN EITHER THE TRANSMITTING OR NON-TRANSMITTING MODE.
C THIS ROUTINE USES STRAIGHT Z-DIRECTED ELEMENTS.
C THE VARIABLE 'END(3,N)' MUST CONATIN THE HALF-LENGTH
C FOR ELEMENTS IN THE N.TH ARRAY.
C.IN  MED   :INDEX OF MEDIUM
C.IN  NAR   :NUMBER OF THE SELECTED ARRAY
C.IN  ITR   :1=TRANSMITTING, -1=NON-TRANSMITTING
C.OUT PATX  :X COMPONENT OF TOTAL PATTERN
C.OUT PATZ  :Z COMPONENT OF TOTAL PATTERN
C
        COMPLEX PATX,PATZ
        INCLUDE 'COMMON.CMN'
        BD=BETA(1)*SRER(NAR)
        BDLE=BD*EFFL(NAR)
        BDDL=BD*(EFFL(NAR)-END(3,NAR))
        BRZ=BETA(MED)*RZKN(MED)
        BRZL=BRZ*END(3,NAR)
        COSBL=COS(BDLE)
```

```
      P=(COS(BDDL+BRZL)-COSBL)/(BD-BRZ)
     1   +(COS(BDDL-BRZL)-COSBL)/(BD+BRZ)
      PATX=C0
      PATZ=CMPLX(P/SIN(BDLE),0.0)
      RETURN
      END
C$$$$$$$$$$$$$$$$$$$$$$$$$$$$$$$$$$$$$$$$$$$$$$$$$$$$$$$$$$$$$$$$$$$$$$$$
      SUBROUTINE OPCOMP(MED,CX,CY,CZ,ORTH,PARAL)
C
C FIND THE ORTHOGONAL AND PARALLEL COMPONENTS OF CX,CY,CZ
C WITH RESPECT TO RXKN,RYKN,RZKN
C.IN  MED       :INDEX OF MEDIUM
C.IN  CX,CY,CZ :INPUT VECTOR(COMPLEX)
C.OUT ORTH      :ORTHOGONAL COMPONENT
C.OUT PARAL    :PARALLEL COMPONENT
C
      COMPLEX CX,CY,CZ,ORTH,PARAL
      INCLUDE 'COMMON.CMN'
      SRXZ=SQRT(RXKN(MED)**2 + RZKN(MED)**2)
      IF(SRXZ.EQ.0.) THEN
              ORTH=CZ
              PARAL=CX
              RETURN
      END IF
C ORTHOGONAL PATTERN FACTOR
      ORTH=CZ*RXKN(MED)/SRXZ
C PARALLEL PATTERN FACTOR
      PARAL=-CZ*RZKN(MED)*RYKN(MED)/SRXZ
      RETURN
      END
C$$$$$$$$$$$$$$$$$$$$$$$$$$$$$$$$$$$$$$$$$$$$$$$$$$$$$$$$$$$$$$$$$$$$$$$$
      SUBROUTINE TFACTD(MED,TFO,TFP,K,N)
C  SUBROUTINE TO CALCULATE T-FACTOR FOR ONE DIPOLE ARRAY.FREE
C  SPACE IS IN MEDIA 1 AND 4 WHICH ARE TO THE LEFT AND RIGHT
C  OF MEDIA 2 AND 3 (THE ARRAY IS LOCATED BETWEEN MEDIA 2 AND
C  3 SO THESE MUST HAVE THE SAME DIELECTRIC CONSTANT).A GROUND
C  PLANE EXISTS AT THE LEFT OF MEDIUM 2 IF ITYP=1.  VARIABLES
C  ENDING IN 'O' REFER TO THE ORTHOGONAL COMPONENT AND THOSE
C  ENDING IN 'P' REFER TO THE PARALLEL COMPONENT.  D(2) IS THE
C  DISTANCE FROM THE ARRAY TO THE LEFT INTERFACE AND D(3) IS
C  THE DISTANCE TO THE RIGHT INTERFACE.
      COMPLEX GAM34O,GAM34P,GAM21O,GAM21P,TFO,TFP
      COMPLEX EGAMMA,TEXP,DSFO,DSFP,TPE,TED2,TED3
      INCLUDE 'COMMON.CMN'
C
      GAM34O=EGAMMA(1)                     !ORTHOG. GAMMA
      GAM34P=EGAMMA(2)                     !PARALLEL GAMMA
      IF(ITYP.EQ.1) THEN
              GAM21O=-C1                   !GROUND PLANE
              GAM21P=-C1                   !TO LEFT
```

```
        ELSE
                GAM21O=GAM34O                   !FREE SPACE
                GAM21P=GAM34P                   !TO LEFT
        END IF
        TPE=TEXP(D(2) + D(3))
        DSFO=GAM21O*GAM34O*TPE
        DSFP=GAM21P*GAM34P*TPE
        TED2=TEXP(D(2))
        TED3=TED2                               !D(3)=D(2)
C
        TFO=( (1. + GAM21O*TED2)*(1. + GAM34O*TED3) )
        1       /(1. - DSFO)
C
        TFP=( (1. + GAM21P*TED2)*(1. + GAM34P*TED3) )
        1       /(1. - DSFP)
C
        RETURN
        END
C$$$$$$$$$$$$$$$$$$$$$$$$$$$$$$$$$$$$$$$$$$$$$$$$$$$$$$$$$$$$$$$$$
        FUNCTION TEXP(DARG)
        COMPLEX TPARG,TEXP
        INCLUDE 'COMMON.CMN'
        TPARG=-CJ*2.*BETA(2)*DARG*RYKN(2)
        TEXP=CEXP(TPARG)
        RETURN
        END
C$$$$$$$$$$$$$$$$$$$$$$$$$$$$$$$$$$$$$$$$$$$$$$$$$$$$$$$$$$$$$$$$$
        FUNCTION EGAMMA(IFIELD)
C  CALCULATES THE E-FIELD REFLECTION COEFFICIENT FROM MEDIUM
C  WITH INTRINSIC IMPEDANCE ZIMP(2) TO MEDIUM WITH INTRINSIC
C  IMPEDANCE ZIMP(1).
C               IFIELD=1 => ORTHOGONAL
C               IFIELD=2 => PARALLEL
C
        COMPLEX EGAMMA,R12,R21,T1,T2
        INCLUDE 'COMMON.CMN'
C
        IF(IFIELD.EQ.1) THEN
                R12=RYKN(2)
                R21=RYKN(1)
        ELSE
                R12=RYKN(1)
                R21=RYKN(2)
        END IF
        T1=ZIMP(1)*R12
        T2=ZIMP(2)*R21
        EGAMMA=(T1 - T2)/(T1 + T2)
        RETURN
        END
C$$$$$$$$$$$$$$$$$$$$$$$$$$$$$$$$$$$$$$$$$$$$$$$$$$$$$$$$$$$$$$$$$
```

```
      SUBROUTINE TFACT(MED,TFO,TFP,K,N)
C
C COMPUTE "T FACTOR" FOR SLOT ARRAY CASES
C.IN  MED   :INDEX OF MEDIUM
C.OUT TFO   :ORTHOGONAL T FACTOR
C.OUT TFP   :PARALLEL T FACTOR
C
      COMPLEX TFO,TFP,NUM,EXP,GMA,EX,HGAMMA,F
      COMPLEX GMA3,GMA4,G3EX,G4EX
      INCLUDE 'COMMON.CMN'
C
      EXP=CEXP(-CJ*2.*BETA(MED)*D(MED)*RYKN(MED))
      IF(ITYP.EQ.1) THEN
            TFO=2.*(1. + EXP)/(1. - EXP)
            TFP=TFO
      ELSE
            GMA3=HGAMMA(3)
            GMA4=HGAMMA(4)
            G3EX=GMA3*EXP
            G4EX=GMA4*EXP
            TFO=2.*(1. + G3EX)/(1. - G3EX)
            TFP=2.*(1. + G4EX)/(1. - G4EX)
      END IF
      RETURN
      END
C$$$$$$$$$$$$$$$$$$$$$$$$$$$$$$$$$$$$$$$$$$$$$$$$$$$$$$$$$$$$$$$$$$$
      FUNCTION HGAMMA(IFIELD)
C
C GENERATE REFELECTION COEFFICIENT; HGAMMA
C.IN  IFIELD:FIELD TYPE (3=ORTH-H, 4=PARAL-H)
C
      COMPLEX HGAMMA,R12,R21,T1,T2
      INCLUDE 'COMMON.CMN'
C
      IF(IFIELD.EQ.3) THEN
            R12=RYKN(IMED)
            R21=RYKN(1)
      ELSE
            R12=RYKN(1)
            R21=RYKN(IMED)
      END IF
      T1=YADM(1)*R12
      T2=YADM(IMED)*R21
      HGAMMA=(T1 - T2)/(T1 + T2)
      RETURN
      END
C$$$$$$$$$$$$$$$$$$$$$$$$$$$$$$$$$$$$$$$$$$$$$$$$$$$$$$$$$$$$$$$$$$$
      SUBROUTINE DELL(HL,W,T,RLAMDA,SRER,DL)
C
C CALCULATION OF AN INCREMENTAL LENGTH TO BE ADDED TO
```

```
C A SLOT OR FLAT WIRE DIPOLE DUE TO END EFFECTS.
C SEE DISSERTATION BY B. MUNK, APPENDIX A
C KHAT: EQ(A-19), XHAT: EQ(A-33), DL: EQ(A-23) & EQ(A-30)
C
C ALL OF THE DIMENSIONS HAVE THE SAME UNITS. EG. CM
C.IN  HL   :HALF-LENGTH, (HL.LT.0)=SLOTS, (HL.GT.0)=DIPOLES
C.IN  W,T    :WIDTH & THICKNESS OF SLOT OR DIPOLE
C.IN  RLAMDA :FREE SPACE WAVELENGTH
C.IN  SRER   :SQUARE ROOT OF EFFECTIVE DIELECTRIC CONSTANT
C.OUT DL        :'DELTA L', TO BE ADDED TO HALF-LENGTH
C
        DATA PI,PI2 /3.14159265, 1.57079633/
        B=2.0*PI/RLAMDA
C
C*** CALCULATE ELECTRICAL LENGTHS ***
C
        EL=ABS(HL)*SRER
        EW=W*SRER
        ET=T*SRER
        BL=B*EL
        BL2=2.0*BL
        BL4=4.0*BL
C
        CALL SICI(SIBL,CIBL,BL)
        SIBL=SIBL+PI2
        CALL SICI(SI2BL,CI2BL,BL2)
        SI2BL=SI2BL+PI2
        CALL SICI(SI4BL,CI4BL,BL4)
        SI4BL=SI4BL+PI2
C
        KHAT=120.0*(ALOG(RLAMDA/(PI*EW))+CIBL+0.769357926)
        IF(2.0*EL/EW.LT.15.0)KHAT=KHAT-41.58883083
C
        XHAT=60.0*SI2BL+30.0*(2.0*SI2BL-SI4BL)*COS(BL2)+30.0*
        1   (CI4BL+2.0*CIBL-2.0*CI2BL-ALOG(BL4)+2.19537305)*
        1   SIN(BL2)
C
        EDL=XHAT/(B*KHAT)+SIGN(1.0,HL)*1.8E-3*EW*KHAT/ALOG
        1                                         (1.5*EW/ET)
C
        DL=EDL/SRER
C
        RETURN
        END
C$$$$$$$$$$$$$$$$$$$$$$$$$$$$$$$$$$$$$$$$$$$$$$$$$$$$$$$$$$$$$$$$$$$$$
        SUBROUTINE SICI(SI,CI,X)
C
C COMPUTATION OF SINE & COSINE INTEGRALS
C
C.IN  X :ARGUMENT
```

```
C.OUT SI     :VALUE OF SINE INTEGRAL
C.OUT CI     :VALUE OF COSINE INTEGRAL
C
             Z=ABS(X)
             IF(Z-4.0) 100,100,400
100          Y=(4.0-Z)*(4.0+Z)
             SI=-1.570797E0
             IF(Z) 300,200,300
200          CI=-1.0E38
             RETURN
300          SI=X*(((((1.753141E-9*Y+1.568988E-7)*Y+1.374168E-5)*Y
             1  +6.939889E-4)*Y+1.964882E-2)*Y+4.395509E-1+SI/X)
             CI=((5.772156E-1+ALOG(Z))/Z-Z*(((((1.386985E-10*Y
             1  +1.584996E-8)*Y+1.725752E-6)*Y+1.185999E-4)*Y
             1  +4.990920E-3)*Y+1.315308E-1))*Z
             RETURN
400          SI=SIN(Z)
             Y=COS(Z)
             Z=4.0/Z
             U=((((((((4.048069E-3*Z-2.279143E-2)*Z+5.515070E-2)*Z
             1  -7.261642E-2)*Z+4.987716E-2)*Z-3.332519E-3)*Z
             1  -2.314617E-2)*Z-1.134958E-5)*Z+6.250011E-2)*Z+
             1                               2.583989E-10
             V=(((((((((-5.108699E-3*Z+2.819179E-2)*Z-6.537283E-2)*Z
             1  +7.902034E-2)*Z-4.400416E-2)*Z-7.945556E-3)*Z+
             1  2.601293E-2)*Z
             1  -3.764000E-4)*Z-3.122418E-2)*Z-6.646441E-7)*Z
             1  +2.5000000E-1
             CI=Z*(SI*V-Y*U)
             SI=-Z*(SI*U+Y*V)
             IF(X) 500,600,600
500          SI=-3.141593E0-SI
600          RETURN
             END
```

APPENDIX I
COMPUTER PROGRAM CMPLOT

CMPLOT is an operator interactive FORTRAN language program which uses the output files of program SLOT or DIPOLE as its input and calculates the desired element by element admittances or impedances of the slot or dipole arrays, respectively. The output can take the form of values printed to the terminal, values written to a data file, or plots of immittances as a function of element position displayed to a CRT graphics display or a paper plotter. As stated in Appendix G, CMPLOT uses the values of F of Equation (G10) as input, calculates the Fourier coefficients for the aperture distribution which the operator specifies, calculates Y, the slot element admittance of Equation (G8) (or dipole impedance if that is desired), and outputs this information in the operator specified mode. All transform method immittance plots in this study were drawn by this program and all numerical values of immittance were calculated by it. Figure I1 gives the contents of file CMPLOT.CMN, the common statements.

Branching to different parts of the code is accomplished by using two non-standard subroutines, COMD and COMDFL, whose function can best be understood by example. When the code is executed, the first executable lines assign values to variables TWOPI and PID2. After two system subroutines are executed the line CALL COMDFL(2H.) is executed. This routine outputs a prompt (the dot) to the terminal. To the operator, it appears as if execution stops here until a three letter command is entered through the terminal. If, for example, the operator entered "INS", the computer would start executing after line 2350. Two WRITE statements to logical unit 8, the terminal, would then be executed. When the next COMD statement, line 5000, is encountered the program appears to branch back to line 2350, the COMDFL statement, and again the dot prompt appears at the terminal. If "REA" is then entered at the terminal, the program branches to line 5000 and the portion of the code reading the input data is executed. When line 6650 is encountered, the prompt again appears at the terminal. The COMD call can have one other format as shown in line 14500. Typing in "CAS" after the prompt forces branching to line 14500 as before. However, if the lines above 14500 were being executed, which would be the case if "FDE" has been entered into the terminal, and this statement were encountered, program execution would branch to FORTRAN line 200 (line 24000 in the listing).

Each possible instruction is listed below with a short explanation as to the purpose of that particular portion of the code.

INS INSTRUCTIONS TO TERMINAL
The list of possible commands is printed to the terminal (logical unit 8).

REA READ
The terminal requests a file name and the indicated file (which has to be written by either program DIPOLE or SLOT) is read. The default array sixe KX=KZ=31 is assigned.

CKK CHANGE KX AND KZ
The values of KX and KZ are output to the terminal and new values are requested.

PT1 PATTERN IN ONE-DIMENSION
The pattern in the x-y plane is calculated using one-dimensional input data

PT2 PATTERN IN TWO-DIMENSIONS
The patterns from two dimensional data can be calculated. This operation is very time consuming and an alternative method is suggested.

FDE FILE DESCRIPTION
The description of a file can be examined without reading in all of the data.

CAS SUM OR DIFFERENCE CASE
The value of CASE can be changed. 0 signifies a sum file, 1 a difference pattern in the x-y plane and 2 a difference pattern in the z-y plane.

CSX COSINE ALONG X (1-D)
Calculate the cosine Fourier coefficients for one-dimensional data. NZ must be zero for one-dimensional apertures.

COS COSINE ALONG X AND Z (2-D)
Calculate the coefficients for cosine distributions in the x and z directions.

CPL COSINE ALONG X, PULSE ALONG Z (2-D)
Calculate the coefficients for this two-dimensional distribution.

TR2 TRAPEXOID ALONG X AND Z (2-D)
Calculate the coefficients for this two-dimensional distribution.

TRX TRAPEZOID ALONG X (1-D)
Calculate the coefficients for this one-dimensional distribution.

TRC TRAPEZOID ALONG X COSINE ALONG Z (2-D)

PLD PULSE DIFFERENCE ALONG (1-D)

DIF SMOOTH DIFFERENCE ALONG X, COSINE ALONG Z (2-D)

DFX SMOOTH DIFFERENCE ALONG X (1-D)

PLC PULSE ALONG X, COSINE ALONG Z(2-D)

PLX PULSE ALONG X (1-D)

PL2 PULSE ALONG X AND Z (2-D)

STC STEP ALONG X, COSINE ALONG Z(2-D)

STP STEP ALONG X AND Z (2-D)

CST CHANGE STEP PARAMETERS
Change the size of the numbers describing the size and shape of the step distributions. See Appendix D.

OUT OUTPUT TO OUTFILE
An output file name is requested. The current data description is output to this file and the program branches to command IND (see below). The data calculated there goes to the output file rather than the terminal as is the case if the command IND is entered.

COF CLOSE OUTPUT FILE

DES DESCRIPTION
The description of the current data is printed to the terminal.

XPL CALCULATE DATA ALONG X (NECESSARY FOR PLOTTING)
The value of the row (m) is requested and the values of the current, voltage, and immittance are calculated for the entire row for the elements from -99 to +99. Either XPL or ZPL must be executed before plotting.

ZPL CALCULATE DATA ALONG Z (NECESSARY FOR PLOTTING)
Same as XPL if it is desired to plot the values along one column of elements along z. Either XPL or ZPL must be executed before plotting.

IND CALCULATE INDIVIDUAL ELEMENT VALUES
The values are calculated for operator specified elements. For example entering "-15,15,0,0" would enable calculation of the values for the center row along x from the -15th element to the 15th element. The values are output to the terminal unless the OUT command is being executed.

PON OPEN THE PLOTTER FILE (UNIQUE TO OHIO STATE UNIVERSITY ELECTROSCIENCE LAB VAX COMPUTER FACILITY)

MPL PLOT TO CRT GRAPHICS DISPLAY (UNIQUE TO OSU-EL)

PLN PLOT FROM FILE TO PLOTTER (UNIQUE TO OSU-ESL)

SLW SET LINE WIDTH (UNIQUE TO OSU-ESL)

GRD PLACE GRID ON PLOTS (UNIQUE TO OSU-ESL)

SPL SET PHASE LIMITS
Change plot phase max-min. Default is -30 degrees to +30 degrees.

PLO PLOT DATA (UNIQUE TO OSU-ESL)
Plot in the form of Figure 17.

PEX PLOT EXPANDED (UNIQUE TO OSU-ESL)
Plot in the form of Figure 18.

STO STORE XPL OR ZPL DATA
Store data to be plotted in the form of Figure 19.

PL4 PLOT 4 PLOTS ON ONE PAGE (UNIQUE TO OSU-ESL)
Plot in the form of Figure 19.

AMX SET AXIS MAXIMUM
Set immittance maximum on plots of the form PEX, PLO, or PL4.

NMP NEW METATEK PAGE (UNIQUE TO OSU-ESL)
Erase the CRT screen so that a new graph can be plotted.

POF PLOTTER OFF (UNIQUE TO OSU-ESL)
Close plotter file or erase and relinquish CRT screen.

EXI EXIT FROM PROGRAM

```
00100          COMMON /LAB/CF
00200          COMPLEX CF(241,81)
```

Figure I1. The contents of file CMPLOT.CMN which contains the COMMON statements for program CMPLOT and subroutine MNSUM.

```
C**************************   . ****************************
C###########################################################
C                                                          #
C                         PROGRAM CMPLOT                   #
C                                                          #
C                                                          #
C  MUST BE COMPILED WITH                                   #
C        $FORTRAN/NOOPTIMIZE                               #
C  MUST BE LINKED WITH                                     #
C        $LINK CMPLOT,CMSUBS,[RC4652]RCLIB/LIB,'PLOTLIB     #
C                                                          #
C                                                          #
C###########################################################
        DIMENSION AMQ(1049),GMAG(1049),DUM(10),APATD(181)
        DIMENSION AMQS(1049),GMAGS(1049)
        DIMENSION FLAMZ(250),FLAMX(250),XEL(1049),ZMAG(1049)
        DIMENSION XELS(1049),ZMAGS(1049),ZPHS(1049),ZMPH(1049)
        DIMENSION GPHS(1049),GMPH(1049),EPAT(181)
        DIMENSION VP1(1049),VP2(1049),VP3(1049),VP4(1049)
        DIMENSION AMD(41,4),GMD(41,4),ZMD(41,4),ALD(4),ETD(4)
        COMPLEX S1PHASE,S2PHASE,EPATC,T2S(-50:50)
        COMPLEX T4S(-50:50,-50:50),TSZ,TSX
        BYTE BDATE(9),BTIME(8)
        INCLUDE 'CMPLOT.CMN'
        COMPLEX ZM(1049),FSM(1049),GMQ,CO,GMQARR(1049),ZM1
        DIMENSION XT(2),YT(2)
        REAL IMAG,IMAX
        INTEGER TNNZP1,TNNXP1,QQ
        INTEGER GGX,GGZ,FFX,FFZ
        CHARACTER*40 FILEIN,FILEOT
        DATA ISC,SGPCM,DIEL1,DIEL2,DUM,NPN
        1  /0,0.,1.,1.,10*0.,3/
        DATA XT,YT/0.,1.,0.,0./
        DATA KKX,KKZ,INDAT,MPL/31,31,0,0/
        DATA LM1,LM2,IGRID/'88888888'X,'AAAAAAAA'X,0/
        DATA PI,CO/3.1415926535,(0.,0.)/
        DATA IXPL,IDS,IFD,INDO,IOUT,ISTP,ISTX
        1  /0,0,0,0,8,0,0/
        DATA CASE,IDIFF,YPMAX/0.,0,30./
        EQUIVALENCE (TVETO,DUM(8)),(DIPOLE,DUM(9))
        EQUIVALENCE (CASE,DUM(1))
        EQUIVALENCE (GPLI,DUM(2))        !GRND PLANE INDICATOR
        TWOPI=2.*PI                      !THROUGH DUM(1),DUM(2)
        PID2=PI/2.
        CALL SETMSG(0)                   !PLOTTER SUBROUTINE
        CALL DATE(BDATE)
        CALL COMDFL(2H. )                !DEFINES CALL COMMAND
C                                        !PROMPT
C************************** INS ****************************
C
```

```
        CALL COMD(3HINS)                    !INSTRUCTIONS TO TTY
        WRITE(8,2)
2       FORMAT(
        1  10X,'REA=READ INPUT FILE',/,
        1  10X,'CKK=CHANGE KKX,KKZ',/,
        1  10X,'PT1=CALCULATE PATTERN 1-D CASE',/,
        1  10X,'PT2=CALCULATE PATTERN 2-D CASE ',/,
        1  10X,'PLX=PULSE DIST. X-DIRECTION ONLY',/,
        1  10X,'TRX=TRAPEZOID DIST. X-DIRECTION ONLY',/,
        1  10X,'CSX=COSINE DIST. X-DIRECTION ONLY',/,
        1  10X,'COS=COSINE DIST. TWO-DIMENSIONAL',/,
        1  10X,'CPL=COS-X,PULSE-Z',/,
        1  10X,'DES=DESCRIPTION OF DATA PARAMETERS',/,
        1  10X,'FDE=FILE DESCRIPTION TO TERMINAL',/,
        1  10X,'XPL=CALCULATE ADMITTANCE OF MTH ROW',/,
        1  10X,'ZPL=CALCULATE ADMITTANCE OF QTH COLUMN',/,
        1  10X,'IND=CALCULATE INDIVIDUAL ADMITTANCES',/,
        1  10X,'OUT=OUPUT DESCRIPTION AND DATA TO OUT FILE',/,
        1  10X,'COF=CLOSE OUTPUT FILE',/,
        1  10X,'STP=2-D STEP APERTURE',/,
        1  10X,'CST=CHANGE STEP PARAMETERS',/,
        1  10X,'STC=STEP-X, COS-Z',/,
        1  10X,'CAS=SUM OR DIFFERENCE CASE',/,
        1  10X,'DIF=SMOOTH DIFFERENCE DISTRIBUTION',/,
        1  10X,'DFX=DIFFERENCE ALONG X ONLY',/,
        1  10X,'PLD=PULSE DIFF X-DIR ONLY',/,
        1  10X,'PLC=PULSE ALONG X,COSINE ALONG Z',/,
        1  10X,'PL2=PULSE ALONG X AND Z',/,
        1  10X,'TR2=TRAPEZOID ALONG X AND Z',/,
        1  10X,'TRC=TRAPEZOID-X, COS-Z')
        WRITE(8,3)
3       FORMAT(
        1  10X,'PON=PLOTTER ON, OPEN PLOTTER FILE',/,
        1  10X,'PLN=PLOT NOW, DATA TO PLOTTER',/,
        1  10X,'SLW=SET LINE WIDTH ON PLOTS',/,
        1  10X,'GRD=SET GRID INDICATOR',/,
        1  10X,'SPL=SET PHASE PLOT LIMITS',/,
        1  10X,'PLO=PLOT FROM ELEMENT -50 TO 50',/,
        1  10X,'PEX=PLOT EXPANDED (FROM -20 TO 20 )',/,
        1  10X,'STO=STORE PLOT FOR COMPARISON DISPLAY',/,
        1  10X,'PL4=4 PLOTS ON ONE PAGE',/,
        1  10X,'AMX=SET AXIS MAX ON PEX PLOT',/,
        1  10X,'MPL=PLOT TO MEGATEK',/,
        1  10X,'NMP=NEW MEGATEK PLOT',/,
        1  10X,'POF=CLOSE PLOTTER FILE',/,
        1  10X,'EXI=EXIT FROM PROGRAM')
C
C*************************** REA *****************************
C
        CALL COMD(3HREA)                    !READ INPUT FILE
```

```
        WRITE(8,4)
4       FORMAT(2X,'ENTER: INPUT FILE NAME',2X,$)
        READ(8,554) FILEIN
554     FORMAT(A30)
        OPEN(UNIT=7,NAME=FILEIN,TYPE='OLD',FORM='UNFORMATTED'
        1  ,ERR=599)
        READ(7) ALPHA,ETA               !DATA FROM PROGRAM
        READ(7) NNX,NNZ,IIX,IIZ,VETO    !DKSZ
        READ(7) FREQ,ISC,SGPCM,DIEL1,DIEL2
        READ(7) DX,DZ,SLWCM,SLTHCM,SLSTCM,SLENCM
        READ(7) DUM
        TNNXP1=(2*NNX)+1
        TNNZP1=(2*NNZ)+1
        DO 11 NU=1,TNNXP1
        READ(7) (CF(NU,MU),MU=1,TNNZP1)
11      CONTINUE
        CLOSE(UNIT=7)
        IF(DIPOLE.EQ.1.) THEN
                PAMX=500.
                FACN=1.
        ELSE
                PAMX=5.
                FACN=1000.
        END IF
        GO TO 600
599     CONTINUE
        WRITE(8,598)
598     FORMAT(2X,'***INPUT FILE DOES NOT EXIST***')
600     CONTINUE
C
C************************** CKK *****************************
C
        CALL COMD(3HCKK)                !CHANGE KKX,KKZ
        WRITE(8,10) KKX,KKZ
10      FORMAT(2X,'KKX= ',I4,7X,'KKZ= ',I4
        1       ,/,2X,'ENTER: KKX,KKZ  ',$)
        READ(8,*) KKX,KKZ
C
C************************** PT1 *****************************
C
        CALL COMD(3HPT1)                !X-Y PLANE PATTERN
        EPMAX=0.
        FLAMDA=(30./FREQ)/SQRT(DIEL1)   !1-DIMENSIONAL
        FLAMODI=FLAMDA/(DX*IIX)
        BETADX=TWOPI*DX/FLAMDA
        IF(NNZ.NE.0) GO TO 600
        SX0=SIN(ETA*PI/180.)*COS(ALPHA*PI/180.)
        DO 577 NQ=-KKX/2,KKX/2
        TPNQ=BETADX*NQ
        T2S(NQ)=C0
```

```
        DO 576 NU=-NNX,NNX
        IF(NU.LT.0) THEN
                COEF=FLAMX(-NU)/2.
        ELSE IF(NU.GT.0) THEN
                COEF=FLAMX(NU)/2.
        ELSE
                COEF=FLAMX0
        END IF
        SMNFDI=SX0-NU*FLAMODI
        ARG=TPNQ*SMNFDI
        S2PHASE=CEXP(CMPLX(0.,-ARG))
        T2S(NQ)=T2S(NQ) + COEF*S2PHASE
576     CONTINUE
577     CONTINUE
        DO 579 IPAT=-90,90
        IP=IPAT + 91
        APATD(IP)=IPAT
        APATR=APATD(IP)*PI/180.
        SNA=SIN(APATR)
        SNMSX=SNA
        EPATC=C0
        DO 578 NQ=-KKX/2,KKX/2
        TPNQ=BETADX*NQ
        ARG=TPNQ*SNMSX
        S1PHASE=CEXP(CMPLX(0.,ARG))
        EPATC=EPATC + S1PHASE*T2S(NQ)
578     CONTINUE
        EPAT(IP)=CABS(EPATC)
        IF(EPAT(IP).GT.EPMAX) EPMAX=EPAT(IP)
579     CONTINUE
        DO 581 I=1,181
        EPAT(I)=20.*ALOG10(EPAT(I)/EPMAX)
        IF(EPAT(I).LT.-40.) EPAT(I)=-40.
581     CONTINUE
        CALL PLTPKG(APATD,EPAT,181,-181,1,0,1)
        CALL PLTPKG(APATD,EPAT,181,-181,1,0,1)
C
C**************************** PT2 *****************************
C
        CALL COMD(3HPT2)                !PATTERN
C$$$$$$$$$$$$$$$$$$$$$$$$$$$$$$$$$$$$$$$$$$$$$$$$$$$$$$$$$$$$$$$$
C$$$$$$$$$$$$$$$$$$$$$$$$$$$$$$$$$$$$$$$$$$$$$$$$$$$$$$$$$$$$$$$$
C                       WARNING
C  CALCULATING THE PATTERN USING THIS COMMAND CAN BE VERY
C  TIME CONSUMING.  IT IS RECOMMENDED THAT ONE USE THE
C  ONE DIMENSIONAL CASE UNDER COMMAND PT1.
C
C$$$$$$$$$$$$$$$$$$$$$$$$$$$$$$$$$$$$$$$$$$$$$$$$$$$$$$$$$$$$$$$$$
C$$$$$$$$$$$$$$$$$$$$$$$$$$$$$$$$$$$$$$$$$$$$$$$$$$$$$$$$$$$$$$$$$
        WRITE(8,562)                    !2-DIMENSIONAL
```

```
562   FORMAT(2X,'ENTER: ALPHA PLANE OF PATTERN',/,
      1       2X,'X-Y PLANE=0, Z-Y PLANE=90, ETC. ',$)
      READ(8,*) ALPHAP
      ALPHAP=ALPHAP*PI/180.
      FLAMDA=(30./FREQ)/SQRT(DIEL2)
      BETADX=TWOPI*DX/FLAMDA
      BETADZ=TWOPI*DZ/FLAMDA
      FLAMODX=FLAMDA/(DX*IIX)
      FLAMODZ=FLAMDA/(DZ*IIZ)
      SXO=SIN(ETA*PI/180.)*COS(ALPHA*PI/180.)
      SZO=SIN(ETA*PI/180.)*SIN(ALPHA*PI/180.)
      EPMAX=0.
      DO 568 MM=-KKZ/2,KKZ/2
      BDZM=BETADZ*MM
      DO 566 NQ=-KKX/2,KKX/2
      T4S(NQ,MM)=CO
      BDXQ=BETADX*NQ
      DO 564 MU=-NNZ,NNZ
      ARG=DDZM*(SZO + MU*FLAMODZ)
      TSZ=CEXP(CMPLX(0.,-ARG))
      IF(MU.LT.0) THEN
              COEFZ=FLAMZ(-MU)/2.
      ELSE IF(MU.GT.0) THEN
              COEFZ=FLAMZ(MU)/2.
      ELSE
              COEFZ=FLAMZO
      END IF
      DO 563 NU=-NNX,NNX
      ARG=BDXQ*(SXO + NU*FLAMODX)
      TSX=CEXP(CMPLX(0.,-ARG))
      IF(NU.LT.0) THEN
              COEFX=FLAMX(-NU)/2.
      ELSE IF(NU.GT.0) THEN
              COEFX=FLAMX(NU)/2.
      ELSE
              COEFX=FLAMXO
      END IF
      T4S(NQ,MM)=T4S(NQ,MM) + COEFX*COEFZ*TSZ*TSX
563   CONTINUE
564   CONTINUE
566   CONTINUE
568   CONTINUE
      DO 569 IPAT=-90,90
      IP=IPAT + 91
      APATD(IP)=IPAT
      SPX=COS(ALPHAP)*SIN(APATD(IP)*PI/180.)
      SPZ=SIN(ALPHAP)*SIN(APATD(IP)*PI/180.)
      EPATC=CO
      DO 572 MM=-KKZ/2,KKZ/2
      BDZM=BETADZ*MM
```

```
              ARG=BDZM*SPZ
              TSZ=CEXP(CMPLX(0.,ARG))
              DO 571 NQ=-KKX/2,KKX/2
              BDXQ=BETADX*NQ
              ARG=BDXQ*SPX
              TSX=CEXP(CMPLX(0.,ARG))
              EPATC=EPATC + T4S(NQ,MM)*TSX*TSZ
      571     CONTINUE
      572     CONTINUE
              EPAT(IP)=CABS(EPATC)
              IF(EPAT(IP).GT.EPMAX) EPMAX=EPAT(IP)
      569     CONTINUE
              DO 570 I=1,181
              EPAT(I)=20.*ALOG10(EPAT(I)/EPMAX)
              IF(EPAT(I).LT.-40.) EPAT(I)=-40.
      570     CONTINUE
              CALL PLTPKG(APATD,EPAT,181,-181,1,0,1)
              CALL PLTPKG(APATD,EPAT,181,-181,1,0,1)
      C
      C************************** FDE ****************************
      C
              CALL COMD(3HFDE)                !READ DESCR. FROM FILE
      333     WRITE(8,334)
      334     FORMAT(2X,'ENTER: FILE NAME',2X,$)
              READ(8,554) FILEIN
              OPEN(UNIT=7,NAME=FILEIN,TYPE='OLD',FORM='UNFORMATTED'
              1  ,ERR=599)
              READ(7) ALPHA,ETA
              READ(7) NNX,NNZ,IIX,IIZ,VETO
              READ(7) FREQ,ISC,SGPCM,DIEL1,DIEL2
              READ(7) DX,DZ,SLWCM,SLTHCM,SLSTCM,SLENCM
              READ(7) DUM
              CLOSE(UNIT=7)
              IOUT=8
              INDO=0
              IF(IFD.NE.0) IOUT=17
      C
      C*************************** CAS ****************************
      C
              CALL COMD(3HCAS,&200)           !SUM OR DIFF. CASE
              WRITE(8,583) CASE
      583     FORMAT(2X,'CASE=',F3.0)
              WRITE(8,584)
      584     FORMAT(2X,'ENTER: CASE #  0=SUM,1=X-DIF,2=Z-DIF',X,$)
              READ(8,*) CASE
      C
      C************************** CSX ****************************
      C
              CALL COMD(3HCSX)                !COSINE ALONG X
              CASE=0.                         !SUM PATTERN CASE
```

```
        FLAMZO=1.
        CALL COS1D(KKX,IIX,NNX,FLAMXO,FLAMX)
C
C************************** COS ****************************
C
        CALL COMD(3HCOS)                  !COSINE ALONG X AND Z
        CASE=0.                           !SUM PATTERN CASE
        CALL COS1D(KKX,IIX,NNX,FLAMXO,FLAMX)
        CALL COS1D(KKZ,IIZ,NNZ,FLAMZO,FLAMZ)
C
C************************** CPL ****************************
C
        CALL COMD(3HCPL)                  !COS-X,PUL-Z
        CASE=0.                           !SUM PATTERN CASE
        CALL COS1D(KKX,IIX,NNX,FLAMXO,FLAMX)
        CALL PUL1D(KKZ,IIZ,NNZ,FLAMZO,FLAMZ)
C
C************************** TR2 ****************************
C
        CALL COMD(3HTR2)                  !TRAPEZOID ALONG X,Z
        CASE=0.                           !SUM PATTERN CASE
        WRITE(8,77)
77      FORMAT(2X,'GZ=',2X,$)
        READ(8,*) GZ
        CALL TRAP1D(KKZ,IIZ,NNZ,GZ,FLAMZO,FLAMZ)
C
C************************** TRX ****************************
C
        CALL COMD(3HTRX,&89)              !TRAPEZOID FOR X ONLY
        CASE=0.                           !SUM PATTERN CASE
        FLAMZO=1.
89      WRITE(8,7)
7       FORMAT(2X,'GX=  ',2X,$)
        READ(8,*) GX
        CALL TRAP1D(KKX,IIX,NNX,GX,FLAMXO,FLAMX)
C
C************************** TRC ****************************
C
        CALL COMD(3HTRC)                  !TRAP-X, COS-Z
        CASE=0.                           !SUM PATTERN CASE
        CALL COS1D(KKZ,IIZ,NNZ,FLAMZO,FLAMZ)
C
C************************** PLD ****************************
C
        CALL COMD(3HPLD,&89)              !PULSE DIFF X-ONLY
        CASE=1.                           !DIFF. PATTERN ALONG X
        FLAMZO=1.
        FLAMXO=0.
        DO 9 N=1,NNX
        TDNPI=2./(N*PI)
```

```
        PINKI=N*PI*KKX/IIX
        FLAMX(N)=TDNPI*(1.-COS(PINKI))
9       CONTINUE
C
C*************************** DIF ****************************
C
        CALL COMD(3HDIF)                 !SMOOTH DIFF DISTRIB.
        CASE=1.                          !DIFF. PATTERN ALONG X
        CALL COS1D(KKZ,IIZ,NNZ,FLAMZ0,FLAMZ)
        CALL SMDIFF(KKX,IIX,NNX,FLAMX0,FLAMX)
C
C*************************** DFX ****************************
C
        CALL COMD(3HDFX)                 !DIFF. ALONG X ONLY
        CASE=1.
        FLAMZ0=1.
        CALL SMDIFF(KKX,IIX,NNX,FLAMX0,FLAMX)
C
C*************************** PLC ****************************
C
        CALL COMD(3HPLC)                 !PULSE-X,COS-Z
        CASE=0.                          !SUM PATTERN CASE
        CALL PUL1D(KKX,IIX,NNX,FLAMX0,FLAMX)
        CALL COS1D(KKZ,IIZ,NNZ,FLAMZ0,FLAMZ)
C
C*************************** PLX ****************************
C
        CALL COMD(3HPLX)                 !PULSE ALONG X ONLY
        CASE=0.                          !SUM PATTERN CASE
        FLAMZ0=1.
        CALL PUL1D(KKX,IIX,NNX,FLAMX0,FLAMX)
C
C*************************** PL2 ****************************
C
        CALL COMD(3HPL2)                 !PULSE ALONG X AND Z
        CASE=0.                          !SUM PATTERN CASE
        CALL PUL1D(KKX,IIX,NNX,FLAMX0,FLAMX)
        CALL PUL1D(KKZ,IIZ,NNZ,FLAMZ0,FLAMZ)
C
C*************************** STC ****************************
C
        CALL COMD(3HSTC)                 !STEP-X, COS-Z
        CASE=0.                          !SUM PATTERN CASE
        CALL COS1D(KKZ,IIZ,NNZ,FLAMZ0,FLAMZ)
        ISTX=1
C
C*************************** STP ****************************
C
        CALL COMD(3HSTP,&537)            !2-D STEP APERTURE
        CASE=0.                          !SUM PATTERN CASE
```

```
537     IF(ISTP.EQ.0) THEN
                ISTP=1
                AA=.3333                !THESE VALUES MAY BE
                BB=.6667                !CHANGED IN COMMAND
                CC=1.000                !CST
                FFX=21
                GGX=11
                FFZ=21
                GGZ=11
        END IF
        CMB=CC-BB
        BMA=BB-AA
        FLAMX0=(CMB*GGX+BMA*FFX+AA*KKX)/FLOAT(IIX)
        DO 54 N=1,NNX
        PINKDI=PI*N*KKX/IIX
        PINGDI=PI*N*GGX/IIX
        PINFDI=PI*N*FFX/IIX
        FLAMX(N)=(2./(N*PI))*(CMB*SIN(PINGDI) +
        1       BMA*SIN(PINFDI) + AA*SIN(PINKDI))
54      CONTINUE
        IF(ISTX.EQ.1) THEN
                ISTX=0
                ISTP=0
                GO TO 600
        END IF
        FLAMZ0=(CMB*GGZ+BMA*FFZ+AA*KKZ)/FLOAT(IIZ)
        DO 55 N=1,NNZ
        PINKDI=PI*N*KKZ/IIZ
        PINGDI=PI*N*GGZ/IIZ
        PINFDI=PI*N*FFZ/IIZ
        FLAMZ(N)=(2./(N*PI))*(CMB*SIN(PINGDI) +
        1       BMA*SIN(PINFDI) + AA*SIN(PINKDI))
55      CONTINUE
C
C************************** CST ****************************
C
        CALL COMD(3HCST)                        !CHANGE STEP
        IF(ISTP.EQ.1) THEN                      !PARAMETERS
                WRITE(8,56) AA,BB,CC,FFX,GGX,FFZ,GGZ
56              FORMAT(2X,'A=',F8.4,3X,'B=',F8.4,3X,'C=',F8.4,
        1       /,2X,'FFX=',I3,3X,'GGX=',I3,/,
        1       2X,'FFZ=',I3,3X,'GGZ=',I3)
                WRITE(8,57)
57              FORMAT(2X,
        1       'ENTER ABOVE NUMBERS IN SAME ORDER ',$)
                READ(8,*) AA,BB,CC,FFX,GGX,FFZ,GGZ
        ELSE
                WRITE(8,58)                     !ISTP=0
58              FORMAT(2X,'*** STP MUST BE EXECUTED ***')
        END IF
```

```
C
C*************************** OUT ****************************
C
        CALL COMD(3HOUT)                 !OUTPUT WRITTEN TO
        IF(INDO.EQ.0) THEN               !OUTFILE
                WRITE(8,60)
60              FORMAT(2X,'ENTER: OUTPUT FILE NAME   ',$)
                READ(8,554) FILEOT
                OPEN(UNIT=6,NAME=FILEOT,TYPE='NEW')
                IOUT=6
                INDO=1
        END IF
        WRITE(IOUT,61)
61      FORMAT(//)
C
C*************************** COF ***************************
C
        CALL COMD(3HCOF,&200)            !CLOSE OUTPUT FILE
        IF(INDO.EQ.1) THEN
                CLOSE(UNIT=6)
                INDO=0
                IOUT=8
        END IF
C
C*************************** DES ***************************
C
        CALL COMD(3HDES)                 !DESCRIPTION OF DATA
        IOUT=8                           !TO TERMINAL
        INDO=0
200     CONTINUE
        WRITE(IOUT,213) FILEIN
213     FORMAT(//,2X,'FILE:',2X,A30)
        WRITE(IOUT,201) ALPHA,ETA
201     FORMAT(2X,'ALPHA=',F6.1,'       ETA=',F6.1)
        WRITE(IOUT,202) NNX,NNZ,IIX,IIZ,VETO,TVETO
202     FORMAT(2X,'NNX=',I4,'  NNZ=',I4,'  IIX=',I4
        1  ,'  IIZ=',I4,'  VETO=',F6.3,'  TVETO=',1PG12.3)
        WRITE(IOUT,203) KKX,KKZ,FREQ
203     FORMAT(2X,'KKX=',I3,'  KKZ=',I3,'    FREQ=',F5.2)
        WRITE(IOUT,204) DX,DZ,SGPCM
204     FORMAT(2X,'DX= ',F7.4,'  DZ= ',F7.4,'   ARRAY TO GP= '
        1       ,F7.4)
        WRITE(IOUT,205) SLWCM,SLTHCM,SLSTCM,SLENCM
205     FORMAT(2X,'ELEMENT WIDTH= ',F8.6,' ELEMENT THICKNESS='
        1 ,F8.6 ,/,2X,'ELEMENT START= ',F7.4
        1       ,'  ELEMENT END= ',F7.4)
        WRITE(IOUT,206) DIEL1,DIEL2
206     FORMAT(2X,'DIEL1= ',F7.4,'   DIEL2= ',F7.4)
        IF(DIPOLE.EQ.1.) THEN
                WRITE(IOUT,211)
```

```
211             FORMAT(2X,'DIPOLES')
        ELSE
                WRITE(IOUT,212)
212             FORMAT(2X,'SLOTS')
        END IF
        IF(GPLI.EQ.1.) WRITE(IOUT,207)
        IF(GPLI.NE.1.) WRITE(IOUT,208)
207     FORMAT(2X,'GROUND PLANE PRESENT')
208     FORMAT(2X,'NO GROUND PLANE')
        IF(INDO.EQ.1) GO TO 38
C
C************************* XPL *****************************
C
        CALL COMD(3HXPL)                  !CALCULATE ALONG X
        IXPL=1                            !INDICATES CALCULATED
        WRITE(8,13)                       !DATA IS ALONG X
13      FORMAT(2X,'ENTER: M   ',2X,$)     !DIRECTION
        READ(8,*) MM
        MMQQ=MM                           !VALUE OUTPUT TO
        IDIFF=0                           !OUTFILE
        IF(CASE.EQ.2.) IDIFF=1            !IDIFF=1 FOR Z DIFF PAT
        CALL DENOM(FLAMZ0,FLAMZ,NNZ,MM,IIZ,DMUM,IDIFF)
        DO 25 NU=1,TNNXP1
        IF(CASE.EQ.2.) IDIFF=1            !IDIFF=1 FOR Z DIFF PAT
        CALL MNSUM(FLAMZ0,FLAMZ,NNZ,MM,IIZ
        1  ,NNX,NU,TNNZP1,FSM(NU),1,IDIFF)
25      CONTINUE
        DO 40 LQ=1,IIX
        LQM=LQ-(IIX/2)
        IF(LQM.LT.-52) GO TO 40
        IF(LQM.GT.52) GO TO 40
        XEL(LQ)=FLOAT(LQM)
        IF(CASE.EQ.1.) IDIFF=1            !IDIFF=1 FOR X DIFF PAT
        CALL MNSUM2(FLAMX0,FLAMX,NNX,LQM,IIX,FSM,TNNXP1,GMQ,
        1                                         IDIFF)
        GMQARR(LQ)=GMQ
        IF(CASE.EQ.1.) IDIFF=1            !IDIFF=1 FOR X DIFF PAT
        CALL DENOM(FLAMX0,FLAMX,NNX,LQM,IIX,DNUQ,IDIFF)
        AMQ(LQ)=DNUQ*DMUM
        IF(AMQ(LQ).EQ.0) THEN
                ZM(LQ)=ZM(LQ-1)
        ELSE
                ZM(LQ)=GMQ/AMQ(LQ)
        END IF
        ZMAG(LQ)=CABS(ZM(LQ))
        GMAG(LQ)=CABS(GMQ)
        GMPH(LQ)= BTAN2(AIMAG(GMQ),REAL(GMQ))*180./PI
        ZMPH(LQ)= BTAN2(AIMAG(ZM(LQ)),REAL(ZM(LQ)))*180./PI
40      CONTINUE
        IMARG=IIX/2
```

```
        YMX=ZMAG(IMARG)
        TYMX=4.*YMX
        WRITE(8,41) YMX
41      FORMAT(2X,'Y CENTER=',1PE12.5)
        IPS=1
        INDAT=1
C
C************************** ZPL ****************************
C
C
        CALL COMD(3HZPL)                !CALCUTE ALONG Z
        IXPL=0                          !INDICATES DATA
        WRITE(8,413)                    !CALCULATED ALONG Z
413     FORMAT(2X,'ENTER: Q  ',2X,$)
        READ(8,*) QQ
        MMQQ=QQ                         !VALUE  TO OUTFILE
        IDIFF=0
        IF(CASE.EQ.1.) IDIFF=1          !IDIFF=1 FOR X DIFF PAT
        CALL DENOM(FLAMX0,FLAMX,NNX,QQ,IIX,DNUQ,IDIFF)
        DO 425 MU=1,TNNZP1
        IF(CASE.EQ.1.) IDIFF=1          !IDIFF=1 FOR X DIFF PAT
        CALL MNSUM(FLAMX0,FLAMX,NNX,QQ,IIX
        1  ,NNZ,MU,TNNXP1,FSM(MU),2,IDIFF)
425     CONTINUE
        DO 440 LM=1,IIZ
        LMQ=LM-(IIZ/2)
        IF(LMQ.LT.-52) GO TO 440
        IF(LMQ.GT.52) GO TO 440
        XEL(LM)=FLOAT(LMQ)
        IF(CASE.EQ.2.) IDIFF=1          !IDIFF=1 FOR Z DIFF PAT
        CALL MNSUM2(FLAMZ0,FLAMZ,NNZ,LMQ,IIZ,FSM,TNNZP1,GMQ,
        1                                                IDIFF)
        GMQARR(LM)=GMQ
        IF(CASE.EQ.2.) IDIFF=1          !IDIFF=1 FOR Z DIFF PAT
        CALL DENOM(FLAMZ0,FLAMZ,NNZ,LMQ,IIZ,DMUM,IDIFF)
        AMQ(LM)=DNUQ*DMUM
        IF(AMQ(LM).EQ.0.) THEN
                ZM(LM)=ZM(LM-1)
        ELSE
                ZM(LM)=GMQ/AMQ(LM)
        END IF
        ZMAG(LM)=CABS(ZM(LM))
        GMAG(LM)=CABS(GMQ)
        GMPH(LM)= BTAN2(AIMAG(GMQ),REAL(GMQ))*180./PI
        ZMPH(LM)= BTAN2(AIMAG(ZM(LM)),REAL(ZM(LM)))*180./PI
440     CONTINUE
        IMARG=IIZ/2
        YMX=ZMAG(IMARG)
        TYMX=4.*YMX
        WRITE(8,441) YMX
```

```
441     FORMAT(2X,'Y CENTER=',1PE12.5)
        IPS=1
        INDAT=1
C
C************************** IND ****************************
C
        CALL COMD(3HIND)                  !CALCULATE INDIVIDUAL
38      WRITE(8,39)                       !ELEMENTS
39      FORMAT(2X,'ENTER: Q START,STOP,M START,STOP',2X,$)
        READ(8,*) LQB,LQE,LMB,LME
        WRITE(IOUT,319)
319     FORMAT(3X,'(X)  (Z)')
        WRITE(IOUT,320)
320     FORMAT(4X,'Q',4X,'M',6X,'YMAG',9X,'YPHASE(DEG)'
        1       ,5X,'VOLTAGE',16X,'CURRENT')
        IPS=2
        IDIFF=0
        DO 350 LQ=LQB,LQE
        IF(CASE.EQ.1.) IDIFF=1            !IDIFF=1 FOR X DIFF PAT
        CALL DENOM(FLAMX0,FLAMX,NNX,LQ,IIX,DNUQ,IDIFF)
        DO 325 MU=1,TNNZP1
        IF(CASE.EQ.1.) IDIFF=1            !IDIFF=1 FOR X DIFF PAT
        CALL MNSUM(FLAMX0,FLAMX,NNX,LQ,IIX
        1  ,NNZ,MU,TNNXP1,FSM(MU),2,IDIFF)
325     CONTINUE
        DO 340 LM=LMB,LME
        IF(CASE.EQ.2.) IDIFF=1            !IDIFF=1 FOR Z DIFF PAT
        CALL MNSUM2(FLAMZ0,FLAMZ,NNZ,LM,IIZ,FSM,TNNZP1,GMQ,
        1                                                   IDIFF)
        IF(CASE.EQ.2.) IDIFF=1            !IDIFF=1 FOR Z DIFF PAT
        CALL DENOM(FLAMZ0,FLAMZ,NNZ,LM,IIZ,DMUM,IDIFF)
        DN=DNUQ*DMUM
        IF(DN.NE.0.) THEN
                ZM1=GMQ/DN
        END IF
        ZRL=REAL(ZM1)
        ZIM=AIMAG(ZM1)
        ZMAG1=CABS(ZM1)
        ZCOMR=ZRL*Z0SQD4
        ZCOMI=ZIM*Z0SQD4
        GM=CABS(GMQ)
        GP=BTAN2(AIMAG(GMQ),REAL(GMQ))*180./PI
        PHASE=BTAN2(ZIM,ZRL)*180./PI
        WRITE(IOUT,331) LQ,LM,ZMAG1,PHASE,DN,GM,GP
331     FORMAT(2X,I3,2X,I3,2X,1PE12.4,4X,0PF8.2
        1       ,6X,1PG12.4,4X,1PE12.4,2X,0PF8.2)
340     CONTINUE
350     CONTINUE
C
C************************** PON ****************************
```

```
C
        CALL COMD(3HPON)                 !OPEN PLOTTER FILE
        IF(IPLO.EQ.0) THEN
              IPLO=1
              CALL PLOTS(0,0,0)
              CALL NEWPEN(NPN)           !SET LINE WIDTH
        END IF
C
C************************** MPL ****************************
C
        CALL COMD(3HMPL)                 !PLOT TO MEGATEK
        IF(IPLO.EQ.0) THEN
              IPLO=1
              CALL VPLOTS(2,5,0)
              MPL=1
        END IF
C
C************************** PLN ****************************
C
        CALL COMD(3HPLN)                 !PLOT NOW
        IF(IPLO.EQ.1) THEN               !PLOTTING INFO. TO
              CALL PLOT(0.,0.,999)       !VERSATEC PLOTTER
              IPLO=0
              CALL PLOTNOW(L)            !PLOT DATA NOW
              OPEN(UNIT=59,NAME='PARM.PLV',TYPE='OLD'
        1         ,DISPOSE='DELETE')
              CLOSE(UNIT=59)
              OPEN(UNIT=59,NAME='VECTR2.PLV',TYPE='OLD'
        1         ,DISPOSE='DELETE')
              CLOSE(UNIT=59)
        END IF
C
C************************** SLW ****************************
C
        CALL COMD(3HSLW)                 !SET PLOTTER LINE
        WRITE(8,360)                     !WIDTH
360     FORMAT(2X,'ENTER: LINE WIDTH (1-5)  ',$)
        READ(8,*) NPN
        CALL NEWPEN(NPN)
C
C************************** GRD ****************************
C
        CALL COMD(3HGRD)                 !PLACE GRID ON PLOTS
        WRITE(8,361)
361     FORMAT(2X,'ENTER: IGRID (1=GRID,0=NOGRID)  ',$)
        READ(8,*) IGRID
C
C************************** SPL ****************************
C
        CALL COMD(3HSPL)                 !SET PHASE PLOT LIMITS
```

```
      WRITE(8,362)
362   FORMAT(2X,'ENTER: PHASE MAX ON PLOT  ',$)
      READ(8,*) YPMAX
C
C************************** PLO ****************************
C
      CALL COMD(3HPLO)                  !PLOT FROM -50 TO 50
      IF(INDAT.EQ.0) THEN
            WRITE(8,363)
363         FORMAT(15X,'*** CALCULATE DATA FIRST ***')
            GO TO 600
      END IF
      IF(IPLO.EQ.0) THEN
            IPLO=1
            CALL PLOTS(0,0,0)
            CALL NEWPEN(NPN)            !SET LINE WIDTH
      END IF
      FAC=.8
      CALL TIME(BTIME)
      CALL NEWPEN(1)                    !NARROW LINE
      CALL SYMBOL(.3,.4,.08,DDATE,0.,9)
      CALL SYMBOL(.3,.2,.08,BTIME,0.,8)
      CALL SYMBOL(5.5,.3,.08,%REF(FILEIN),0.,30)
      CALL NEWPEN(NPN)                  !SET LINE WIDTH
      CALL PLOT(1.75,2.3,-3)
      XLN=4.4
      YLN=3.
      IF(IGRID.EQ.1) CALL GRID(0.,0.,50,XLN/50,
     1                        25,YLN/25,LM1)
      IF(IGRID.EQ.1) CALL GRID(0.,0.,10,XLN/10,
     1                        5,YLN/5,LM2)
500   CONTINUE
      IIXZ=IIZ
      IF(IXPL.EQ.1) IIXZ=IIX
      XSMIN=-100/2.
      XDS=100./XLN
      XSPACE=XLN/10.
      IF(IXPL.EQ.1) THEN
         CALL FFAXIS(0.,0.,6HX AXIS,-6,XLN,0.,XSMIN
     1         ,XDS,XSPACE,-1,FAC,4)
      ELSE
         CALL FFAXIS(0.,0.,6HZ AXIS,-6,XLN,0.,XSMIN
     1         ,XDS,XSPACE,-1,FAC,4)
      END IF
      YSMIN=0.
      YDS=1./YLN
      YSPACE=YLN/5.
      IF(DIPOLE.EQ.1.) THEN
        CALL FFAXIS(0.,0.,17HINPUT CURRENT (A),17
     1  ,YLN,90.,YSMIN,YDS,YSPACE,1,FAC,4)
```

```
          ELSE
            CALL FFAXIS(0.,0.,17HINPUT VOLTAGE (V),17
          1  ,YLN,90.,YSMIN,YDS,YSPACE,1,FAC,4)
          END IF
          YDS5=(1./YLN)*PAMX
          IM1D2=((IIXZ-100)/2)-1
          DO 480 I=1,101
          AMQS(I)=AMQ(I+IM1D2)
          GMAGS(I)=GMAG(I+IM1D2)*FACN
          ZMAGS(I)=ZMAG(I+IM1D2)*FACN
          XEL(I)=I-51
          IF(AMQS(I).GT.1.2) AMQS(I)=1.2
          IF(GMAGS(I).GT.PAMX) GMAGS(I)=PAMX
          IF(ZMAGS(I).GT.PAMX) ZMAGS(I)=PAMX
480       CONTINUE
          CALL STRYP(XEL,XSMIN,XDS,AMQS,YSMIN,YDS,101,1.,-4)
          CALL STRYP(XEL,XSMIN,XDS,GMAGS,YSMIN,YDS5,101,1.,-2)
          CALL STRYP(XEL,XSMIN,XDS,ZMAGS,YSMIN,YDS5,101,1.,-1)
          IF(DIPOLE.EQ.1.) THEN
            CALL FFAXIS(XLN,0.,13HIMPED. (OHMS),-13,YLN
          1       ,90.,YSMIN,YDS5,YSPACE,101,FAC,4)
          ELSE
            CALL FFAXIS(XLN,0.,13HY (MILLIMHOS),-13,YLN
          1       ,90.,YSMIN,YDS5,YSPACE,1,FAC,4)
          END IF
          CALL PLOT(-.5,0.,-3)
C
C**************************** PEX *****************************
C
          CALL COMD(3HPEX,&516)            !PLOT DATA TO FILE
          IF(INDAT.EQ.0) THEN
                WRITE(8,363)
                GO TO 600
          END IF
          IF(IPLO.EQ.0) THEN
                IPLO=1
                CALL PLOTS(0,0,0)
                CALL NEWPEN(NPN)           !SET LINE WIDTH
          END IF
          CALL TIME(BTIME)
          CALL NEWPEN(1)                   !NARROW LINE WIDTH
          CALL SYMBOL(.3,.4,.08,BDATE,0.,9)
          CALL SYMBOL(.3,.2,.08,BTIME,0.,8)
          CALL SYMBOL(1.1,.3,.08,%REF(FILEIN),0.,30)
          CALL NEWPEN(NPN)                 !SET LINE WIDTH
510       CONTINUE
          CALL PLOT(1.75,5.,-3)
          FAC=.8
          YPLN=2.
          YPMIN=-YPMAX
```

```
      YPDS=2.*YPMAX/YPLN
      YPSP=YPLN/2.
      XELN=4.4
      XEMIN=-20.
      XEDS=40./XELN
      XESP=10.*XELN/40.
      YELN=2.5
      IF(IGRID.EQ.1)CALL GRID(0.,0.,20,.22,25,YELN/25,LM1)
      IF(IGRID.EQ.1)CALL GRID(0.,0.,4,1.1,5,YELN/5,LM2)
      IF(IXPL.EQ.1) THEN
              CALL FFAXIS(0.,0.,6HX AXIS,-6,XELN,0.,XEMIN
      1       ,XEDS,XESP,-1,FAC,4)
      ELSE
              CALL FFAXIS(0.,0.,6HZ AXIS,-6,XELN,0.,XEMIN
      1       ,XEDS,XESP,-1,FAC,4)
      END IF
      YEMIN=0.
      YEDS=(1./YELN)
      YESP=(YELN/5.)
      IF(DIPOLE.EQ.1.) THEN
      CALL FFAXIS(0.,0.,17HINPUT CURRENT (A),17
      1       ,YELN,90.,YEMIN,YEDS,YESP,1,FAC,4)
      ELSE
      CALL FFAXIS(0.,0.,17HINPUT VOLTAGE (V),17
      1       ,YELN,90.,YEMIN,YEDS,YESP,1,FAC,4)
      END IF
      YEDS5=(1./YELN)*PAMX
      IIXZ=IIZ
      IF(IXPL.EQ.1) IIXZ=IIX
      ID2M20=(IIXZ/2)-20
      ID2P20=(IIXZ/2)+20
      INC=0
      DO 515 I=ID2M20,ID2P20
      INC=INC+1
      AMQS(INC)=AMQ(I)
      GMAGS(INC)=GMAG(I)*FACN
      ZMAGS(INC)=ZMAG(I)*FACN
      XELS(INC)=INC-21
      GPHS(INC)=GMPH(I)
      ZPHS(INC)=ZMPH(I)
      IF(AMQS(INC).GT.1.20) AMQS(INC)=1.20
      IF(GMAGS(INC).GT.PAMX) GMAGS(INC)=PAMX
      IF(ZMAGS(INC).GT.PAMX) ZMAGS(INC)=PAMX
      IF(GPHS(INC).LT.YPMIN) GPHS(INC)=YPMIN
      IF(GPHS(INC).GT.YPMAX) GPHS(INC)=YPMAX
      IF(ZPHS(INC).LT.YPMIN) ZPHS(INC)=YPMIN
      IF(ZPHS(INC).GT.YPMAX) ZPHS(INC)=YPMAX
515   CONTINUE
      CALL STRYP(XELS,XEMIN,XEDS,AMQS,YEMIN,YEDS,41,1.,-4)
      CALL STRYP(XELS,XEMIN,XEDS,GMAGS,YEMIN,YEDS5,41,1.,-2)
```

```
      CALL STRYP(XELS,XEMIN,XEDS,ZMAGS,YEMIN,YEDS5,41,1.,-1)
      IF(DIPOLE.EQ.1.) THEN
        CALL FFAXIS(XELN,0.,13HIMPED. (OHMS),-13,YELN
     1                ,90.,YEMIN,YEDS5,YESP,101,FAC,4)
      ELSE
        CALL FFAXIS(XELN,0.,13HY (MILLIMHOS),-13,YELN
     1                ,90.,YEMIN,YEDS5,YESP,1,FAC,4)
      END IF
      CALL PLOT(0.,-2.7,-3)
      IF(IGRID.EQ.1)CALL GRID(0.,0.,20,.22,12,YPLN/12,LM1)
      IF(IGRID.EQ.1)CALL GRID(0.,0.,4,1.1,6,YPLN/6,LM2)
      IF(IXPL.EQ.1) THEN
              CALL FFAXIS(0.,0.,6HX AXIS,-6,XELN,0.,XEMIN
     1        ,XEDS,XESP,-1,FAC,4)
      ELSE
              CALL FFAXIS(0.,0.,6HZ AXIS,-6,XELN,0.,XEMIN
     1        ,XEDS,XESP,-1,FAC,4)
      END IF
      CALL FFAXIS(0.,0.,11HPHASE (DEG),11,YPLN,90.,
     1        YPMIN,YPDS,YPSP,1,FAC,2)
      CALL STRYP(XELS,XEMIN,XEDS,ZPHS,YPMIN,YPDS,41
     1                                  ,1.,-1)
      CALL PLOT(-.5,0.,-3)
516   CONTINUE
      CALL SYMBOL(.2,-.8,.08,
     1   32HIX    IZ    KX    KZ    NX    NZ,0.,32)
      CALL SYMBOL(.2,-1.45,.08,4HFREQ,0.,4)
      FPN=IIX
      CALL NUMBER(.1,-.95,.08,FPN,0.,-1)
      FPN=IIZ
      CALL NUMBER(.65,-.95,.08,FPN,0.,-1)
      FPN=KKX
      CALL NUMBER(1.2,-.95,.08,FPN,0.,-1)
      FPN=KKZ
      CALL NUMBER(1.68,-.95,.08,FPN,0.,-1)
      FPN=NNX
      CALL NUMBER(2.1,-.95,.08,FPN,0.,-1)
      FPN=NNZ
      CALL NUMBER(2.67,-.95,.08,FPN,0.,-1)
      IF(IXPL.EQ.1) FPN=MM
      IF(IXPL.NE.1) FPN=QQ
      CALL NUMBER(.21,-1.6,.08,FREQ,0.,1)
      CALL SYMBOL(.2,-1.15,.08,
     1        23HALPHA     ETA         DX,0.,23)
      CALL SYMBOL(2.5,-1.15,.08,2HDZ,0.,2)
      CALL NUMBER(.3,-1.3,.08,ALPHA,0.,-1)
      CALL NUMBER(.9,-1.3,.08,ETA,0.,2)
      CALL NUMBER(1.75,-1.3,.08,DX,0.,3)
      CALL NUMBER(2.4,-1.3,.08,DZ,0.,3)
      CALL SYMBOL(1.,-1.45,.08,2HGP,0.,2)
```

```
      IF(GPLI.EQ.1.) CALL SYMBOL(1.,-1.6,.08,3HYES,0.,3)
      IF(GPLI.NE.1.) CALL SYMBOL(1.,-1.6,.08,3HNO ,0.,3)
      IF(DIPOLE.EQ.1.) THEN
            CALL SYMBOL(3.75,-.6,.08,7HDIPOLES,0.,7)
      ELSE
            CALL SYMBOL(3.75,-.6,.08,5HSLOTS,0.,5)
      END IF
      CALL SYMBOL(1.6,-1.45,.08,7HEPSILON,0.,7)
      CALL NUMBER(1.8,-1.6,.08,DIEL2,0.,1)
      CALL SYMBOL(2.5,-1.45,.08,2HD2,0.,2)
      CALL NUMBER(2.4,-1.6,.08,SGPCM,0.,3)
      CALL PLOT(3.35,-.8,-3)
      IF(DIPOLE.EQ.1.) THEN
            CALL SYMBOL(1.2,0.,.08,7HCURRENT,0.,7)
            CALL SYMBOL(1.2,-.25,.08,7HVOLTAGE,0.,7)
            CALL SYMBOL(1.2,-.5,.08,7HIMPED. ,0.,7)
      ELSE
            CALL SYMBOL(1.2,0.,.08,7HVOLTAGE,0.,7)
            CALL SYMBOL(1.2,-.25,.08,7HCURRENT,0.,7)
            CALL SYMBOL(1.2,-.5,.08,7HADMITT.,0.,7)
      END IF
      CALL STRYP(XT,0.,1.,YT,0.,1.,2,1.,-4)
      CALL PLOT(0.,-.25,-3)
      CALL STRYP(XT,0.,1.,YT,0.,1.,2,1.,-2)
      CALL PLOT(0.,-.25,-3)
      CALL STRYP(XT,0.,1.,YT,0.,1.,2,1.,-1)
      IF(MPL.EQ.0) CALL PLOT(0.,0.,-999)
C
C************************** STO ****************************
C
      CALL COMD(3HSTO)                  !STORE PLOTS FOR
      IF(INDAT.EQ.0) THEN               !COMPARISON DISPLAY
            WRITE(8,363)
            GO TO 600
      END IF
      WRITE(8,520)
520   FORMAT(2X,'ENTER: PLOT # (1-4)  ',$)
      READ(8,*) IPL
      IF(IPL.GT.4) GO TO 600
      IF(IXPL.EQ.1) THEN
            IIXZ=IIX
      ELSE
            IIXZ=IIZ
      END IF
      ID2M20=(IIXZ/2)-20
      ID2P20=(IIXZ/2)+20
      INC=0
      DO 523 I=ID2M20,ID2P20
      INC=INC+1
      AMD(INC,IPL)=AMQ(I)
```

```
      GMD(INC,IPL)=GMAG(I)*FACN
      ZMD(INC,IPL)=ZMAG(I)*FACN
      XELS(INC)=INC-21
      IF(AMD(INC,IPL).GT.1.2) AMD(INC,IPL)=1.2
      IF(GMD(INC,IPL).GT.PAMX) GMD(INC,IPL)=PAMX
      IF(ZMD(INC,IPL).GT.PAMX) ZMD(INC,IPL)=PAMX
523   CONTINUE
      ALD(IPL)=ALPHA
      ETD(IPL)=ETA
C
C************************** PL4 ****************************
C
      CALL COMD(3HPL4)                  !4 PLOTS ON 1 PAGE
      IF(INDAT.EQ.0) THEN               !COMPARISON DISPLAY
            WRITE(8,363)
            GO TO 600
      END IF
      IF(IPLO.EQ.0) THEN
            IPLO=1
            CALL PLOTS(0,0,0)
            CALL NEWPEN(NPN)
      END IF
      XELN=4.
      XEMIN=-20.
      XEDS=40./XELN
      XESP=10.*XELN/40.
      YELN=1.3
      YEMIN=0.
      YEDS=(1./YELN)
      YESP=(YELN/2.)
      YEDS5=(1./YELN)*PAMX
      FAC=.75
      CALL PLOT(1.75,6.2,-3)
      DO 330 IPL=1,4
      CALL FFAXIS(0.,0.,1H ,-1,XELN,0.,XEMIN,XEDS,XESP
      1   ,-1,FAC,4)
      IF(DIPOLE.EQ.1.) THEN
      CALL FFAXIS(0.,0.,11HCURRENT (A),11,YELN,90.,
      1       YEMIN,YEDS,YESP,1,FAC,1)
      ELSE
      CALL FFAXIS(0.,0.,11HVOLTAGE (V),11,YELN,90.,
      1       YEMIN,YEDS,YESP,1,FAC,1)
      END IF
      DO 329 I=1,41
      AMQS(I)=AMD(I,IPL)
      GMAGS(I)=GMD(I,IPL)
      ZMAGS(I)=ZMD(I,IPL)
329   CONTINUE
      CALL STRYP(XELS,XEMIN,XEDS,AMQS,YEMIN,YEDS,41,1.,-4)
      CALL STRYP(XELS,XEMIN,XEDS,GMAGS,YEMIN,YEDS5,41,1.,-2)
```

```
          CALL STRYP(XELS,XEMIN,XEDS,ZMAGS,YEMIN,YEDS5,41,1.,-1)
          IF(DIPOLE.EQ.1.) THEN
             CALL FFAXIS(XELN,0.,6H(OHMS),-6,YELN,90.,YEMIN
          1                 ,YEDS5,YESP,101,FAC,1)
          ELSE
            CALL FFAXIS(XELN,0.,11H(MILLIMHOS),-11,YELN,90.,YEMIN
          1             ,YEDS5,YESP,1,FAC,1)
          END IF
          IF(IGRID.EQ.1)CALL GRID(0.,0.,20,XELN/20.,20,YELN/20.
          1                             ,LM1)
          IF(IGRID.EQ.1)CALL GRID(0.,0.,4,XELN/4.,4,YELN/4.,LM2)
          CALL SYMBOL(2.2,1.35,.08,6HALPHA=,0.,6)
          CALL NUMBER(2.8,1.35,.08,ALD(IPL),0.,-1)
          CALL SYMBOL(3.2,1.35,.08,4HETA=,0.,4)
          CALL NUMBER(3.6,1.35,.08,ETD(IPL),0.,2)
          CALL PLOT(0.,-1.8,-3)
330       CONTINUE
          CALL PLOT(0.,1.2,-3)
          IF(DIPOLE.EQ.1.) THEN
                  CALL SYMBOL(.2,0.,.08,7HCURRENT,0.,7)
                  CALL SYMBOL(1.8,0.,.08,7HVOLTAGE,0.,7)
                  CALL SYMBOL(3.3,0.,.08,7HIMPED. ,0.,7)
          ELSE
                  CALL SYMBOL(.2,0.,.08,7HVOLTAGE,0.,7)
                  CALL SYMBOL(1.8,0.,.08,7HCURRENT,0.,7)
                  CALL SYMBOL(3.3,0.,.08,7HADMITT.,0.,7)
          END IF
          CALL PLOT(0.,.25,-3)
          CALL STRYP(XT,0.,1.,YT,0.,1.,2,1.,-4)
          CALL PLOT(1.6,0.,-3)
          CALL STRYP(XT,0.,1.,YT,0.,1.,2,1.,-2)
          CALL PLOT(1.4,0.,-3)
          CALL STRYP(XT,0.,1.,YT,0.,1.,2,1.,-1)
          IF(MPL.EQ.0) CALL PLOT(0.,0.,-999)
C
C************************** AMX ****************************
C
          CALL COMD(3HAMX)                !SET AXIS MAXIMUM
          WRITE(8,517)
517       FORMAT(2X,'ENTER: AXIS MAX ON PEX   ',$)
          READ(8,*) PAMX
C
C************************** NMP ****************************
C
          CALL COMD(3HNMP)                !NEW MEGATEK PLOT
          IF(MPL.EQ.1) CALL PLOT(0.,0.,-999)
C
C************************** POF ****************************
C
          CALL COMD(3HPOF)                !CLOSE PLOT FILE
```

```
      IF(IPLO.EQ.1) THEN
            IPLO=0
            CALL PLOT(0.,0.,999)
            MPL=0
      END IF
C
C************************** EXI ****************************
C
      CALL COMD(3HEXI)                !EXIT FROM PROGRAM
      IF(IPLO.EQ.1) CALL PLOT(0.,0.,999)
      CALL EXIT
      END
C
C$$$$$$$$$$$$$$$$$$$$$$$$$$$$$$$$$$$$$$$$$$$$$$$$$$$$$$$$$$$$$$$$$$
C
      SUBROUTINE DENOM(TO,TARR,NN,MQ,II,DOUT,IDIFF)
      DIMENSION TARR(1)
      DATA PI/3.1415926535/
      DOUT=1.
      IF(NN.EQ.0) IDIFF=0
      IF(NN.EQ.0) RETURN
      ISM=1
      IF(IDIFF.EQ.1) ISM=0
      DOUT=TO*ISM                                   !DC TERM ZERO
      DO 1 L=1,NN                                   !DIFF. PATTERN
      TPML=2.*PI*MQ*L/II
      DOUT=DOUT+TARR(L)*(ISM*COS(TPML)        !COS FOR SUM PAT
      1                +IDIFF*SIN(TPML))      !SIN FOR DIFF PAT
1     CONTINUE
      IDIFF=0
      RETURN
      END
C
C$$$$$$$$$$$$$$$$$$$$$$$$$$$$$$$$$$$$$$$$$$$$$$$$$$$$$$$$$$$$$$$$$$
C
      SUBROUTINE MNSUM(TO,TARR,NN1,MQ,II1
      1  ,NN2,MUNU,ITNN1,FSM,ISW,IDIFF)
C  ISW IS A SWITCH WHICH DETERMINES IF THE ARRAY CF
C  IS USED ROW-WISE OR COLUMNWISE.  TO PLOT AS
C  A FUNCTION OF X, ROWS ARE USED, FOR Z COLUMNS
C  ARE USED.
      INCLUDE 'CMPLOT.CMN'
      COMPLEX FSM,CO,CARG,C1,CJ,ALAM,CSC
      DIMENSION TARR(1)
      DATA PI,CO/3.1415926535,(0.,0.)/
      DATA C1,CJ/(1.,0.),(0.,1.)/
      IF(IDIFF.EQ.1) THEN
            IDSN=-1
            ISM=0
            CSC=CJ
```

```
                IDIFF=0
        ELSE
                IDSN=1
                ISM=1
                CSC=C1
        END IF
        LMN=0
        FSM=C0
        DO 1 MN=-NN1,NN1
        LMN=LMN+1
        MMN=-MN
        ALAM=CMPLX(T0*ISM,0.)
        IF(MN.LT.0) ALAM=CSC*IDSN*TARR(MMN)*.5
        IF(MN.GT.0) ALAM=CSC*TARR(MN)*.5
        TPM=2.*PI*MQ*MN/II1
        CARG=CMPLX(0.,-TPM)
        IF(ISW.EQ.1) THEN
                FSM=FSM + ALAM*CEXP(CARG)*CF(MUNU,LMN)
        ELSE
                FSM=FSM + ALAM*CEXP(CARG)*CF(LMN,MUNU)
        END IF
1       CONTINUE
        RETURN
        END
C
C$$$$$$$$$$$$$$$$$$$$$$$$$$$$$$$$$$$$$$$$$$$$$$$$$$$$$$$$$$$$$$$$$
C
        SUBROUTINE MNSUM2(T0,TARR,NN1,MQ,II1,FSM,ITNN1
        1                                        ,GNQ,IDIFF)
        COMPLEX GNQ,C0,FSM(1),CARG,C1,CJ,ALAM,CSC
        DIMENSION TARR(1)
        DATA PI,C0/3.1415926535,(0.,0.)/
        DATA C1,CJ/(1.,0.),(0.,1.)/
        IF(IDIFF.EQ.1) THEN
                IDSN=-1
                ISM=0
                CSC=CJ
                IDIFF=0
        ELSE
                IDSN=1
                ISM=1
                CSC=C1
        END IF
        GNQ=C0
        LMN=0
        DO 1 MN=-NN1,NN1
        LMN=LMN+1
        MMN=-MN
        ALAM=CMPLX(T0*ISM,0.)
        IF(MN.LT.0) ALAM=CSC*IDSN*TARR(MMN)*.5
```

```
      IF(MN.GT.0) ALAM=CSC*TARR(MN)*.5
      TPM=2.*PI*MQ*MN/II1
      CARG=CMPLX(0.,-TPM)
      GMQ=GMQ + ALAM*CEXP(CARG)*FSM(LMN)
1     CONTINUE
      RETURN
      END
C
C$$$$$$$$$$$$$$$$$$$$$$$$$$$$$$$$$$$$$$$$$$$$$$$$$$$$$$$$$$$$$$$$$$$$$$$
C
      FUNCTION BTAN2(Y,X)
C  THIS ROUTINE IS USED TO COMPUTE THE ARCTANGENT. IT IS
C  SIMILAR TO ATAN2 EXCEPT IT AVOIDS THE RUN TIME ERRORS.
      DATA PI,TPI,DPR/3.14159265,6.2831853,57.29577958/
      IF(ABS(X).GT.1.E-10) GO TO 50
      IF(ABS(Y).GT.1.E-10) GO TO 10
      BTAN2=0.
      RETURN
10    BTAN2=PI/2.
      IF(Y.LT.0.) BTAN2=-BTAN2
      RETURN
50    BTAN2=ATAN2(Y,X)
      RETURN
      END
C
C$$$$$$$$$$$$$$$$$$$$$$$$$$$$$$$$$$$$$$$$$$$$$$$$$$$$$$$$$$$$$$$$$$$$$$$
C
C  THIS SUBROUTINE CALCULATES THE FOURIER COEFFICIENTS
C  FOR ONE DIMENSION OF THE EVEN PULSE FUNCTION
C  CENTERED AT ZERO.
      SUBROUTINE PUL1D(KK,II,NN,FLAM0,FLAM)
      DIMENSION FLAM(1)
      DATA PI/3.1415926535/
      FLAM0=FLOAT(KK)/II
      DO 1 N=1,NN
      PINKDI=PI*N*KK/II
      FLAM(N)=(2./(N*PI))*SIN(PINKDI)
1     CONTINUE
      RETURN
      END
C
C$$$$$$$$$$$$$$$$$$$$$$$$$$$$$$$$$$$$$$$$$$$$$$$$$$$$$$$$$$$$$$$$$$$$$$$
C
C  THIS SUBROUTINE CALCULATES THE FOURIER COEFFICIENTS
C  FOR ONE DIMENSION OF THE EVEN COSINE FUNCTION
C  CENTERED AT ZERO.
      SUBROUTINE COS1D(KK,II,NN,FLAM0,FLAM)
      DIMENSION FLAM(1)
      DATA PI/3.1415926535/
      PID2=PI/2.
```

```
      TKD=2.*KK/(II*PI)
      FLAMO=TKD
      DO 1 N=1,NN
      FIM=(II - 2.*N*KK)/II
      FIP=(II + 2.*N*KK)/II
      FLAM(N)=TKD*(SIN(PID2*FIM)/FIM + SIN(PID2*FIP)/FIP)
1     CONTINUE
      RETURN
      END
C
C$$$$$$$$$$$$$$$$$$$$$$$$$$$$$$$$$$$$$$$$$$$$$$$$$$$$$$$$$$$$$$$$$$$$$$
C
C  THIS SUBROUTINE CALCULATES THE FOURIER COEFFICIENTS
C  FOR ONE DIMENSION OF THE EVEN TRAPEZOID FUNCTION
C  CENTERED AT ZERO.
      SUBROUTINE TRAP1D(KK,II,NN,G,FLAMO,FLAM)
      DIMENSION FLAM(1)
      DATA PI/3.1415926535/
      FLAMO=(2.*FLOAT(KK) + G)/(2.*FLOAT(II))
      GPK=G + KK
      DO 1 N=1,NN
      GNPI=G*N*PI
      PIN=PI*N
      FLAM(N)=(-2.*II/(GNPI*PIN))
      1       *(COS(PIN*GPK/II) - COS(PIN*KK/II))
1     CONTINUE
      RETURN
      END
C
C$$$$$$$$$$$$$$$$$$$$$$$$$$$$$$$$$$$$$$$$$$$$$$$$$$$$$$$$$$$$$$$$$$$$$$
C
C  THIS SUBROUTINE CALCULATES THE FOURIER COEFFICIENTS
C  FOR ONE DIMENSION OF THE ODD SMOOTH DIFFERENCE
C  DISTRIBUTION CENTERED AT ZERO.  THE VALUE OF THE DISTIB.
C  AT DISTANCE X FROM THE ORIGIN IS 2*X*COS(PI*X/KK).
      SUBROUTINE SMDIFF(KK,II,NN,FLAMO,FLAM)
      DIMENSION FLAM(NN)
      DATA PI/3.1415926535/
      FLAMO=0.
      F8DI=8./FLOAT(II)
      XX=FLOAT(KK)/2.
      DO 1 N=1,NN
      BPA=PI*(2.*N*KK + II)/FLOAT(II*KK)
      BMA=PI*(2.*N*KK - II)/FLOAT(II*KK)
      T1=-(XX/2.)*(COS(BMA*XX)/BMA + COS(BPA*XX)/BPA)
      T2=(1./(2.*BMA*BMA))*SIN(BMA*XX)
      T3=(1./(2.*BPA*BPA))*SIN(BPA*XX)
      FLAM(N)=0.1*F8DI*(T1 + T2 + T3)
1     CONTINUE
      RETURN
      END
```

REFERENCES

1. L. Stark, "Microwave Theory of Phased-Array Antennas - A Review," Proc. IEEE, Vol. 62, NO. 12, pp. 1161-1701, December 1974.

2. T. C. Cheston, "Phased Arrays for Radars," IEEE Spectrum, Vol. 5, No. 11, pp. 102-111, November 1968.

3. L. Stark, op. cit., pp. 1661-1662.

4. Carl A. Mentzer, "Transmission Properties of Tuned Resonant Windows," Report 2382-8, 14 January 1969, The Ohio State University ElectroScience Laboratory, Department of Electrical Engineering; prepared under Contract F33615-67-C-1507 for Air Force Avionics Laboratory, Wright-Patterson Air Force Base, Ohio. (AFAL-TR-68-306) (AD 394981)

5. Carl A. Mentzer, and B. A. Munk, "Resonant Metallic Radome," Report 2382-21, 21 June 1970, The Ohio State University ElectroScience Laboratory, Department of Electrical Engineering; prepared under Contract F33615-67-C-1507 for Air Force Avionics Laboratory, Wright-Patterson Air Force Base, Ohio. (AFAL-TR-70-86) (AD 509525)

6. E. L. Pelton, "A Streamlined Metallic Radome with High Transmission Performance," Report 2989-11, March 1973, The Ohio State University ElectroScience Laboratory, Department of Electrical Engineering; prepared under Contract F 33(615)-70-1439 for Air Force Avionics Laboratory, Wright-Patterson Air Force Base, Ohio. (AFAL-TR-73-100) (AD 909 360L)

7. C. J. Larson, "Modified Center Layer Metallic Biplanar Radome Design," Report 784346-2, March 1978, The Ohio State University ElectroScience Laboratory, Department of Electrical Engineering; prepared under Contract F33615-76-C-1024 for Aeronautical Systems Division, Wright-Patterson Air Force Base, Ohio. (AFAL-TR-78-28)(AD/B043 262L)

8. T. W. Kornbau, and B.A. Munk, "Design of a Metallized Radome for the C-140 Aircraft," Report 784346-4, May 1979, The Ohio State University ElectroScience Laboratory, Department of Electrical Engineering; prepared under Contract F33615-76-C-1024 for Aeronautical Systems Division, Wright-Patterson Air Force Base, Ohio. (AFAL-TR-79-1103)(AD/B043 935L)

9. C. J. Larson, "Effects of Transmission Lines and Antennas Incorporated with Metallic Radomes," Report 784346-8, May 1978, The Ohio State University ElectroScience Laboratory, Department of Electrical Engineering; prepared under Contract F33615-76-C-1024 for Aeronautical Systems Division, Wright-Patterson Air Force Base, Ohio. (AFAL-TR-78-100) (AD/B043 752L)

10. B.A. Munk and J.F. Stosic, "Radome Panels of Slotted Arrays Located in a Stratified Dielectric Medium" Report 784346-10, June 1979, The Ohio State University ElectroScience Laboratory, Department of Electrical Engineering; prepared under Contract F33615-76-C-1024 for Aeronautical Systems Division, Wright-Patterson Air Force Base, Ohio. (AFAL-TR-79-1158) (AD/B044 224L)

11. J.S. Ernst "Broadband Metallic Radome," Report 784346-11, September 1979, The Ohio State University ElectroScience Laboratory, Department of Electrical Engineering; prepared under Contract F33615-76-C-1024 for Aeronautical Systems Division, Wright-Patterson Air Force Base, Ohio. (AFAL-TR-79-1142) (AD/A084 663)

12. J.F. Stosic, "Multilayer Metallic Radome Panel Design with Modified Center Layers," M.Sc. Thesis, The Ohio State University, Columbus, March 1980.

13. B. A. Munk and E. L. Pelton, "A Streamlined Metallic Radome," IEEE Transactions on Antennas and Propagation, Vol. AP-22, No. 6, pp. 799-803, November 1974.

14. B.A. Munk, G.A. Burrell and T.W. Kornbau, "A General Theory of Periodic Surfaces in Stratified Dielectric Media," Report 784346-1, Nobember 1977, The Ohio State University ElectroScience Laboratory; Department of Electrical Engineering; prepared under Contract F33615-76-C-1024 for Aeronautical Systems Division, Wright-Patterson Air Force Base, Ohio. (AFAL-TR-77-219) (AD/B030 544L)

15. T.W. Kornbau, "Application of the Plane Wave Expansion Method to Periodic Arrays Having a Skewed Grid Geometry," Report 784346-3, June 1977, The Ohio State University ElectroScience Laboratory, Department of Electrical Engineering; prepared under Contract F33615-76-C-1024 for Aeronautical Systems Division, Wright-Patterson Air Force Base, Ohio. (AFAL-TR-77-112) (AD/A047 311)

16. B.A. Munk, T.W. Kornbau, and R.D. Fulton, "Scan Independent Phased Arrays," Radio Science, Vol. 14, No. 6, pp. 979-990, November 1979.

17. N. Amitay, V. Galindo, and C.P. Wu, Theory and Analysis of Phased Arrays, John Wiley and Sons, New York, 1972.

18. B.A. Munk and T.W. Kornbau, "Mono-planar Arrays of Generalized Three-Legged Elements in a Stratified Dielectric Medium," Report 784346-6, May 1978, The Ohio State University ElectroScience Laboratory, Department of Electrical Engineering; prepared under Contract F33615-76-C-1024 for Aeronautical Systems Division, Wright-Patterson Air Force Base, Ohio. (AFAL-TR-78-43) (AD/B030 753L)

19. B.A. Munk and J.S. Ernst, "A Dipole-Reflector Phased Array Imbedded in Dielectric Slabs," Report 784346-9, October 1979, The Ohio State University ElectroScience Laboratory, Department of Electrical Engineering; prepared under Contract F33615-76-C-1024 for Aeronautical Systems Division, Wright-Patterson Air Force Base, Ohio. (AFAL-TR-79-1157) (AD/C021 655)

20. B.A. Munk and G.A. Burrell, "Plane-Wave Expansion for Arrays of Arbitrarily Oriented Piecewise Linear Elements and Its Application in Determining the Impedance of a Single Linear Antenna in a Lossy Half-Space," IEEE Transactions on Antennas and Propagation, May 1979, Vol. AP-27, No. 3.

21. E.L. Pelton and B.A. Munk, "Scattering from Periodic Arrays of Crossed Dipoles," IEEE Transactions on Antennas and Propagation, May 1979, Vol. AP-27, No. 3

22. R.J. Luebbers and B.A. Munk, "Mode Matching Analysis of Biplanar Slot Arrays," IEEE Transactions on Antennas and Propagation, May 1979, Vol. AP-27, No. 3.

23. C.J. Larson, "The Broadband Frequency Response of Periodic Surfaces," Ph.D. Dissertation, The Ohio State University, Columbus, Ohio, March 1980.

24. A.J. Fenn, G.A. Thiele and B.A. Munk, "Moment Method Calculation of Reflection Coefficient for Waveguide Elements in a Finite Planar Phased Antenna Array," Report 784372-7, September 1978, The Ohio State University ElectroScience Laboratory, Department of Electrical Engineering; prepared under Contract N00014-76-C-0573 for Office of Naval Research. (AD/A060 071)

25. M.A. Hidayet, J.A.M. Lyon, and C.B. Loftis, "VHF-UHF Phased Array Techniques, Part II: Mutual Effects in Finite Arrays of Slots," Tech. Rep. AFAL-TR-73-399, Part II, The University of Michigan Radiation Laboratory, Ann Arbor (1973).

26. J. Luzwick and R.F. Harrington, "Mutual Coupling in a Finite Planar Rectangular Waveguide Antenna Array," Tech. Rept. No. 7, Contract No. N00014-76-C-0225, Office of Naval Research, June 1978.

27. B.A. Munk, T.W. Kornbau, and R.D. Fulton, op. cit.

28. B.A. Munk, G.A. Burrell, and T.W. Kornbau, op. cit.

29. ibid.

30. B.A. Munk, G.A. Burrell, and T.W. Kornbua, op. cit., pp. 40-41.

31. R.F. Harrington, Time-Harmonic Electromagnetic Fields, New York, N.Y., McGraw-Hill Book Company, 1961, p. 77.

32. R.F. Harrington, op. cit., pp. 81-82.

33. S.A. Schelkunoff and H.T. Friis, Antennas Theory and Practice, J. Wiley and Sons, 1952, p. 298, Equation (100) and p. 366, Equation (26).

34. B.A. Munk, G.A. Burrell, and T.W. Kornbau, op. cit., pp. 61-71.

35. B.A. Munk, G.A. Burrell, and T.W. Kornbau, op. cit., pp. 53-57.

36. E.C. Jordan and K.G. Balmain, Electromagnetic Waves and Radiating Systems, Englewood Cliffs, New Jersey, Prentice-Hall, Inc., 1968, pp. 517-519.

37. B.A. Munk, G.A. Burrell, and T.W. Kornbau, op. cit., pp. 61-71.

38. B.A. Munk, "Resonant Frequency of Periodic Surfaces for Oblique Incidence," Report 2148-5, November 1966, The Ohio State University ElectroScience Laboratory, Department of Electrical Engineering; prepared under Contract AF 33(615)-361 for Air Force Avionics Laboratory, Wright-Patterson Air Force Base, Ohio. (AD806 089)

39. J.H. Richmond, "Radiation and Scattering by Thin-Wire Structures in the Complex Frequency Domain," Report 2902-10, July 1973, The Ohio State University ElectroScience Laboratory, Department of Electrical Engineering; prepared under Grant No. NGL 36-008-138 for National Aeronautics and Space Administration, Hampton. VA.

40. B.A. Munk, T.W. Kornbau, and R.D. Fulton, op. cit., p. 986.

41. R.F. Harrington, op. cit., pp. 164-165.

42. J.D. Kraus, Antennas, McGraw-Hill, 1950, pp. 348-349.

43. E. Kreyszig, Advanced Engineering Mathematics, Wiley, 1967, pp. 681-684.

44. J.W. Goodman, Introduction to Fourier Optics, McGraw-Hill, 1968, pp. 11-25.

45. B.A. Munk, G.A. Burrell, and T.W. Kornbau, op. cit., pp. 40-47.

46. R.F. Harrington, op. cit., p. 100.

47. A. Papoulis, The Fourier Integral and Its Applications, McGraw-Hill, 1962, pp. 47-49.

48. H. Bateman, Table of Integral Transforms, Vol. I, McGraw-Hill, 1954.

49. M. Abramowitz and I.A. Stegun, Handbook of Mathematical Functions, Dover Publications, Inc., New York, 1972.

50. R.F. Harrington, op. cit., p. 77.

51. B.A. Munk, G.A. Burrell, and T.W. Kornbau, op. cit., pp. 58-60.

52. C.J. Larson, op. cit., p. 263.

53. B.A. Munk, op. cit.

54. T.W. Kornbau, B.A. Munk, and C.J. Larson, op. cit., p. 32.

55. B.A. Munk, G.A. Burrell, and T.W. Kornbau, op. cit., pp. 53-57.

56. O. R. Price and R. F. Hyneman, "Distribution Functions for Monopulse Antenna Difference Patterns," IRE Transactions on Antennas and Propagation, Vol. AP-8, No. 6, November 1960.

57. J.H. Richmond, op. cit.

58. R.F. Harrington, op. cit., p. 167.

59. C.J. Larson, op. cit., pp. 182-210.

60. S.A. Schelkunoff and H.T. Friis, op. cit.

61. C.J. Larson, op. cit.

62. J.F. Stosic, op. cit.